

Mössbauer Spectroscopy – Principles and Applications

Philipp Gütlich



Institut für Anorganische Chemie und Analytische Chemie
Johannes Gutenberg-Universität Mainz

Acknowledgement

I am thankful to Dr. Maksym Seredyuk, Dr. Matthias Grunert, Dr. Vadim Ksenofontov, Dr. Ulrich Stumm and Iris Fleischer for their assistance in preparing this lecture series. Also, I wish to extend my sincere thanks to all my graduate students, post-doctoral fellows and colleagues for their successful and pleasant collaboration.

Financial help from the Deutsche Forschungsgemeinschaft, Fonds der Chemischen Industrie, University of Mainz, Federal Government of Germany and the European Community for carrying out research in this field is gratefully acknowledged.

P.G.

Introduction

Nearly fifty years ago Rudolf L Mössbauer, whilst working on his doctoral thesis under Professor Maier-Leibnitz in Heidelberg, discovered the recoilless nuclear resonance absorption of gamma rays which became known as the Mössbauer Effect [1-3]. The phenomenon rapidly developed to a new spectroscopic technique which now bears his name. The Mössbauer Effect has been observed for about 100 nuclear transitions in some 80 nuclides in nearly fifty elements. Not all of these transitions are suitable for actual exploitation but, as will be shown here, the technique has made valuable contributions to the physical-, chemical-, biological- and earth-sciences.

“Mössbauer’s discovery that γ -ray emission and absorption can occur in a recoil-free fashion might have seemed at first glance to be no more than just an interesting new phenomenon. However, as soon as it became generally realized that the Mössbauer resonance line is extremely narrow and allows hyperfine interactions to be resolved and evaluated in a rather straightforward way, this handy new method created an avalanche of research activity. Within a few years nearly all disciplines in the natural sciences enjoyed a boom in the application of Mössbauer spectroscopy. Some journals were swamped to such an extent that editorials were written to limit the publication of Mössbauer results....Rudolf Mössbauer’s concluding remark concerning the effect that bears his name in his Nobel Laureate speech of December 1961 has proved to be correct and has retained its significance to the present day; it can also be regarded as a prognosis for the future. “We may therefore hope that this young branch of physics stands only at its threshold, and that it will be developed in the future, not only to extend the application of existing knowledge but to make possible new advances in the exciting world of unknown phenomena and effects.”

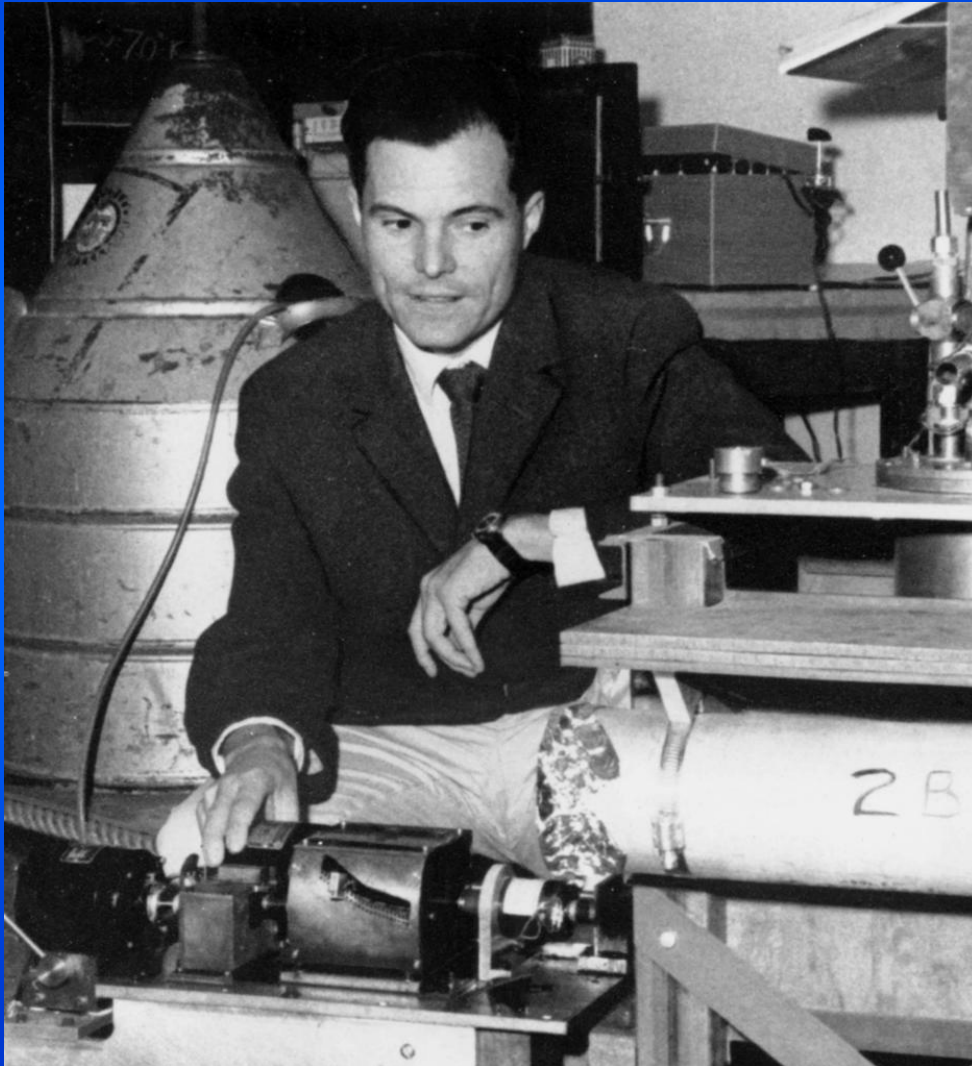
There have, over the past forty years, been excellent books devoted to Mössbauer spectroscopy [4-17] and numerous reviews. The purpose of the material shown here is to use schematic representations with the minimum of text to describe the principles and applications of Mössbauer spectroscopy and encourage the reader to consult other material for the detail.

References

1. R.L. Mössbauer, Z. Physik, 1958, 151, 124.
2. R.L. Mössbauer, Naturwissenschaften, 1958, 45, 538.
3. R.L. Mössbauer, Z. Naturforsch, 1959, 14a, 211.
4. U. Gonser (ed), Mössbauer Spectroscopy, Topics in Applied Physics, Vol 5, Springer, Berlin-Heidelberg-New York, 1975.
5. H. Fauenfelder, The Mössbauer Effect, Benjamin, New York, 1962.
6. G.K. Wertheim, Mössbauer Effect: Principles and Applications, Academic Press, New York, 1964.
7. V.I. Goldanskii and R. Herber (eds), Chemical Applications of Mössbauer Spectroscopy, Academic Press, New York, 1968.
8. L. May (ed) An Introduction to Mössbauer Spectroscopy, Plenum Press, New York, 1971.
9. N.N. Greenwood and T.C. Gibb, Mössbauer Spectroscopy, Chapman and Hall London, 1971.
10. G.M. Bancroft, Mössbauer Spectroscopy, An Introduction for Inorganic Chemists and Geochemists, McGraw-Hill London-New York, 1973.
11. T.C. Gibb, Principles of Mössbauer Spectroscopy, Chapman and Hall, London 1976.
12. P. Gütlich, R. Link, A. Trautwein, Mössbauer Spectroscopy and Transition Metal Chemistry, Springer-Verlag, Berlin-Heidelberg-New York, 1978.
13. A. Vértes, L. Korecz, K. Burger, Mössbauer Spectroscopy, Elsevier Scientific Publ. Comp. Amsterdam, Oxford, 1979
14. D. Barb, Grundlagen und Anwendungen der Mössbauerspektroskopie, Akademie-Verlag Berlin, 1980
15. R.H. Herber (ed) Chemical Mössbauer Spectroscopy, Plenum, New York, 1984.
16. G.J. Long (ed), Mössbauer Spectroscopy Applied to Inorganic Chemistry, Vol 1, Plenum, New York, 1984 and subsequent volumes.
17. D.P.E. Dickson and F.J. Berry, Mössbauer Spectroscopy, Cambridge University Press, Cambridge, 1986.

Rudolf L. MÖSSBAUER

discovers the “Recoilless Nuclear Resonance Absorption of γ -Radiation” in 1958
and receives the Nobel Prize in 1961



R.L. Mössbauer made his first
observation of recoilless nuclear
resonant absorption in ^{191}Ir !

R.L. Mössbauer,
Z. Physik, 1958, 151, 124.

R.L. Mössbauer,
Naturwissenschaften, 1958, 45, 538

The Principle of the Mössbauer Effect and Basic Concepts of Mössbauer Spectroscopy

For pedagogical reasons the following presentations refer to the most prominent Mössbauer active nuclide ^{57}Fe

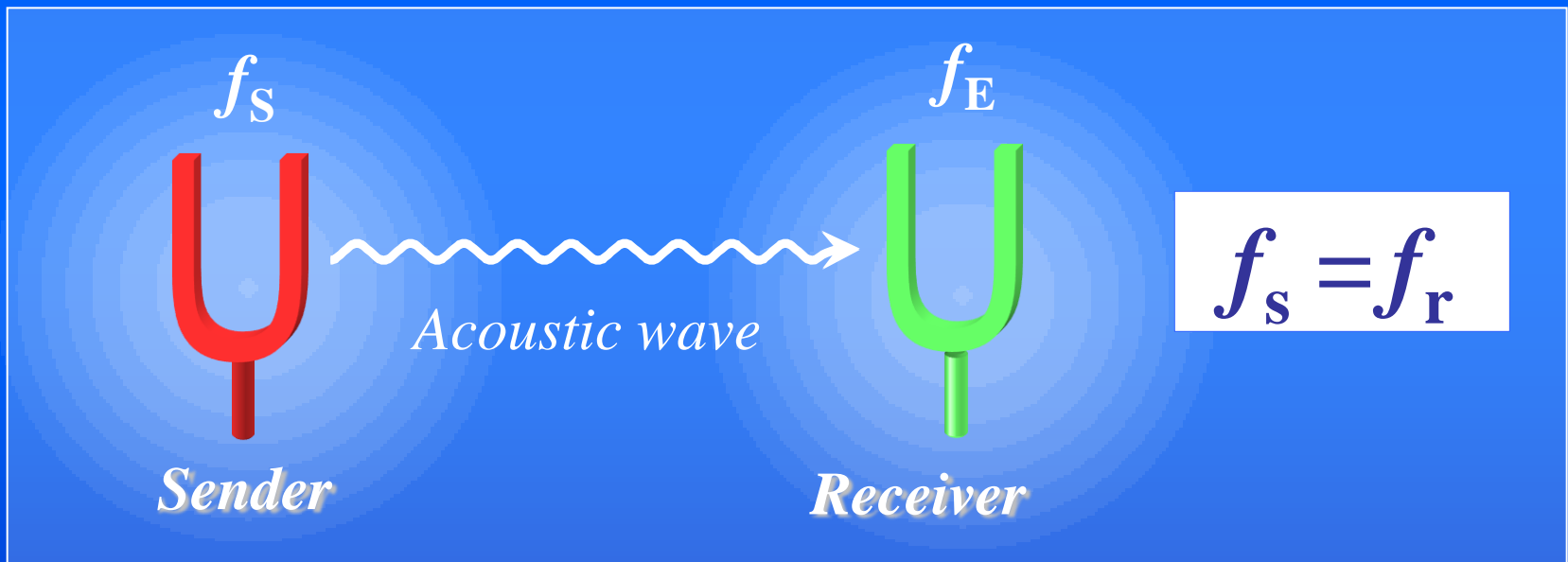
Mössbauer effect:

“Recoilless nuclear resonance absorption of γ -rays“

similar to

Acoustic resonance between two tuning forks with

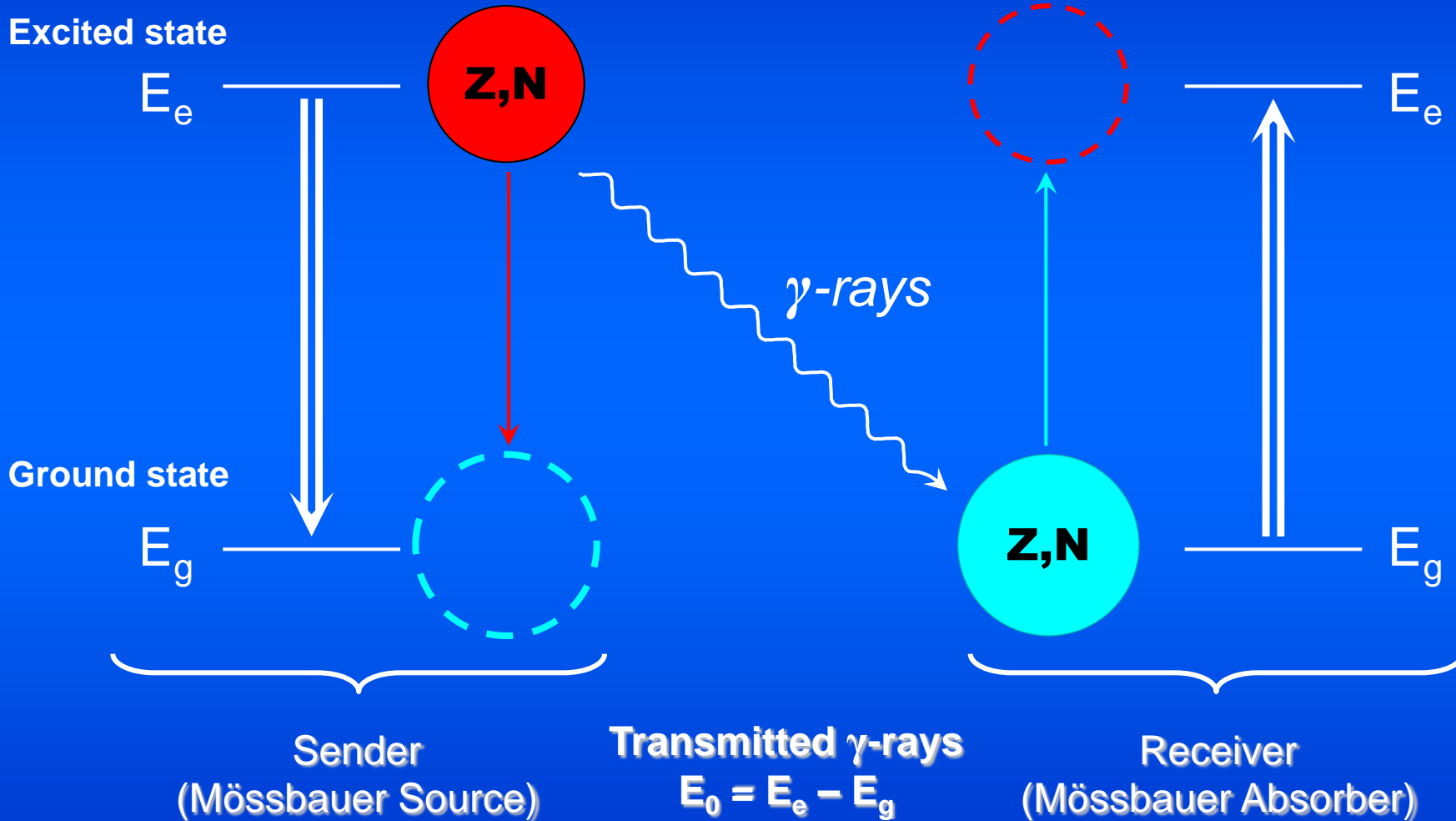
same frequency $f_s = f_r$



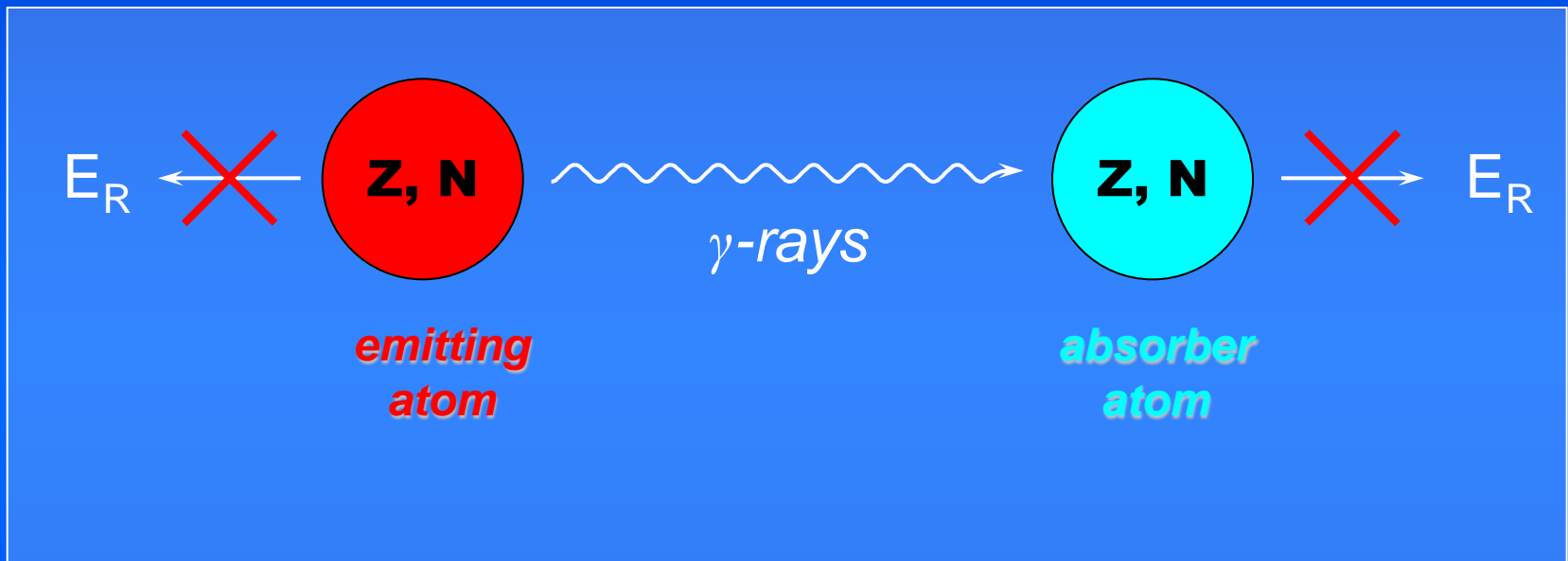
Mössbauer effect: Atomic nuclei instead of tuning forks

Nucleus 1

Nucleus 2

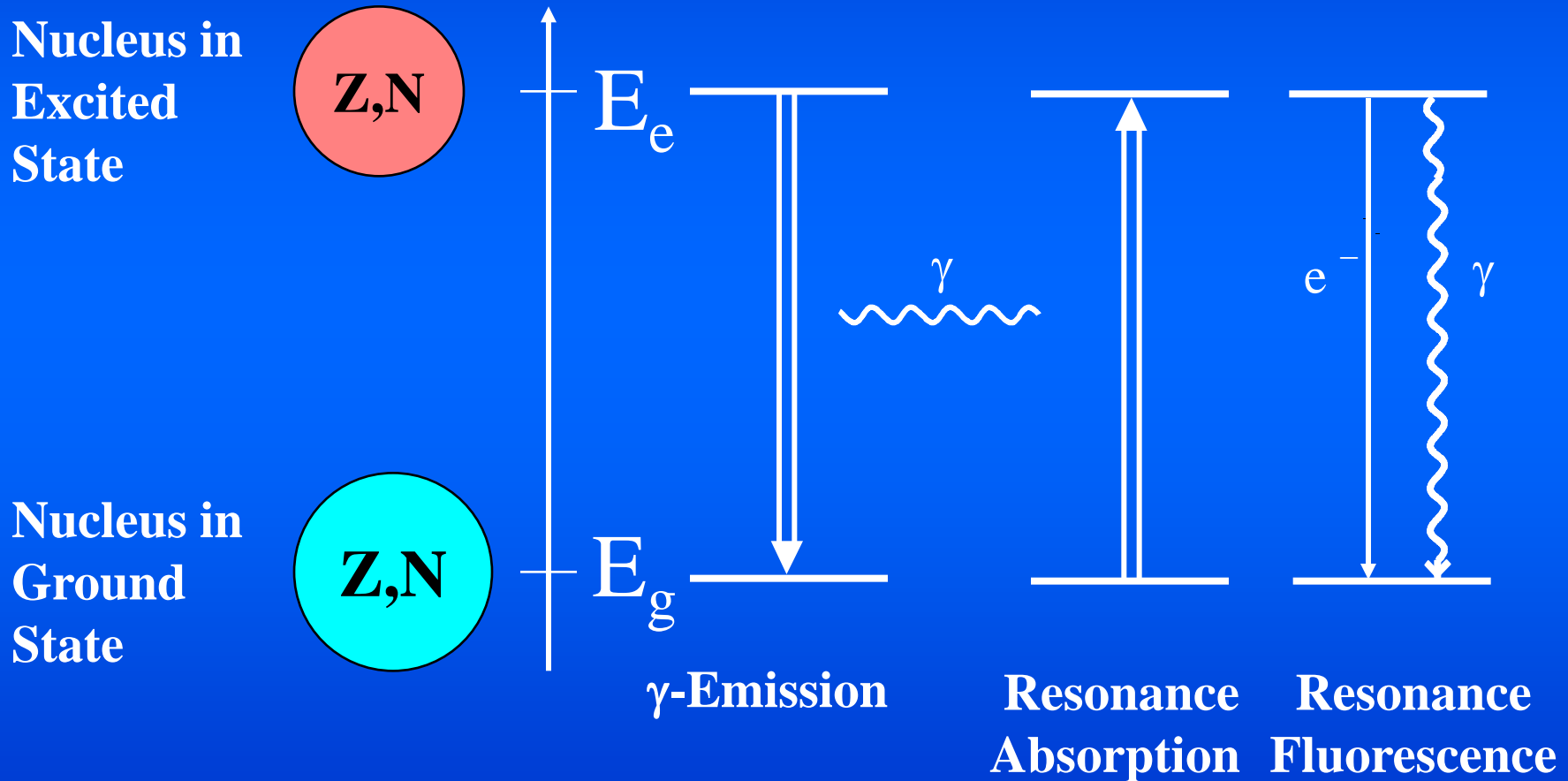


Important:
Elimination of recoil effect
upon emission and absorption of γ -rays!



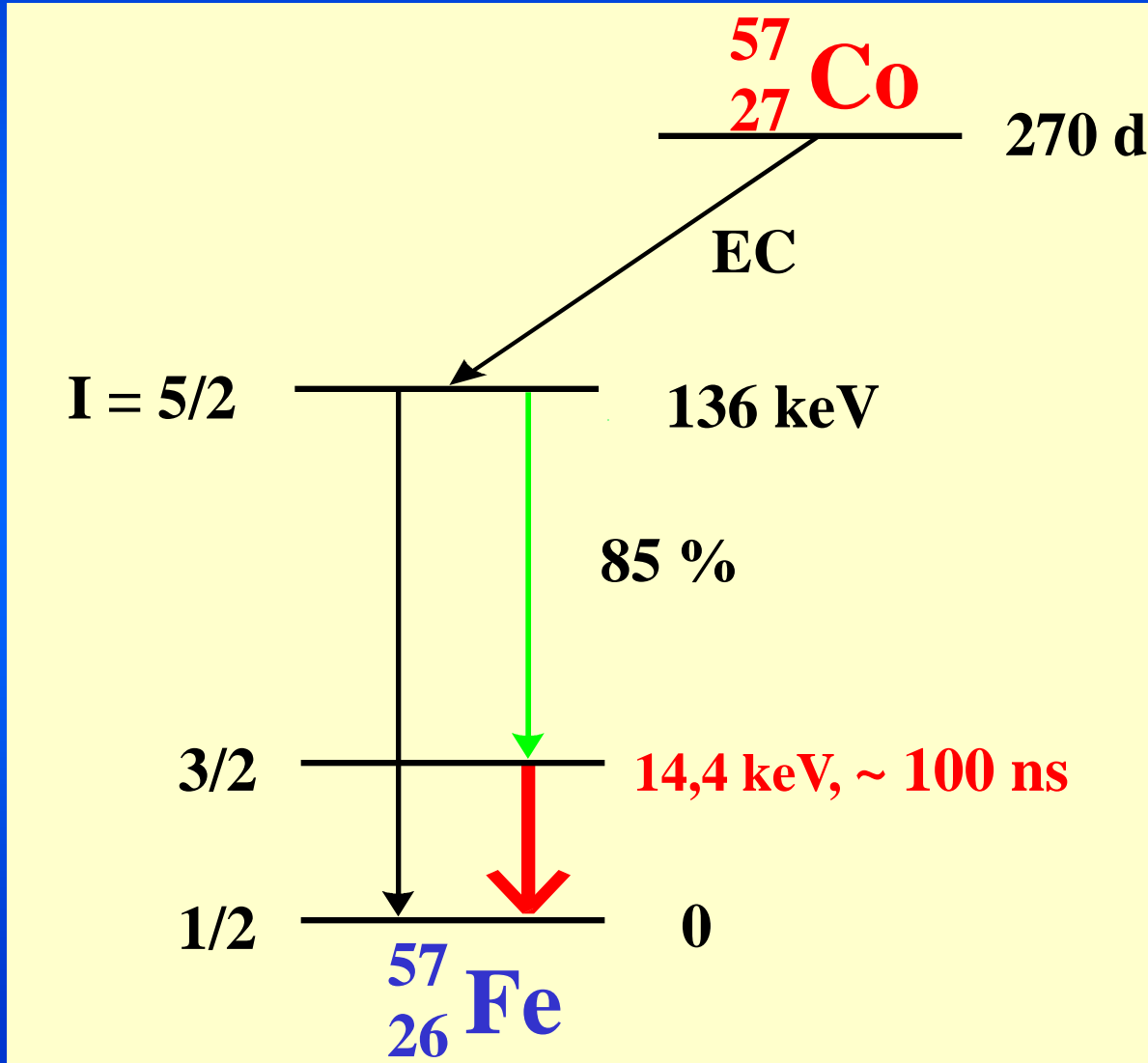
$$E_R = E_\gamma^2 / 2mc^2$$

Recoilless Nuclear Resonance Absorption and Fluorescence of γ -Radiation



A nucleus with Z protons and N neutrons in an excited state of energy E_e undergoes transition to the ground state of energy E_g by emitting a gamma quantum of energy $E_e - E_g$. The gamma quantum may be absorbed by the nucleus of the same kind (same Z and N) in its ground state, whereby transition to the excited state of energy E_e takes place (resonance absorption). The subsequent transition to the ground state emits a conversion electron e^- or a γ -quantum (resonance fluorescence).

Nuclear Decay Scheme for ^{57}Fe Mössbauer Resonance



Radioactive ^{57}Co with 270 days half-life, which may be generated in a cyclotron and diffused into a noble metal like rhodium, serves as the gamma radiation source for ^{57}Fe Mössbauer spectroscopy. ^{57}Co decays by electron capture (EC from K-shell, thereby reducing the proton number, from 27 to 26 corresponding to ^{57}Fe) and initially populates the 136 keV nuclear level of ^{57}Fe with nuclear spin quantum number $I = 5/2$. This excited state decays after ca. 10 ns and populates, with 85 % probability the 14.4 keV level by emitting 122 keV gamma quanta, with 15 % probability the 136 keV level decays directly to the ground state of ^{57}Fe . The 14.4 keV nuclear state has a half-life of ca. 100 ns. Both the half-life and the emitted gamma quanta of 14.4 keV energy are ideally suited for ^{57}Fe Mössbauer spectroscopy.

$I = 3/2$ and $I = 1/2$ are the nuclear spin quantum numbers of the excited state (14.4 keV) and the ground state, respectively.

The internal conversion coefficient α (= the number of ejected K-shell electrons for each γ -quantum interacting with the K-shell) is 9.7.

Mössbauer Active Elements

IA																		VIIIA
H	IIA											IIIA	IVA	VA	VIA	VIIA		He
Li	Be											B	C	N	O	F		Ne
Na	Mg	IIIB	IVB	VB	VIB	VIIIB	VIII B			IB	IIB	Al	Si	P	S	Cl		Ar
K	Ca	Sc	Ti	V	Cr	Mn	Fe	Co	Ni	Cu	Zn	Ga	Ge	As	Se	Br		Kr
Rb	Sr	Y	Zr	Nb	Mo	Tc	Ru	Rh	Pd	Ag	Cd	In	Sn	Sb	Te	I		Xe
Cs	Ba	La	Hf	Ta	W	Re	Os	Ir	Pt	Au	Hg	Tl	Pb	Bi	Po	At		Rn
Fr	Ra	Ac																
			Ce	Pr	Nd	Pm	Sm	Eu	Gd	Tb	Dy	Ho	Er	Tm	Yb	Lu		
			Th	Pa	U	Np	Pu	Am	Cm	Bk	Cf	Es	Fm	Md	No	Lw		

Periodic table of the elements. Marked in red are the elements (more than 40) for which the Mössbauer effect has been observed. The most prominent “Mössbauer nuclide” is ^{57}Fe . More than 90 % of the nearby 50 000 publications which have appeared so far refer to ^{57}Fe isotope. Nuclides suitable for Mössbauer spectroscopy should possess excited nuclear states with lifetimes in the range of ca. 10^{-6} to ca. 10^{-11} s, and transition energies between ca. 5 and 180 keV. Longer (shorter) lifetimes than indicated lead, according to the Heisenberg Uncertainty Principle, to too narrow (broad) emission and absorption lines, which no longer effectively overlap. Transition energies beyond ca. 180 keV cause too large recoil effects which destroy the resonance (see next figure). Gamma quanta with energies smaller than ca. 5 keV will mostly be absorbed in the source and absorber material.

The Mössbauer effect has been detected with a total of nearly 90 γ -ray transitions in 72 isotopes of 42 different elements. Due to several criteria (suitable lifetime of nuclear excited state, transition energy, easy accessibility and handling) only ca. twenty elements can be studied by Mössbauer spectroscopy, e.g. iron, tin, antimony, tellurium, iodine, gold, nickel, ruthenium, iridium, tungsten, krypton, xenon, many of the rare earth elements, neptunium.

Experimental Resonance Conditions

Transition energy: $E_\gamma = E_a - E_g$

Suitable range: $5 \text{ keV} \leq E_\gamma \leq 180 \text{ keV}$

If $E_\gamma \leq 5 \text{ keV}$: Complete non-resonance absorption

If $E_\gamma \geq 180 \text{ keV}$: Recoil energy $E_R = E_\gamma^2/2mc^2$
becomes too large and destroys
resonance

Nuclear parameters for selected Mössbauer isotopes

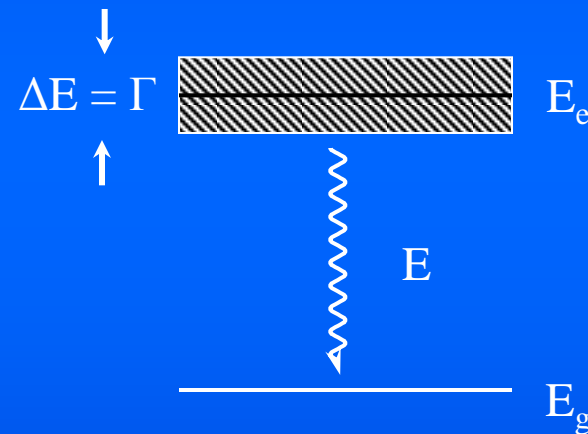
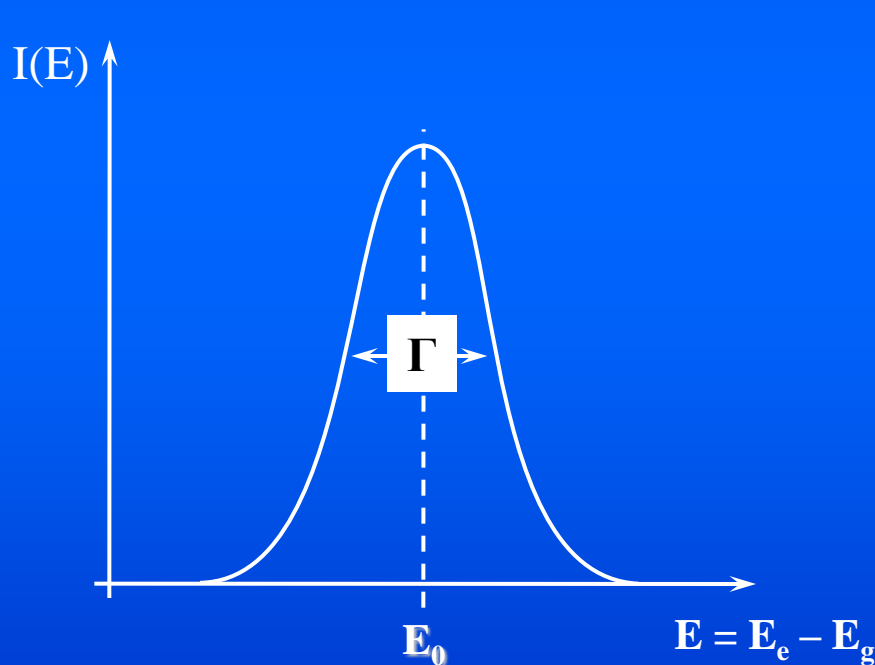
Isotope	E_γ/keV	$\Gamma_r/(\text{mm s}^{-1})$ $= 2 \Gamma_{\text{nat}}$	I_g	I_e	α	Natural abundance %	Nuclear decay*
^{57}Fe	14.41	0.192	1/2-	3/2-	8.17	2.17	$^{57}\text{Co}(\text{EC } 270 \text{ d})$
^{61}Ni	67.40	0.78	3/2-	5/2-	0.12	1.25	$^{61}\text{Co}(\beta^- 99 \text{ m})$
^{119}Sn	23.87	0.626	1/2+	3/2+	5.12	8.58	$^{119\text{m}}\text{Sn}(\text{IT } 50 \text{ d})$
^{121}Sb	37.15	2.1	5/2+	7/2+	~ 10	57.25	$^{121\text{m}}\text{Sn}(\beta^- 76 \text{ y})$
^{125}Te	35.48	5.02	1/2+	3/2+	12.7	6.99	$^{125}\text{I}(\text{EC } 60 \text{ d})$
^{127}I	57.60	2.54	5/2+	7/2+	3.70	100	$^{127\text{m}}\text{Te}(\beta^- 109 \text{ d})$
^{129}I	27.72	0.59	7/2+	5/2+	5.3	nil	$^{129\text{m}}\text{Te}(\beta^- 33 \text{ d})$
^{149}Sm	22.5	1.60	7/2-	5/2-	~ 12	13.9	$^{149}\text{Eu}(\text{EC } 106 \text{ d})$
^{151}Eu	21.6	1.44	5/2+	7/2+	29	47.8	$^{151}\text{Gd}(\text{EC } 120 \text{ d})$
^{161}Dy	25.65	0.37	5/2+	5/2-	~ 2.5	18.88	$^{161}\text{Tb}(\beta^- 6.9 \text{ d})$
^{193}Ir	73.0	0.60	3/2+	1/2+	~ 6	61.5	$^{193}\text{Os}(\beta^- 31 \text{ h})$
^{197}Au	77.34	1.87	3/2+	1/2+	4.0	100	$^{197}\text{Pt}(\beta^- 18 \text{ h})$
^{237}Np	59.54	0.067	5/2+	5/2-	1.06	nil	$^{241}\text{Am}(\alpha 458 \text{ y})$

*EC = electron capture, β^- = beta-decay, IT = isomeric transition, α – alpha-decay

Mean lifetime τ of excited state and natural line width Γ

An excited state (nuclear or electronic) of mean lifetime τ can never be assigned a sharp energy value, but only a value within the energy range ΔE , which correlates with the uncertainty in time Δt via the **Heisenberg Uncertainty Principle**: $\Delta E \Delta t \geq \hbar$. Weisskopf and Wigner have shown that in general $\Gamma \cdot \tau = \hbar$.

$\Gamma = \hbar/\tau = \text{natural line width}$, $\hbar = h/2\pi$ Planck's constant

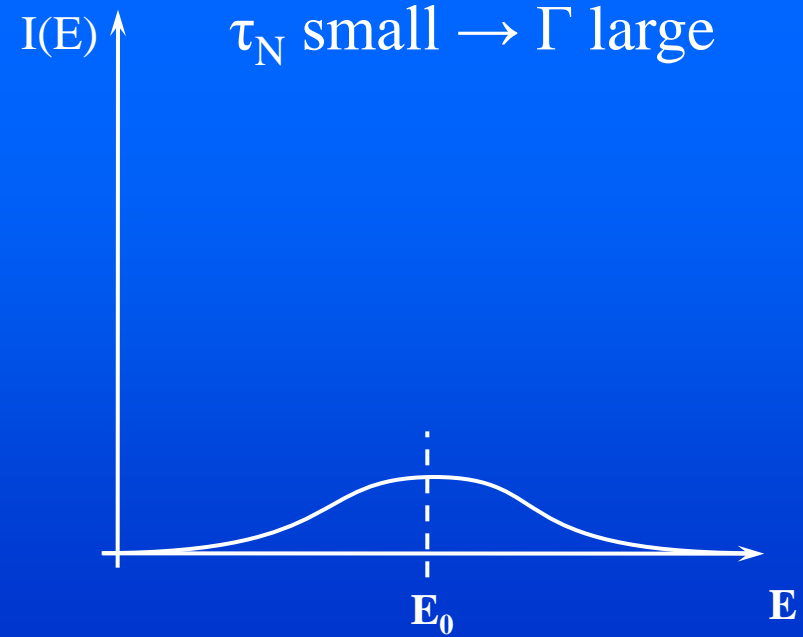
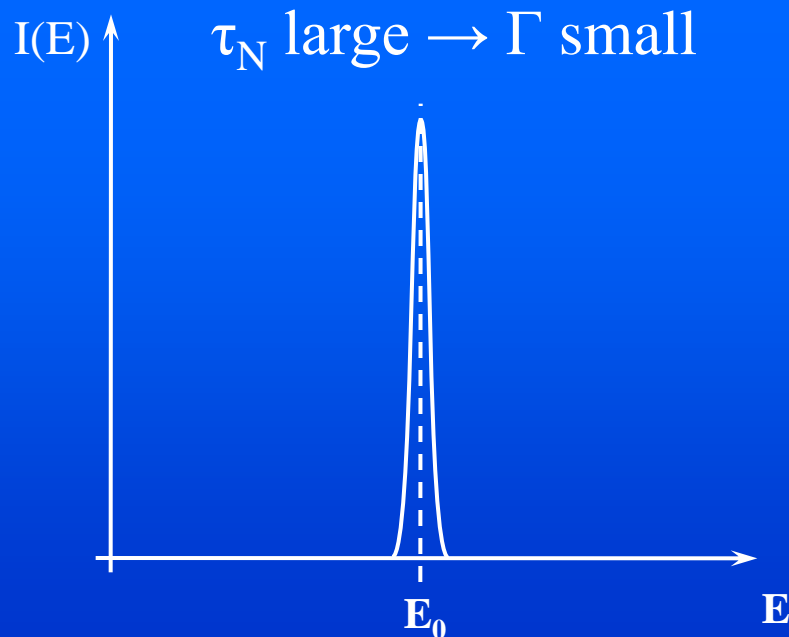


Transitions from an excited state (e) to the ground state (g) or vice versa involve all possible energies within the range of ΔE . The transition probability or intensity as a function of E yields a spectral line centered around the most probable transition energy E_0 .

According to Weisskopf and Wigner the distribution of energies about the energy E_0 (= transition probability as function of transition energy E) is given by the **Breit-Wigner (or Lorentzian) formula**:

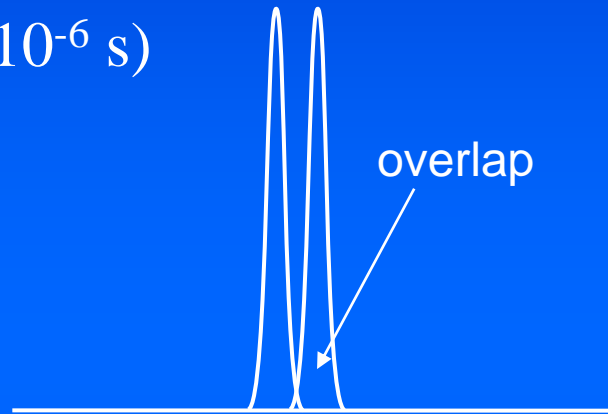
$$I(E) = \frac{(\Gamma/2)^2}{(E - E_0)^2 + (\Gamma/2)^2}$$

The mean lifetime τ determines the width of the resonance lines ($\Gamma \cdot \tau = \hbar$). The mean lifetime τ is related to the half-life $t_{1/2}$ by the relation $\tau = \ln 2 \cdot t_{1/2}$.

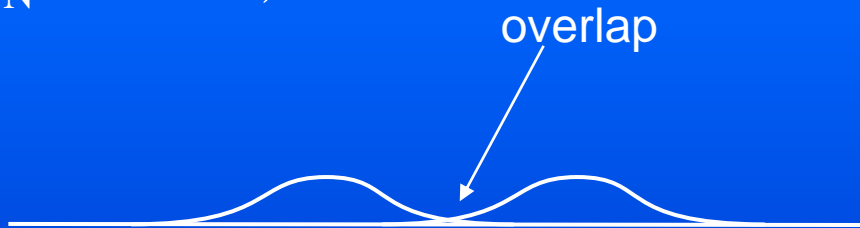


Resonance absorption is observable only if the emission and absorption lines **overlap sufficiently**. This is not the case when the lines are:

- too narrow ($\tau_N \geq 10^{-6}$ s)



- too broad ($\tau_N \leq 10^{-11}$ s)



Resonance absorption is “hidden in the noise”

Suitable for Mössbauer spectroscopy: 10^{-6} s $\geq \tau_N \geq 10^{-11}$ s

Sharpness of resonance Γ/E_γ in Mössbauer effect with nuclear transition E_γ Example ^{57}Fe

$$\tau_N = 1.4 \cdot 10^{-7} \text{ s} \rightarrow \Gamma = \hbar/\tau_N = 4.7 \cdot 10^{-9} \text{ eV}$$

$$\Gamma/E_\gamma = 4.7 \cdot 10^{-9} \text{ eV} / 14\,400 \text{ eV} = \mathbf{3.26 \cdot 10^{-13}}$$

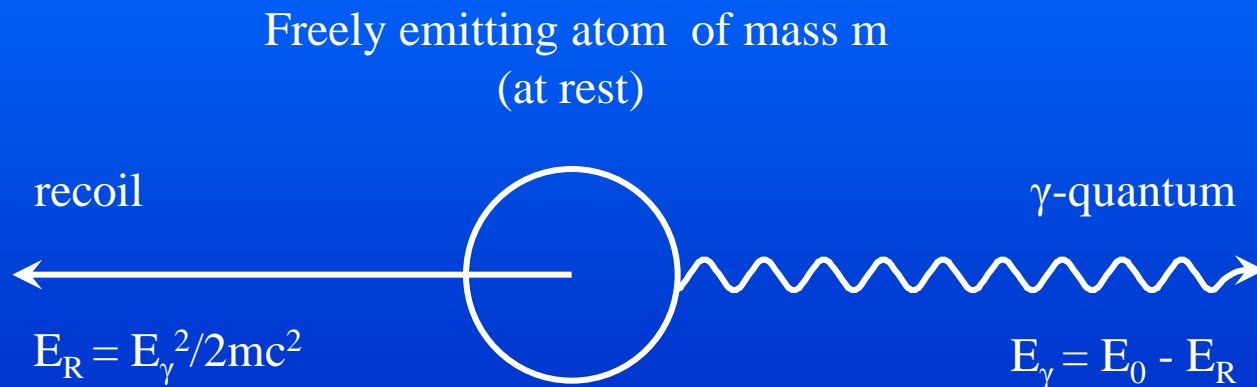
(Optical transitions $\Gamma/E \sim 10^{-8}$)

Recoil Effect

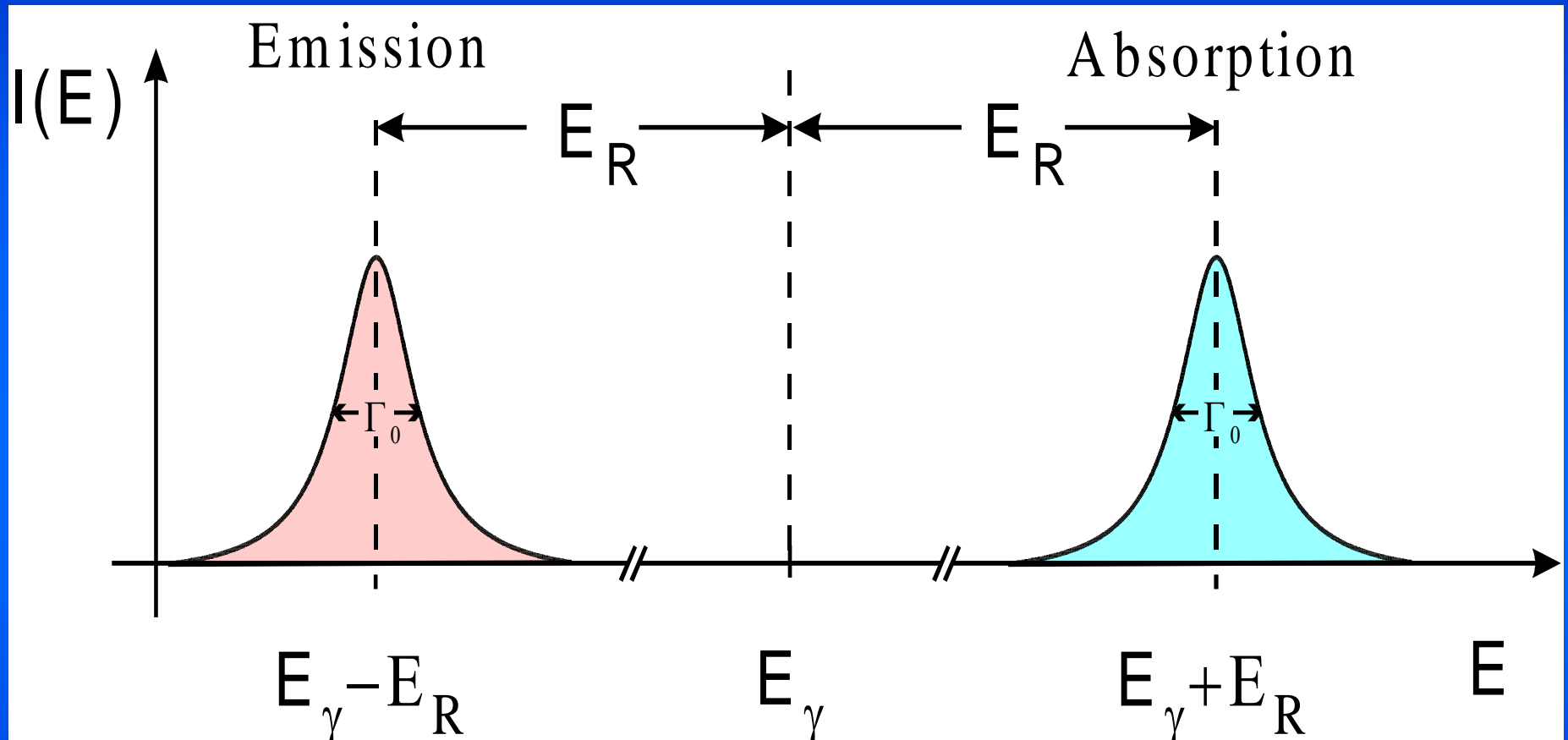
By emission or absorption of γ -quanta with energy E_γ in a **free atom or molecule** (gas, liquid) the atom (molecule) of mass **m** suffers a recoil effect with energy E_R given by the equation

$$E_R = E_\gamma^2 / 2mc^2$$

which is much larger (5-6 orders of magnitude) than the natural line width $\Gamma \rightarrow$ no resonance possible between free atoms or molecules



Recoil Effect



$$E_R = \frac{E_\gamma^2}{2mc^2}$$

$${}^{57}\text{Fe} : E_R = 2 \cdot 10^{-3} \text{ eV}$$
$$\Gamma_0 = 4.7 \cdot 10^{-9} \text{ eV}$$

The figure shows the intensity $I(E)$ as a function of the transition energy for emission and absorption of gamma quanta. The spectral line shape may be described by the **Lorentzian or Breit-Wigner** form. The width at half maximum of the spectral line is called the natural line width Γ_0 and is determined by the mean life time $\tau = t_{1/2}/\ln 2 = 1.43 \times 10^{-7}$ s for the 14.4 keV level of ^{57}Fe , for which $\Gamma_0 = h/2\pi\tau = 4.6 \times 10^{-9}$ eV. The symbol Γ_0 is used here for the natural linewidth to differentiate from the experimental line width, which in actual experiments is always broader than the natural line width due to various broadening effects.

If a **free atom or molecule** with mass m emits or absorbs a gamma quantum of energy E_γ , a linear momentum with recoil energy E_R is imparted to the atom and molecule, respectively, which according to the formula given in the Figure (c = velocity of light) amounts to 2×10^{-3} eV and thus is six orders of magnitude larger than the transition energy E_γ . The recoil effect reduces the transition energy by E_R for the emission process and increases the transition energy by E_R for the absorption process. Thus the emission and the absorption lines are shifted away from each other by $2E_R \approx 10^6 \Gamma_0$, and in view of the huge difference between Γ_0 and E_R an appreciable overlap resonance is not possible. This means, that **the Mössbauer effect cannot be observed for freely moving atoms or molecules, i.e. in gaseous or liquid state.**

So far we have considered a freely emitting and absorbing atom or molecule **at rest** before and after emission and absorption. This, however, is against reality and we must take into account the additional movement of atoms or molecules (even if bound in a crystal lattice) due to thermal energy, which leads to **thermal broadening** of emission and absorption lines, not only of nuclear but also of optical transitions.

Free-atom Recoil and Thermal Broadening

We consider the emission of a γ -quantum of initial energy E_0 from an atom with mass m moving with velocity v_N in the direction of the γ -ray propagation.

Before emission: $E_0 + \frac{1}{2} m v_N^2$

After emission: $E_\gamma + \frac{1}{2} m (v_N + v_R)^2$ $v_R =$ velocity due to recoil
(opposite to v_N)

Conservation of energy: $E_0 + \frac{1}{2} m v_N^2 = E_\gamma + \frac{1}{2} m (v_N + v_R)^2$

Difference between nuclear transition energies before and after emission:

$$\delta E = E_0 - E_\gamma = \underbrace{\frac{1}{2} m v_R^2}_{\text{Recoil energy } E_R} + \underbrace{m v_N v_R}_{\text{Doppler energy } E_D}$$

Some typical energies

Mössbauer γ -ray energies (E_γ):	$10^4 - 10^5$ eV
Chemical bonds and lattice energies:	$1 - 10$ eV
Electronic transitions:	$0.5 - 5$ eV
Molecular vibrations:	$5 \cdot 10^{-2} - 5 \cdot 10^{-1}$ eV
Lattice vibrations:	$10^{-3} - 10^{-1}$ eV
Nuclear recoil and Doppler energies (E_D, E_R):	$10^{-4} - 10^{-1}$ eV
Nuclear quadrupole coupling:	$< 10^{-5}$ eV
Nuclear Zeeman splitting:	$< 10^{-5}$ eV
Heisenberg natural line width:	$10^{-9} - 10^{-6}$ eV

$$1 \text{ eV} = 23.06 \text{ kcal/mole} = 96.49 \text{ kJ/mole}$$

Comparison Between Electronic and Nuclear Transitions

	ELECTRONIC TRANSITION SODIUM D LINE	NUCLEAR TRANSITION FE-57
ENERGY OF TRANSITION, E (eV)	2.1	14.413
MEAN LIFE TIME OF EXCITED STATE, τ (SEC)	1.5×10^{-8}	1.4×10^{-7}
NATURAL WIDTH OF RESONANCE LINE, $\Gamma = \hbar/\tau$ (eV)	4.4×10^{-8}	4.6×10^{-9}
RESOLVING POWER, Γ/E	2.1×10^{-8}	3.1×10^{-13}
RECOIL ENERGY, E_R (eV)	$\sim 10^{-10}$	1.9×10^{-3}
RATIO E_R/Γ	$\sim 2.3 \times 10^{-3}$	4.1×10^5

Energy and Momentum Transfer to the Lattice

In the solid state, crystalline or non-crystalline, **recoilless emission and absorption** of gamma quanta is possible, and the essentially unshifted transition lines can (at least partially) overlap and nuclear resonance absorption can be observed. The reason is that due to the much larger mass M of a solid particle as compared to that of an atom or a molecule, the linear momentum created by emission and absorption of a gamma quantum practically vanishes. The recoil energy caused by an emitting and absorbing atom, which is tightly bound in the lattice, is mostly transferred to the lattice vibrational system. There is a certain probability f (known as *Debye-Waller factor* or *Lamb-Mössbauer factor*) that no lattice excitation (*zero-phonon processes*) takes place during γ -emission or γ -absorption. f denotes the fraction of nuclear transitions which occur without recoil. Only for this fraction is the Mössbauer effect observable. Within the Debye model for solids, f increases with decreasing transition energy E_γ , with decreasing temperature, and with increasing Debye temperature $\theta_D = h\omega_D/2\pi k_B$ (ω_D = vibrational frequency of Debye oscillator, k_B = Boltzmann factor). θ_D is a measure for the strength of the bonds between the Mössbauer atom and the lattice. It is high ($>$ room temperature) for metallic materials and low ($<$ room temperature) for soft compounds.

In a solid (e.g. crystal)

the recoil energy E_R is partitioned according to

$$E_R = E_{\text{transl}} + E_{\text{vib}}$$

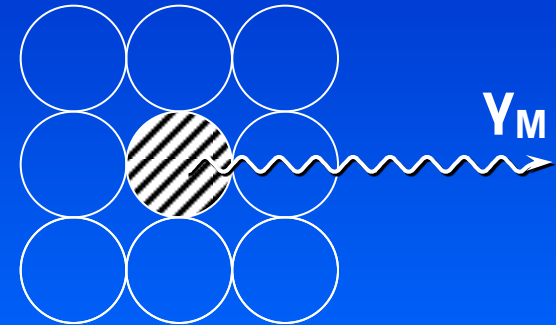
E_{transl} refers to the linear momentum imparted to the whole particle (crystal) of mass M .

$E_{\text{transl}} \ll \Gamma$, since $M \gg m$.

E_{vib} is converted into phonons (excitation of lattice vibrations).

E_{vib} is quantized. Within the Einstein model or Debye model:

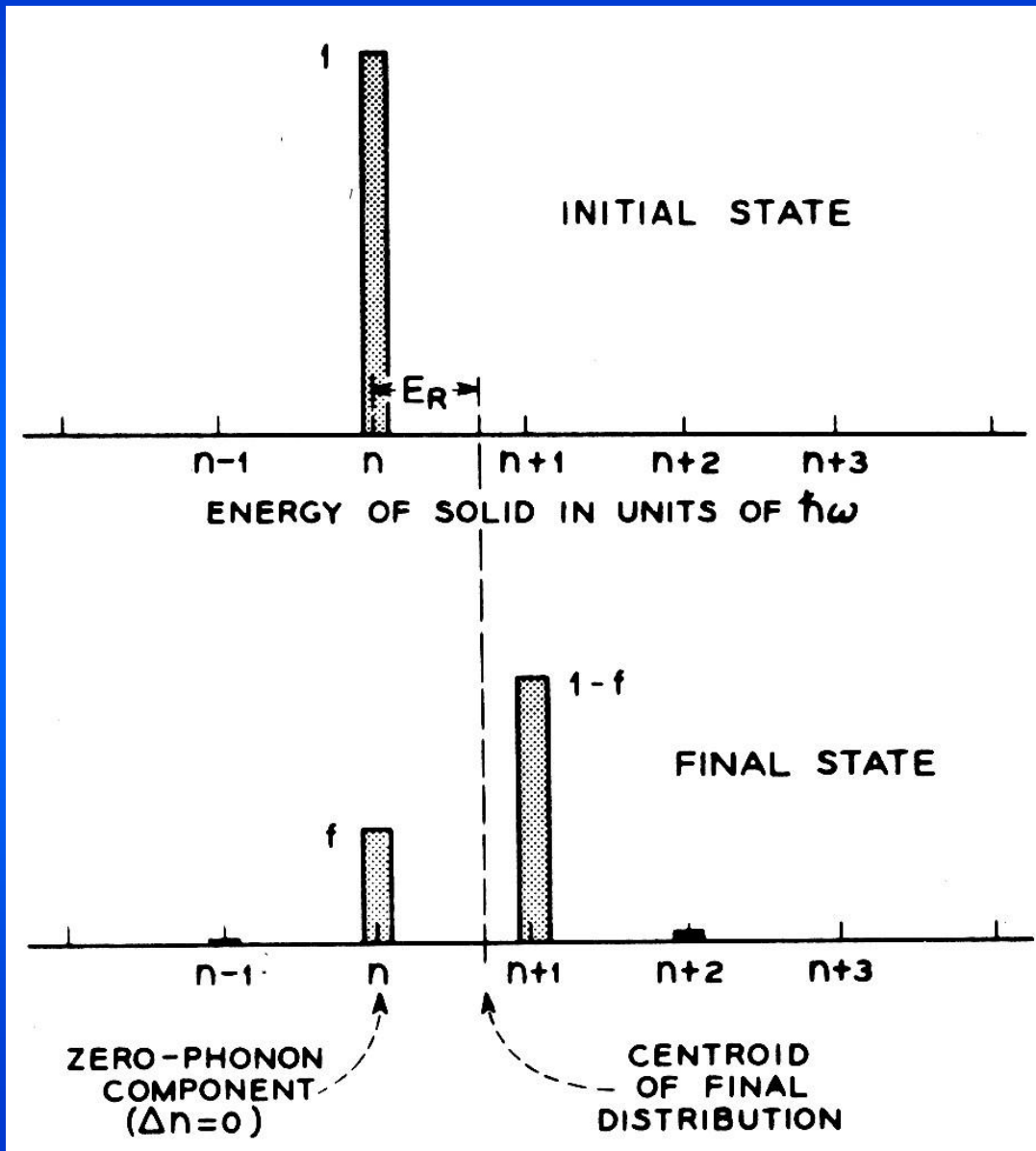
The vibrational energy of the lattice as a whole can only change by discrete amounts $0, \pm\hbar\omega, \pm2\hbar\omega, \dots$



With probability f (**Debye-Waller factor**, often denoted as **Lamb-Mössbauer factor**) the quantum mechanical phonon system remains unchanged (i.e. no excitation of lattice vibrations = *zero phonon processes*) during emission or absorption of γ -quanta.

Only this parameter f is useful for nuclear resonance absorption (fluorescence) → **Mössbauer effect**

The recoil-free fraction in the Einstein model



The solid may be characterized by the quantum numbers of its N oscillators having the same frequency for the $3N$ vibrational modes. The only possible changes are an increase or decrease in one or more of the quantum numbers. These correspond to the absorption or emission of quanta of energy $\hbar\omega$. The emission of a γ -quantum is accompanied by a transfer of integral multiples of this phonon energy ($0, \pm\hbar\omega, \pm 2\hbar\omega, \dots$).

The fraction f produces no change in the quantum state of the lattice. In the remaining, $1-f$, an energy $\hbar\omega$ is transferred. The processes with $\Delta n = -1$ and 2 may be neglected.

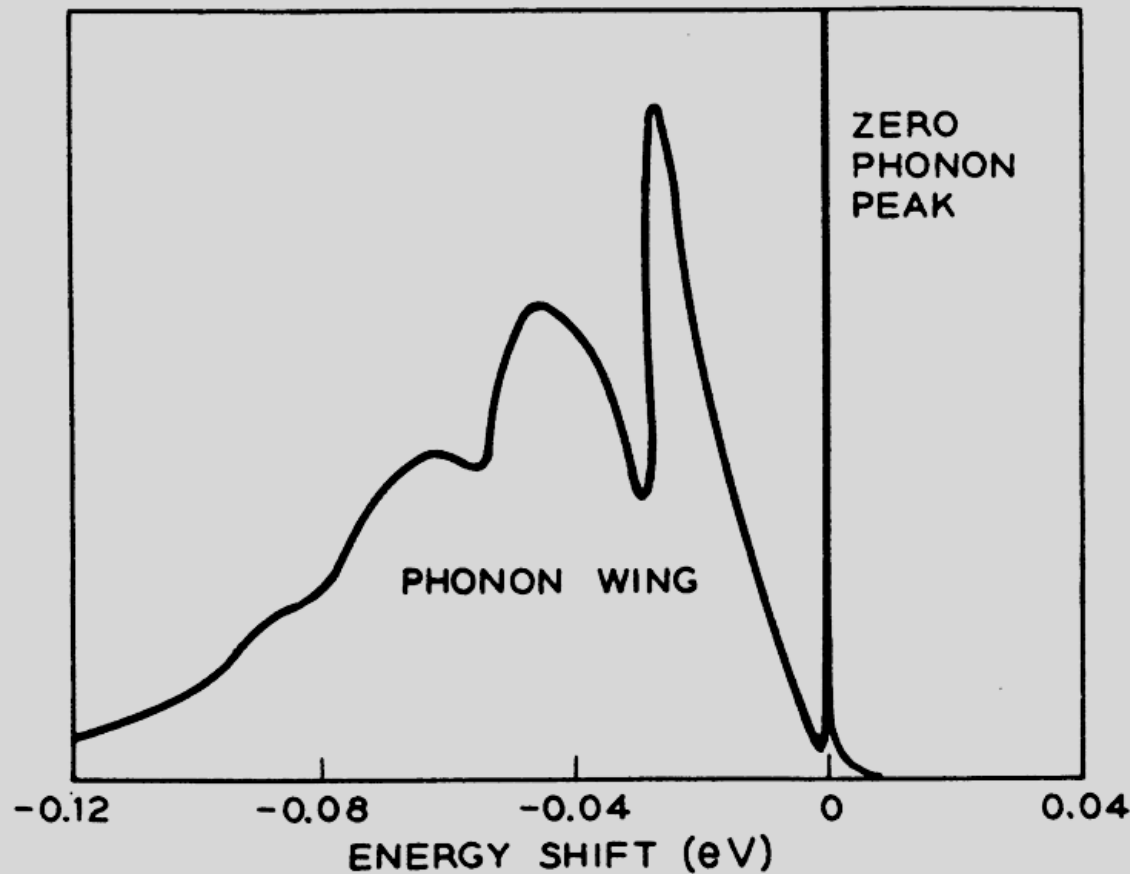


FIG. 1. The theoretical spectrum of the 129 keV gamma ray of Ir¹⁹¹ emitted by an atom in iridium metal at low temperature [2]. The Mössbauer spectrometer is sensitive only to the narrow, recoil-free line at zero energy shift, which contains 5.7% of the total area under the curve.

[1] W.M. Visscher, *Ann. Phys.* 9, 194, 1960

Lamb-Mössbauer-Factor (Debye-Waller-Factor)

f is known as the *recoil-free fraction* and denotes the fraction of γ -quanta, which are emitted and absorbed **without recoil**.

The parameter f is related to the vibrational properties of the crystal lattice and can be expressed as:

$$f = \exp -\{(\langle x^2 \rangle / \lambda^2)(2\pi)^2\} = \exp -\{(2\pi)^2 E_\gamma^2 \langle x^2 \rangle / (hc)^2\}$$

$\langle x^2 \rangle$: mean square vibrational amplitude in x direction

λ : wave length of gamma radiation with $E_\gamma = h\nu = h \cdot c / \lambda$

This means:

the weaker the bonding in the crystal,

- the larger is $\langle x^2 \rangle$
- the smaller is f
- the smaller the resonance effect

and the larger the transition energy E_γ

- the smaller is λ
- the smaller is the resonance effect

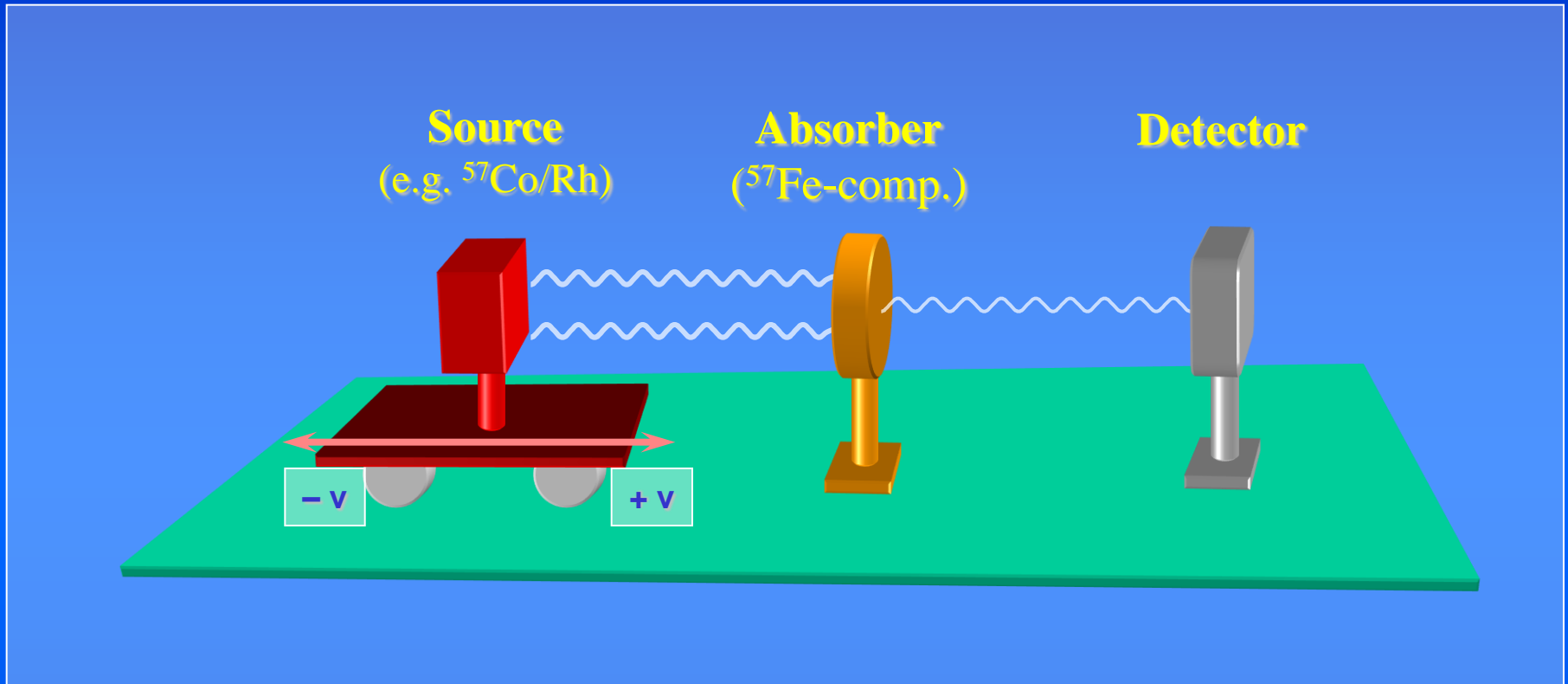
Debye model: For the low-temperature approximation, $T \ll \Theta_D$:

$$f = \exp \left[- \frac{E_R}{k_B \Theta_D} \left(\frac{3}{2} + \frac{\pi^2 T^2}{\Theta_D^2} \right) \right]$$

k_B : Boltzmann constant,
 $\Theta_D = \hbar \omega_D / k_B =$
Debye-temperature

f increases a) with **decreasing recoil energy E_R**
b) with **decreasing temperature T**
c) with **increasing Debye-temperature (bondstrength)**

Mössbauer-Experiment



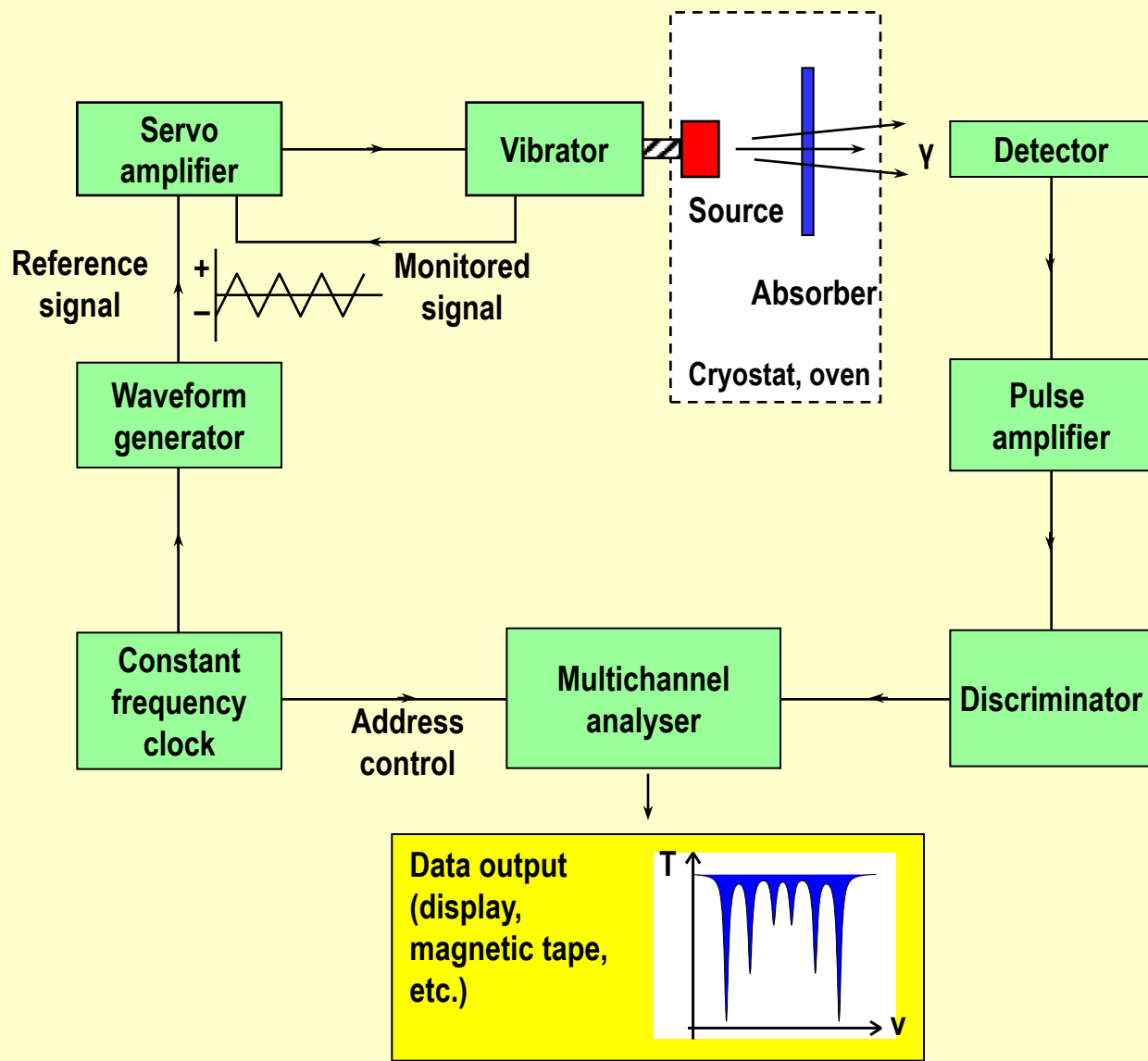
Source and absorber are moved relative to each other with

Doppler velocity $v = c (\Gamma_0/E_\gamma)$

c = velocity
of light

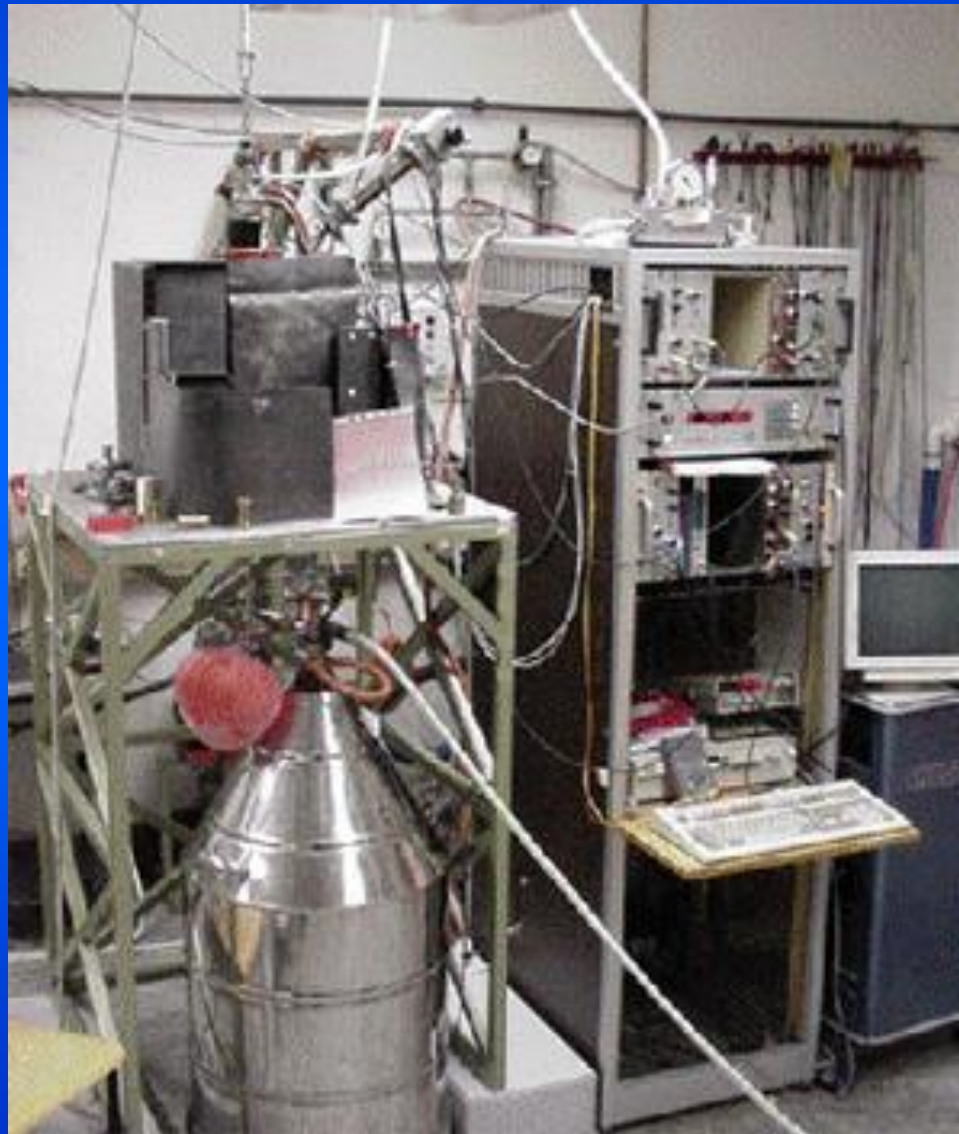
$^{57}\text{Fe} : \Gamma_0 = 4.7 \cdot 10^{-9} \text{ eV}, E_\gamma = 14400 \text{ eV}, v = 0.096 \text{ mm s}^{-1}$

Scheme of Mössbauer Spectrometer



The schematic diagram shows the main components of a Mössbauer spectrometer. The source, for ^{57}Fe spectroscopy one uses e.g. commercially available $^{57}\text{Co}/\text{Rh}$, is mounted on the shaft of a *vibrator*. While the source is generally kept at room temperature, the absorber (sample under study) may be thermostated in a cryostat for cooling down to liquid nitrogen or liquid helium temperatures, or for controlled heating in an oven. The γ -rays are detected by a scintillation counter, gas proportional counter or a semiconductor detector. The pulses from the *detector* are amplified and pass through a *discriminator*, where most of the non-resonant background radiation is rejected, and finally are fed into the open channel address of a *multi-channel analyser* (e.g. a computer) with several hundred channels, which is synchronised with the vibrator making use of the so-called *feed-back control system*. A *constant frequency clock* synchronises a voltage waveform (usually triangular yielding a linear Doppler velocity scale) which serves as a reference signal to the servo-amplifier controlling the electro-mechanical vibrator. The difference between the monitored signal and the reference signal is amplified and drives the vibrator at the same frequency (typically 50 s^{-1}) as the channel address advance. Each channel corresponds to a certain relative velocity and is held open for a fixed time interval depending on the frequency and number of channels used. The incoming γ -counts are collected in their corresponding channels during the sequential accessing e.g. 50 times per second, until satisfactory resolution is reached. The measured Mössbauer spectrum is analysed using special least squares fitting programs.

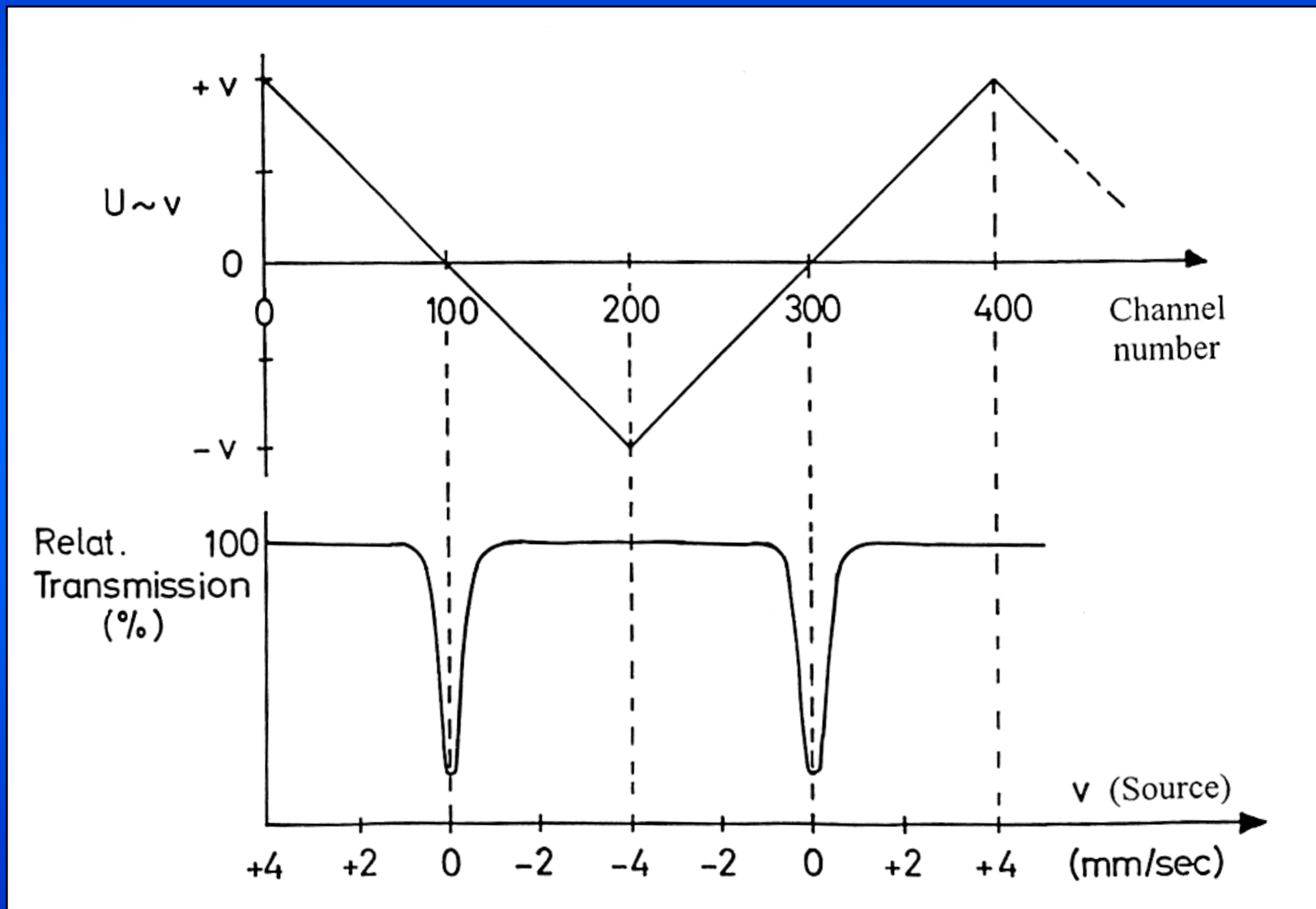
Mössbauer Spectrometer

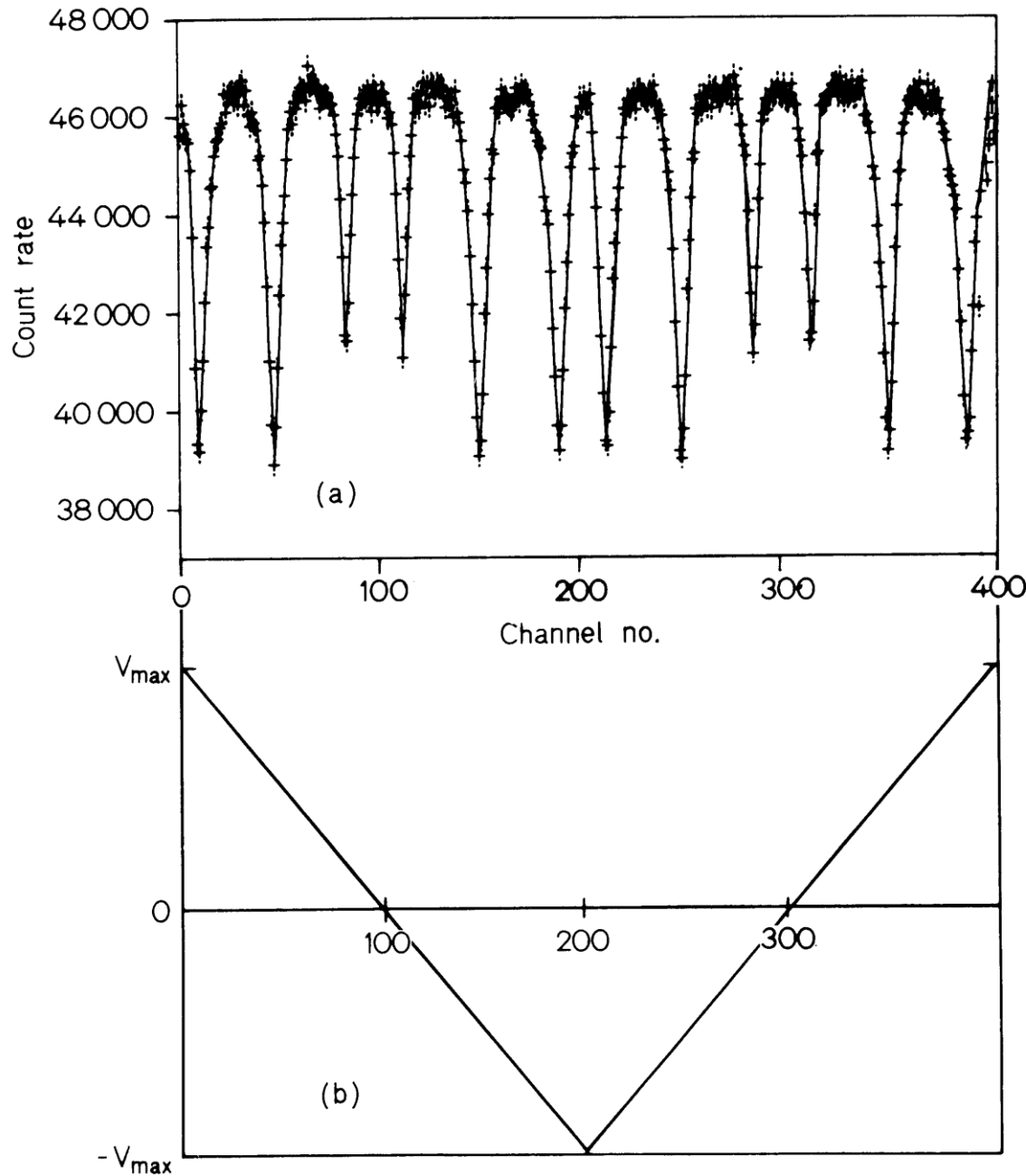


The picture shows a typical Mössbauer spectrometer with low temperature facility for cooling the sample down to 4.2 K (boiling point of liquid helium). Further cooling to ca. 1.5 K is possible by pumping on the liquid helium vessel. The cryostat can be furnished with a super-conducting solenoid for measuring the sample in an applied magnetic field. It is also possible to mount a pressure cell inside the cryostat for studying the sample properties under pressure.

As will be described below, a miniaturised version of a Mössbauer spectrometer, almost as small as a cigarette box, has been designed and constructed which has successfully been employed in many outdoor applications and quite recently in studying soil and rocks on the surface of Mars (NASA mission 2003/2004).

Correlation of count rate with channel number and relative velocity

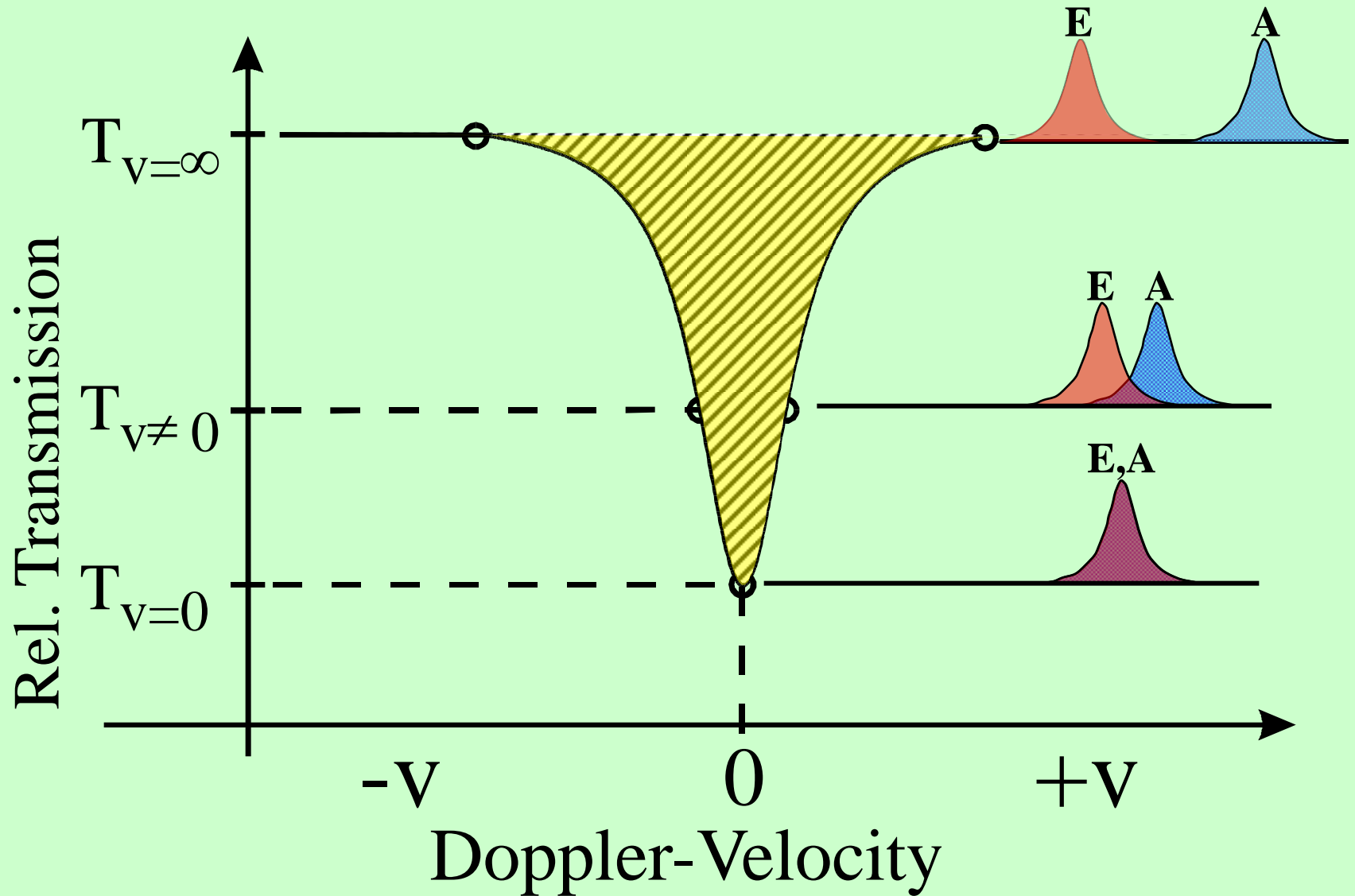




a) Mössbauer spectrum of metallic iron taken with a $^{57}\text{Co}/\text{Rh}$ source. The count rate is plotted as function of the channel number. The solid line drawn through the data points represents the least squares fit of the magnetic hyperfine pattern to the experimental data points

b) Velocity as a function of the channel number

Mössbauer Spectrum



Recoilless resonant absorption is necessary for maximum overlap of the emission line (E) and absorption line (A). Only for identical materials, e.g. ^{57}Co diffused into stainless steel as a source and stainless steel containing ^{57}Fe (to 2.2 % natural abundance) as absorber at the same temperature can total overlap be expected. If, however, the source and the absorber consist of different materials, which is usually the case when studying an iron-containing sample as absorber with a $^{57}\text{Co}/\text{Rh}$ source, the resonance effect may be perturbed due to electric and magnetic **hyperfine interactions** between the nuclei and electric and magnetic fields set up by electrons interacting with the nuclei (see below). Such hyperfine interactions not only shift, but may also split degenerate nuclear levels resulting in several transition lines. The Mössbauer source is always prepared such that it emits a single transition line E and we assume, for the sake of simplicity, that the absorber shows also only one transition line A. But E and A now have slightly modified transition energies E_γ ; the perturbation energies are of the order of 10^{-8} eV (comparable to the natural linewidth), which shifts the transition lines away from each other such that the overlap decreases or disappears entirely. Perfect overlap can be restored again by making use of the **Doppler effect**, i.e. by moving the absorber (generally kept fixed) and the source (generally mounted on a vibrator) relative to each other. In the case of ^{57}Fe spectroscopy, Doppler velocities of up to a few mm s^{-1} are sufficient to make up for the perturbing hyperfine interaction energies and bring emission and absorption lines to perfect overlap, i.e. resonance. The **hyperfine interaction energy ε** (of interest) is correlated with the Doppler velocity v via $\varepsilon = (v/c) E_\gamma$ and can be measured in this way. The plot of the relative transmission of the gamma radiation as a function of the Doppler velocity v is called the **Mössbauer spectrum**.

The schematised Mössbauer spectrum in the above illustration refers to identical source and absorber material; maximum overlap occurs at zero Doppler velocity.

Hyperfine Interactions between Nuclei and Electrons and Mössbauer Parameters

- Electric Monopole Interaction
⇒ Isomer Shift δ
- Electric Quadrupole Interaction
⇒ Quadrupole Splitting ΔE_Q
- Magnetic Dipole Interaction
⇒ Magnetic Splitting ΔE_M

Three kinds of hyperfine interactions may be observed in a Mössbauer spectrum:

Electric monopole interaction between protons of the nucleus and electrons (mainly s-electrons) penetrating the nuclear field. The observable Mössbauer parameter is the “isomer shift δ “. Isomer shift values give information on the oxidation state, spin state, and bonding properties such as covalency and electronegativity.

Electric quadrupole interaction between the nuclear quadrupole moment and an inhomogeneous electric field at the nucleus. The observable Mössbauer parameter is the “quadrupole splitting ΔE_Q “. The information derived from the quadrupole splitting refers to oxidation state, spin state and site symmetry.

Magnetic dipole interaction between the nuclear magnetic dipole moment and a magnetic field at the nucleus. The observable Mössbauer parameter is the “magnetic splitting ΔE_M “. This quantity gives information on the magnetic properties of the material under study.

The following viewgraphs show the conditions, regarding the electronic and the nuclear properties, which lead to the three kinds of hyperfine interactions which may be observed in a Mössbauer spectrum.

Hyperfine Interactions and Mössbauer Parameters

Mössbauer Parameter	Type of Interaction	Information for Chemistry
Isomer Shift δ (mm/sec)	Electric Monopole (Coulombic) interaction between nucleus (protons) and electrons	Oxidation state Electronegativity of ligands Character of bonds Spin state (HS, IS, LS)
Quadruple splitting ΔE_Q (mm/sec)	Electric quadrupole interaction between nuclear quadrupole moment and inhomogeneous electric field	Molecular symmetry Oxidation state Character of bonds Spin state (HS, IS, LS)
Magnetic splitting ΔE_M (mm/sec)	Magnetic dipole interaction between nuclear magnetic dipole moment and magnetic field	Magnetic interactions e.g. ferromagnetism, antiferromagnetism

Conditions for Hyperfine Interactions

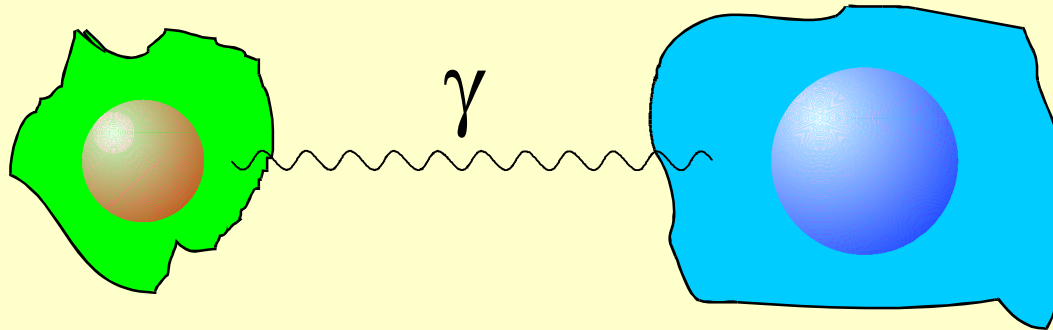
Type of Interaction	Nuclear Condition	Electronic Condition	Consequence
Electric Monopole interaction	$R_e^2 \neq R_g^2$	$ \Psi(0) _A^2 \neq \Psi(0) _S^2$	Different shift of nuclear levels \Rightarrow Isomer shift δ
Electric Quadrupole interaction	Electric quadrupole moment $eQ \neq 0$ ($I > 1/2$)	EFG $\neq 0$	Nuclear states split into $I + 1/2$ substates $ I, \pm m_I\rangle$ (twofold degenerate) \Rightarrow Quadrupole Splitting ΔE_Q
Magnetic dipole interaction	Magn. dipole moment $\mu \neq 0$ ($I > 0$)	$H \neq 0$	Nuclear states $ I\rangle$ split into $2I+1$ substates $ I, m_I\rangle$ with $m_I = +I, +I-1, \dots, -I$ \Rightarrow Magnetic dipole splitting ΔE_M

Electric Monopole Interaction

Isomer Shift δ

Source (S)

Absorber (A)



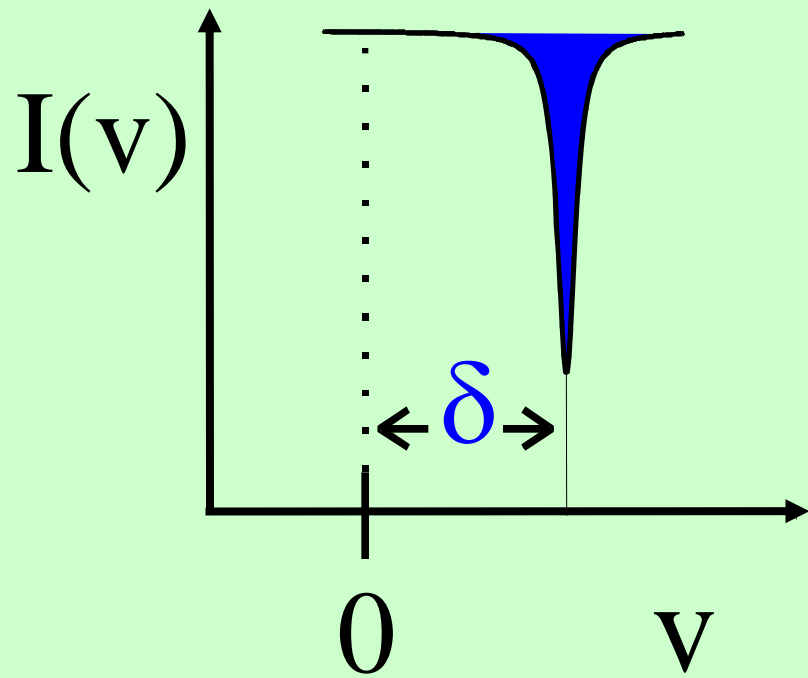
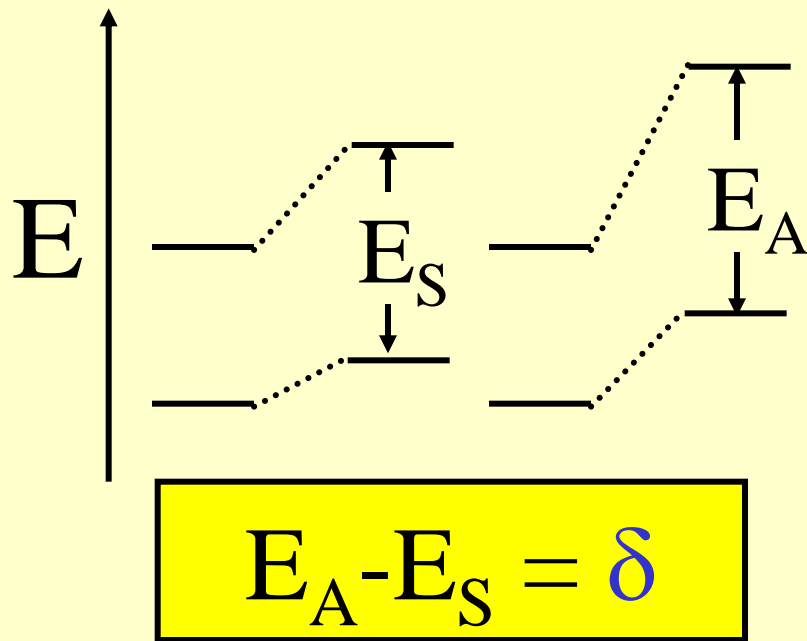
Nuclear radius

$$R_e \neq R_g$$

Electron density

$$\rho_S \neq \rho_A$$

In a typical Mössbauer experiment, the source (S) material (e.g. ^{57}Co embedded in Rh metal) is generally different from the absorber (A) material under study. The nuclear radius in the excited state (red) is different (in the case of ^{57}Fe it is smaller) than that in the ground state (blue): $R_e \neq R_g$. The electronic structure requirement is only fulfilled if the source and absorber materials are different. In this case the electronic densities set up by all s-electrons (1s, 2s, 3s, etc.) of the electronic shells are different at the nuclei of the source and the absorber: $\rho_S \neq \rho_A$. The result is that the **electric monopole interactions** (Coulomb interactions) are different in the source and the absorber and therefore affect the nuclear ground and excited state levels to a different extent. This leads to the measured isomer shift δ as sketched in the next viewgraph.



Oxidation state
Spin state
Bond properties
Covalency
Electronegativity

The fictitious energy levels of the ground and excited states of a bare nucleus (no surrounding electrons) are perturbed and shifted by electric monopole interactions. The shifts in the ground and excited states differ because of the different nuclear radii in the two states, which cause different Coulombic interactions. The energy differences E_S and E_A in the source and absorber also differ because of the different electron densities in the source and absorber material. The individual energy differences E_S and E_A cannot be measured individually, a Mössbauer experiment measures only the difference of the transition energies $\delta = E_A - E_S$, which is the **isomer shift**. This shift appears in the spectrum as the difference between the position of the baricenter of the resonance signal and zero Doppler velocity.

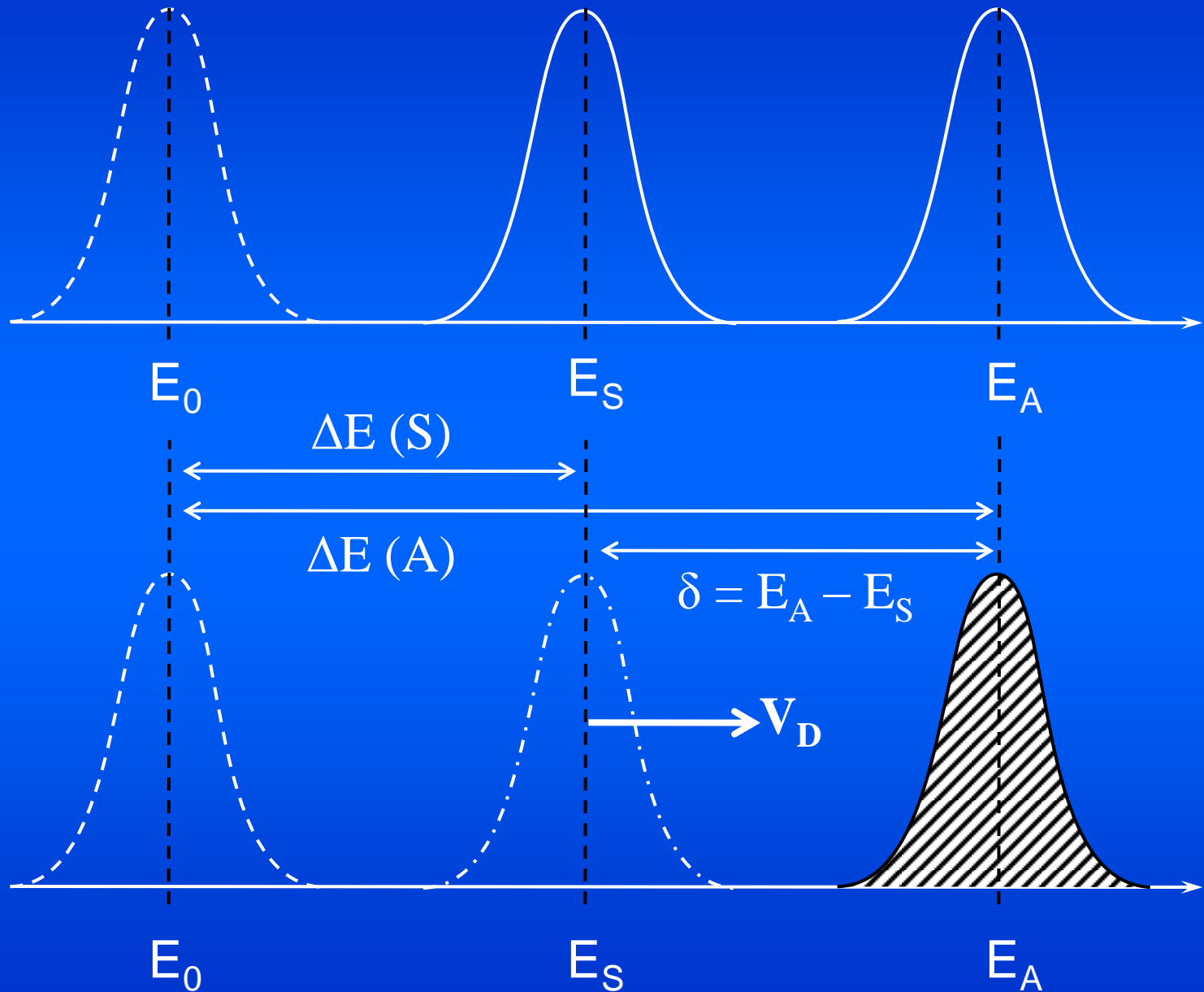
The isomer shift is given by the following expression:

$$\delta = E_A - E_S = \text{const.} (\rho_A - \rho_S)(R_e^2 - R_g^2), \text{ where } \text{const} = (2/3)\pi Ze^2.$$

The isomer shift depends directly on the s-electron densities (as sum of all s-electron shells), but may be influenced indirectly via shielding effects of p-, d- and f-electrons, which are not capable (if neglecting relativistic effects) of penetrating the nuclear field.

The most valuable information derived from isomer shift data refers to the valence state of a Mössbauer-active atom embedded in a solid material. The following viewgraph shows ranges of isomer shift values expected for different oxidation and spin states of iron.

Measuring the Isomer Shift by making use of the Doppler effect



$$\Delta E(S) = E_S - E_0 = C |\Psi(0)|_S^2 (R_e^2 - R_g^2), \quad C = (2/3)\pi Z e^2$$

$$\Delta E(A) = E_A - E_0 = C |\Psi(0)|_A^2 (R_e^2 - R_g^2)$$

$$\delta = \Delta E(A) - \Delta E(S) = E_A - E_S$$

$$\delta = C \{ |\Psi(0)|_A^2 - |\Psi(0)|_S^2 \} (R_e^2 - R_g^2)$$

If the source is unchanged: $|\Psi(0)|_S^2 = \text{const}$

$$\longrightarrow \delta = C' \{ |\Psi(0)|_A^2 \} (R_e^2 - R_g^2)$$

The Doppler velocity v_D , which is necessary to restore resonance between source and absorber in a Mössbauer experiment, is given by

$$v_D = (\delta c/E_\gamma) = (c/E_\gamma) C \{ |\Psi(0)|_A^2 - |\Psi(0)|_S^2 \} (R_e^2 - R_g^2)$$

Influence on $|\Psi(0)|^2$:

a) Direct:

Change of electron population in s -orbitals (mainly valence s -orbitals) changes directly $|\Psi(0)|^2$.

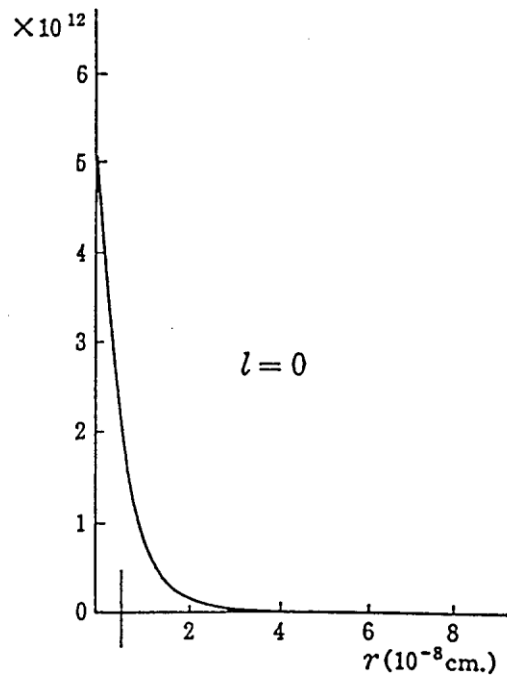
b) Indirect: (shielding by p -, d -, f - electrons)

Increase of electron density in p -, d -, f -orbitals increases shielding effect for s -electrons from the nuclear charge
→ s -electron cloud expands, $|\Psi(0)|^2$ at nucleus decreases.

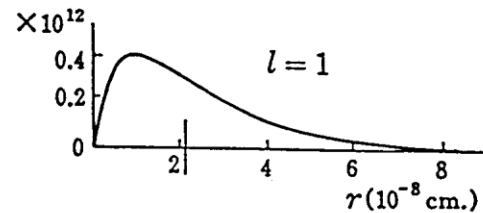
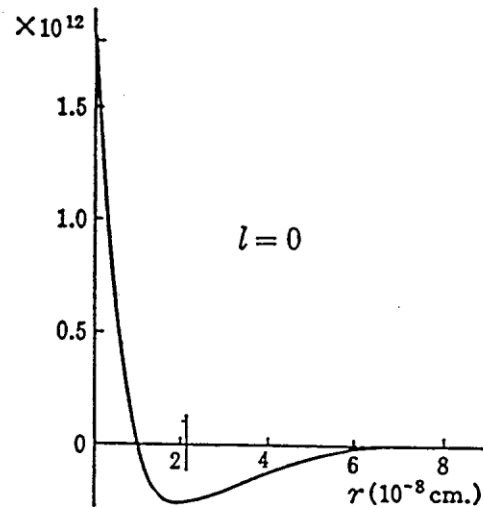
Chemical bonds between metal ion and ligands in co-ordination compounds can be viewed as the result of the balance between **σ -donation** (s -electrons from ligands are donated into s orbitals of the metal) and **d_{π} - p_{π} back donation** (d -electrons move from d -orbitals of the metal to empty π -orbitals of the ligands). Both bonding mechanisms influence the isomer shift in the same direction, but to different extent, depending on the nature of the ligands and thus on the weight of the atomic orbitals of the metal and ligands participating in the molecular orbitals. This is the reason why isomer shift scales for different compounds of the same oxidation state often cover a broad range of values.

Radial Part of Hydrogen Eigenfunctions for $n = 1, 2, 3$

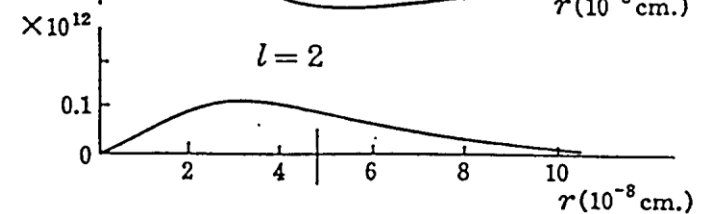
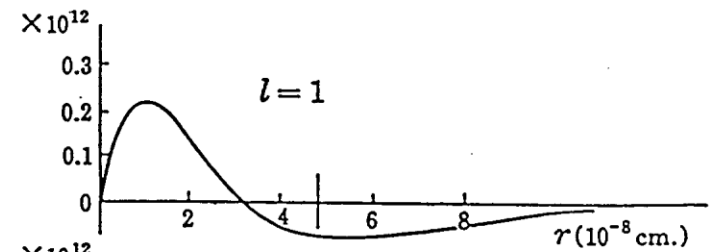
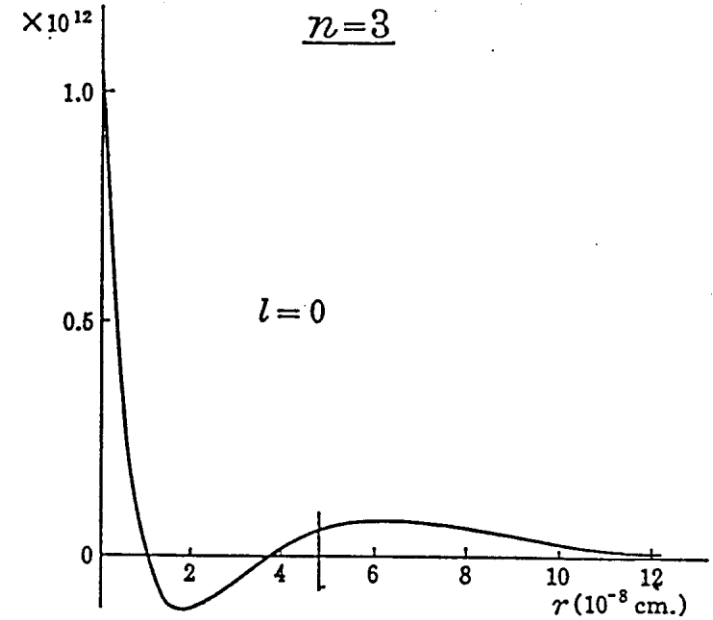
$n=1$



$n=2$



$n=3$



Electron densities at the nucleus ($r = 0$) for different configurations of an Fe atom [1,2]

The following partial electron densities refer to one electron each in 1s, 2s, 3s, 4s-orbitals. The total s-electron density at $r = 0$ is twice the sum of the partial one-electron contributions (since all s-orbitals are doubly occupied).

Electrons per cubic Bohr radius	$3d^8$	$3d^7$ Fe ⁺	$3d^6$ Fe ²⁺	$3d^5$ Fe ³⁺	$3d^6 4s^2$ free atom
$ \psi_{1s}(0) ^2$	5378.005	5377.973	5377.840	5377.625	5377.873
$ \psi_{2s}(0) ^2$	493.953	493.873	493.796	493.793	493.968
$ \psi_{3s}(0) ^2$	67.524	67.764	68.274	69.433	68.028
$ \psi_{4s}(0) ^2$					3.042
$2 \sum_n \psi_{ns}(0) ^2$	11878.9	11879.2	11879.8	11881.7	11885.8

[1] Watson, R. E. (1960) *Phys. Rev.*, **118**, 1036.

[2] Watson, R. E. (1960) *Phys. Rev.*, **119**, 1934.

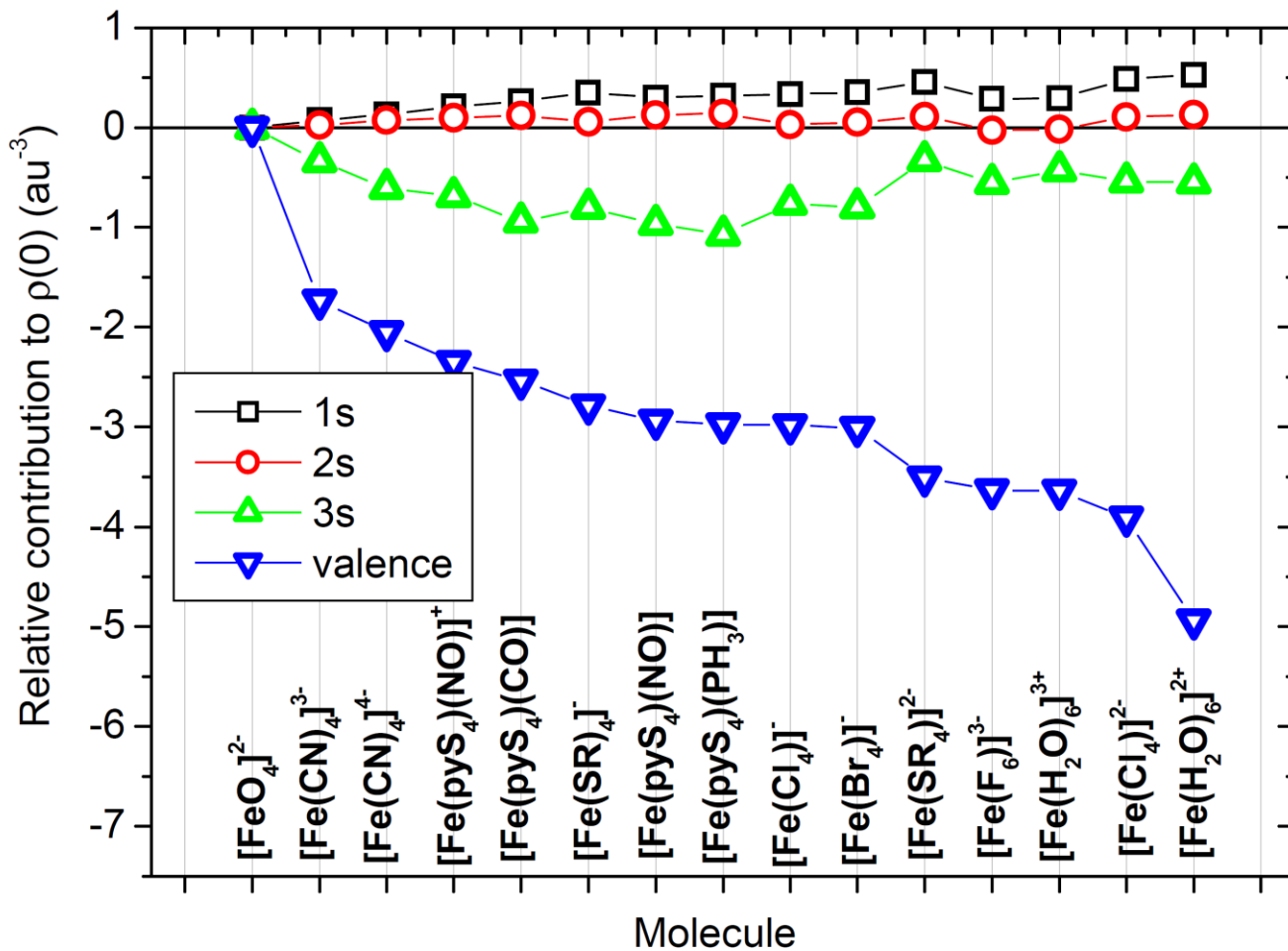
	Fe ⁽⁰⁾			Fe ¹⁺		
	s ² d ⁶	s ¹ d ⁷	s ⁰ d ⁸	s ² d ⁵	s ¹ d ⁶	s ⁰ d ⁷
1s	10689,72	10690,01	10690,18	10689,37	10689,77	10690,02
2s	981,99	982,04	982,19	981,99	981,92	982,00
3s	134,80	132,63	131,46	137,35	134,37	132,53
4s	6,12	2,05	-	9,55	4,09	-

Contributions of ns Orbitals to the total Electron density at the Fe nucleus (in au⁻³) as a function of Oxidation state and Configuration (from Spin-averaged Hartree-Fock calc. and large Uncontracted Gaussian Basis set.

	Fe ²⁺			Fe ³⁺		
	s ² d ⁴	s ¹ d ⁵	s ⁰ d ⁶	s ² d ³	s ¹ d ⁴	s ⁰ d ⁵
1s	10688,86	10689,43	10689,79	10688,24	10688,92	10689,45
2s	982,19	981,86	981,85	982,63	982,06	981,80
3s	141,09	136,82	134,24	145,65	140,65	136,81
4s	12,44	5,51	-	15,68	6,89	-

F. Neese et al.
(2009)

Calculated 1s-, 2s-, 3s- and 4s-electron contributions to the total electron density at the Fe nucleus



Nonrelativistic B₃LYP DFT calculations (F. Neese et al. 2009)

From the table we notice:

- a) On going from one electron configuration to another, differences in $|\Psi(0)|^2$ originate from 1s, 2s, 3s contributions, where the contribution from the 3s shell dominates.
- b) Removal of 3d electrons (oxidation of an iron compound) leads to an increase of $|\Psi(0)|^2$ due to decreased shielding of the 3s electrons from the nuclear charge by 3d electrons.
- c) Adding 4s electrons, e.g. on going from Fe^{2+} ($3d^6$) to metallic iron ($3d^6 4s^2$), increases markedly the electron density at the nucleus.

Isomer Shifts δ of Iron Compounds

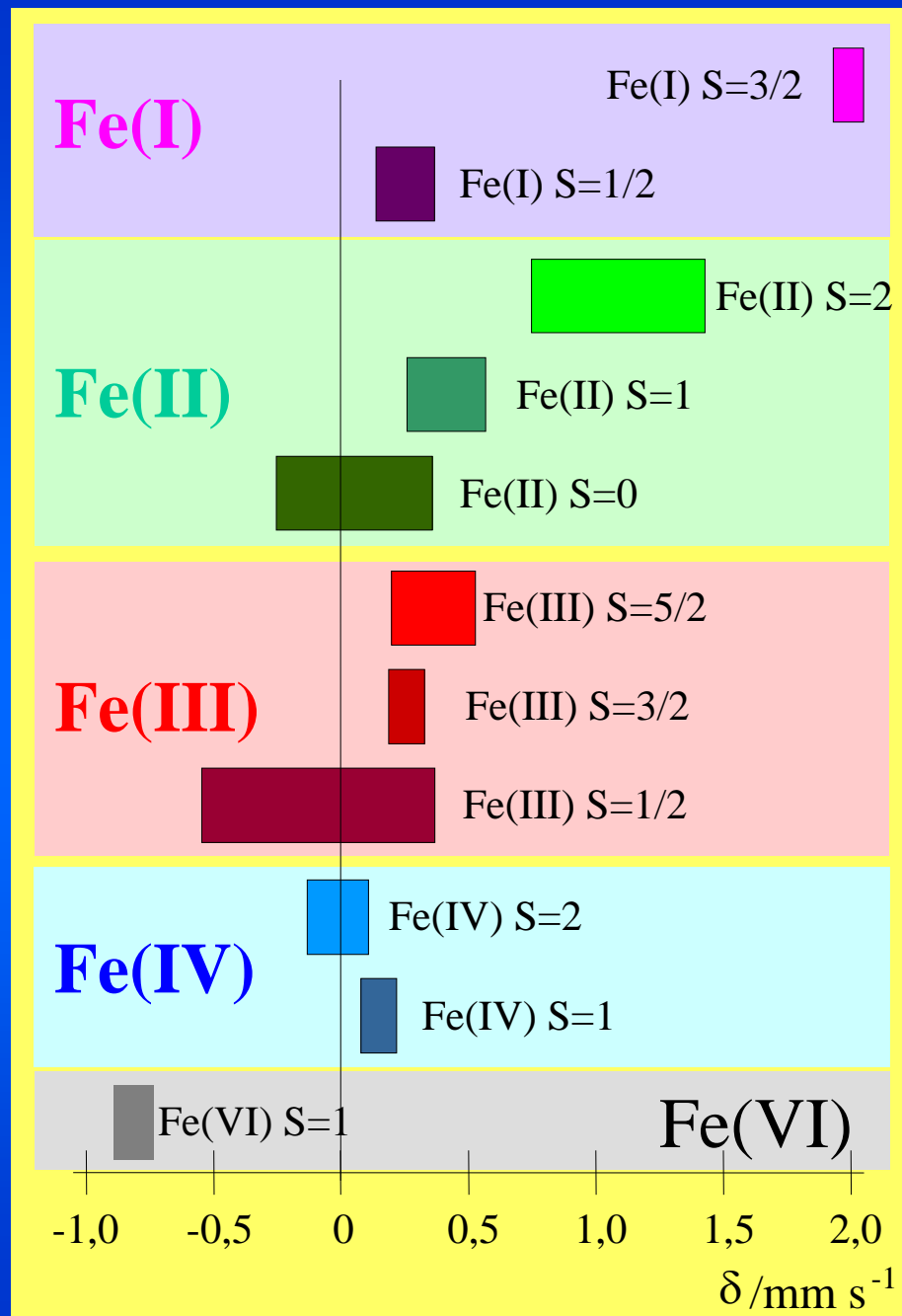
$$\delta = C' \{|\Psi(0)|_A^2\} (R_e^2 - R_g^2)$$

Note:

For ^{57}Fe : $(R_e^2 - R_g^2) < 0$

Increase of $\{|\Psi(0)|_A^2\}$

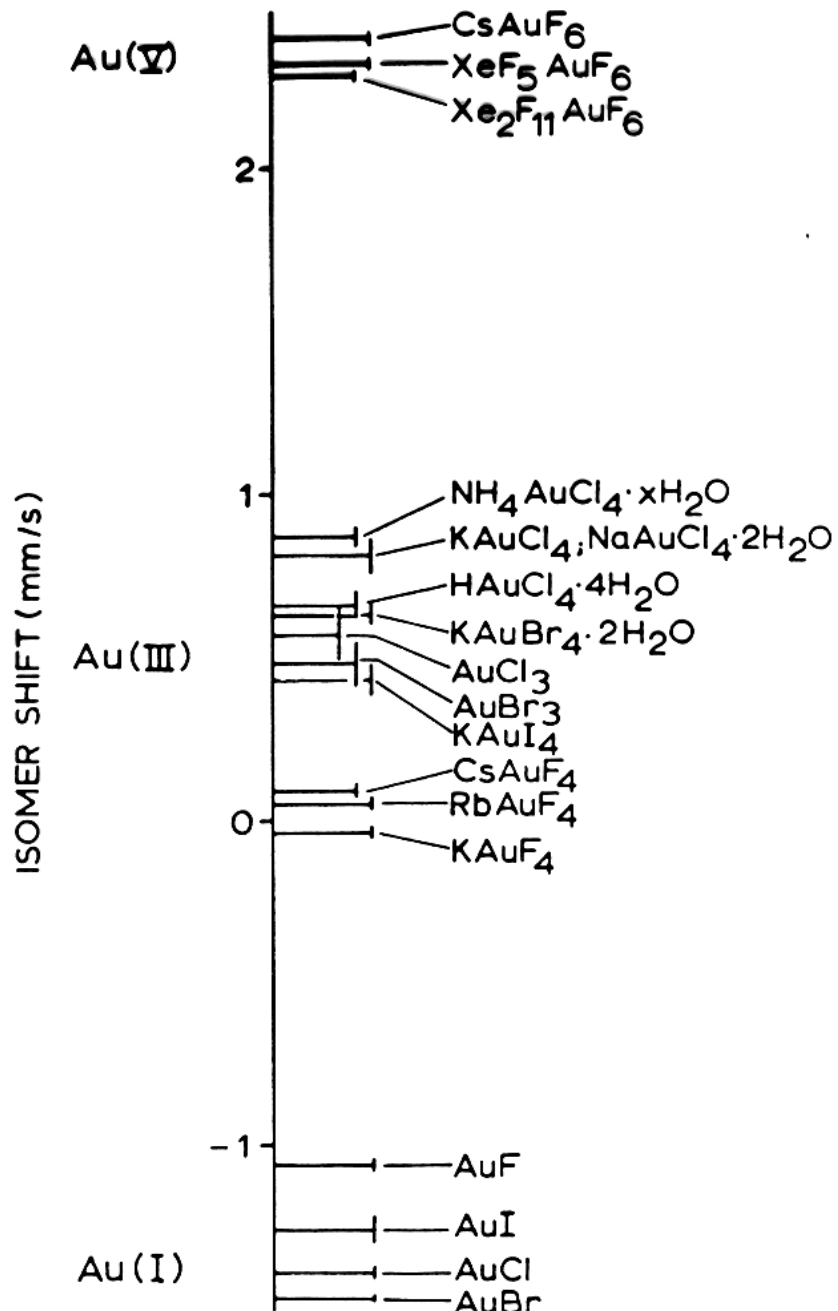
⇒ δ more negative



The table shows ranges of isomer shift values expected for different oxidation and spin states. The most positive isomer shift occurs with iron(I) compounds with spin $S = 3/2$. In this case, the seven d-electrons exert a very strong shielding of the s-electrons towards the nuclear charge, this reduces markedly the s-electron density ρ_A giving a strongly negative quantity ($\rho_A - \rho_S$). As the nuclear factor ($R_e^2 - R_g^2$) is negative for ^{57}Fe , the measured isomer shift becomes strongly positive. At the other end of the isomer shift scale are strongly negative values expected for iron(VI) compounds with spin $S = 1$. The reason is that iron(VI) compounds have only two d-electrons, the shielding effect for s-electrons is very weak in this case and the s-electron density ρ_A at the nucleus becomes relatively high which – multiplied by the negative nuclear factor ($R_e^2 - R_g^2$) – pushes the isomer shift value strongly in a negative direction.

It is seen from the table that some isomer shift regions do not overlap, e.g. iron(II) high spin compounds with $S = 2$ can be easily assigned from a Mössbauer spectrum. In other cases with more or less strong overlapping δ values unambiguous assignment to certain oxidation and spin states may not be possible. In such cases the quadrupole splitting parameter ΔE_Q will be included in the analysis and leads to a conclusive characterisation in most cases.

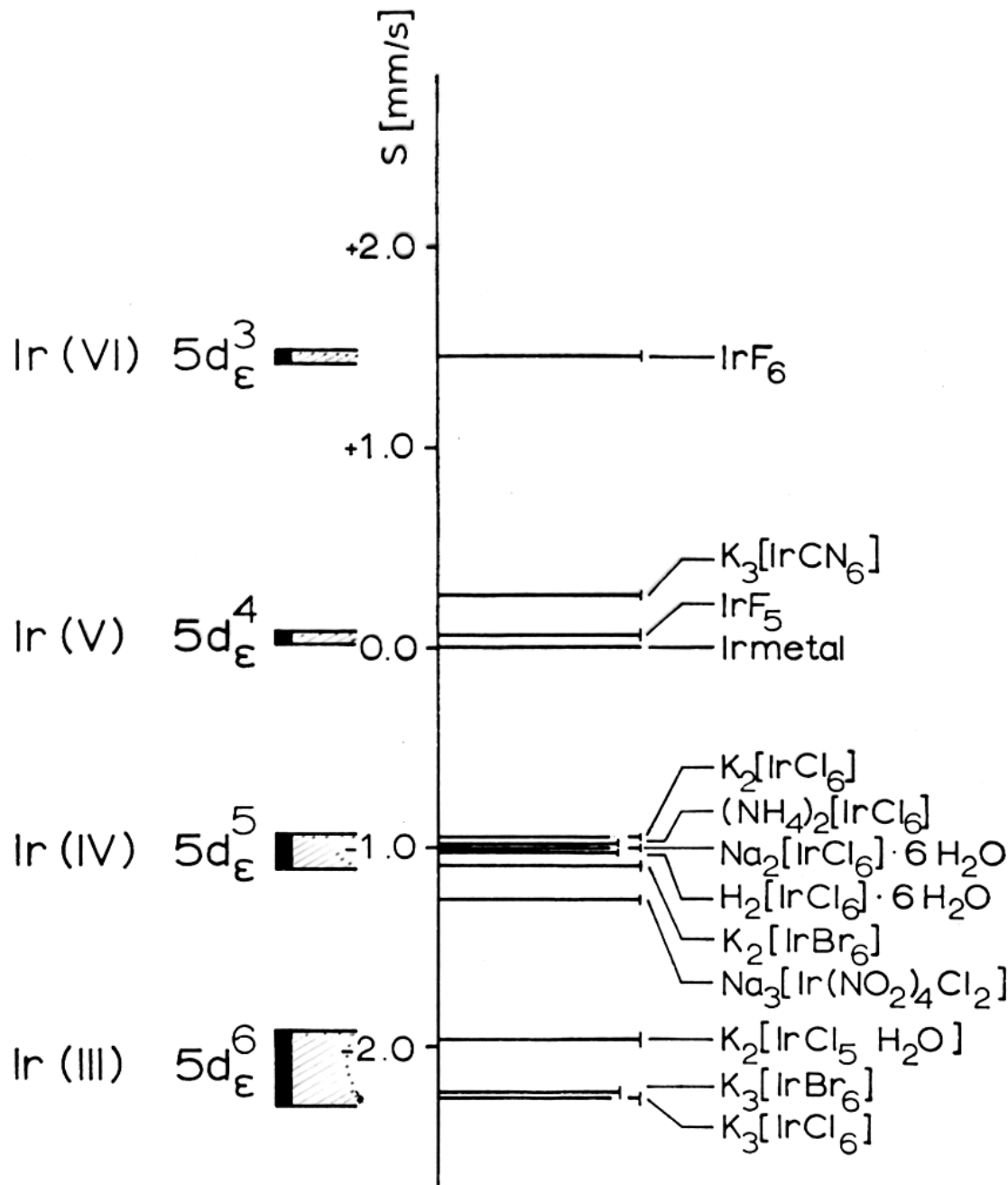
Isomer shifts of Gold Compounds from ^{197}Au Mössbauer Spectroscopy



$$^{197}\text{Au} : (R_e^2 - R_g^2) > 0$$

(F. Wagner et al.)

Isomer shifts of Iridium Compounds from ^{193}Ir Mössbauer Spectroscopy



$$^{193}\text{Ir} : (\mathbf{R}_e^2 - \mathbf{R}_g^2) > 0$$

(F. Wagner et al.)

Second-order Doppler shift:

The isomer shifts δ , i.e. the resonance peak shifts observed in Mössbauer spectra, are composed of two terms:

$$\delta = \delta_C + \delta_{SOD}$$

The first term is the *chemical isomer shift* δ_C , which we have discussed above. δ_C is temperature-independent.

The second term is the *second-order Doppler shift* δ_{SOD} . Since δ_{SOD} is T-dependent, the observed isomer shift δ is also T-dependent.

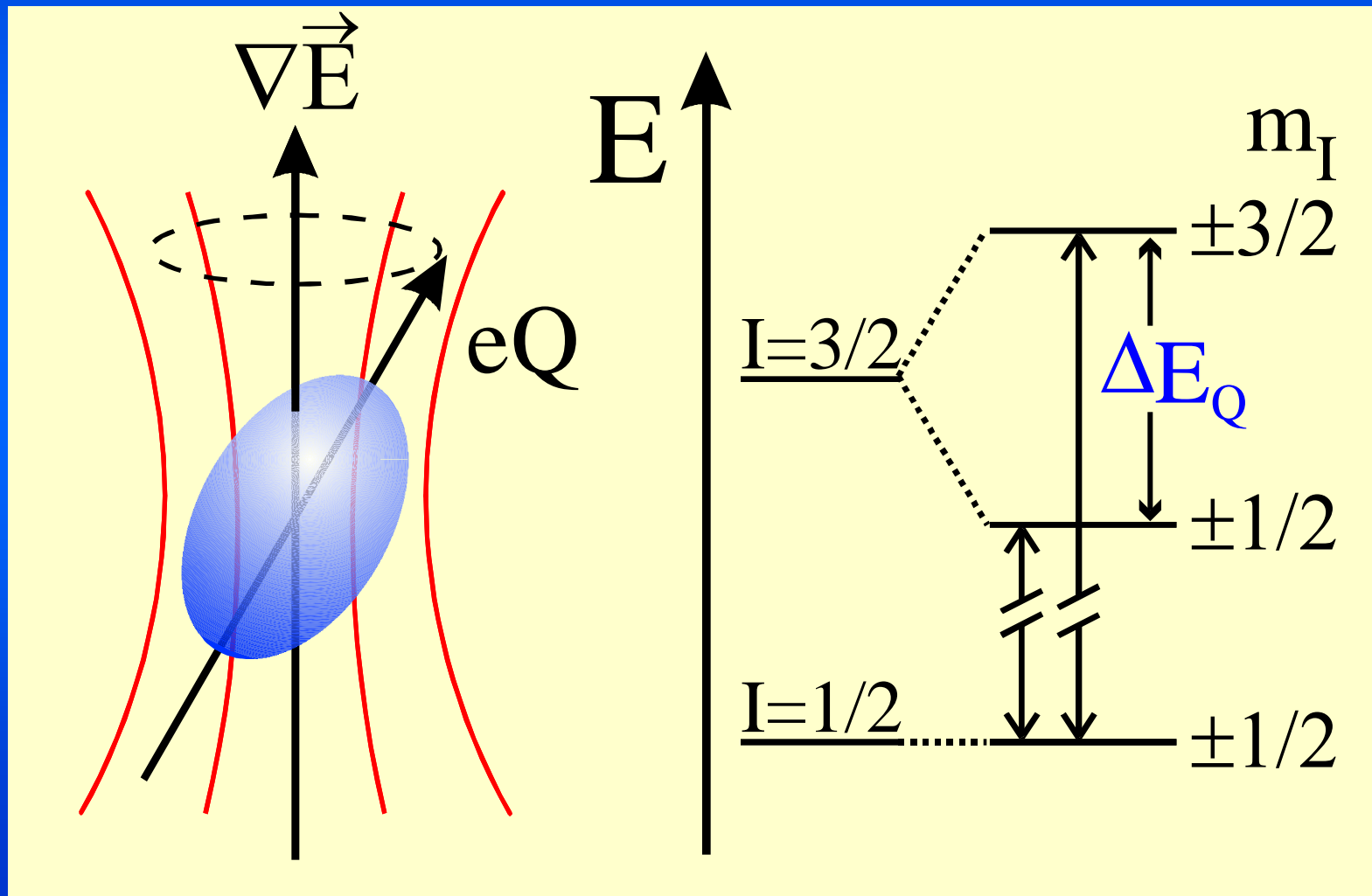
The **second-order Doppler shift** δ_{SOD} is related to the mean-square velocity v of lattice vibrations in the direction of the γ -ray propagation:

$$\delta_{SOD} = \Delta E_{SOD} \frac{c}{E_0} = -\frac{\langle v^2 \rangle}{2c^2} E_0 \frac{c}{E_0} = -\frac{\langle v^2 \rangle}{2c}$$

$\langle v^2 \rangle$ increases with rise in temperature. Accordingly, the Mössbauer resonance signal moves to a more negative velocity with increasing temperature.

Electric Quadrupole Interaction

Quadrupole Splitting ΔE_Q



Electric quadrupole interaction occurs if at least one of the nuclear states involved possesses a quadrupole moment eQ (which is the case for nuclear states with spin $I > 1/2$) and if the electric field at the nucleus is inhomogeneous. In the case of ^{57}Fe the first excited state (14.4 keV state) has a spin $I = 3/2$ and therefore also an electric quadrupole moment.

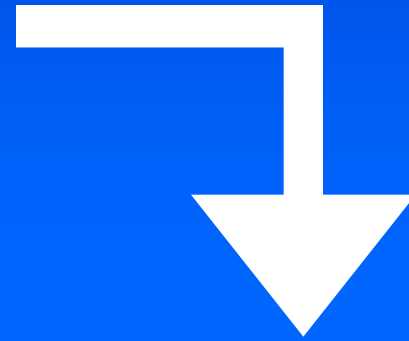
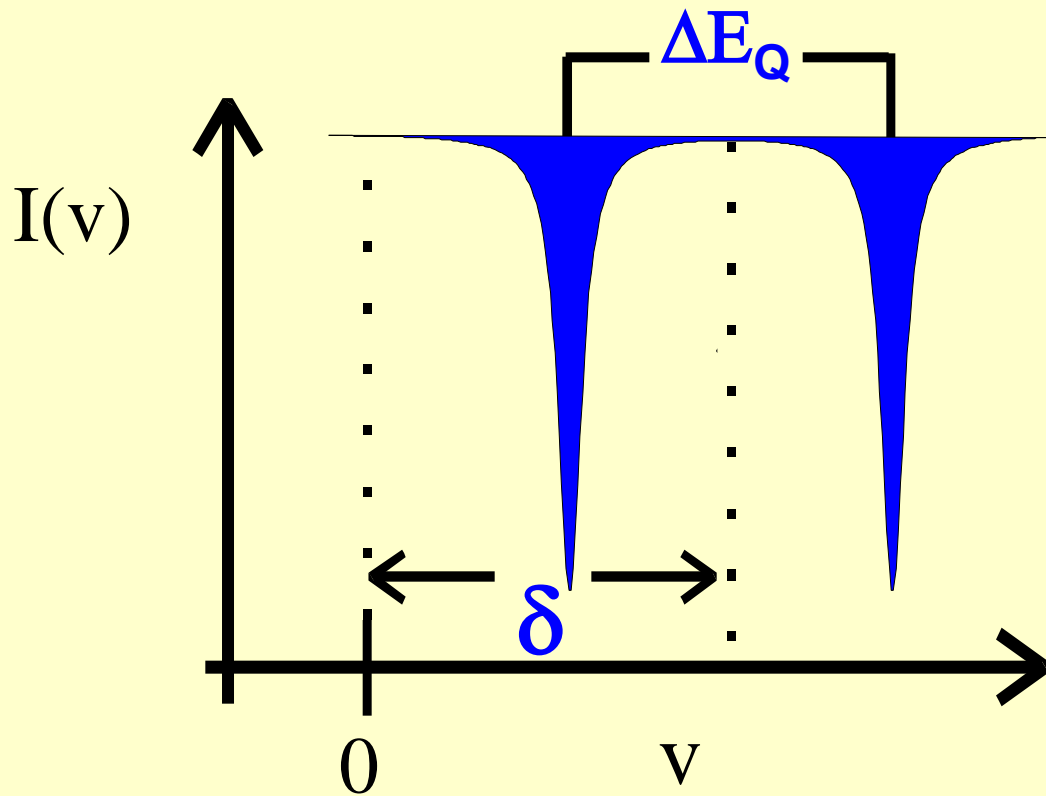
If the electric field gradient (EFG) is non-zero, for instance due to a non-cubic valence electron distribution and/or non-cubic lattice site symmetry, electric quadrupole interaction as visualized by the precession of the quadrupole moment vector about the field gradient axis sets in and splits the degenerate $I = 3/2$ level into two substates with magnetic spin quantum numbers $m_I = \pm 3/2$ and $\pm 1/2$. The energy difference between the two substates ΔE_Q is observed in the spectrum as the separation between the two resonance lines (see next scheme).

These two resonance lines in the spectrum refer to the two transitions between the two substates of the split excited state and the unsplit ground state. The ground state with $I = 1/2$ has no quadrupole moment and remains therefore unsplit, but still twofold degenerate. This degeneracy can be lifted by magnetic dipole interaction (Zeeman effect). The same holds for the two substates of the excited $I = 3/2$ level, which are still twofold degenerate after electric quadrupole interaction. This becomes apparent by looking at the expression for the quadrupolar interaction energies E_Q derived from perturbation theory:

$$E_Q(I, m_I) = (eQV_{zz}/4I(2I-1)[3m_I^2 - I(I+1)]) \text{ (for axial symmetry).}$$

Electric Quadrupole Interaction

Quadrupole Splitting $\Delta E_Q \sim eQ \cdot \nabla E$



Oxidation state
Spin state,
Symmetry

For ^{57}Fe Mössbauer spectroscopy, electric quadrupole interaction in the absence of magnetic dipole interaction leads to a doublet, the separation of the two resonance lines giving the quadrupole interaction energy ΔE_Q which is proportional to the quadrupole moment eQ and the electric field gradient (EFG). The electric field \vec{E} at the nucleus is the negative gradient of the potential, $-\nabla V$, and the electric field gradient EFG is given by the nine components $V_{ij} = (\partial^2 V / \partial i \partial j)$ ($i, j, k = x, y, z$) of the 3×3 second rank EFG tensor. Only five of these components are independent because of the symmetric form of the tensor, i.e. $V_{ij} = V_{ji}$ and because of Laplace's equation which requires that the tensor be traceless: $\sum V_{ii} = 0$ ($i = x, y, z$). In the principal axes system the off-diagonal elements vanish, and for axial symmetry the EFG is then solely given by the tensor component V_{zz} . For non-axial symmetry the asymmetry parameter

$$\eta = (V_{xx} - V_{yy}) / V_{zz} \text{ is required in addition.}$$

In principle, there are two sources which can contribute to the total EFG: charges (or dipoles) on distant ions surrounding the Mössbauer atom in non-cubic symmetry, usually termed *lattice contribution* to the EFG;

anisotropic (non-cubic) electron distribution in the valence shell of the Mössbauer atom, usually called *valence electron contribution* to the EFG.

The electric quadrupole splitting gives information on the oxidation state, the spin state and the local symmetry of the Mössbauer atom.

Note that the isomer shift parameter δ is given by the distance of the baricenter of the quadrupole doublet from zero Doppler velocity.

Electric field gradient (EFG)

A point charge q at a distance $r = (x^2 + y^2 + z^2)^{1/2}$ from the nucleus causes a potential $V(r) = q/r$ at the nucleus. The electric field E at the nucleus is the negative gradient of the potential, $-\nabla V$, and the electric field gradient is given by

$$EFG = \bar{\nabla} \bar{E} = -\bar{\nabla} \bar{\nabla} V = \begin{vmatrix} V_{xx} & V_{xy} & V_{xz} \\ V_{yx} & V_{yy} & V_{yz} \\ V_{zx} & V_{zy} & V_{zz} \end{vmatrix}$$

**3×3 second-rank
EFG tensor**

where

$$V_{ij} = \frac{\partial^2 V}{\partial i \partial j} = q(3ij - r^2 \delta_{ij})r^{-5}, (i, j = x, y, z)$$

Only five V_{ij} components are independent, because:

- symmetric form of the tensor, i.e. $V_{ij} = V_{ji}$,
- Laplace: traceless tensor $\sum_i V_{ii} = 0, \quad i = x, y, z$

Principal axes system:

Choose $|V_{zz}| \geq |V_{xx}| \geq |V_{yy}|$ 

The EFG is given by two independent parameters:

- **Main tensor component V_{zz}**
- **Asymmetry parameter $\eta = (V_{xx} - V_{yy})/V_{zz}$**

Range of η : $0 \leq \eta \leq 1$

For axial systems (tetragonal, trigonal):

$$V_{xx} = V_{yy} \rightarrow \eta = 0$$

Two kinds of contributions to the EFG:

$$(\mathbf{EFG})^{\text{total}} = (\mathbf{EFG})^{\text{val}} + (\mathbf{EFG})^{\text{lat}}$$

or in the principal axes system and $\eta = 0$:

$$(V_{zz})^{\text{total}} = (V_{zz})^{\text{val}} + (V_{zz})^{\text{lat}}$$

The **lattice contribution** $(V_{zz})^{\text{lat}}$ arises from non-cubic arrangement of the next nearest neighbours

$$(V_{zz})^{\text{lat}} = \sum_{i=1}^n q_i r_i^{-3} (3 \cos^2 \vartheta_i - 1)$$

q_i : charge on ligand i

r_i : distance of ligand i from Mössbauer central atom

The **valence contribution** $(V_{zz})^{val}$ arises from anisotropic (noncubic) electron population in the molecular orbitals (or atomic orbitals in simple ligand field theory):

$$(V_{zz})^{val} = -e \sum_i \langle \psi_i | (3 \cos^2 \vartheta_i - 1) r^{-3} | \psi_i \rangle$$

$$\langle r_i^{-3} \rangle = \int R(r) r^{-3} R(r) r^2 dr$$

= expectation value of $1/r^3$, can be factorized out:

$$(V_{zz})^{val} = -e \sum_i \langle \psi_i | (3 \cos^2 \vartheta_i - 1) | \psi_i \rangle \langle r_i^{-3} \rangle$$

For evaluation of η^{val} in the case of non-axial symmetry one must work out:

$$(V_{xx})^{val} = -e \sum_i \langle \psi_i | (3 \sin^2 \vartheta \cos^2 \varphi - 1) | \psi_i \rangle \langle r_i^{-3} \rangle$$

$$(V_{yy})^{val} = -e \sum_i \langle \psi_i | (3 \sin^2 \vartheta \sin^2 \varphi - 1) | \psi_i \rangle \langle r_i^{-3} \rangle$$

Sternheimer Shielding Factors:

The total EFG is described by

$$(V_{zz})^{\text{total}} = (1-\gamma_{\infty})(V_{zz})^{\text{lat}} + (1-R)(V_{zz})^{\text{val}} \quad (\text{for axial systems})$$

$(1-\gamma_{\infty})$: **Sternheimer antishielding factor** (~ 10 for ^{57}Fe),
compensates for distortion of electron shell due to non-cubic
charge distribution in the near crystal lattice.

$(1-R)$: **Sternheimer antishielding factor** ($\sim 0.25-0.35$ for ^{57}Fe),
compensates distortion of inner electron shell by anisotropic
valence electron distribution.

Diagonal (EFG)^{val} tensor elements for p- and d-electrons (per electron)

Orbital	$\frac{(V_{xx})_{val}}{e\langle r^{-3} \rangle}$	$\frac{(V_{yy})_{val}}{e\langle r^{-3} \rangle}$	$\frac{(V_{zz})_{val}}{e\langle r^{-3} \rangle}$
p-Electrons			
p _x	-4/5	+2/5	+2/5
p _y	+2/5	-4/5	+2/5
p _z	+2/5	+2/5	-4/5
d-Electrons			
d _{xy}	-2/7	-2/7	+4/7
d _{xz}	-2/7	+4/7	-2/7
d _{yz}	+4/7	-2/7	-2/7
d _{x²-y²}	-2/7	-2/7	+4/7
d _{z²}	+2/7	+2/7	-4/7

Quadrupole Splitting

In the principal axes system with \vec{z} as axis of quantization:

Hamiltonian:

$$\hat{H}_Q = \hat{\vec{Q}} \cdot \hat{\nabla} \hat{E} = \frac{eQ}{4I(2I-1)} \left(V_{zz} \hat{I}_z^2 + V_{xx} \hat{I}_x^2 + V_{yy} \hat{I}_y^2 \right)$$

eQ: electric quadrupole moment, (3×3) second rank tensor operator with elements

$$Q_{ij} = \int \rho_n(r) (x_i x_j - \delta_{ij} r^2) d\tau$$

ρ_n : nuclear charge

x_i, x_j : cartesian coordinates

In the principal axes system (off-diagonal elements are zero) and with quantisation axis \vec{z} and the transformation $z = r \cdot \cos \vartheta$

$$Q = \frac{1}{e} \int \rho_n(r) (3z^2 - r^2) d\tau = \frac{1}{e} \int \rho_n(r) (3r^2 \cos^2 \vartheta - r^2) d\tau$$

\hat{I} : nuclear spin operator

$\hat{I}_x, \hat{I}_y, \hat{I}_z$: operators of the nuclear spin projections onto the principal axes

With $\hat{I}_{\pm} = \hat{I}_x \pm i\hat{I}_y$ shift operators we obtain

$$\hat{H}_Q = \frac{eQV_{zz}}{4I(2I-1)} \left[3\hat{I}_z^2 - \hat{I}^2 + \frac{\eta}{2}(\hat{I}_+^2 + \hat{I}_-^2) \right]$$

First order perturbation theory for degenerate systems yields the matrix

$$\left\| \langle I, m_I | \hat{H}_Q | I, m'_I \rangle \right\| = 0$$

and the eigenvalues

$$E_Q(I, m_I) = \frac{eQV_{zz}}{4I(2I-1)} \left[3m_I^2 - I(I+1) \right] \left(1 + \frac{\eta^2}{3} \right)^{\frac{1}{2}}$$

with $m_I = +I, +I-1, \dots, -I$

For ^{57}Fe with $I_e = 3/2$, $I_g = 1/2$:

$$E_Q(3/2, \pm 3/2) = 3eQV_{zz}/12 \quad \text{for } I = 3/2, m_I = \pm 3/2$$

$$E_Q(3/2, \pm 1/2) = -3eQV_{zz}/12 \quad \text{for } I = 3/2, m_I = \pm 1/2$$

and for the **quadrupole splitting energy**

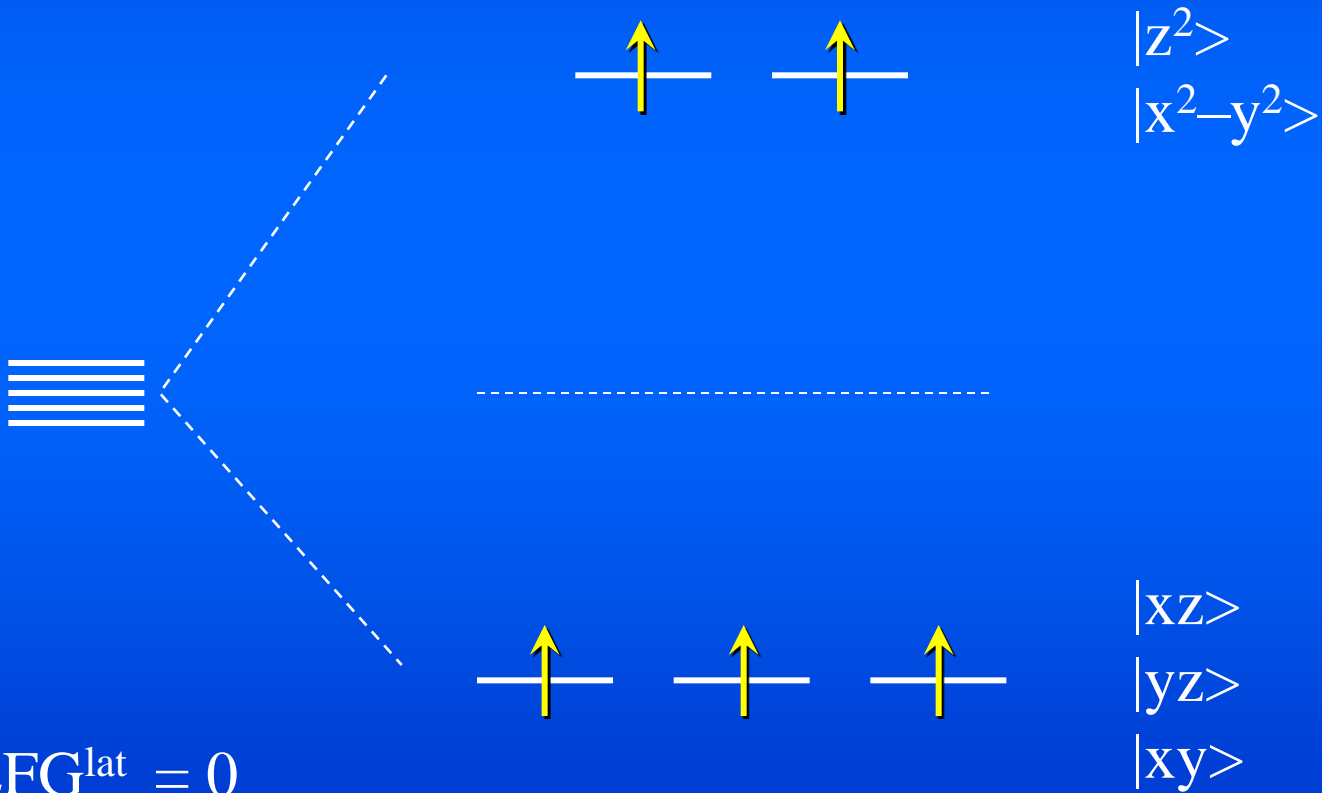
$$\Delta E_Q = E_Q(3/2, \pm 3/2) - E_Q(3/2, \pm 1/2) = eQV_{zz}/2$$

(in axially symmetric systems, $\eta = 0$)

Example: $[\text{Fe}(\text{H}_2\text{O})_6]^{3+}, {}^6\text{A}_1$

Free Ion

$[\text{ML}_6] (\text{O}_h)$

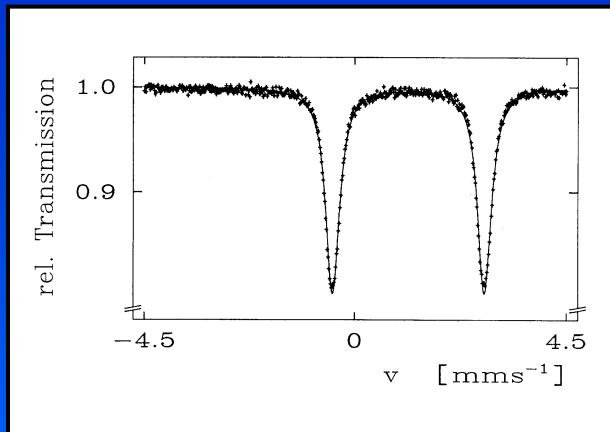


$$\text{EFG}^{\text{lat}} = 0$$

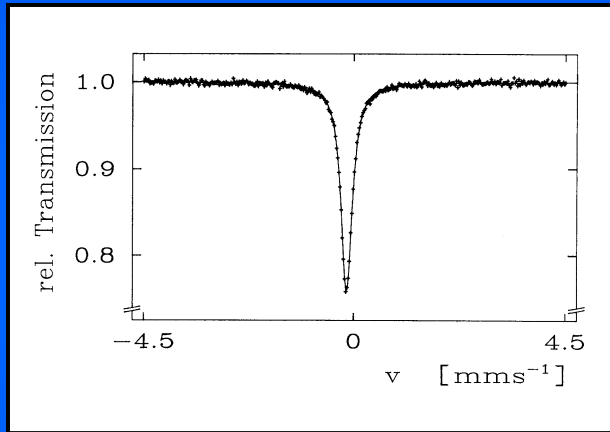
$$\text{EFG}^{\text{val}} = 0$$

Diagonal (EFG)^{val} tensor elements for p- and d-electrons (per electron)

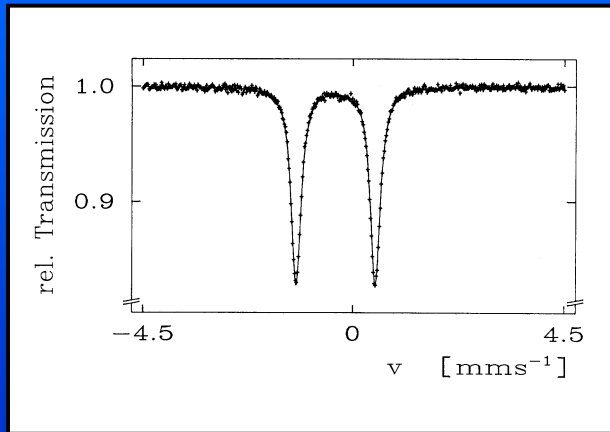
Orbital	$\frac{(V_{xx})_{\text{val}}}{e\langle r^{-3} \rangle}$	$\frac{(V_{yy})_{\text{val}}}{e\langle r^{-3} \rangle}$	$\frac{(V_{zz})_{\text{val}}}{e\langle r^{-3} \rangle}$
p-Electrons			
p _x	-4/5	+2/5	+2/5
p _y	+2/5	-4/5	+2/5
p _z	+2/5	+2/5	-4/5
d-Electrons			
d _{xy}	-2/7	-2/7	+4/7
d _{xz}	-2/7	+4/7	-2/7
d _{yz}	+4/7	-2/7	-2/7
d _{x²-y²}	-2/7	-2/7	+4/7
d _{z²}	+2/7	+2/7	-4/7



$\text{FeSO}_4 \cdot 7\text{H}_2\text{O}$
 $[\text{Fe}(\text{H}_2\text{O})_6]^{2+}$
 Fe(II)-HS, $S=2$



$\text{K}_4[\text{Fe}(\text{CN})_6]$
 Fe(II)-LS, $S=0$
 cubic



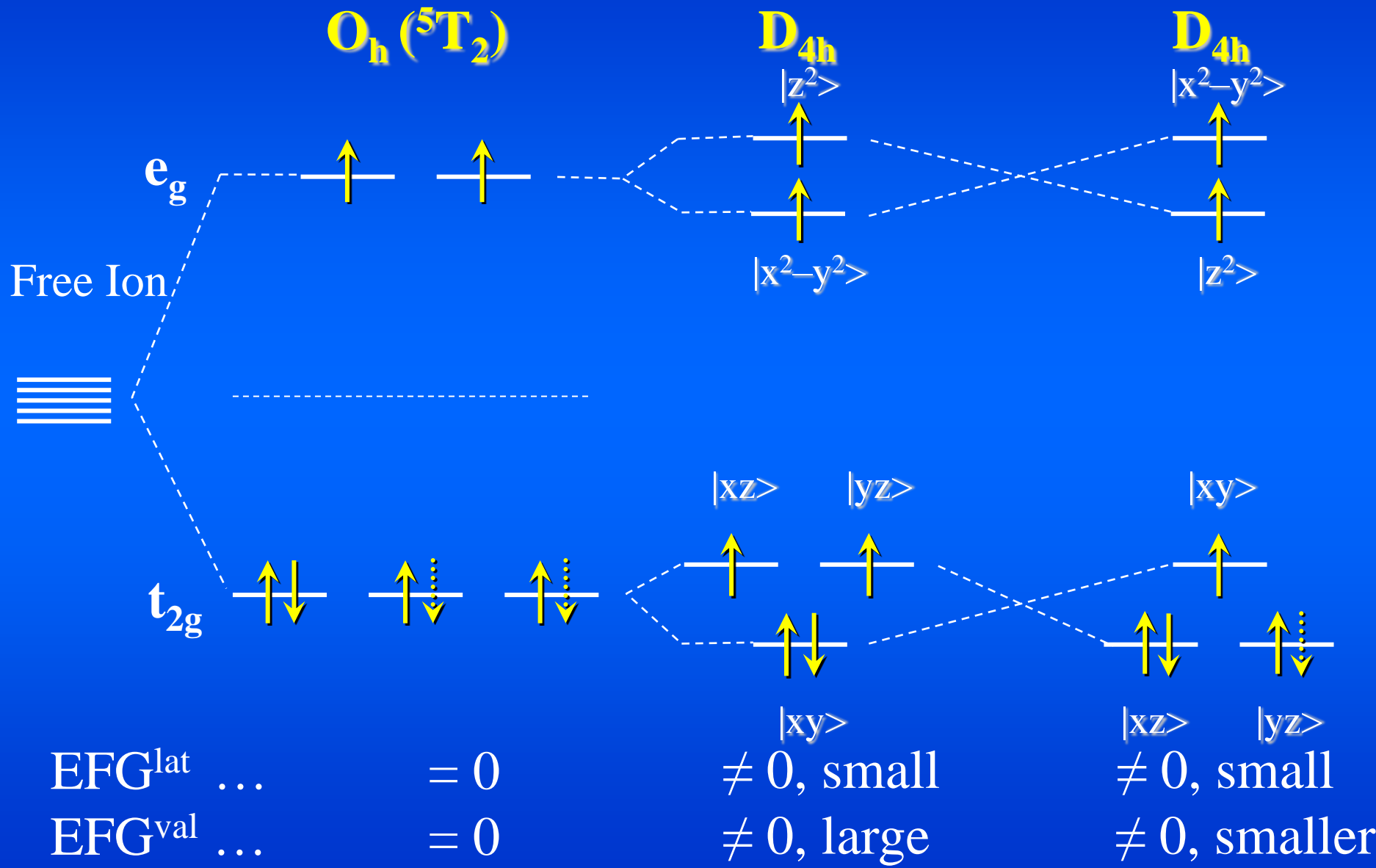
$\text{Na}_2[\text{Fe}(\text{CN})_5\text{NO}]$
 Fe(II)-LS, $S=0$
 tetragonal



Jahn-Teller-Distortion

compressed

elongated

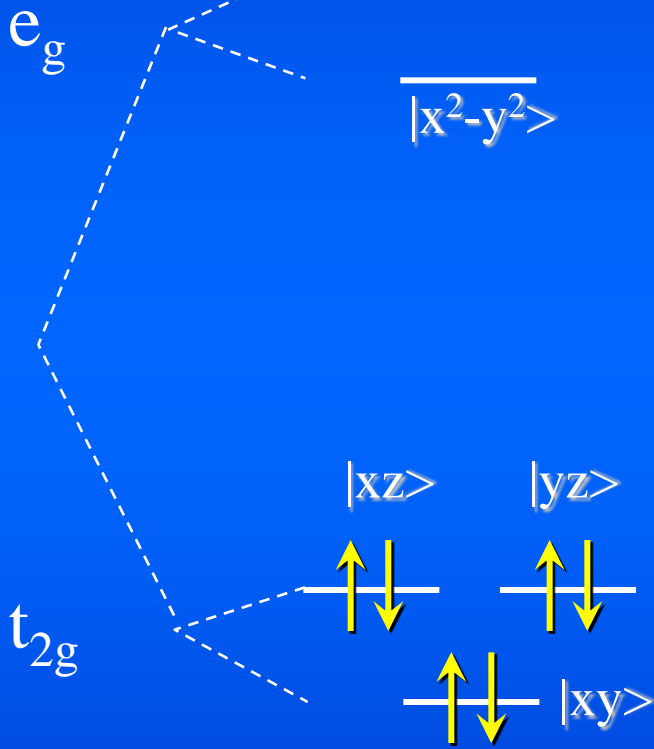
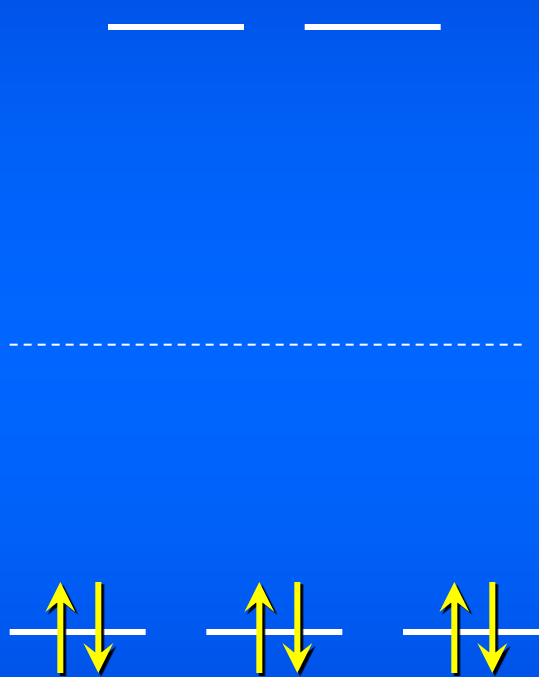




$$O_h$$

$$C_{4v}$$

Free Ion



$$\text{EFG}^{\text{lat}} = 0$$

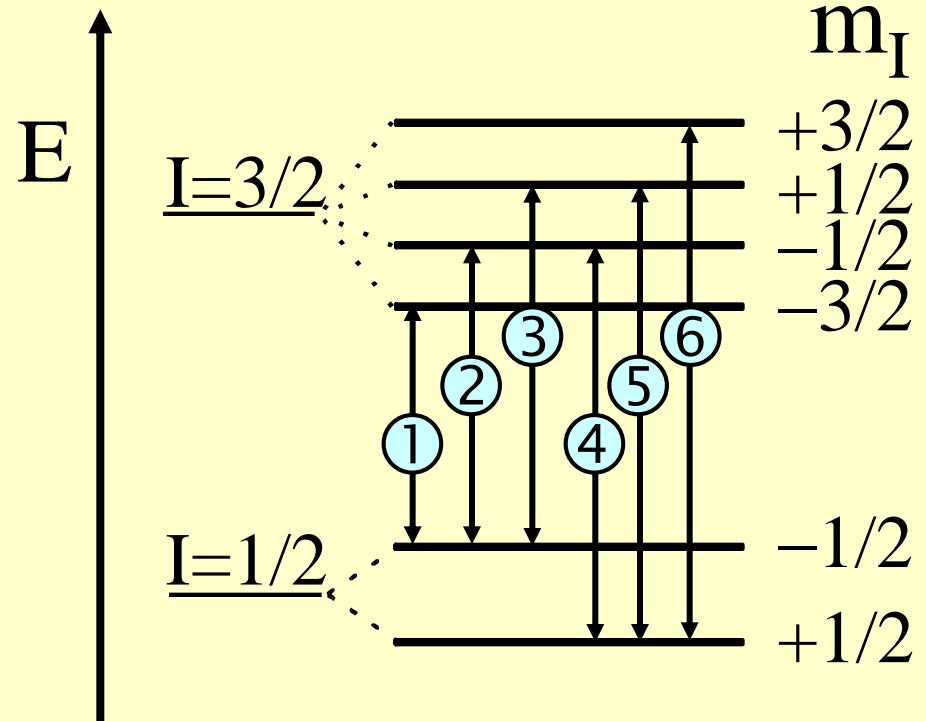
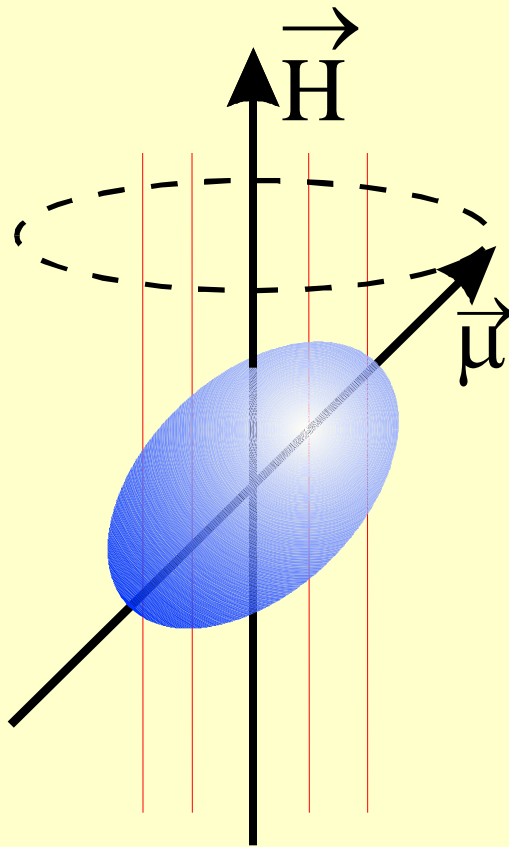
$$\dots \neq 0$$

$$\text{EFG}^{\text{val}} = 0$$

$$\dots = 0$$

Magnetic Dipole Interaction

Magnetic Splitting ΔE_M



$$\Delta I = \pm 1, \Delta m_I = 0, \pm 1$$

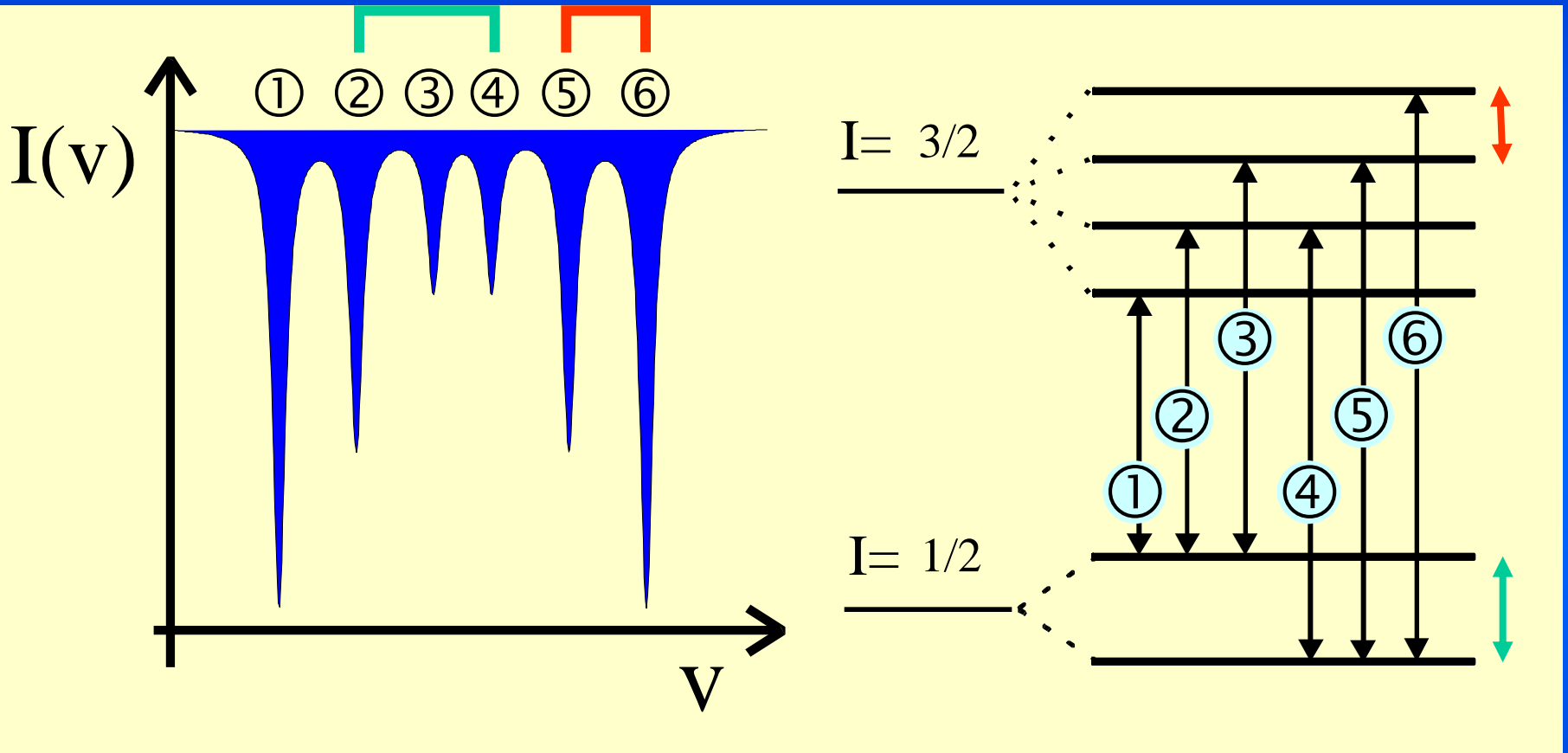
The requirements for magnetic dipole interaction to be observed are that (i) the nuclear states involved possess a magnetic dipole moment and (ii) a magnetic field is present at the nucleus. A nuclear state with spin $I > 1/2$ possesses a magnetic dipole moment μ . This is the case for both the ground state with $I = 1/2$ and the first excited state with $I = 3/2$ of ^{57}Fe . Magnetic dipole interaction (visualized as the precession of the magnetic dipole moment vector about the axis of the magnetic field) leads to splitting of the states $|I, m_I\rangle$ into $2I+1$ substates characterized by the magnetic spin quantum numbers m_I . Thus the excited state with $I = 3/2$ is split into four, and the ground state with $I = 1/2$ into two substates. These substates are no longer degenerate. The energies of the sublevels are given from first-order perturbation theory by

$$E_M(m_I) = -\mu H m_I / I = -g_N \beta_N H m_I,$$

where g_N is the nuclear Landé factor and β_N the nuclear Bohr magneton.

Note that the sign of the magnetic spin quantum numbers m_I of the sublevels have a different sequence in the excited state and the ground state, this being due to the different signs of the magnetic moments of the two states. The allowed gamma transitions between the sublevels of the excited state and those of the ground state are given by the selection rules for magnetic dipole transitions: $\Delta I = \pm 1$, $\Delta m_I = 0, \pm 1$. The six allowed transitions are shown in the picture.

$$E_M(m_I) = -\mu H m_I / I$$



**Ferro-, Antiferro-,
Ferri -magnetism**

The separation between the lines 2 and 4 (also between 3 and 5) refers to the magnetic dipole splitting of the ground state. The separation between lines 5 and 6 (also between 1 and 2, 2 and 3, 4 and 5) refers to the magnetic dipole splitting of the excited $I = 3/2$ state. The magnetic hyperfine splitting enables one to determine the effective magnetic field (size and direction) acting at the nucleus. Such a field can be externally applied. But many substances can also create a magnetic field of their own through various mechanisms, e.g.

the **Fermi contact field** H_C arises from a net spin-up or spin-down s-electron density at the nucleus as a consequence of spin polarization of inner filled s-shells by spin-polarized partially filled outer shells;

a contribution H_L may arise from the **orbital motion** of valence electrons with the orbital momentum quantum number L ;

a contribution H_D , called **spin-dipolar field**, may arise from the total electron spin of the atom under consideration.

All contributions may be present and add to the total effective magnetic field $H_{\text{eff}} = H_C + H_L + H_D$. By applying an external magnetic field of known size and direction one can determine the size and the direction of the intrinsic effective magnetic field H_{eff} of the material under investigation.

Magnetic dipole interaction and electric quadrupole interaction may be present in a material simultaneously (together with the electric monopole interaction which is always present). The perturbations are treated depending on their relative strengths. In the case of relatively weak quadrupole interaction the nuclear sublevels $|I, m_I\rangle$ arising from magnetic dipole splitting are additionally shifted by the quadrupole interaction energies $E_Q(I, m_I)$; as a result, the sublevels of the excited $I = 3/2$ state are no longer equally spaced. The shifts by E_Q are upwards or downwards depending on the direction of the EFG. This enables one to determine the sign of the quadrupole splitting parameter ΔE_Q .

Internal magnetic field

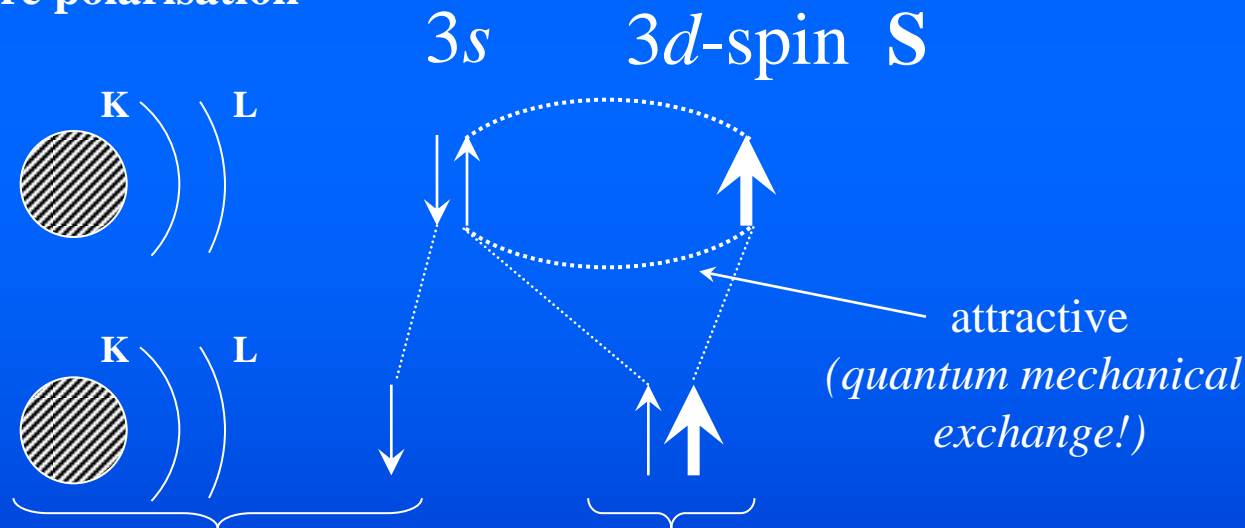
A magnetic field $H_{\text{int}}(r = 0)$ at the nucleus can originate in various ways:

$$\mathbf{H}_{\text{int}} = \mathbf{H}_{\text{C}} + \mathbf{H}_{\text{D}} + \mathbf{H}_{\text{L}} + \mathbf{H}_{\text{ext}}$$

= total internal magnetic field

- Fermi Contact Interaction $\rightarrow \mathbf{H}_{\text{C}}$:

Electron spin S of valence shell (e.g. $S = 5/2$ of Fe^{3+}) polarizes the s-electron density at the nucleus: **core polarisation**



$3s\downarrow$ cause higher net spin density

$$|\Psi(0)\downarrow|^2 > |\Psi(0)\uparrow|^2 \implies \text{magnetic field } H_{\text{C}} \neq 0$$

$$H_C = -\frac{16\pi}{3} \mu_B \left\langle \sum (\rho_S(\uparrow) - \rho_S(\downarrow)) \right\rangle$$

The direct coupling between the nucleus and H_C is called “**Fermi contact interaction**”

- Spin dipolar interaction $\rightarrow H_D$

The magnetic moment of the electron spin \vec{S} gives rise to dipolar interaction with the nucleus. \vec{S} causes a field at $r = 0$ of

$$H_D = -2\mu_B \left\langle 3\vec{r}(\vec{S} \cdot \vec{r})r^{-5} - \vec{S}r^{-3} \right\rangle$$

or

$$H_D = -2\mu_B \langle S \rangle \langle r^{-3} \rangle \langle 3 \cos^2 \vartheta - 1 \rangle$$

for axial symmetry

(ϑ is the angle between the spin vector \vec{S} and the principal axis \vec{Z})

- Orbital dipolar interaction $\rightarrow \mathbf{H}_L$

Electrons with orbital moment $L \neq 0$ give rise to an orbital magnetic moment accompanied by a magnetic field

$$\mathbf{H}_L = -2\mu_B \langle r^{-3} \rangle \langle \mathbf{L} \rangle$$

$\langle \mathbf{L} \rangle$: expectation value of orbital angular momentum.

Pure magnetic dipole interaction

Magnetic dipole interaction (Zeeman effect) is described by the Hamiltonian

$$\hat{H}_M = -\hat{\boldsymbol{\mu}} \cdot \hat{\mathbf{H}} = -g_N \beta_N \hat{\mathbf{I}} \cdot \vec{H}$$

g_N : nuclear Landé-factor

$\beta_N = e\hbar/2Mc$ nuclear Bohr magneton

If $\vec{H} \parallel \vec{z}$:

$$\hat{H}_M = -g_N \beta_N H \hat{I}_z$$

First order perturbation theory yields the matrix (elements) equations:

$$\left\| \left\langle I, m'_I \left| \hat{H}_M \right| I, m_I \right\rangle - E_M \delta_{m'_I m_I} \right\| = 0 \quad \text{with eigenvalues} \quad \mathbf{E}_M(\mathbf{I}, \mathbf{m}_I) = -g_N \beta_N H m_I$$

Combined Magnetic Dipole and Electric Quadrupole Interaction:

Often both perturbations – magnetic dipole and electric quadrupole interactions – are present.

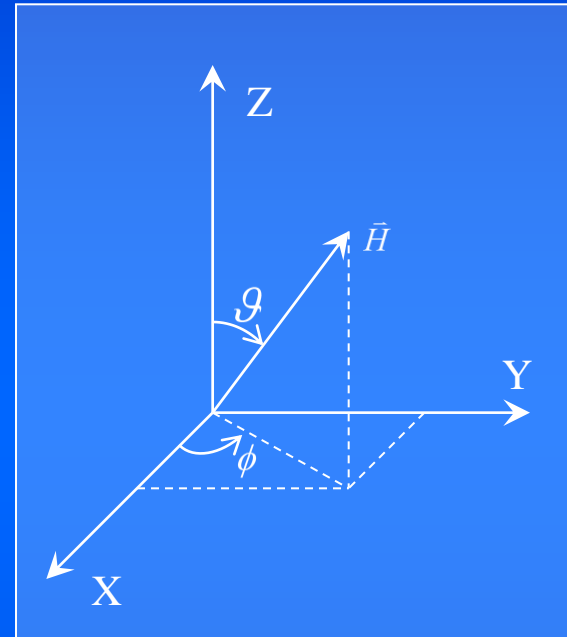
The Hamiltonian then writes:

$$\hat{H} = \hat{H}_M + \hat{H}_Q$$

$$\hat{H}_Q = A \left[3\hat{I}_z^2 - \hat{I}^2 + \eta(\hat{I}_x^2 - \hat{I}_y^2) \right]$$

with $A = eQV_{zz} / 4I(2I - 1)$

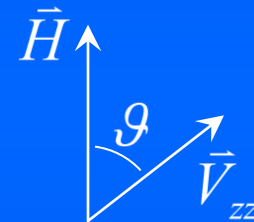
$$\hat{H}_M = -g\beta_N H \left(\hat{I}_z \cos \vartheta + \hat{I}_x \sin \vartheta \cos \phi + \hat{I}_y \sin \vartheta \sin \phi \right)$$



The electric quadrupole interaction is usually much weaker than the magnetic dipole interaction, i.e. it can be treated as a perturbation of the magnetic dipole splitting:

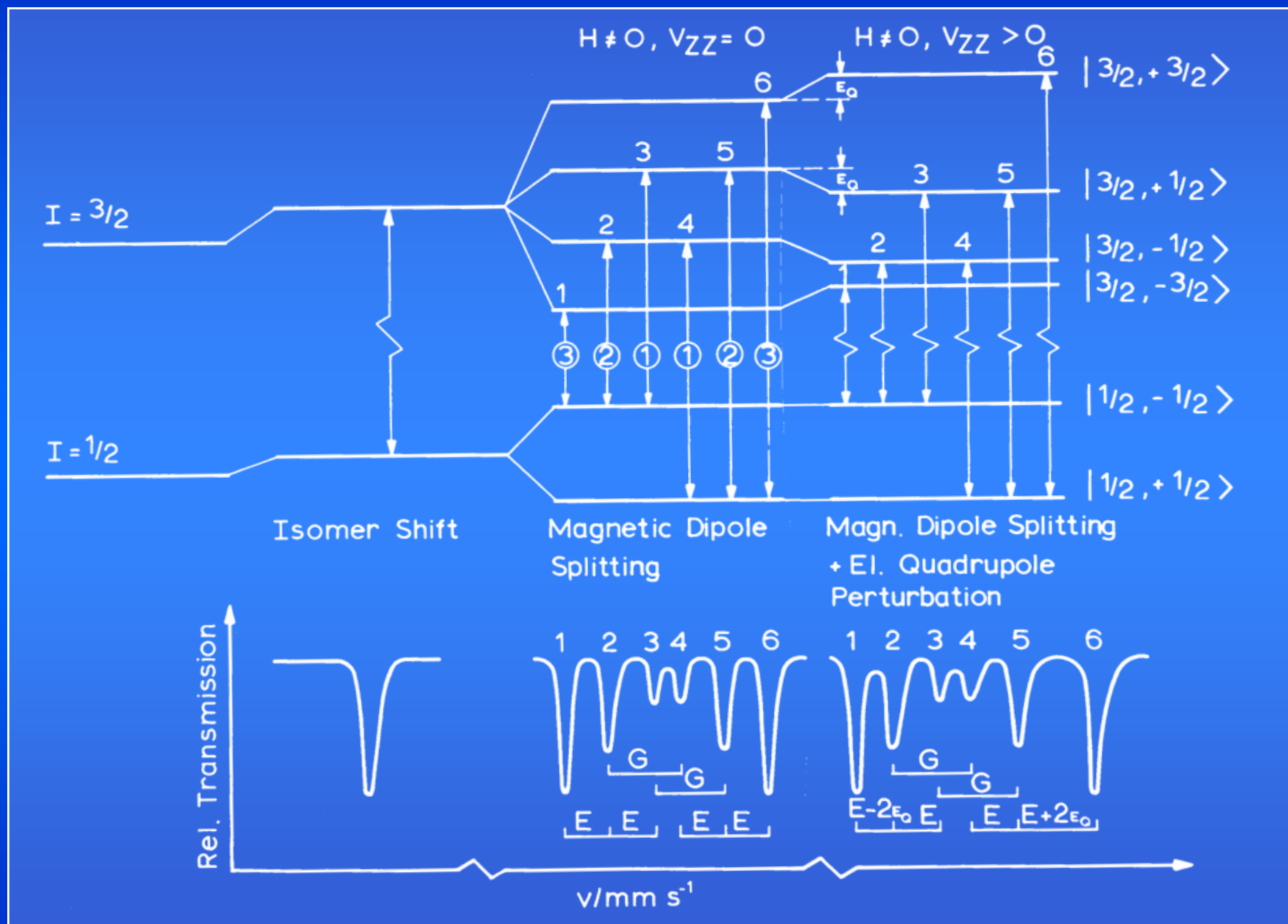
$$\hat{H}_Q \ll \hat{H}_M$$

For ^{57}Fe and axial systems ($\eta = 0$):



$$E_{M,Q}(I, m_I) = -g_N \beta_N H m_I + (-1)^{|m_I|+1/2} (eQV_{zz} / 8) (3 \cos^2 \vartheta - 1)$$

Combined magn. dipole and electr. quadrupole interaction



Information from Magnetic Dipole Splitting

H_{int} normally fluctuates (changes the direction) with $\tau(H_{\text{int}})$.

Magnetic hyperfine interaction in Mössbauer spectrum observable only if

$$\left. \begin{array}{l} \tau(H_{\text{int}}) \\ \text{and } 1/\omega_{\text{Larmor}} \end{array} \right\} > \tau_{\text{N}}$$

Then $|H_{\text{int}}|$ is a specific property of the material.

Some examples:



	$ \mathbf{H}_{\text{int}} $	
Para-, Diamagnetism	0	
Ferro- Antiferro- Ferrimagnetism	$\neq 0$	α -FeOOH orders at RT β -FeOOH orders at $\sim 80\text{K}$ γ -FeOOH orders at $\sim 30\text{K}$
α -Fe ₂ O ₃	520 kOe (RT)	Highest H_{int} and T_{C} of all Fe-oxides
Fe ₃ O ₄	Two H_{int}	Inverse spinel, Fe ^{III} - tetrahedral, Fe ^{II,III} – octahedral with fast electron transfer

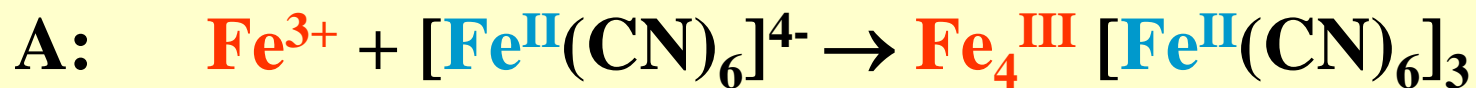
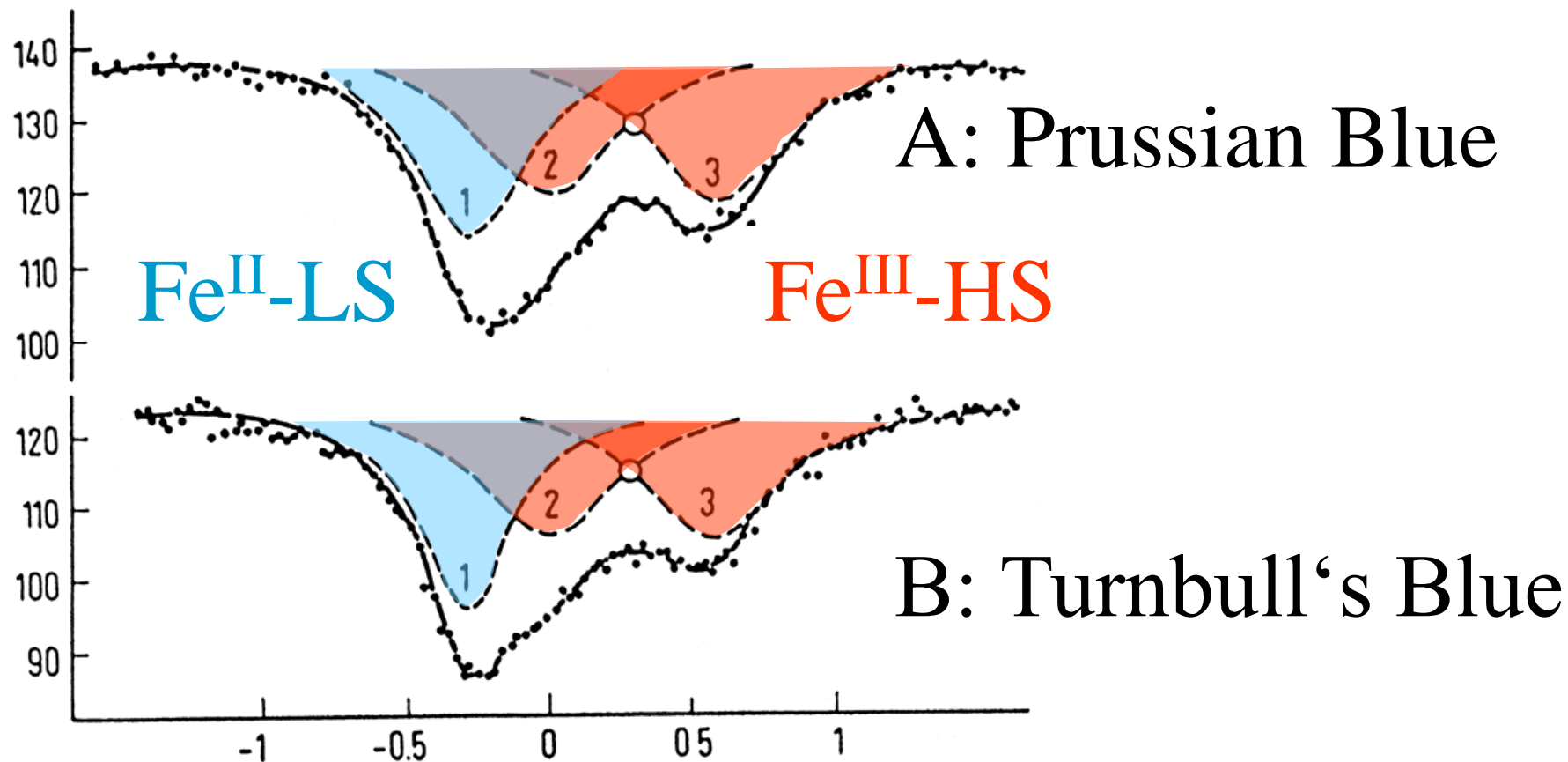
Applications

Transition Metal Compounds

- **Valence State**
- **Structural Properties**
- **Bonding Properties**
- **Solid State Reactions**
- **Mixed Valency**
- **Spin Crossover**
- **Magnetic Properties**

Prussian Blue – Turnbull's Blue

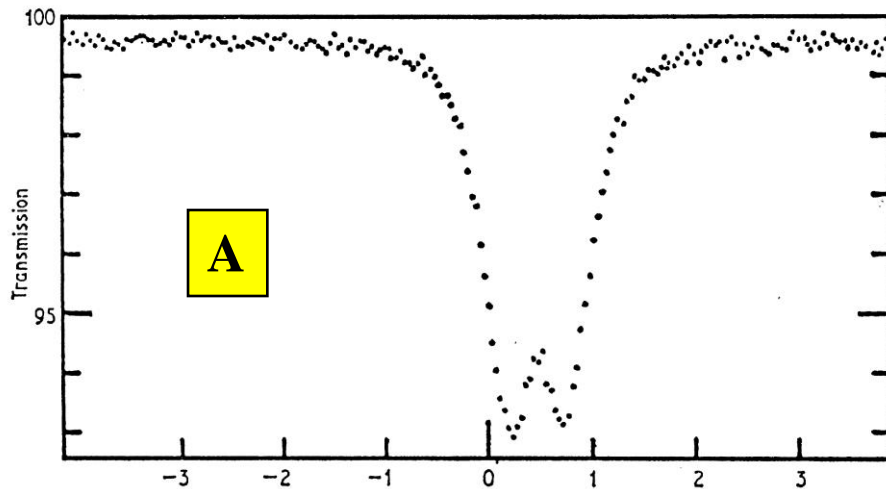
E. Fluck et al. 1963



Soon after the discovery of the *recoilless nuclear resonance absorption of γ -rays* (Mössbauer effect) mainly physicists and chemists began to explore the applicability of the new resonance effect to solve problems in solid state research. Fluck, Kerler and Neuwirth reported already in 1963 on the successful application of the new technique to distinguish between the cyano complexes of iron known as Prussian Blue (PB) and Turnbull's Blue (TB). PB is prepared by adding a solution of an iron(III) salt to a solution of $[\text{Fe}^{\text{II}}(\text{CN})_6]^{4-}$, and TB by adding a solution of an iron(II) salt to a solution of $[\text{Fe}^{\text{III}}(\text{CN})_6]^{3-}$. For a long time one had considered them as chemically different compounds, Prussian Blue with $[\text{Fe}^{\text{II}}(\text{CN})_6]^{4-}$ anions and Turnbull's Blue with $[\text{Fe}^{\text{III}}(\text{CN})_6]^{3-}$ anions, according to the different way of preparing them. However, the Mössbauer spectra recorded by Fluck, Kerler and Neuwirth were nearly identical for both PB and TB showing only the presence of $[\text{Fe}^{\text{II}}(\text{CN})_6]^{4-}$ and Fe^{3+} in the high spin state. This could be confirmed by use of $\text{K}_4[\text{Fe}^{\text{II}}(\text{CN})_6]$ and $\text{K}_3[\text{Fe}^{\text{III}}(\text{CN})_6]$ as reference compounds. The explanation is given in the schemes A and B: Immediately after adding a solution of Fe^{2+} to a solution of $[\text{Fe}^{\text{III}}(\text{CN})_6]^{3-}$ a rapid electron transfer takes place from Fe^{2+} to the anion $[\text{Fe}^{\text{III}}(\text{CN})_6]^{3-}$ with subsequent precipitation of the same material as in scheme A.

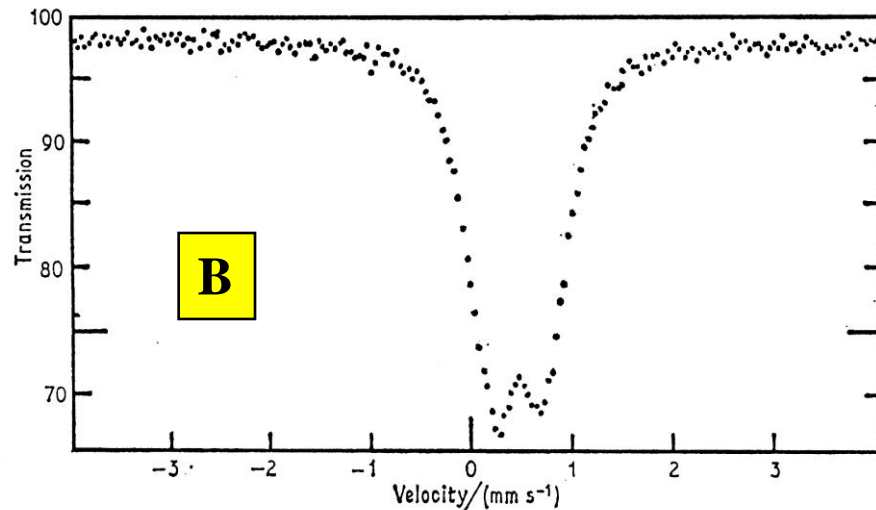
Maer et al. in 1968 confirmed, again by Mössbauer spectroscopy, that Prussian Blue and Turnbull's Blue are identical substances. They carried out the following experiment:

Mössbauer spectra (77 K) of “Prussian Blue” prepared from ...



A

$^{57}\text{Fe}_2(\text{SO}_4)_3$ (enriched) +
 $\text{K}_4[\text{Fe}(\text{CN})_6]$ (unenriched)



B

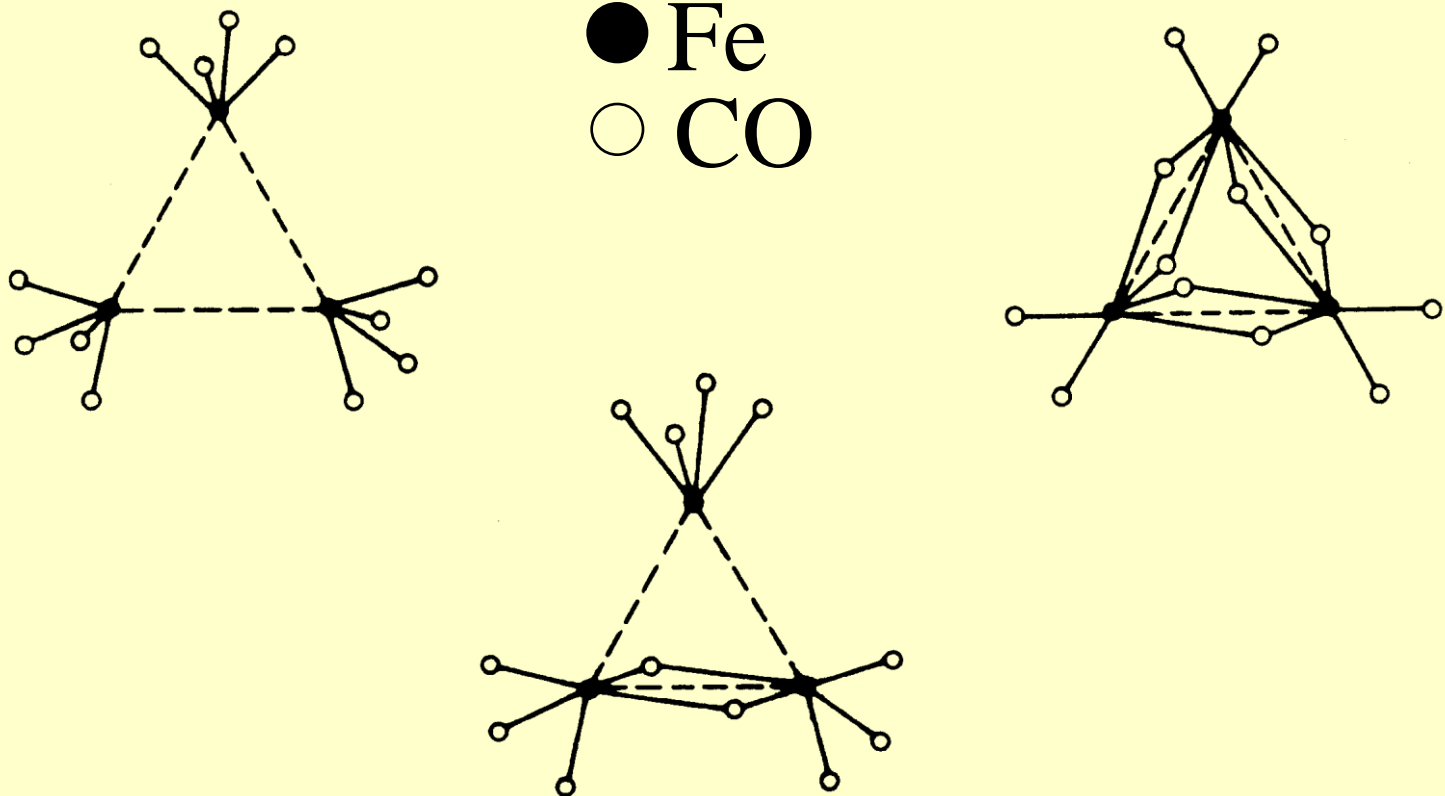
$^{57}\text{FeCl}_2$ (enriched) +
 $\text{K}_3[\text{Fe}(\text{CN})_6]$ (unenriched)

Maer et al., J. Am. Chem. Soc. 90 (1968) 3201

$\text{Fe}_3(\text{CO})_{12}$

Possible Structures from X-Ray Diffraction

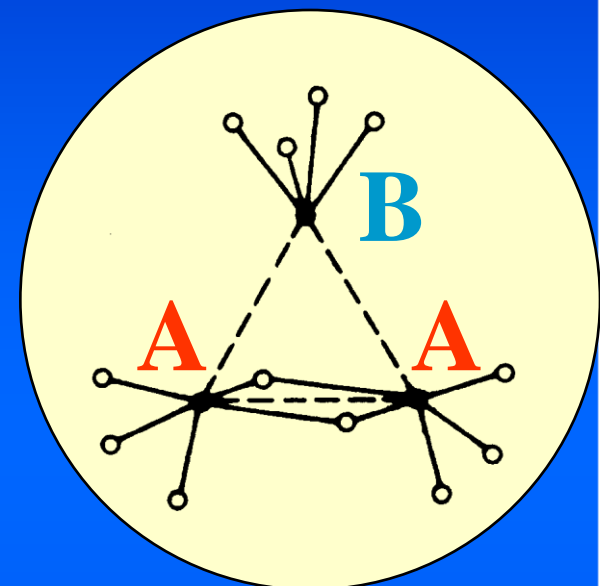
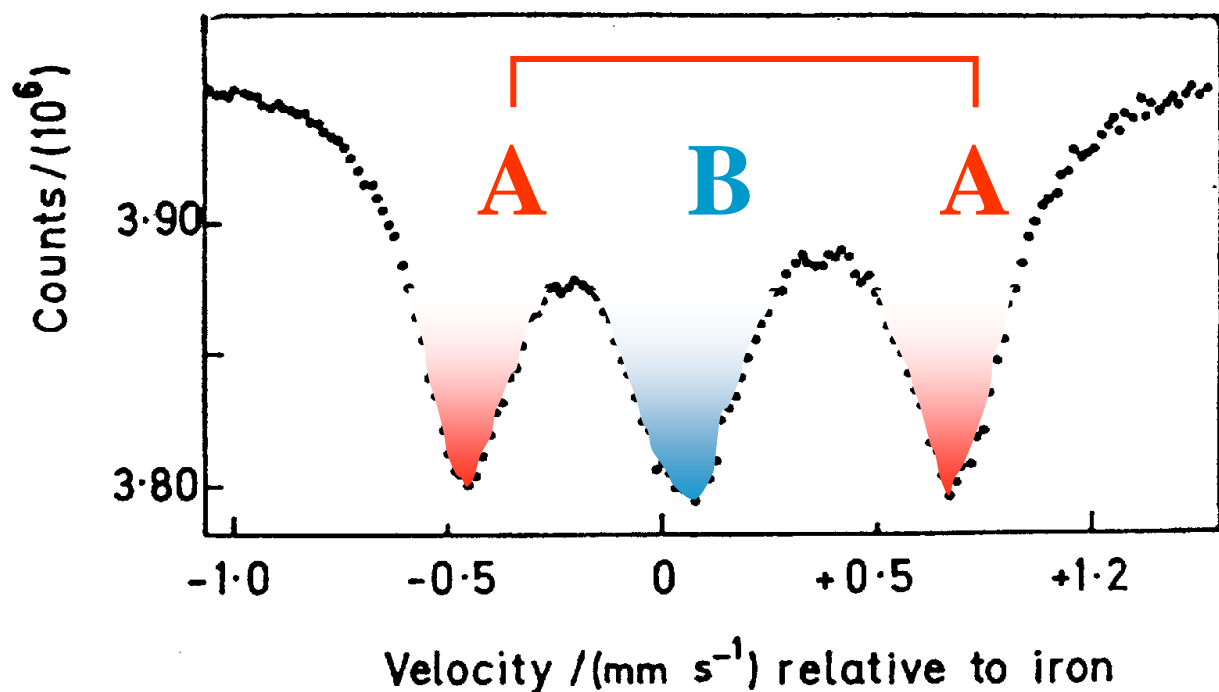
(Erickson, Fairhall 1965)



In 1965 Erickson and Fairhall suggested, on the basis of single crystal X-ray diffraction, three possible molecular structures for $\text{Fe}_3(\text{CO})_{12}$. In all cases the iron atoms form a triangle, but with different surroundings by the CO groups. In the upper two structures the three iron atoms have identical surroundings, the Mössbauer spectrum is expected to show only one type of resonance signal. The lower structure has two identical iron positions and a different one for the third iron atom. In this case the Mössbauer spectrum is expected to show two different types of resonance signals with an area ratio of 2:1. A Mössbauer effect study performed by Greenwood and Greatrex in 1969 indeed showed two types of resonance signals, a quadrupole doublet A and a singlet B with an area ratio of 2:1 confirming the presence of two types of iron positions in $\text{Fe}_3(\text{CO})_{12}$.

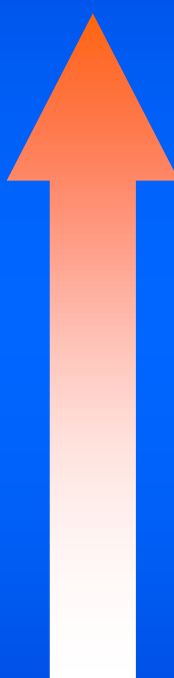
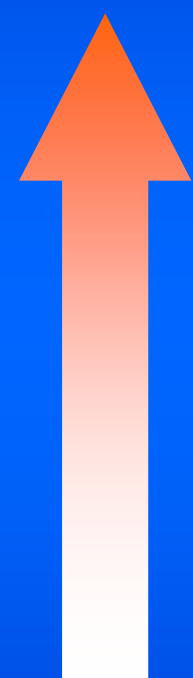
^{57}Fe Mössbauer Spectrum (80K)

(Greenwood, Greatrex 1969)



R. Greatrex, N.N. Greenwood, *Discuss. Faraday Soc. No.47 (1969) 126*

Effect of π -Backdonation in $[\text{Fe}(\text{CN})_5\text{X}^{n-}]^{(3+n)-}$

Ligand X	$\delta/\text{mm s}^{-1}$	$d_\pi \rightarrow p_\pi$	d-shield	$ \Psi_s(\mathbf{0}) ^2$
NO^+	0.00			
CO	+0.15			
SO_3^{2-}	+0.22			
$\text{P}(\text{C}_6\text{H}_5)_3$	+0.23			
NO_2^-	+0.26			
$\text{Sb}(\text{C}_6\text{H}_5)_3$	+0.26			
NH_3	+0.26			
$\text{As}(\text{C}_6\text{H}_5)_3$	+0.29			
H_2O	+0.31			

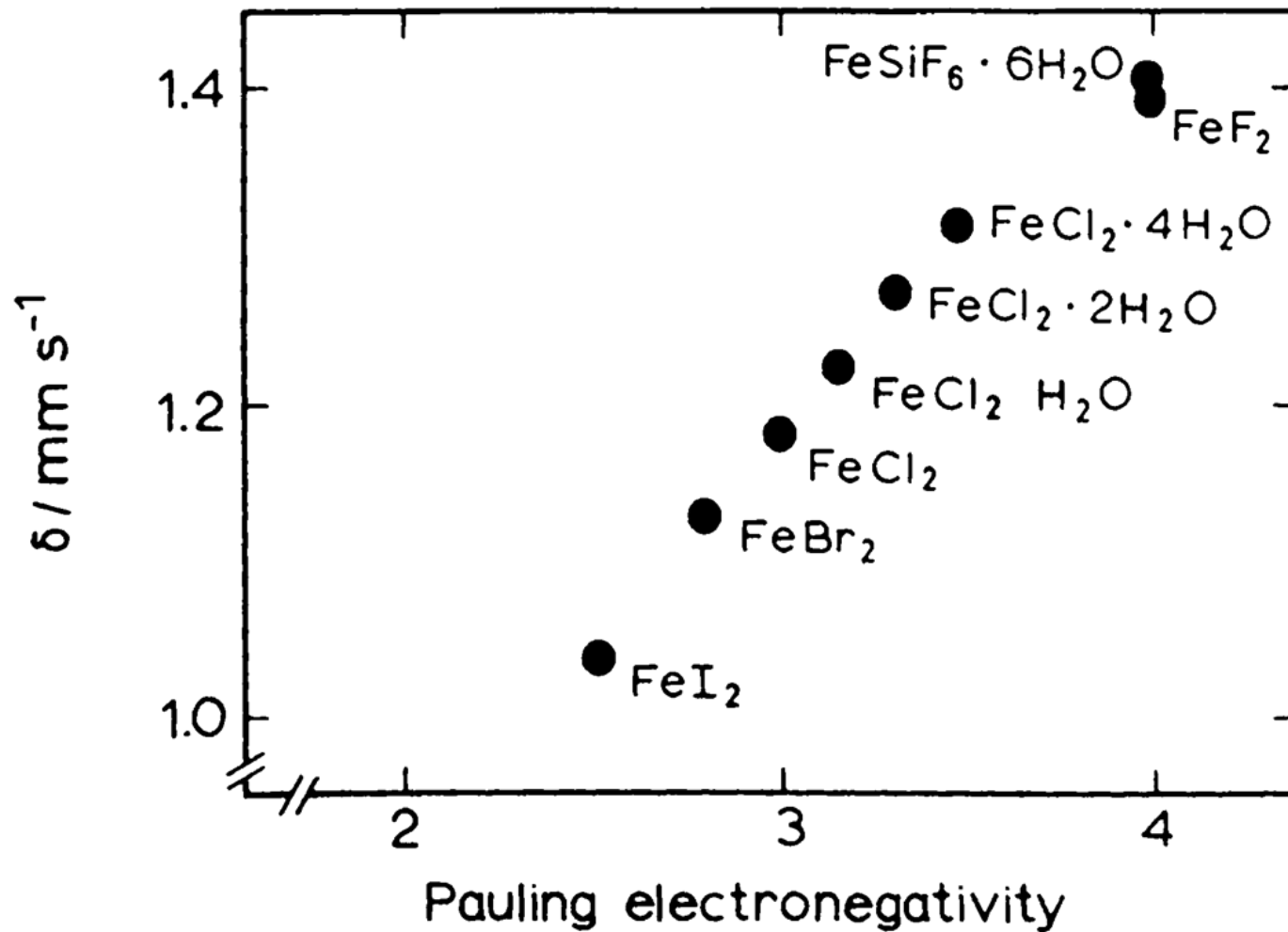
$$\delta \sim |\Psi_s(\mathbf{0})|^2 \frac{\Delta R}{R}$$

$$^{57}\text{Fe}: \frac{\Delta R}{R} < 0$$

This example demonstrates that Mössbauer spectroscopy can help to characterize chemical bond properties. Taking from the literature the isomer shift data for the pentacyano complexes of iron(II) with a different sixth ligand X and normalising the isomer shifts to that of the pentacyanonitrosylferrate complex as zero point, one finds the ordering given in the following table which expresses the varying effects of d_{π} - p_{π} backdonation for the different sixth ligand X.

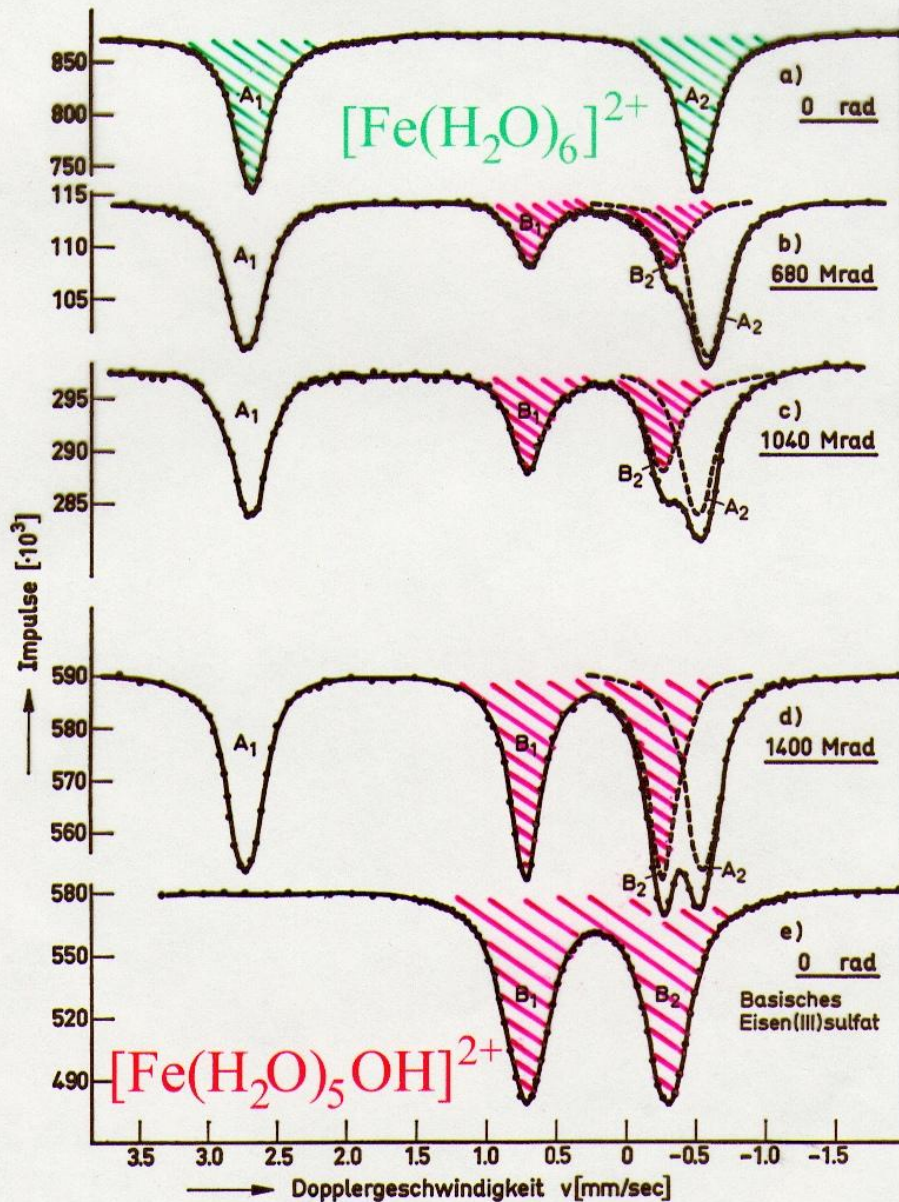
The isomer shift values become more positive on going from NO^+ to H_2O . The reason is that in the same ordering the strength of d_{π} - p_{π} backdonation decreases causing an increasing d-electron density residing near the iron centre and thus effecting stronger shielding of s-electrons by d-electrons, which finally creates lower s-electron density at the nucleus in the case of H_2O as compared to NO^+ . Keeping in mind that the nuclear factor $\Delta R/R$ is negative for ^{57}Fe explains the increasingly positive isomer shift values in the given sequence from NO^+ to H_2O .

Effect of ligand electronegativity



The electronegativity increases from iodine to fluorine. In the same ordering the 4s-electron population decreases and as a direct consequence the s-electron density at the iron nucleus decreases, and due to the fact that $(R_a^2 - R_g) < 0$ for ^{57}Fe the isomer shift increases from iodide to fluoride.

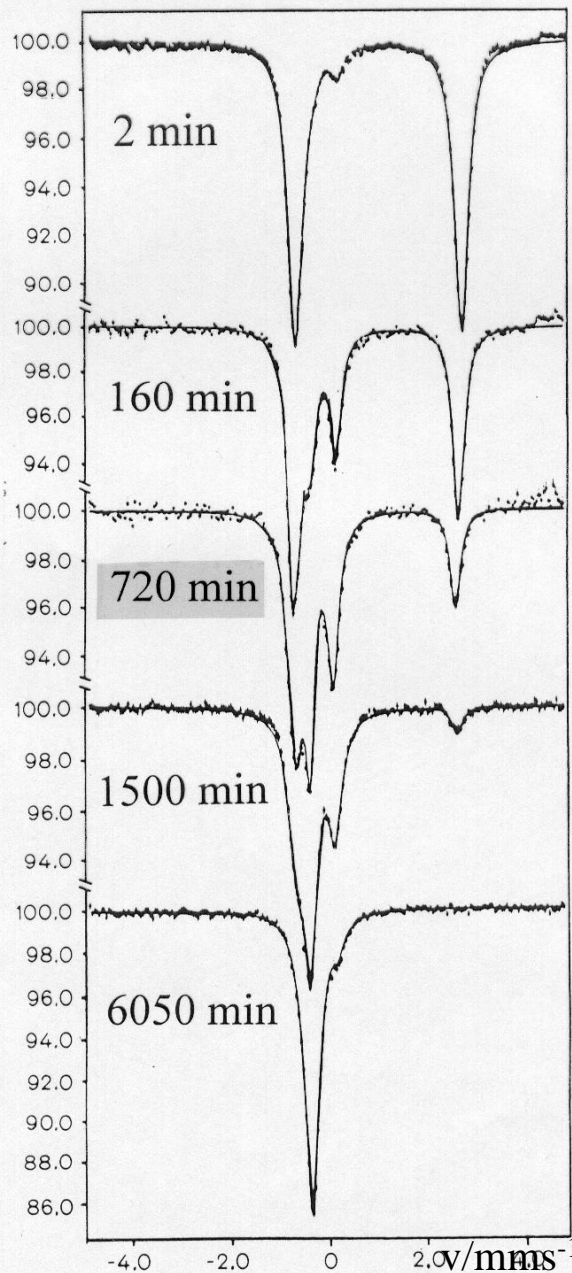
γ -Radiolysis of $\text{FeSO}_4 \cdot 7\text{H}_2\text{O}$ (300K)



P. Gülich, S. Odar,
 B.W. Fitzsimmons, N.E. Erickson,
 Radiochim. Acta 10 (1968) 147

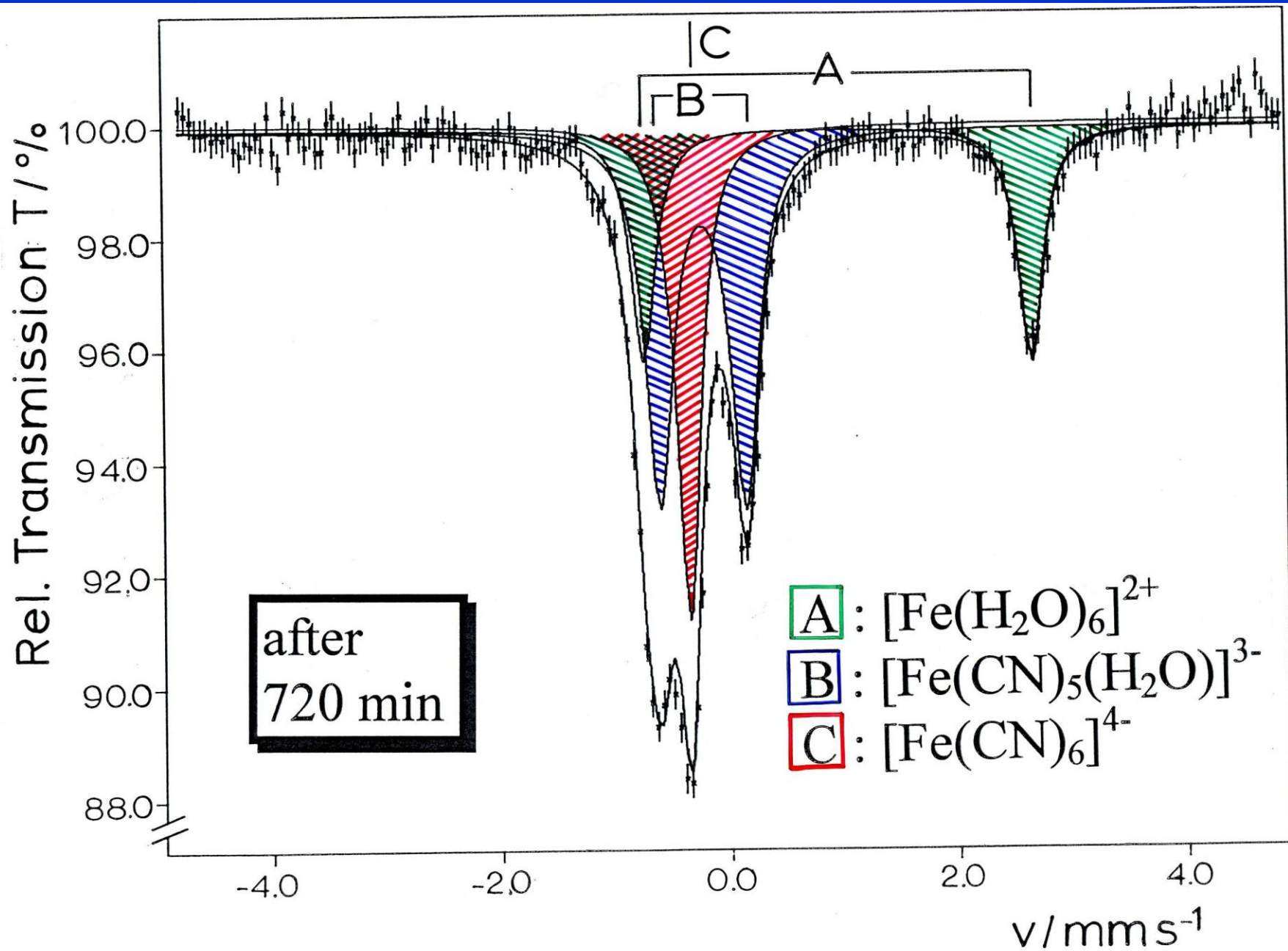
Ligand Exchange Reaction $\text{FeSO}_4 \cdot 7\text{H}_2\text{O} / \text{KCN} (1:6) / 5^\circ\text{C}$

Rel. Transmission / %



A pellet of a polycrystalline mixture of $\text{FeSO}_4 \cdot 7\text{H}_2\text{O} / \text{KCN} (1:6)$ reacted at 5°C for different length of time. ^{57}Fe Mössbauer spectra were recorded at room temperature.

P. Gülich, K.M. Hasselbach,
Ber. Bunsenges. Phys. Chem. 78 (1974) 1017

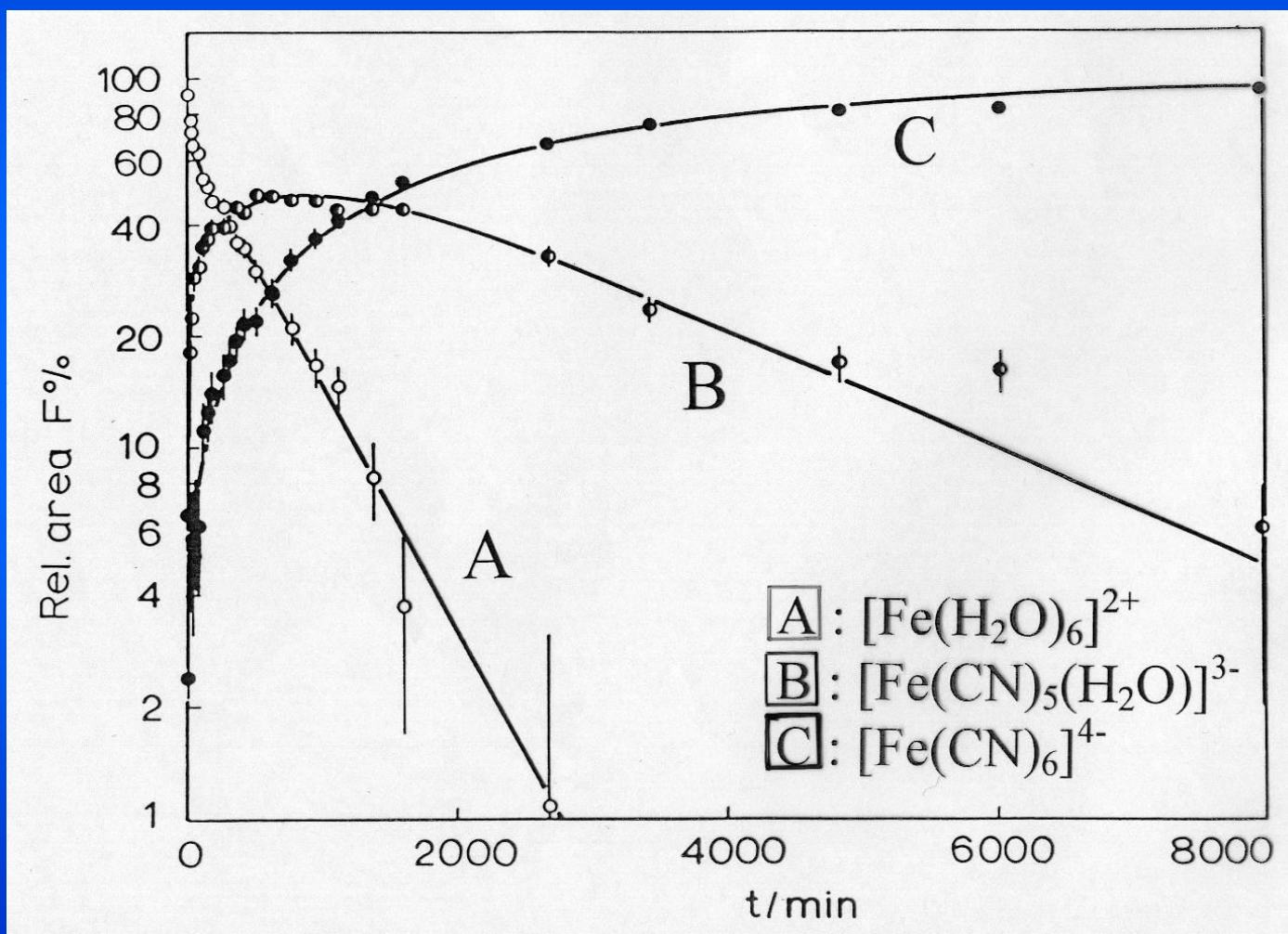


Three resonance signals are detected in the Mössbauer spectra: the quadrupole doublet A (green) of the starting $[\text{Fe}(\text{H}_2\text{O})_6]^{2+}$, the quadrupole doublet of the mixed-ligand complex B (blue) $[\text{Fe}(\text{CN})_5(\text{H}_2\text{O})]^{3-}$, and the singlet of the final complex C (red) $[\text{Fe}(\text{CN})_6]^{4-}$.

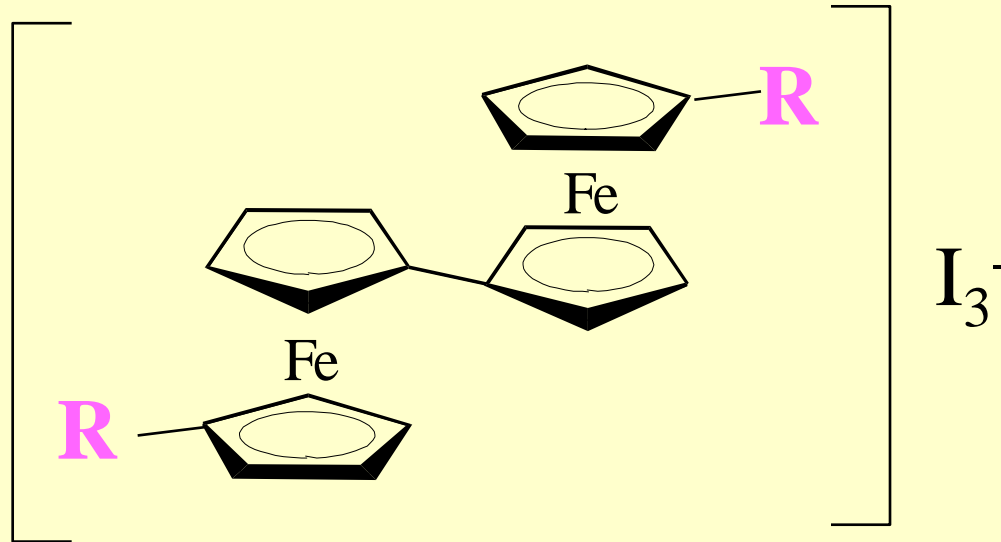
Obviously, the stepwise replacement of water molecules for the cyanide anions is very fast (faster than 10^{-7} s, the Mössbauer time scale) for the first four reaction steps, even though we have started with a solid state mixture of reactants at a relatively low reaction temperature of 5 °C. Taking the Lamb-Mössbauer factors of the three species as nearly the same, we can plot the area fractions as a function of reaction time (at 5°C) and obtain the following graph.

Ligand Exchange Reaction $\text{FeSO}_4 \cdot 7\text{H}_2\text{O} / \text{KCN} (1:6) / 5^\circ\text{C}$

Area fractions from Mössbauer spectra as a function of reaction time



Mixed-Valence Biferrocenes



Depending on **R**:

„localized“ **ferrocene** – **ferrocenium**

„delocalized“ \Rightarrow fast fluctuation ($k > 10^7 \text{ s}^{-1}$)

Time-averaged species

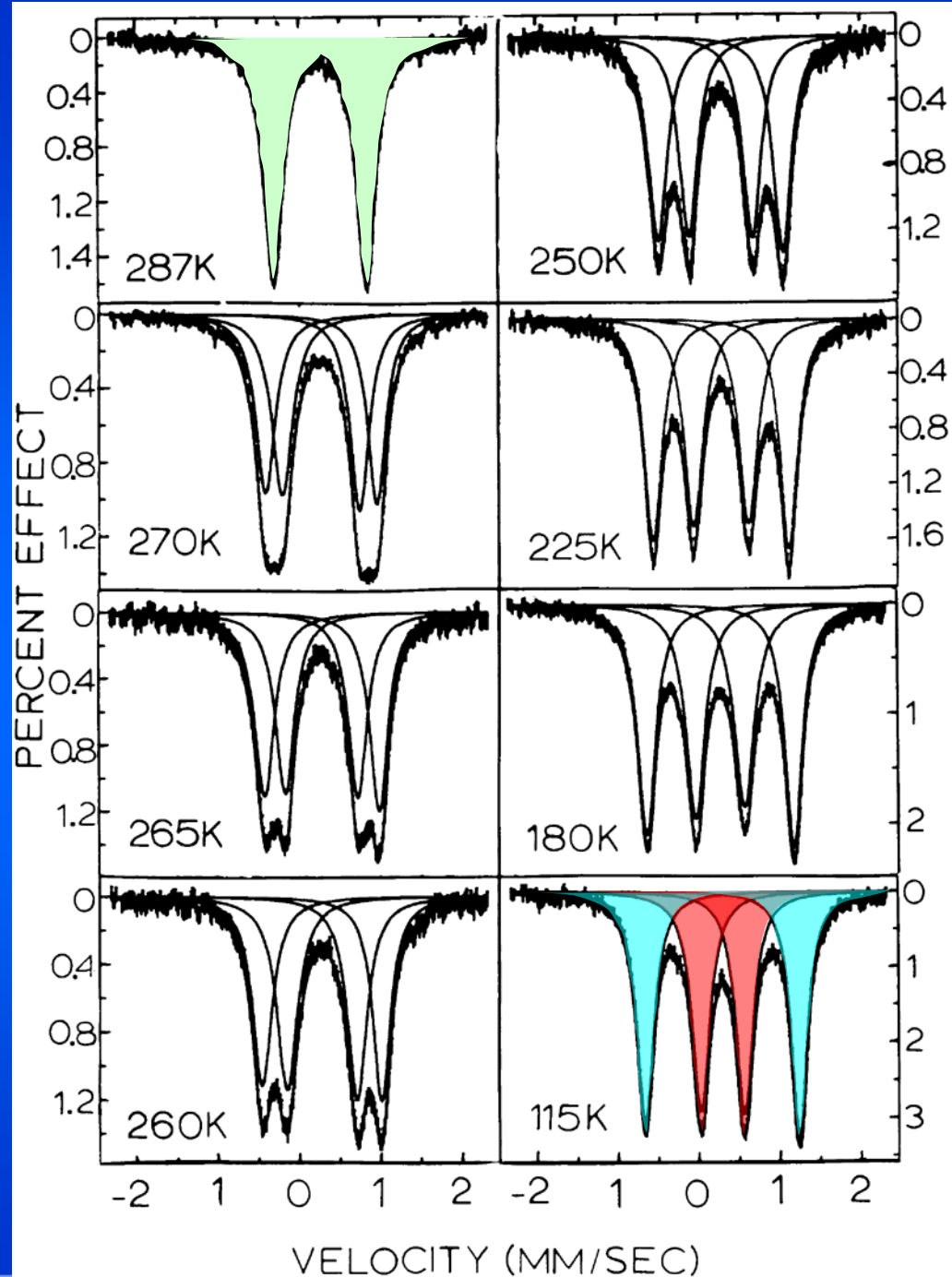
Mixed-valence compounds are known to possess two or more transition metal ions with different oxidation states. The picture shows the example of mixed-valence biferrocenes. Depending on the nature of the substituent R, the iron centres have either static but different electronic structures referred to as “localized” ferrocene and ferricinium, respectively. Or a rapid electron transfer between the two iron centres takes place and as a result of the fast fluctuation one observes a time-averaged species with an electronic structure between the two localized species. With the help of ^{57}Fe Mössbauer spectroscopy one has studied the biferrocenes containing ethyl groups as R substituents as a function of temperature. At 115 K, the spectrum shows two well resolved quadrupole doublets, the light-blue one being characteristic of ferrocene-like iron, the red one of ferrocinium-like iron. With increasing temperature an electron fluctuation sets in and the doublets of the two localized species turn into one quadrupole doublet (shown in green at 287 K) of a time-averaged species, the parameter values of which are different from those of the two localized species. From the sharpness of the quadrupole doublet of the time-averaged species one can conclude that the electron fluctuation rate must be faster than 10^7 s^{-1} , with reference to the time-window of ^{57}Fe Mössbauer spectroscopy given by the lifetime of the excited 14.4 keV nuclear state.

This example demonstrates the thermally induced transition between localized and delocalized electronic structures in a mixed-valence organometallic compound.

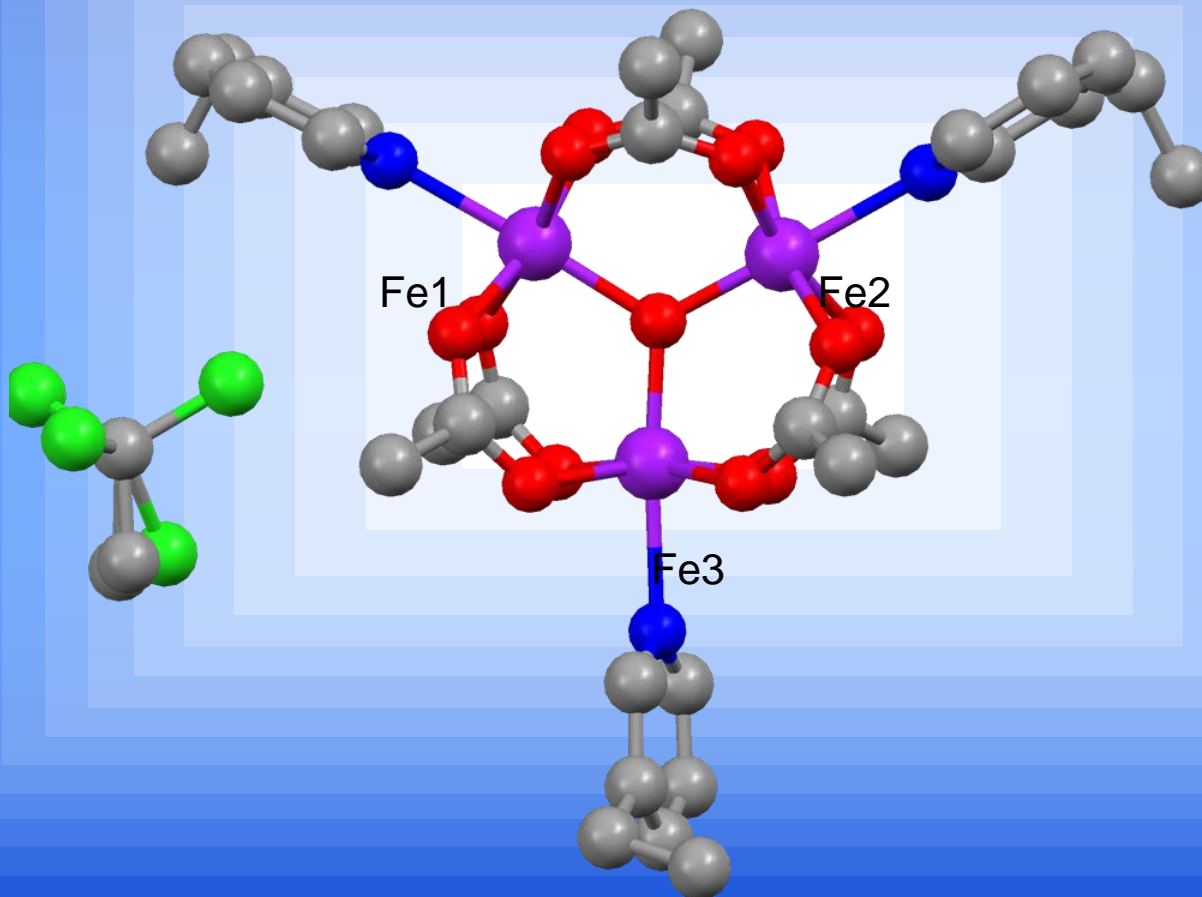
R = Ethyl

Ferrocene-like Fe
Ferrocenium-like Fe
Fast fluctuation
($k > 10^{+7} \text{ s}^{-1}$)

H. Sano et al. 1981;
D.N. Hendrickson et al. 1985



Solvents Molecule Effects in the Valence Detrapping of Mixed-Valence $[\text{Fe}_3\text{O}(\text{O}_2\text{CCH}_3)_3]_6(3\text{-Et-py})_3 \cdot \text{S}$



C.C. Wu, H. G. Jang, A.L. Rheingold, P. Gütlich, D.N. Hendrickson,
Inorg. Chem. 35 (1996) 4137

$[\text{Fe}_3\text{O}(\text{O}_2\text{CCH}_3)_3]_6(3\text{-Et-py})_3 \cdot \text{S}$

A

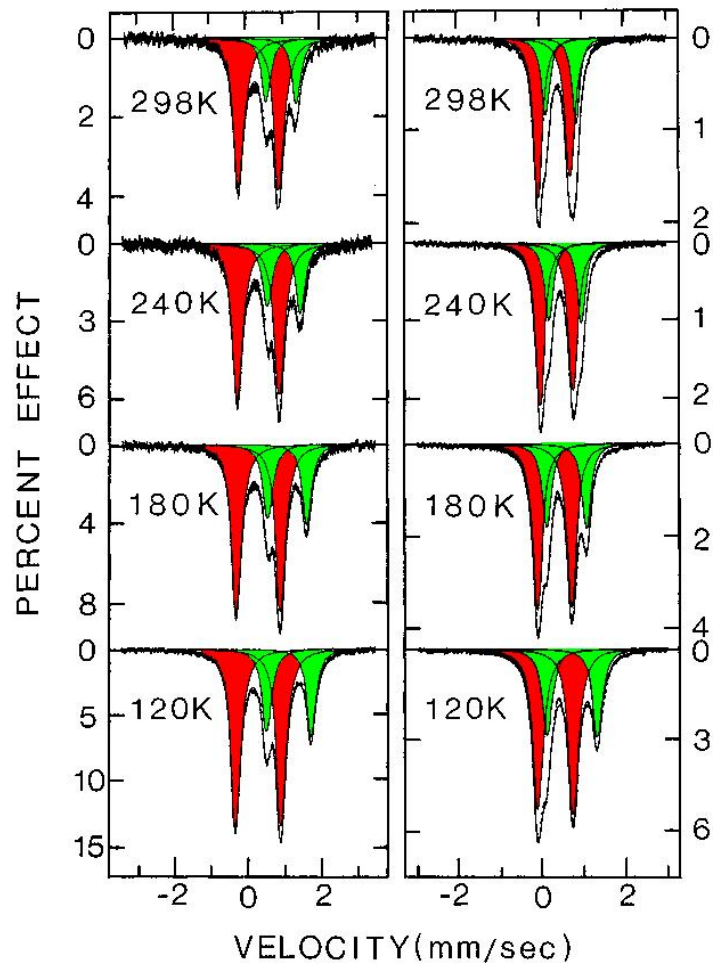
B

C

S = 0.5 benzene

S = CH_3CN

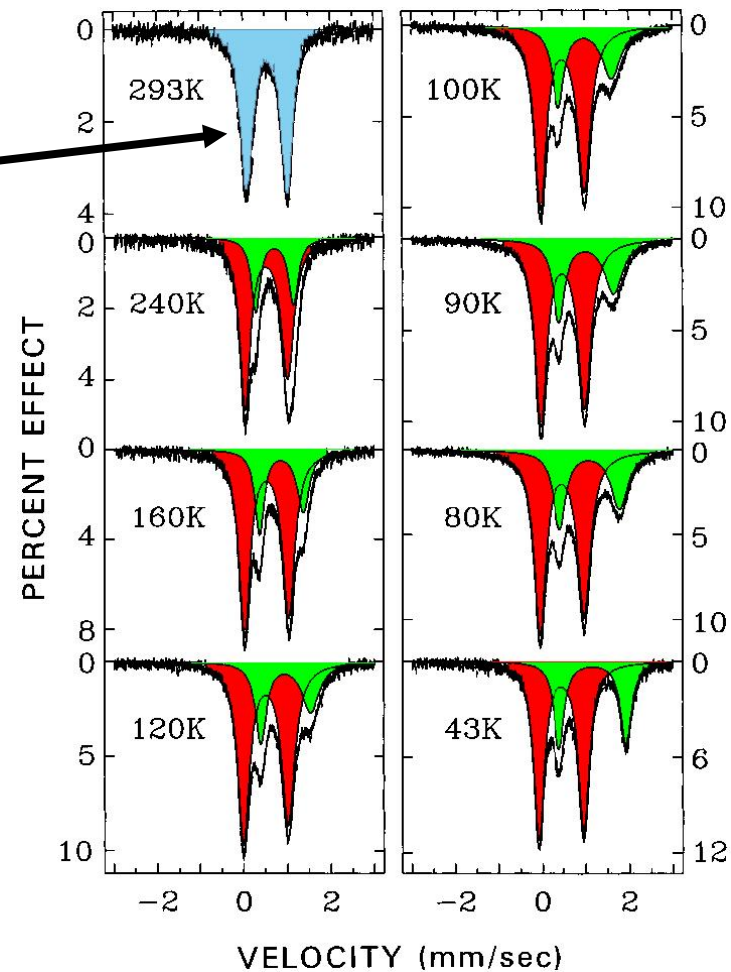
S = CH_3CCl_3



$\text{Fe}^{2.67+}$

Fe^{3+} -HS

Fe^{2+} -HS



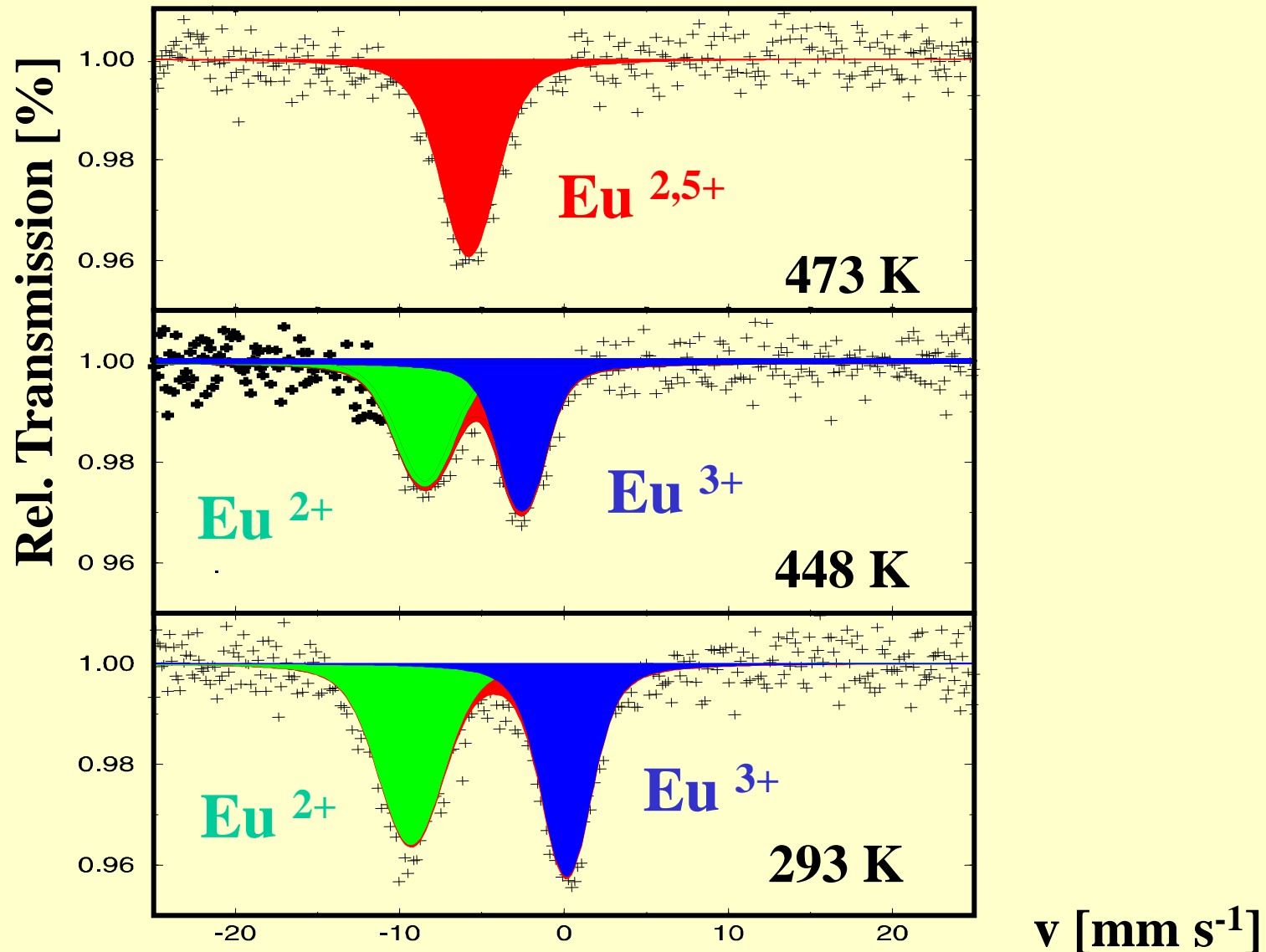
It was found that compound A is the most valence-trapped from 120 to 298 K on the Mössbauer time scale (given by the lifetime of the nuclear excited state. B and C are shown to be valence trapped below ca. 120 K, whereas increasing temperature leads to valence detrapping near room temperature.

In each spectrum the more intense quadrupole doublet marked in red corresponds to the two high spin Fe(III)-HS ions and the less intense doublet is for the one high spin Fe(II) ion. The ratio of the area fractions of Fe(III) to Fe(II) is close to 2 at low temperatures. Towards higher temperatures it tends to become larger than 2, which is due to the larger Lamb-Mössbauer factor of Fe(III) compared to that of Fe(II). At room temperature, complex C shows a single doublet that is a time-averaged signal for all three Fe ions in the Fe₃O complex.

From the results of the variable-temperature Mössbauer spectra and the X-ray structural analysis it is evident that the lattice packing environments of these Fe₃O complexes can control whether a given complex can become valence detrapped. Compound A possesses a stack type structure with relatively strong intermolecular interactions due to overlapping pyridine ligands. B and C are isostructural and of layer-type.

^{151}Eu Mössbauer Spectra of EuNiP

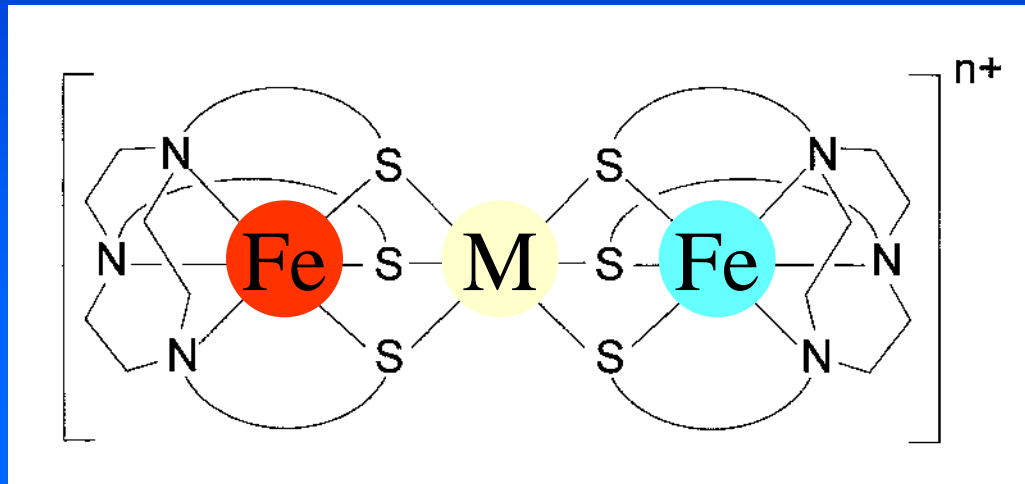
C. Felser, P. Gütlich, V. Ksenofontov, et al. (2000)



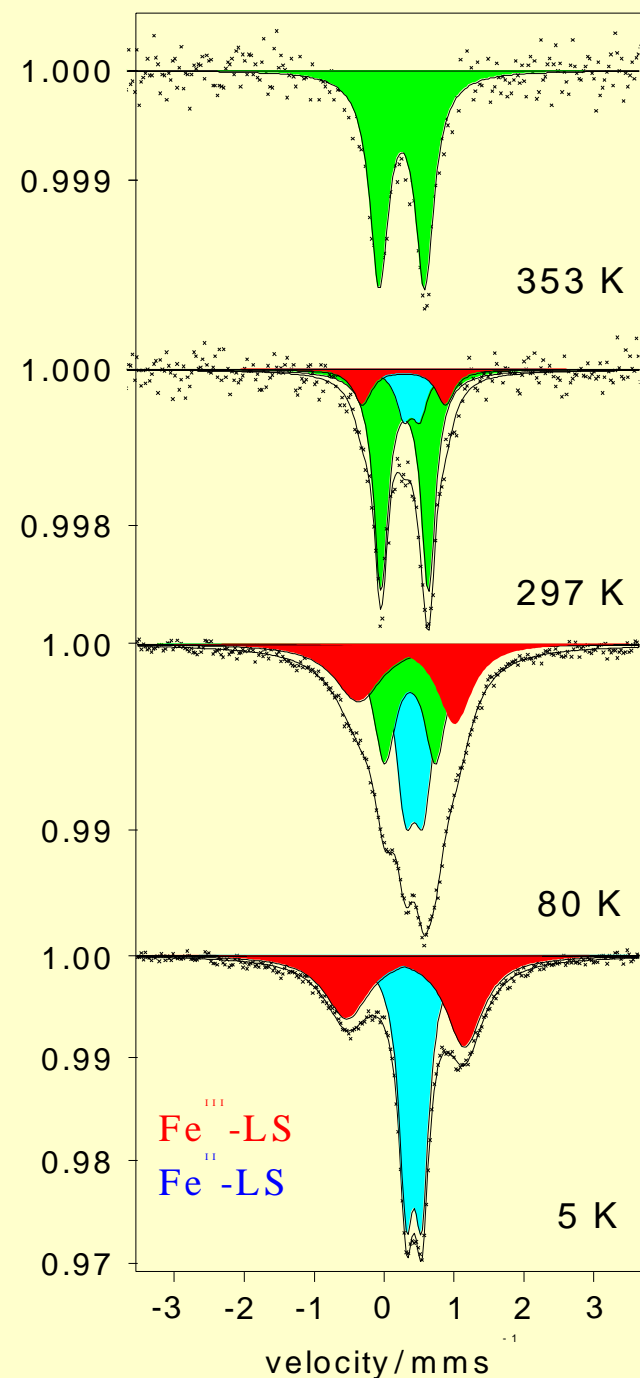
Another example showing mixed-valency and thermally induced transition between localized and delocalized valence states, a Verwey-type charge delocalization, is the intermetallic compound EuNiP . With ^{151}Eu Mössbauer spectroscopy one observes at room temperature still two well resolved signals, one being typical for Eu^{2+} (green) and the other one for Eu^{3+} (blue). With increasing temperature to well above 400 K the electron fluctuation between Eu^{2+} and Eu^{3+} becomes faster than the time-window of ^{151}Eu Mössbauer spectroscopy and one observes a time-averaged oxidation state of $\text{Eu}^{2.5+}$ (red).

V. Ksenofontov, H.C. Kandpal, J. Ensling, M. Waldeck, D. Johrendt, A. Mewis, P. Gütlich, C. Felser,
Europhysics Letters 74 (2006) 672

Valence Fluctuation in



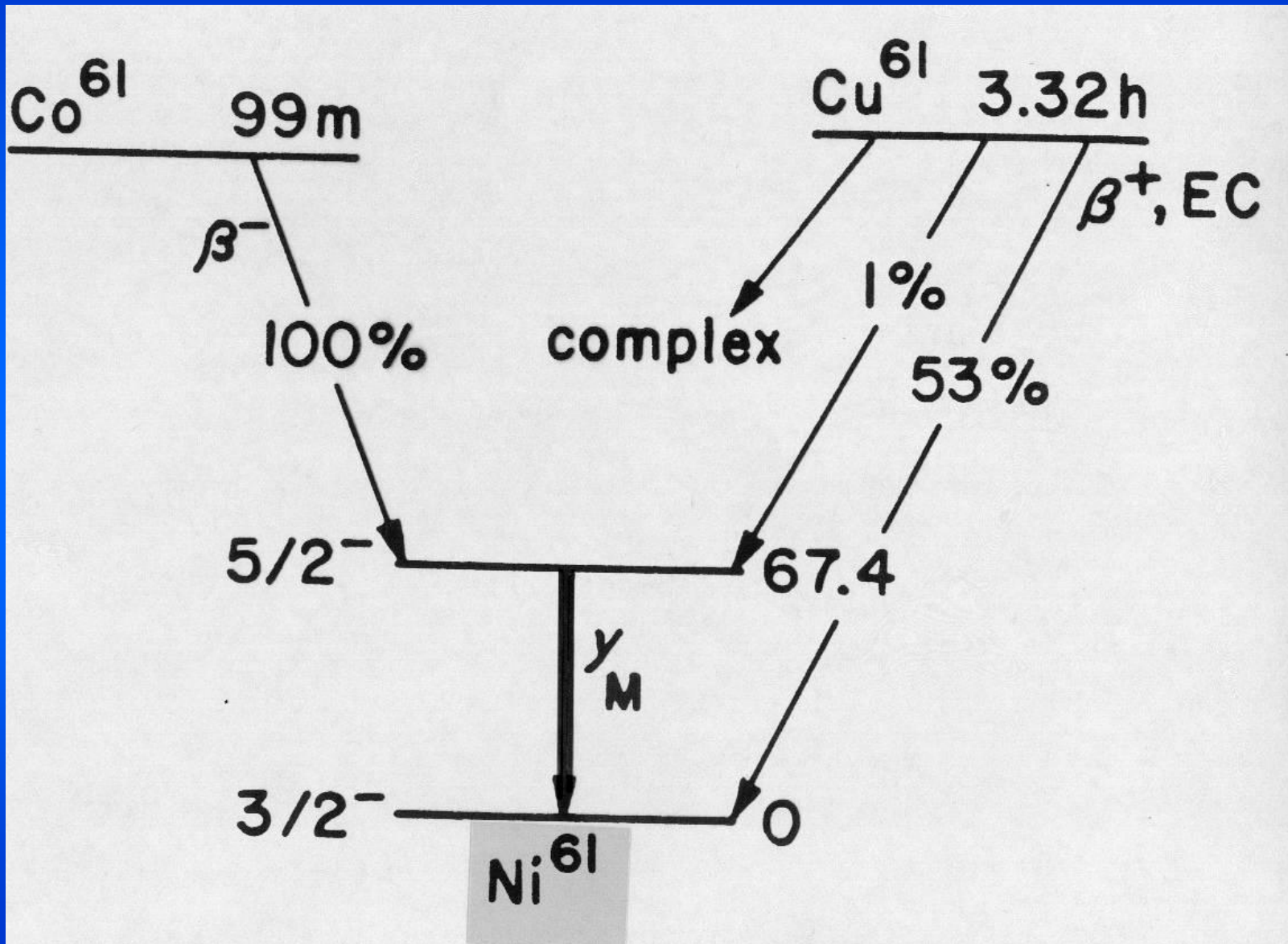
Glaser, Bill, Trautwein, Wieghardt;
JACS 1999



Another interesting example of valence fluctuation and temperature dependent transition between localized and delocalized electronic structures was reported by Bill, Glaser, Trautwein and Wieghardt to occur in a trinuclear transition metal compound. In this case the electron fluctuation takes place between two iron centres of different oxidation states and separated by a diamagnetic Co(III) ion. The ^{57}Fe Mössbauer spectra clearly show that at sufficiently low temperatures, i.e. 5 K, the two iron centres are reflected as localized oxidation states with a well resolved doublet for Fe(III)-low spin (red) and a poorly resolved doublet for Fe(II)-low spin (light-blue). At higher temperatures the intensities of these two resonance signals decrease at the favour of a new resonance signal, another quadrupole doublet (green), arising from a time-averaged species where both iron centres are in an intermediate oxidation state as a result of a fast electron fluctuation through the bridging diamagnetic central Co(III) ion.

**Characterisation of
Nickel Compounds
by
 ^{61}Ni Mössbauer Spectroscopy**

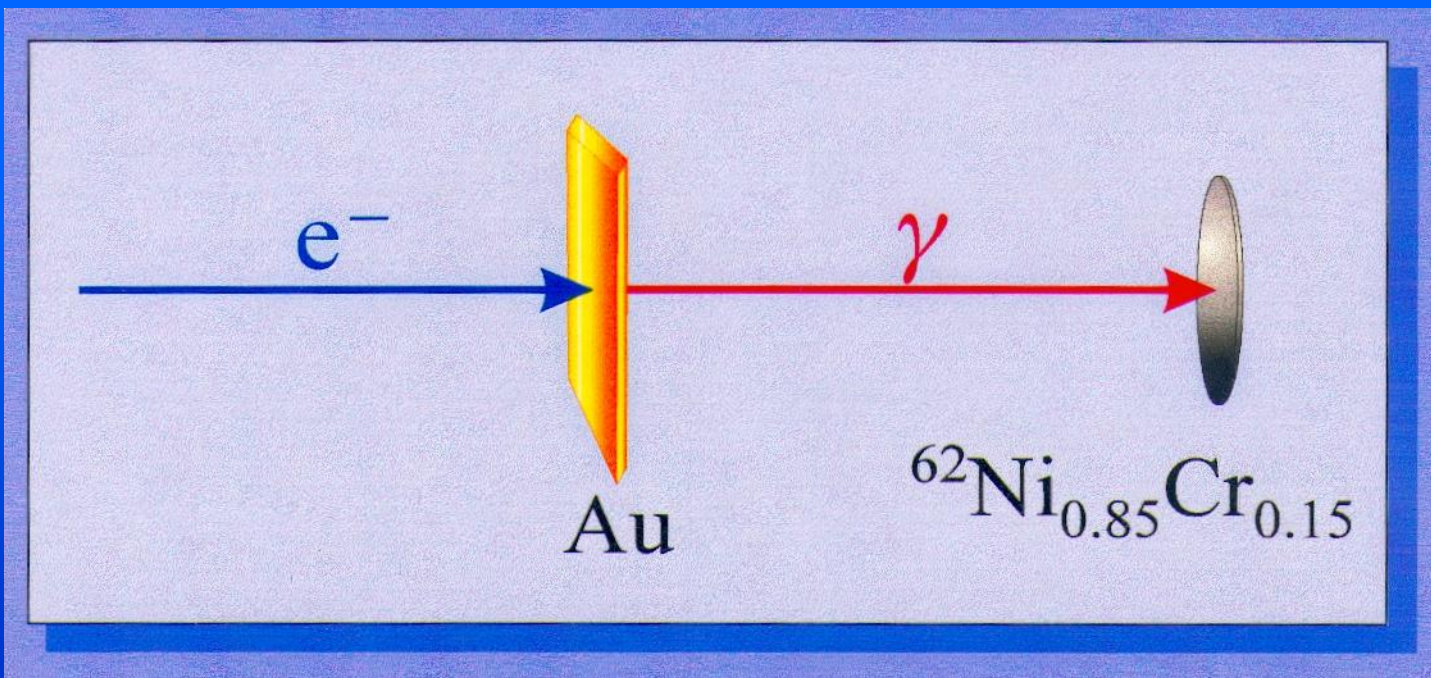
Decay Scheme of ^{61}Ni



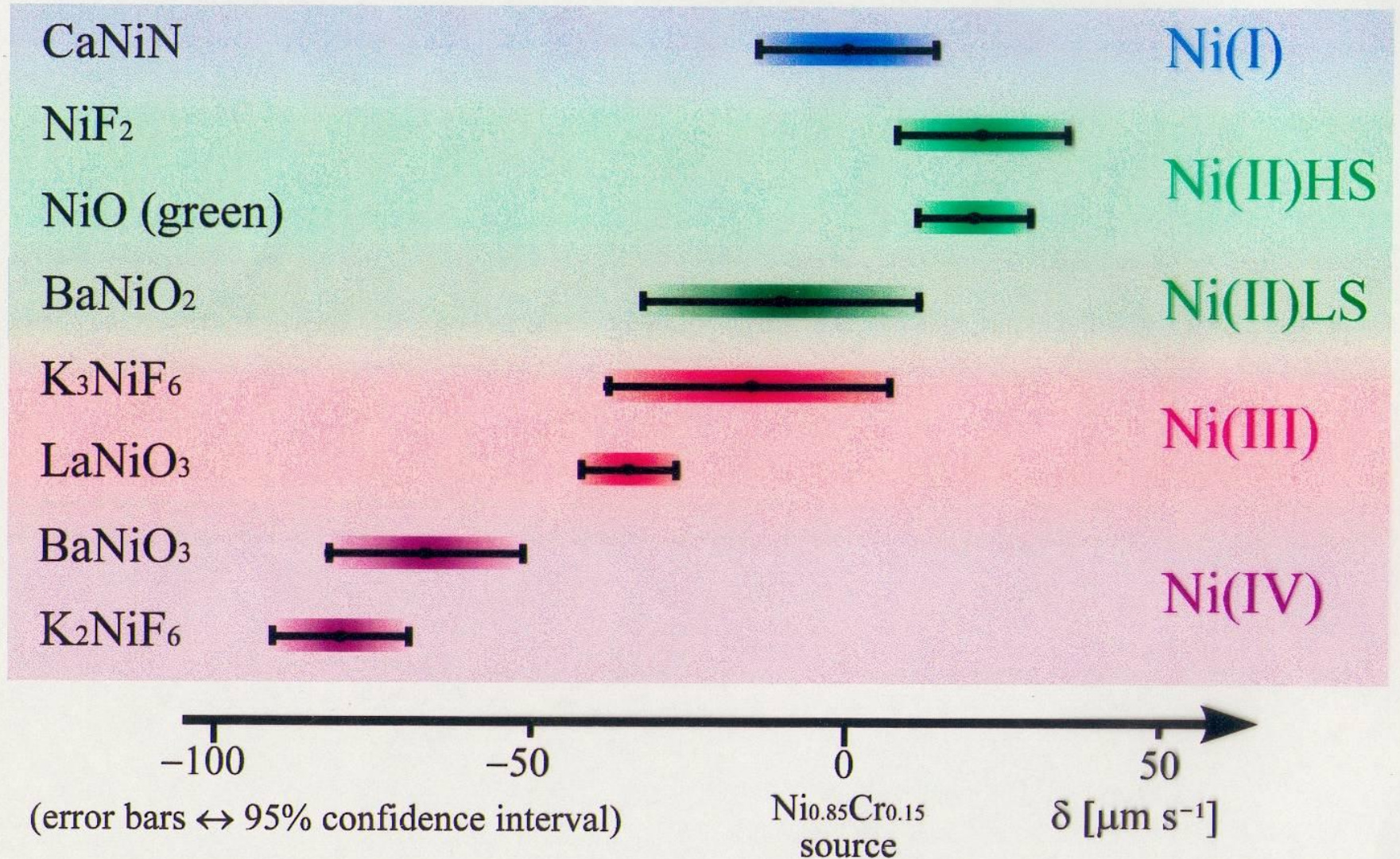
^{61}Ni Source Production

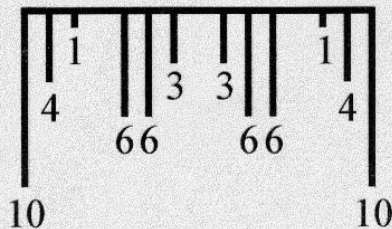
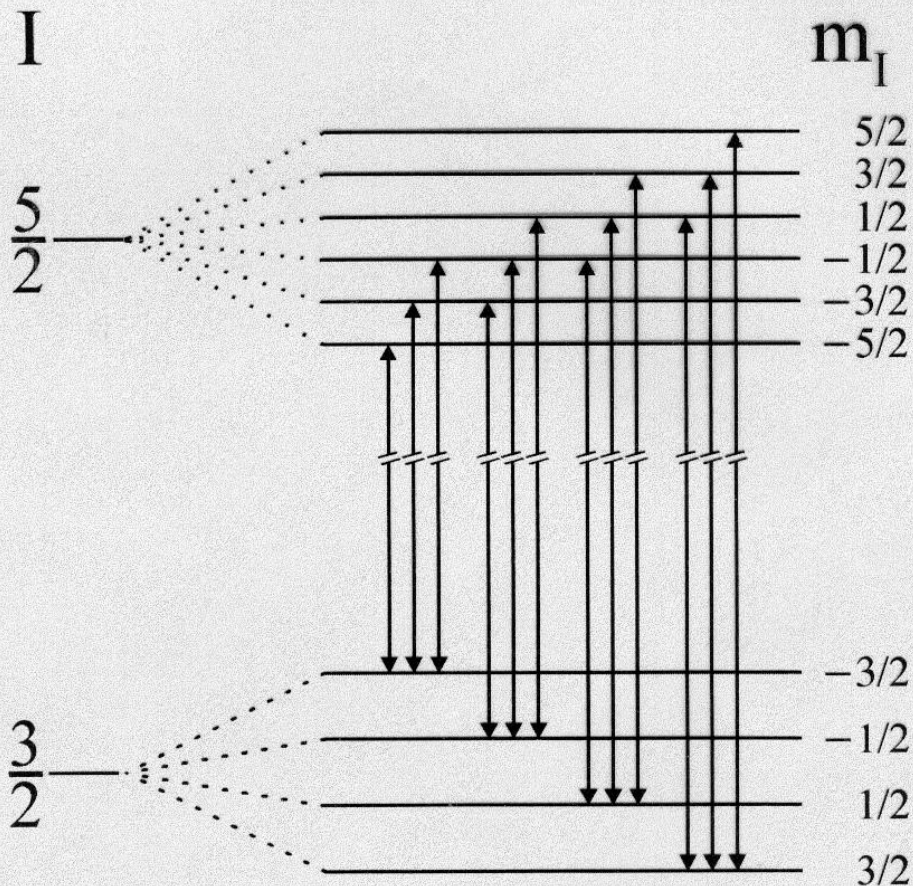


Activation with Bremsstrahlung from the
Electron beam of the **MA**inz **MI**crotron (MAMI)



^{61}Ni Isomer Shifts



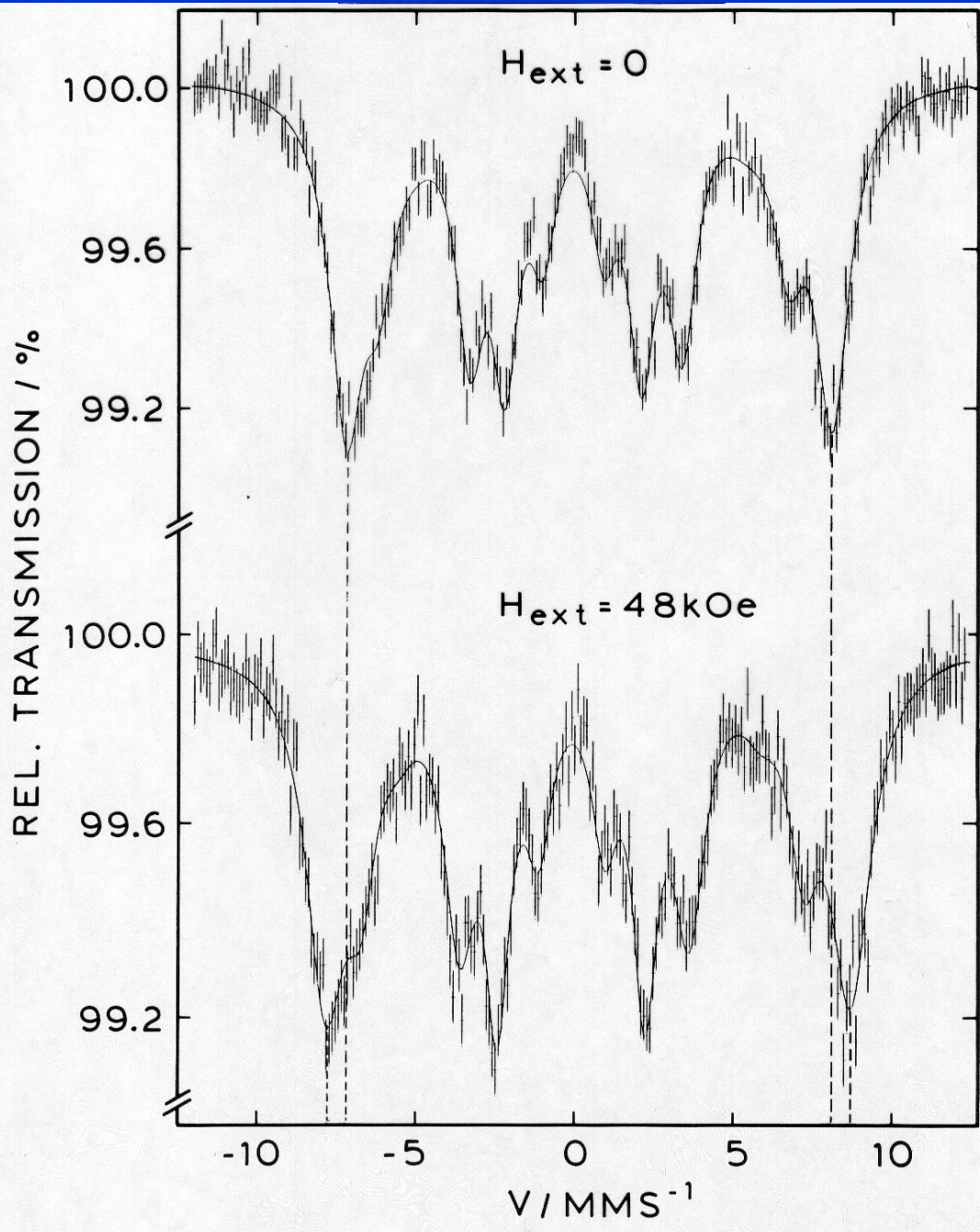


^{61}Ni Magnetic Splitting

12 transition lines
completely resolved
at H_{eff} ca. 50 T

**Sign and Magnitude
of the
Magnetic Hyperfine Field
in
Nickel Spinel Compounds**

NiCr_2O_4 (Ni in tetrahedral sites)

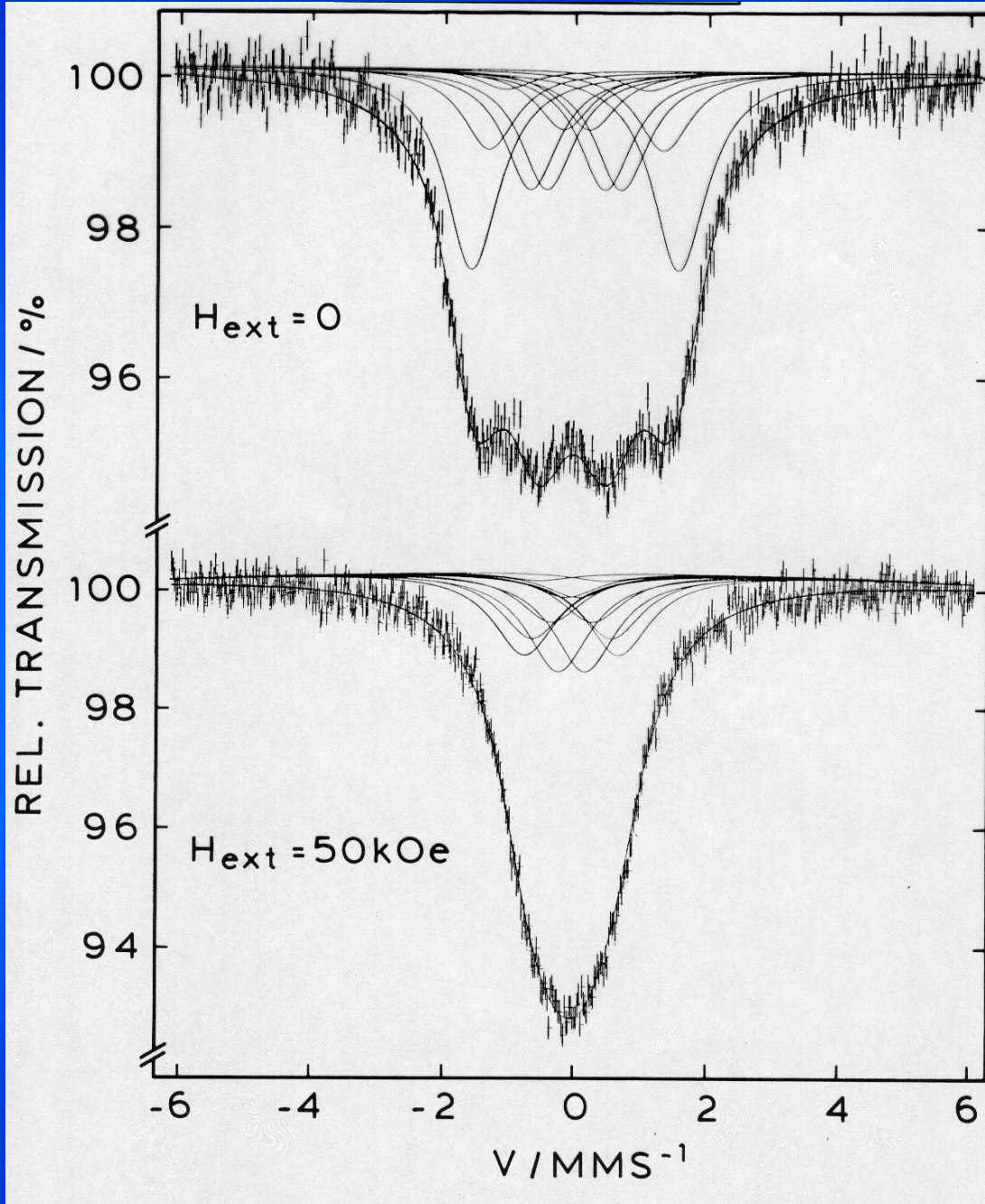


← Applied field
 $H_{\text{ext}} = 0$

← Applied field
 $H_{\text{ext}} = 48 \text{ kOe}$
increases internal
field

Gütlich, Hasselbach,
Rummel, Spiering,
J. Chem. Phys. 81 (1984) 1396

NiFe_2O_4 (Ni in octahedral sites)



← Applied field
 $H_{\text{ext}} = 0$

← Applied field
 $H_{\text{ext}} = 50 \text{ kOe}$
reduces internal
field

Gütlich, Hasselbach,
Rummel, Spiering,
J. Chem. Phys. **81** (1984) 1396

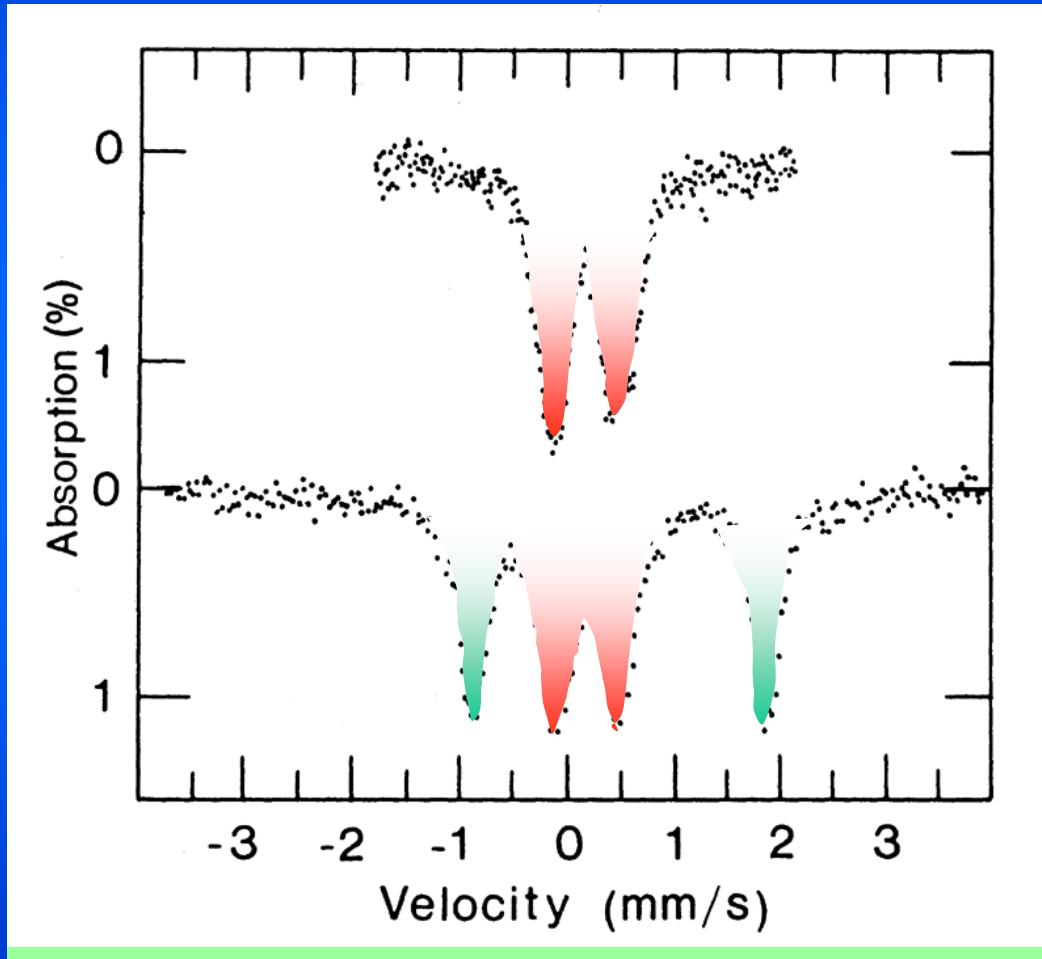
Results:

Ni²⁺(tet) : H_{hf} = + 44.5 T (positive)

Ni²⁺(oct) : H_{hf} = - 9.1 T (negative)

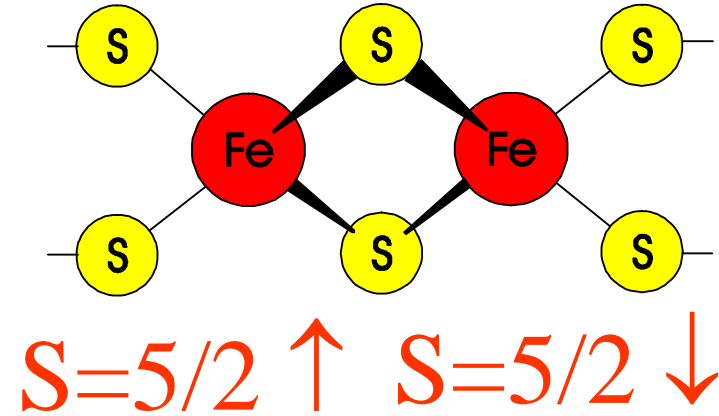
Bioinorganic Compounds

Ferredoxin (green alga) Two-Iron Center Protein

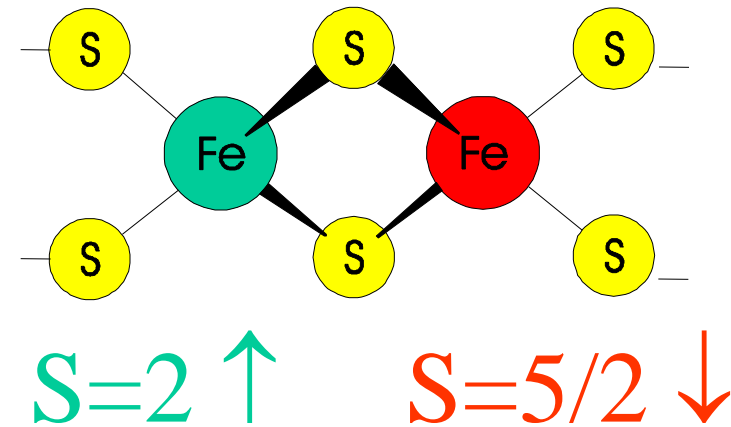


C. E. Johnson et al. (1971)

Oxidized



Reduced

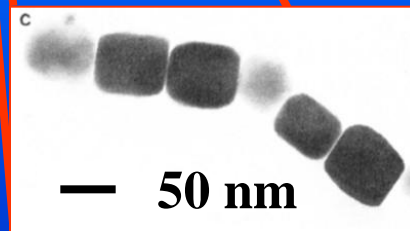
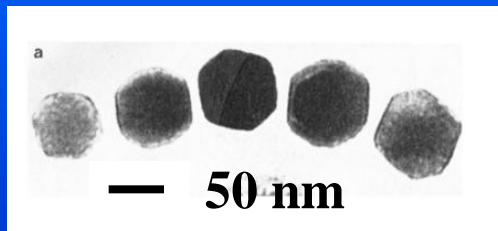


Bioinorganic chemistry is another discipline where Mössbauer spectroscopy has widely been employed by chemists and physicists. Early Mössbauer effect studies by Johnson et al. of Ferredoxin, the two-iron centre of proteins, demonstrate convincingly, as seen in this picture, that the oxidized form with two Fe(III)-high spin centres can be distinguished from the reduced form with one Fe(III)-high spin centre and one Fe(II)-high spin centre.

Fe_3O_4 in Magnetotactic Bacteria

Aquaspirillum Magnetotacticum

Biomagnetic compass:
Microorganisms
follow the geomagnetic
field due to magnetic
particles (40 – 120 nm)



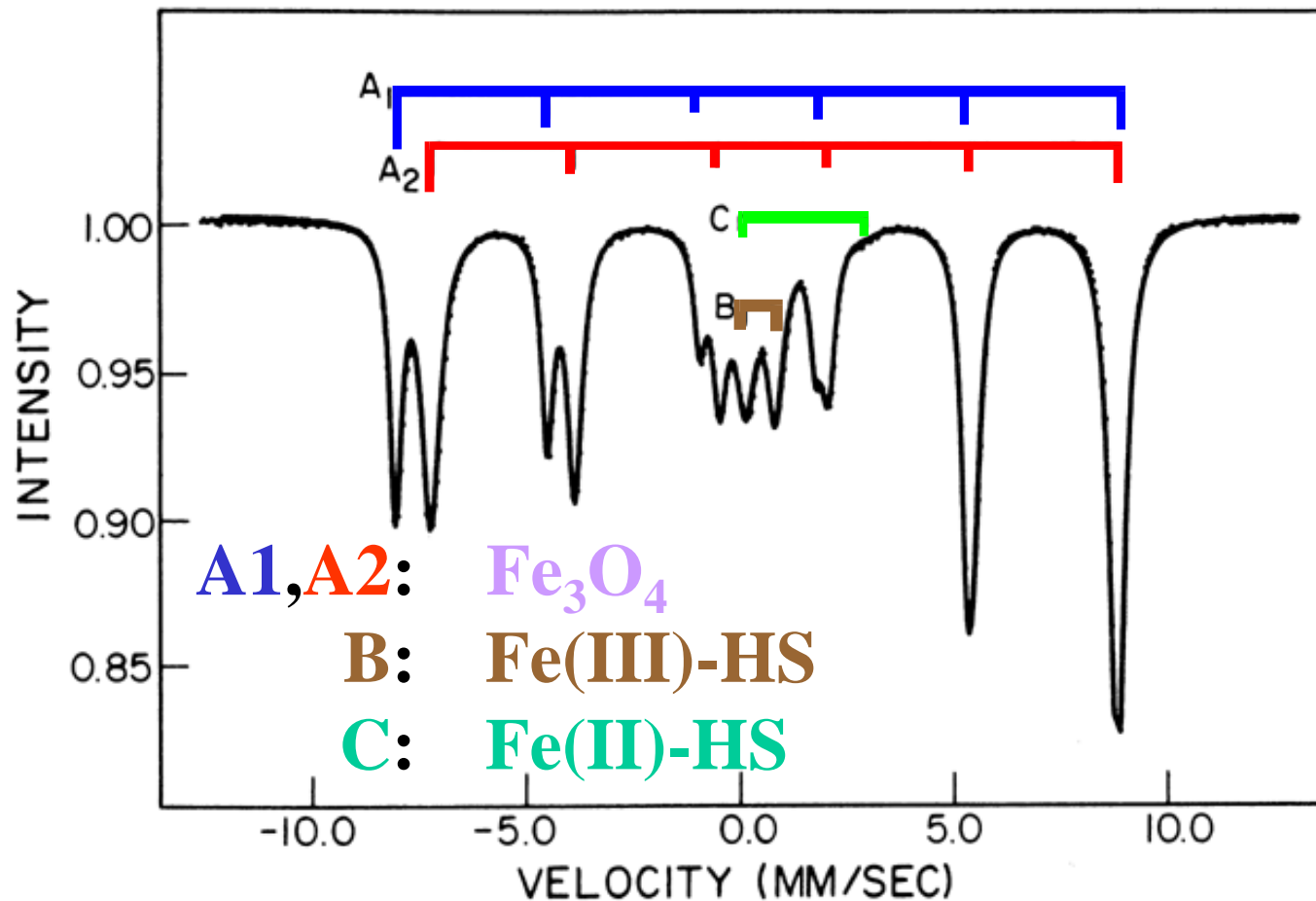
Hexagonal

Cubic

Frankel and Papaefthymiou have investigated the iron containing material in the microorganisms *Aquaspirillum Magnetotacticum*, which are sensitive to the geomagnetic field due to magnetic particles as a kind of biomagnetic compass. The hexagonal and cubic magnetic particles are 40 - 120 nm in size and their chemical nature has been identified by Mössbauer spectroscopy as magnetite, Fe_3O_4 .

^{57}Fe Mössbauer Spectrum of Magnetic Particles in Magnetotactic Bacteria

Frankel, Papaefthymiou, 1983:



Magnetite is a so-called inverse spinel of formula $\text{Fe}^{\text{III}}_{\text{tet}}[\text{Fe}^{\text{II}}\text{Fe}^{\text{III}}]_{\text{oct}}\text{O}_4$. The oxygen atoms form a cubic lattice structure with tetrahedral and octahedral sites. Half of the iron(III) atoms are accommodated in tetrahedral sites, the other half and all of the iron(II) atoms occupy octahedral sites. The ^{57}Fe -Mössbauer spectrum typically shows two magnetic sextets (blue and red), which strongly overlap. One of the sextets arises from the iron atoms in tetrahedral sites and the other one from the iron atoms in octahedral sites. At room temperature and down to ca. 200 K there is fast electron fluctuation between Fe^{2+} and Fe^{3+} ions in octahedral sites giving a time-averaged species with only one magnetic sextet. The components B and C observed in the Mössbauer spectrum refer to paramagnetic compounds from which the magnetite particles are grown in the microorganisms.

Thermal, Optical and Pressure-induced Spin State Switching of Iron Compounds



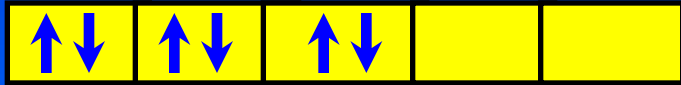
Application in Molecular Devices

Thermal spin transition (spin crossover) is another facet of dynamic electronic structure phenomena that, although first established already several decades ago, in recent years has attracted increasing attention by chemists and physicists because of the promising potential for practical applications in sensors and display devices. Thermally induced spin state transition from a high spin (HS) state with maximum unpaired electrons to a low spin (LS) state with minimum unpaired electrons occurs in coordination compounds with d^4 up to d^7 electron configurations, if the difference between the free energies of the HS and the LS states are comparable to thermal energy: $\Delta E_{\text{HL}} \approx k_{\text{B}}T$ (k_{B} = Boltzmann constant). A large number (a few hundred) of compounds have been synthesized and characterized by now. Among the various physical techniques that are employed to investigate the spin state switching processes in solid material, ^{57}Fe Mössbauer spectroscopy has become one of the most valuable tools.

Thermal spin transition (thermal spin crossover) occurs quite frequently in coordination compounds of iron(II), iron(III) and cobalt(II). The following picture sketches the phenomenon in the case of iron(II) compounds with 6 electrons in the 3d valence shell.

Iron(II), 3d⁶

3d Orbitals



$$S = 0$$

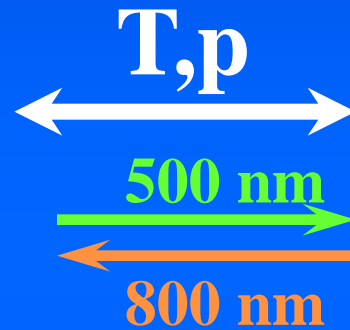
“Low Spin”
diamagn.

3d Orbitals



$$S = 2$$

“High Spin”
paramagn.



Spin Crossover
(Spin Transition)

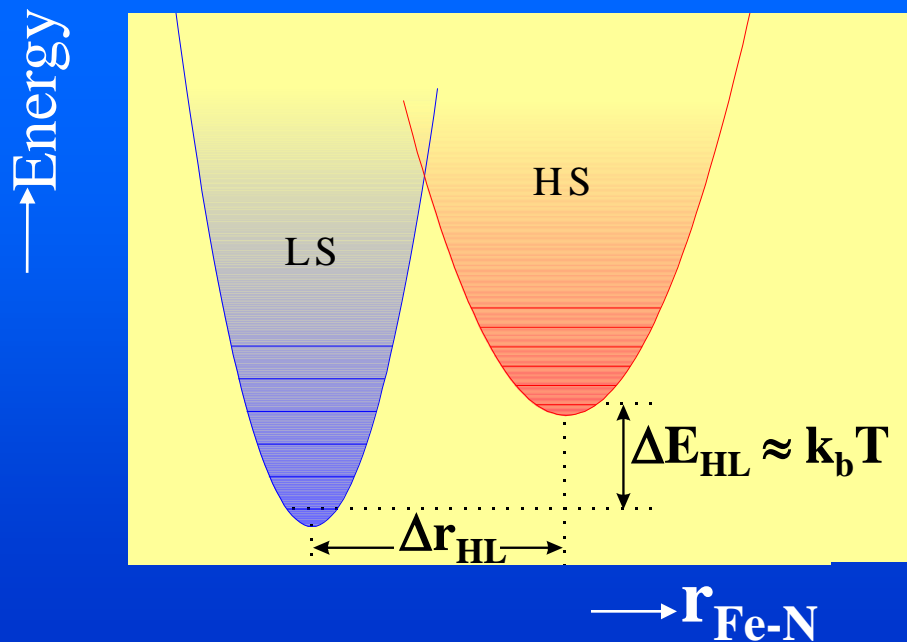
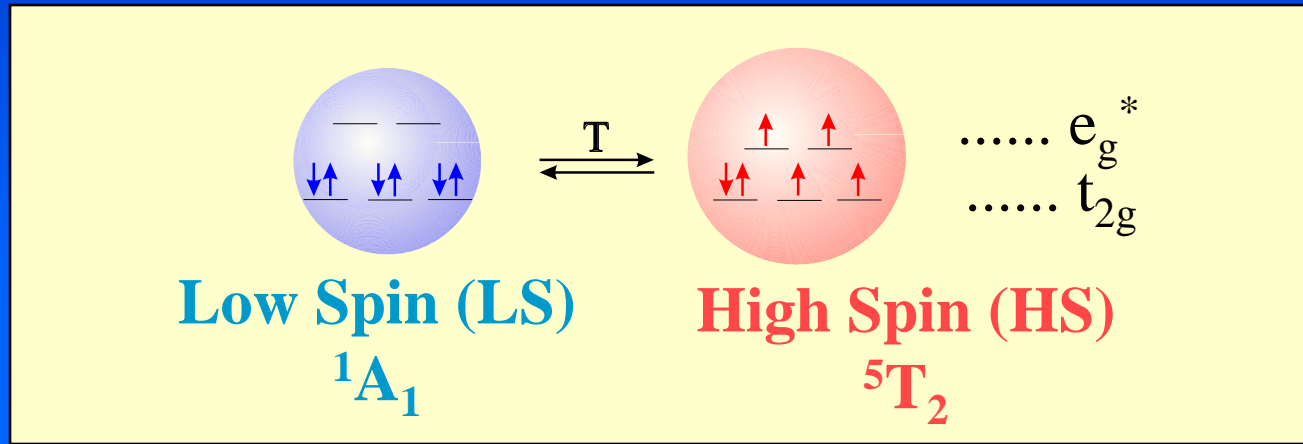


This cartoon introduces on an elementary level the spin crossover phenomenon in Fe(II) complexes with $3d^6$ valence electron configuration. In iron(II) compounds with relatively weak ligands coordinated to the iron ions, e.g. water molecules, the 3d electrons are accommodated spin-free according to Hund's rule of maximum spin of $S = 2$. Such compounds, called *high spin complexes*, are paramagnetic and are generally weakly coloured. In Fe(II) compounds with relatively strong ligands like CN^- ions, the six electrons are arranged spin-paired with total spin $S = 0$. Such compounds are called *low spin complexes*; they are generally diamagnetic and somewhat coloured. If the right kinds of ligands are chosen, e.g. derivatives of tetrazole or triazole, one may observe spin state transition solely by varying the temperature, applying pressure or under irradiation with light as shown in the cartoon.

Thermal spin crossover in iron(II) compounds is reflected by changes in the electron configuration. In the notation of ligand field theoretical concepts, the electron configuration changes from $(t_{2g})^4(e_g)^2$ in the HS state to $(t_{2g})^6$ in the LS state. This *phase transition* between *paramagnetic* and (nearly) *diamagnetic* is easily detected by magnetic susceptibility measurements. As the colour changes simultaneously, too, the transition from one spin state to the other is also easily detected by optical means. As indicated in the picture, the spin transition can also be affected by applying external pressure or by irradiating the material with light, where green light converts the LS to the HS state and red light the HS to the LS state. The light-induced spin state switching has become known as LIESST and reverse-LIESST (LIESST = Light-Induced Excited Spin State Switching).

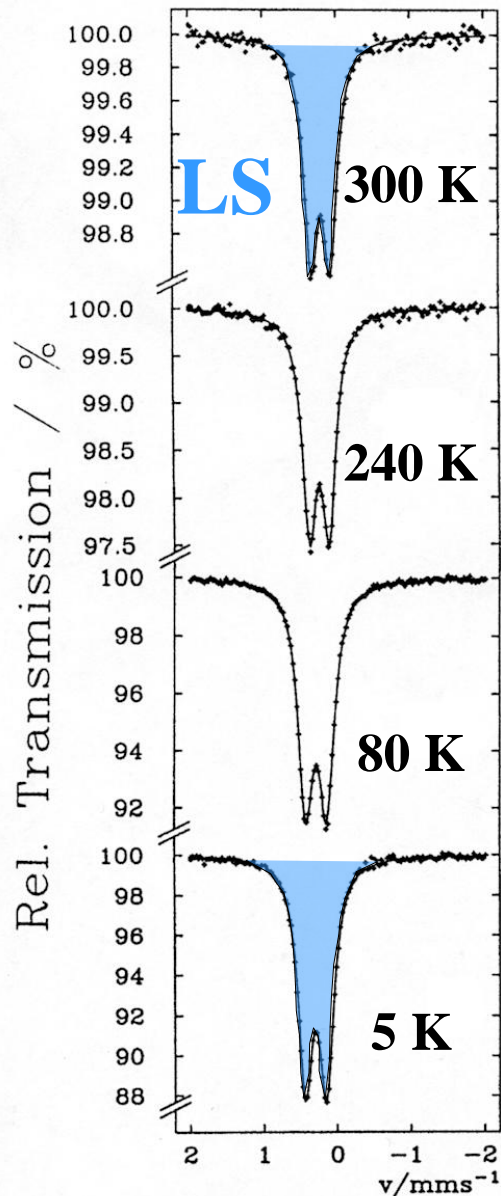
The condition that has to be met in order to observe thermal spin crossover is sketched in the next viewgraph using the orbital term symbols known from ligand field theory.

Condition for Thermal Spin Crossover in Iron(II) Compounds

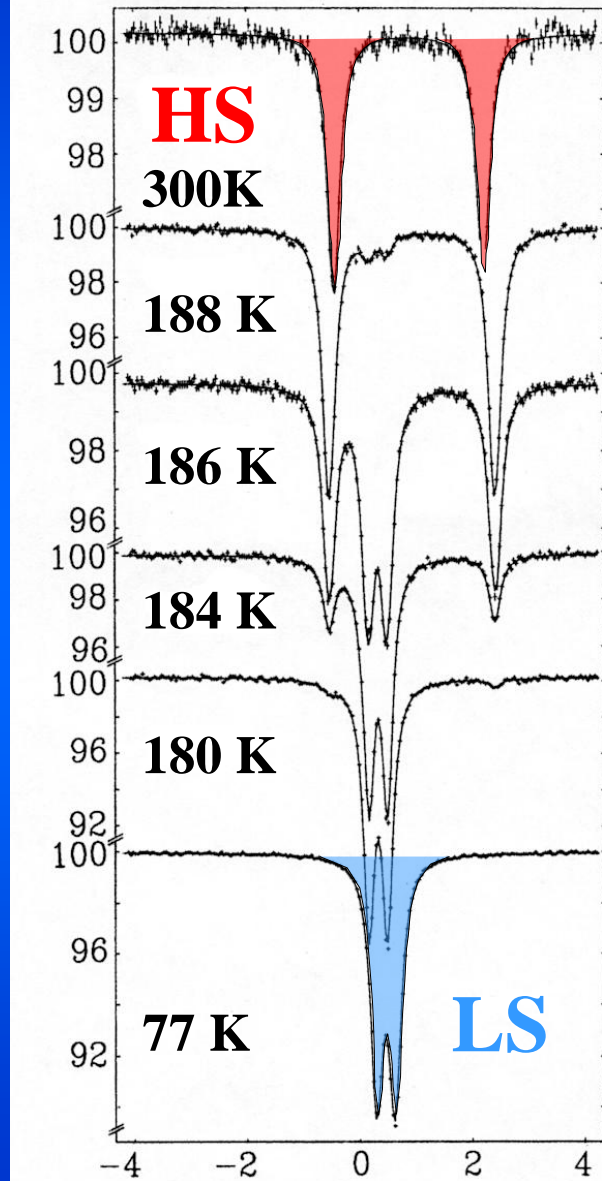


Thermal spin crossover may be observed if the ligand field strength of an iron(II) compound is such that the difference between the lowest “vibronic” energy levels of the high spin state 5T_2 and the low spin state 1A_1 state is comparable with thermal energy $k_B T$ (k_B = Boltzmann constant). The spin transition behaviour can be influenced by chemical alteration, e.g. ligand replacement, change of non-coordinating anion and solvent molecule, substitution of spin state changing metal by another metal, e.g. substitution of iron by zinc. It can also be influenced by physical perturbation such as irradiation with light, applying pressure and a magnetic field. For a comprehensive coverage of chemical and physical influences on the spin transition behaviour see: Gütlich, P.; Hauser, A.; Spiering, H. *Angew. Chem. Int. Ed. Engl.* **1994**, *33*, 2024.

The influence of the ligand molecules on the spin state of the central iron(II) ions is demonstrated with the two examples and their temperature dependent Mössbauer spectra shown in the following picture

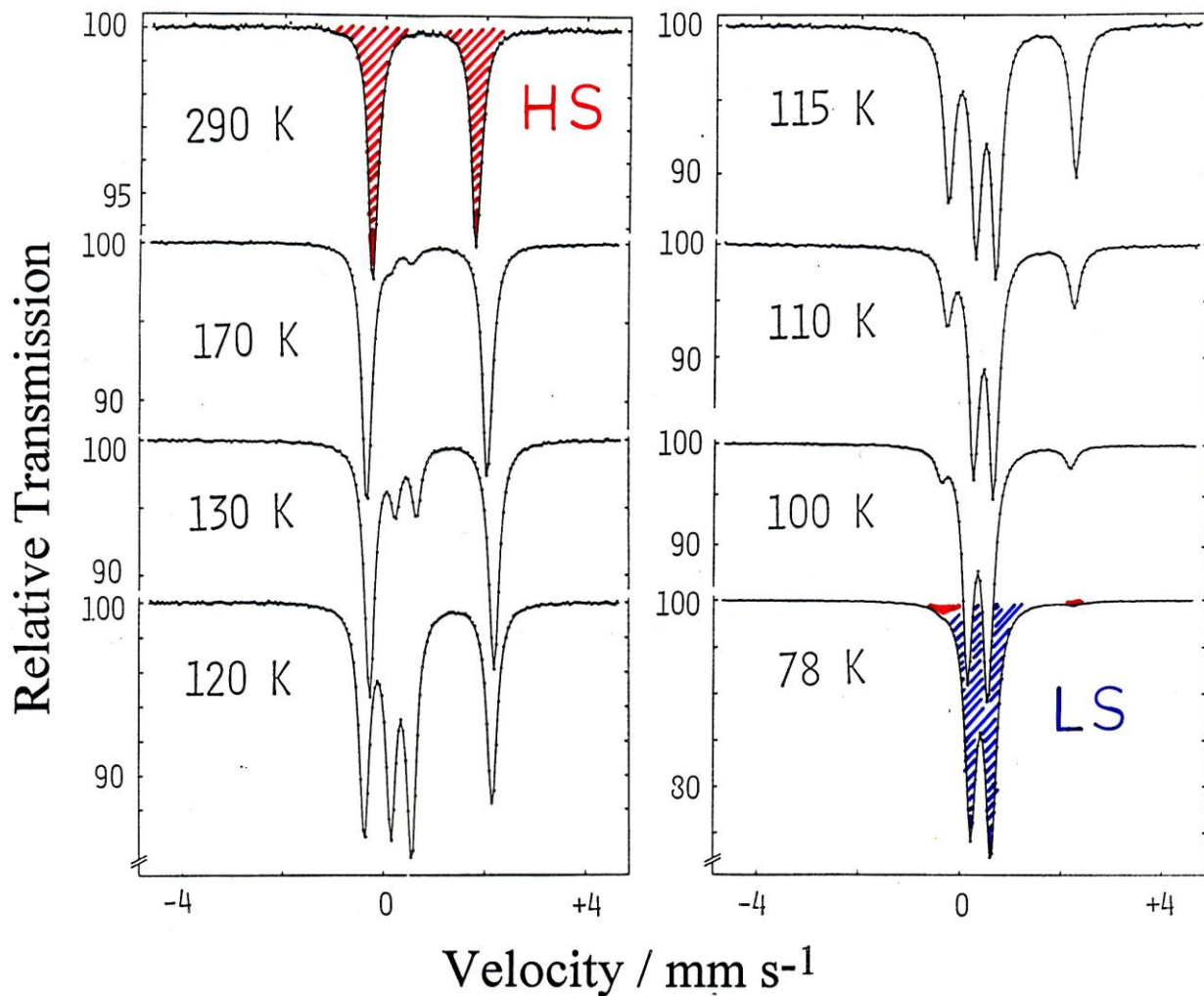


Fine Tuning the
Ligand Field
by Ligand
Replacement

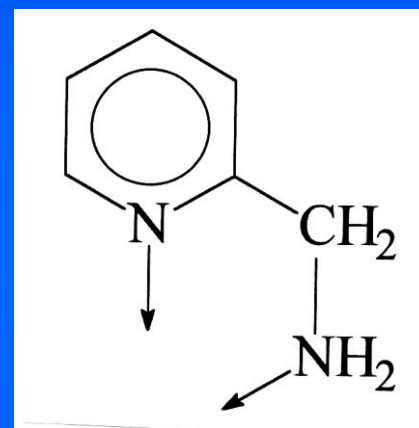


$[\text{Fe}^{\text{II}}(\text{phen})_3]\text{X}_2$ (phen = 1.10-phenanthroline) is a typical low spin compound with the characteristic Mössbauer spectra as shown on the left; the isomer shift is ca. 0.2 and the quadrupole splitting ca. 0.5 mm s⁻¹, nearly independent of temperature. If one of the relatively strong phen ligands, which occupies two coordination positions of the octahedron, is replaced by two monofunctional NCS⁻ groups, the average ligand field strength becomes weaker than the mean spin pairing energy and the compound $[\text{Fe}^{\text{II}}(\text{phen})_2(\text{NCS})_2]$ adopts high spin character at room temperature. The Mössbauer spectrum at 300 K shows the typical features of an iron(II) HS compound with isomer shift of ca. 1 mm s⁻¹ and large quadrupole splitting of ca. 3 mm s⁻¹. However, the compound $[\text{Fe}^{\text{II}}(\text{phen})_2(\text{NCS})_2]$ fulfils the condition for thermal spin crossover to occur, viz. $\Delta E_{\text{HL}} \approx k_{\text{B}}T$. As the temperature is lowered, the compound changes spin state from high spin to low spin near 180 K as is well documented by the Mössbauer spectra as a function of temperature, which was first reported by I. Dezsi et al. in 1967. Since then more than 200 spin crossover compounds of iron(II) and iron(III) have been studied by Mössbauer spectroscopy (see e.g. P. Gütlich, H.A. Goodwin (eds.), *Spin Crossover in Transition Metal Compounds*, Springer Series "Topics in Current Chemistry, Vol. 233, 234, 235, Berlin Heidelberg 2004).

$[\text{Fe}(\text{2-pic})_3]\text{Cl}_2 \cdot \text{EtOH}$

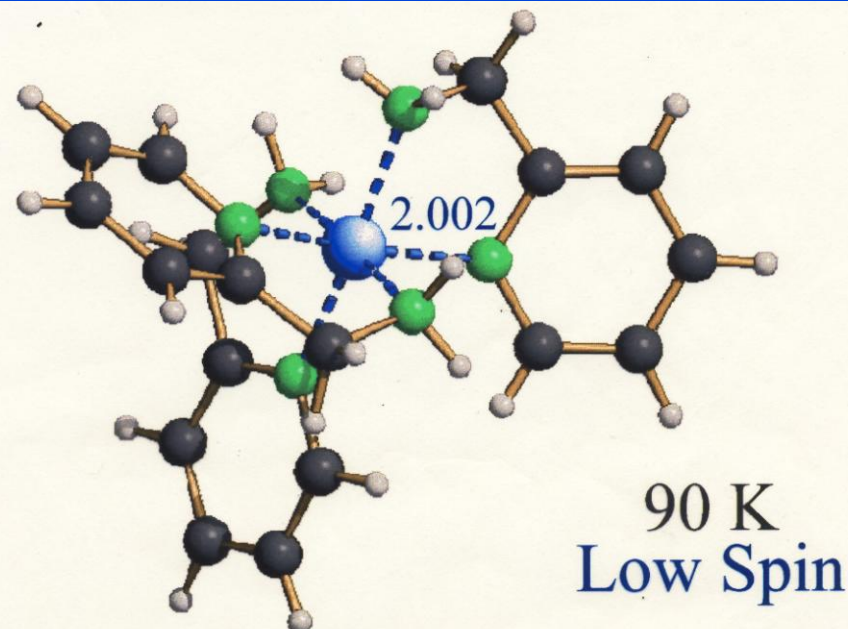
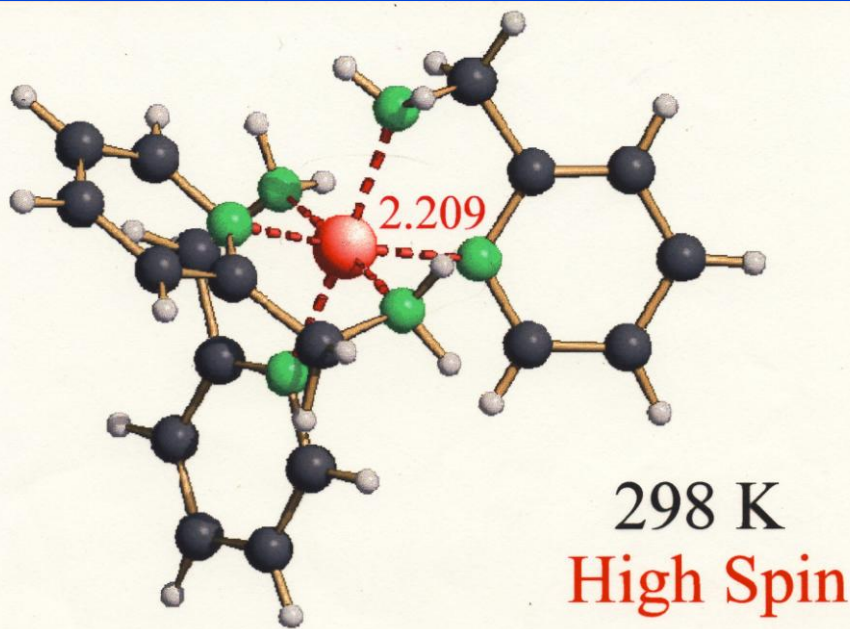


2-pic =
2-picolylamine =
2-aminomethylpyridine



M Sorai, J. Ensling,
P. Gülich
Chem. Phys. 18 (1976) 199

$[\text{Fe}(\text{2-pic})_3]\text{Cl}_2 \cdot \text{EtOH}$



- Monoclinic with space group P21/c in HS and LS state.
- The considerable contraction of the Fe-N(pyr) bond in the LS state is mainly due to π -backbonding.

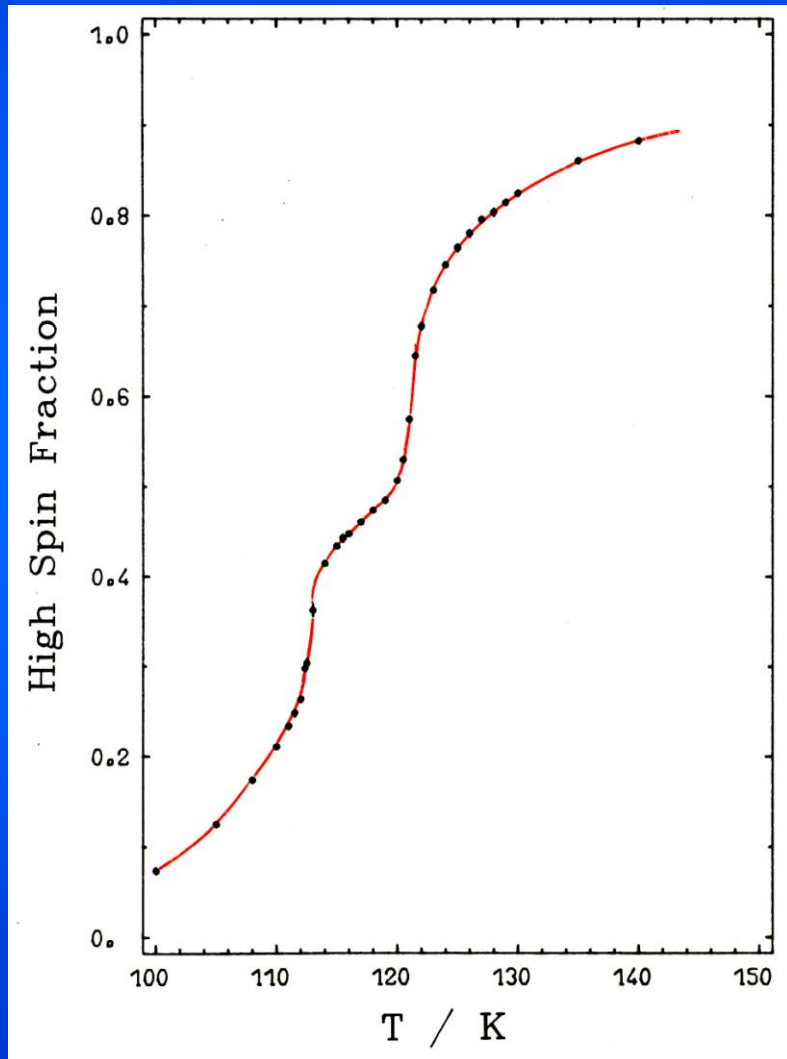
M. Mikami, M. Konno, Y. Saito, *Acta Crystallogr.*, B36 (1980) 275

[Fe(2-pic)₃]Cl₂·EtOH

First observation of “two-step” SCO

by

Mössbauer spectroscopy



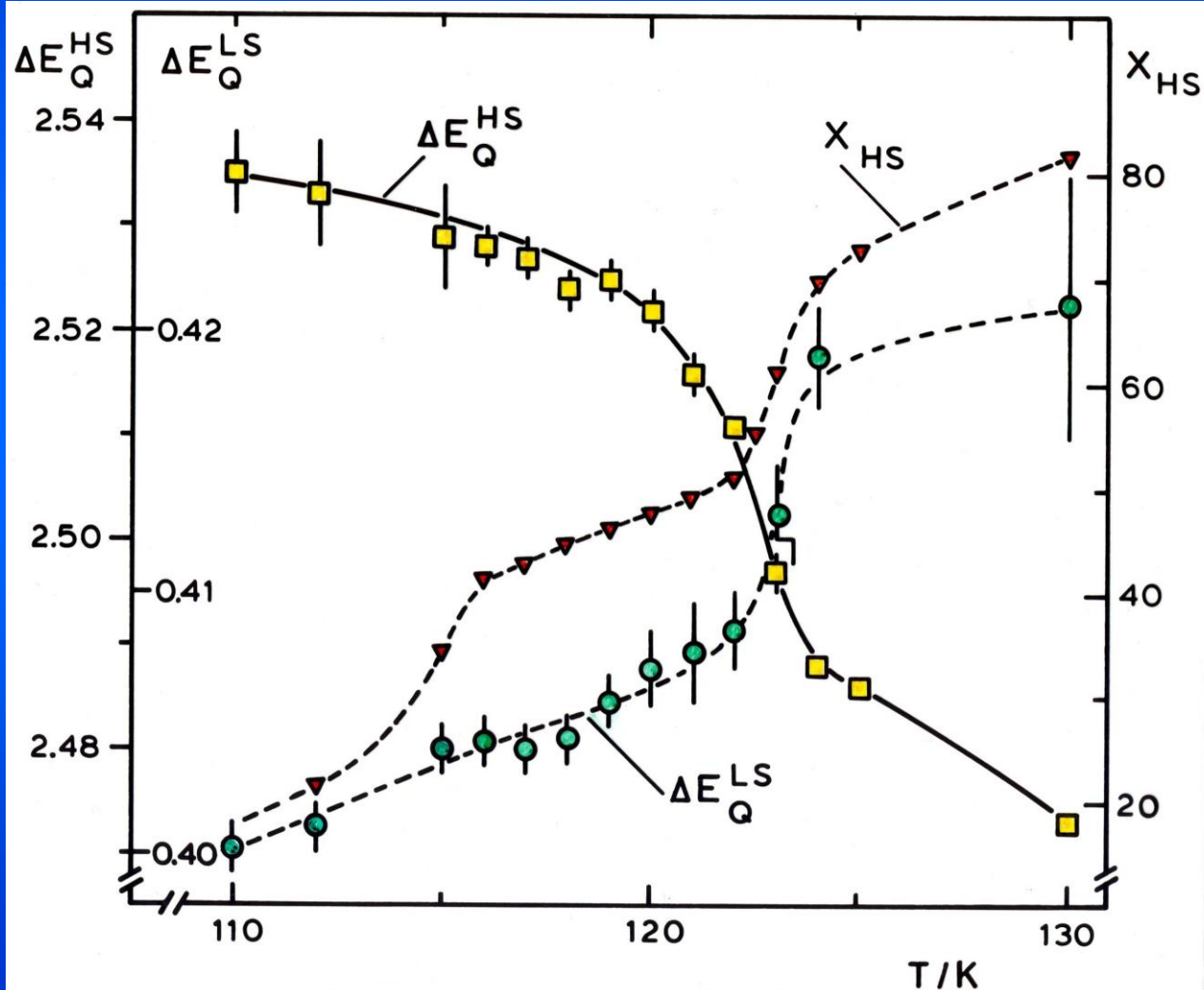
Origin of the step:

- Ordering between HS and LS molecules in the transition region
(R. Jakobi, H. Spiering, P. Gütlich, *J. Phys. Chem. Solids* 53 (1992) 267)
- Formation of “intermediate structural phase”
(H.B. Bürgi et al., *Angew. Chem. Inter. Ed.* 42 (2003) 3825)

H. Köppen, E.W. Müller, C.P. Köhler,
H. Spiering, E. Meissner, P. Gütlich
Chem. Phys. Lett. 91 (1982) 348

[Fe(2-pic)₃]Cl₂·EtOH

First observation of “two-step” SCO

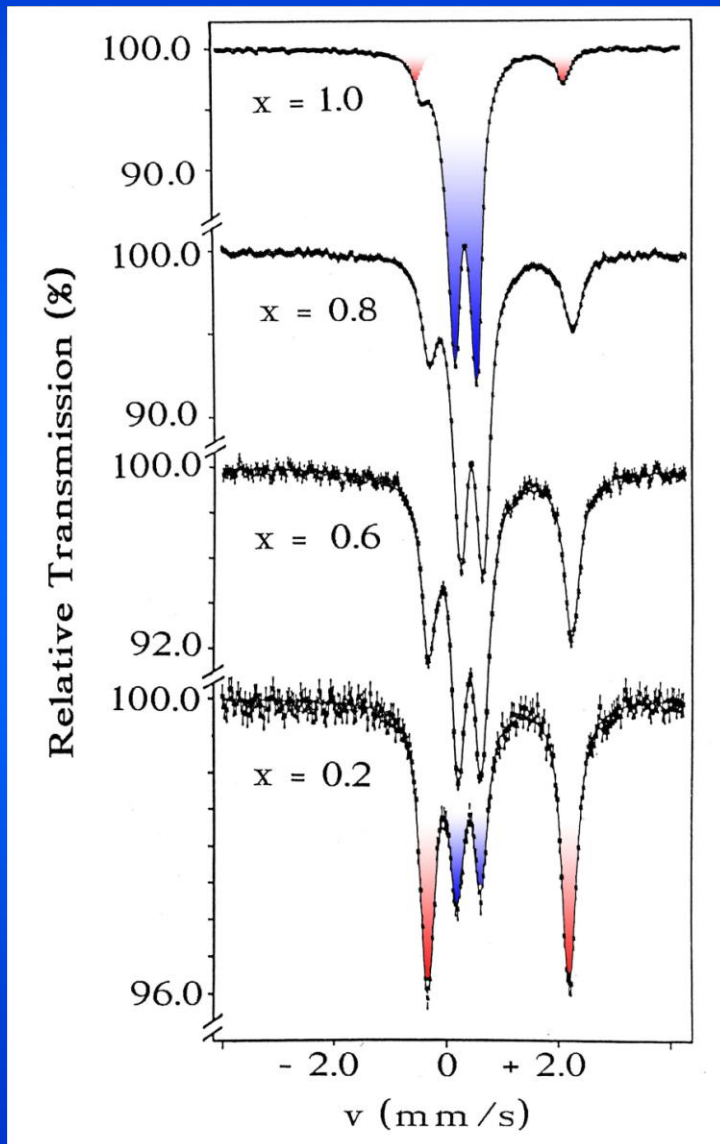


The quadrupole splitting of the HS and the LS state change abruptly in the region of the step.

H. Köppen, E.W. Müller,
C.P. Köhler, H. Spiering,
E. Meissner, P. Gütlich
Chem. Phys. Lett. 91 (1982)
348

$[\text{Fe}_x\text{Zn}_{1-x}(\text{2-pic})_3]\text{Cl}_2 \cdot \text{EtOH}; T = 100 \text{ K}$

Effect of metal dilution Mössbauer spectra recorded at 100 K



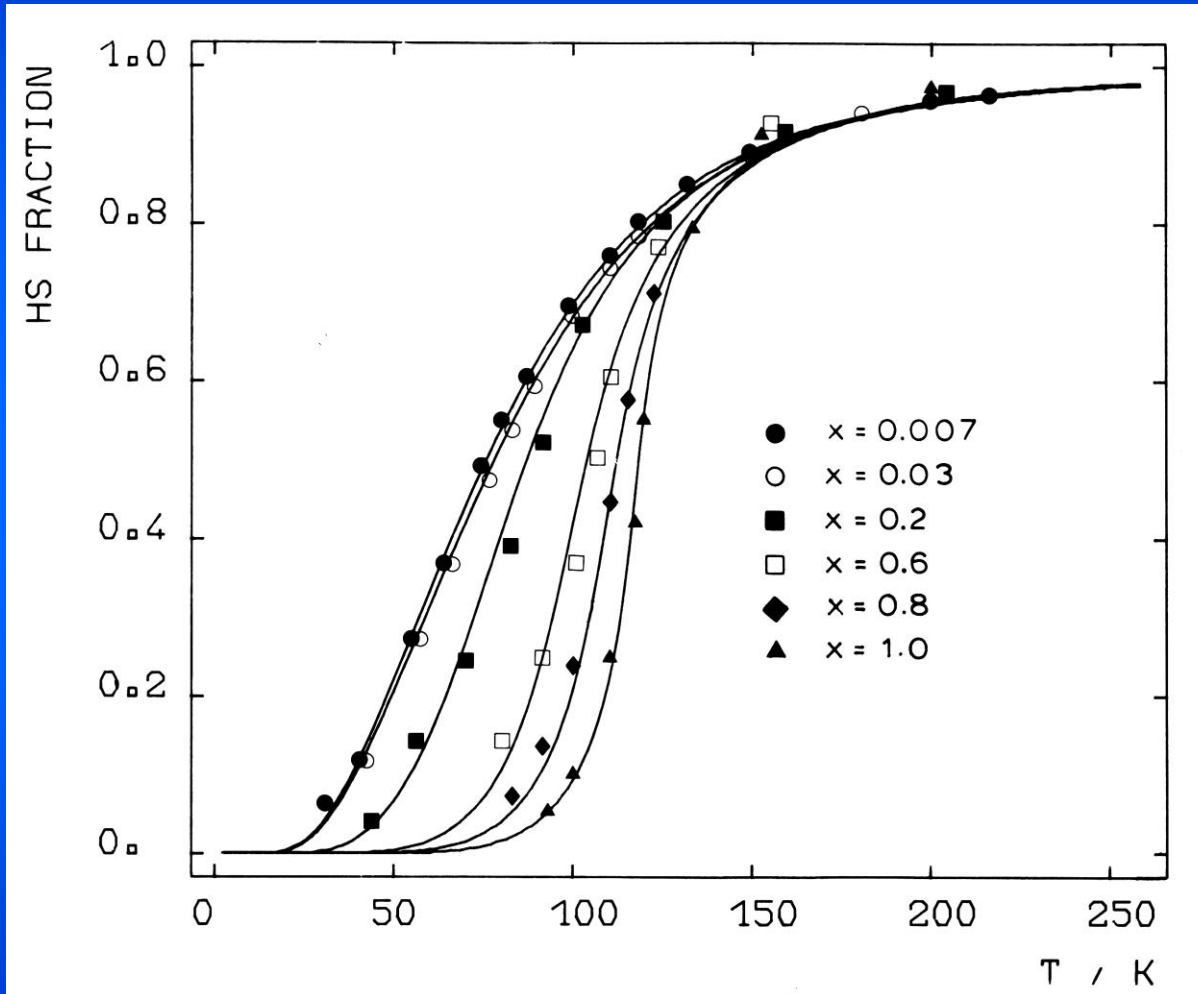
Note:

- The Zn compound is isomorphous with the iron compound.
- With decreasing iron concentration x the intensity of the quadrupole doublet of the HS state (outer two lines) increases.

M Sorai, J. Enslin, P. Gütlich
Chem. Phys. 18 (1976) 199

$[\text{Fe}_x\text{Zn}_{1-x}(\text{2-pic})_3]\text{Cl}_2 \cdot \text{EtOH}$

Molar fraction $\gamma_{\text{HS}}(\text{T})$ as function of T and iron content x



$\gamma_{\text{HS}}(\text{T})$ becomes more gradual and is shifted to lower T with decreasing x.



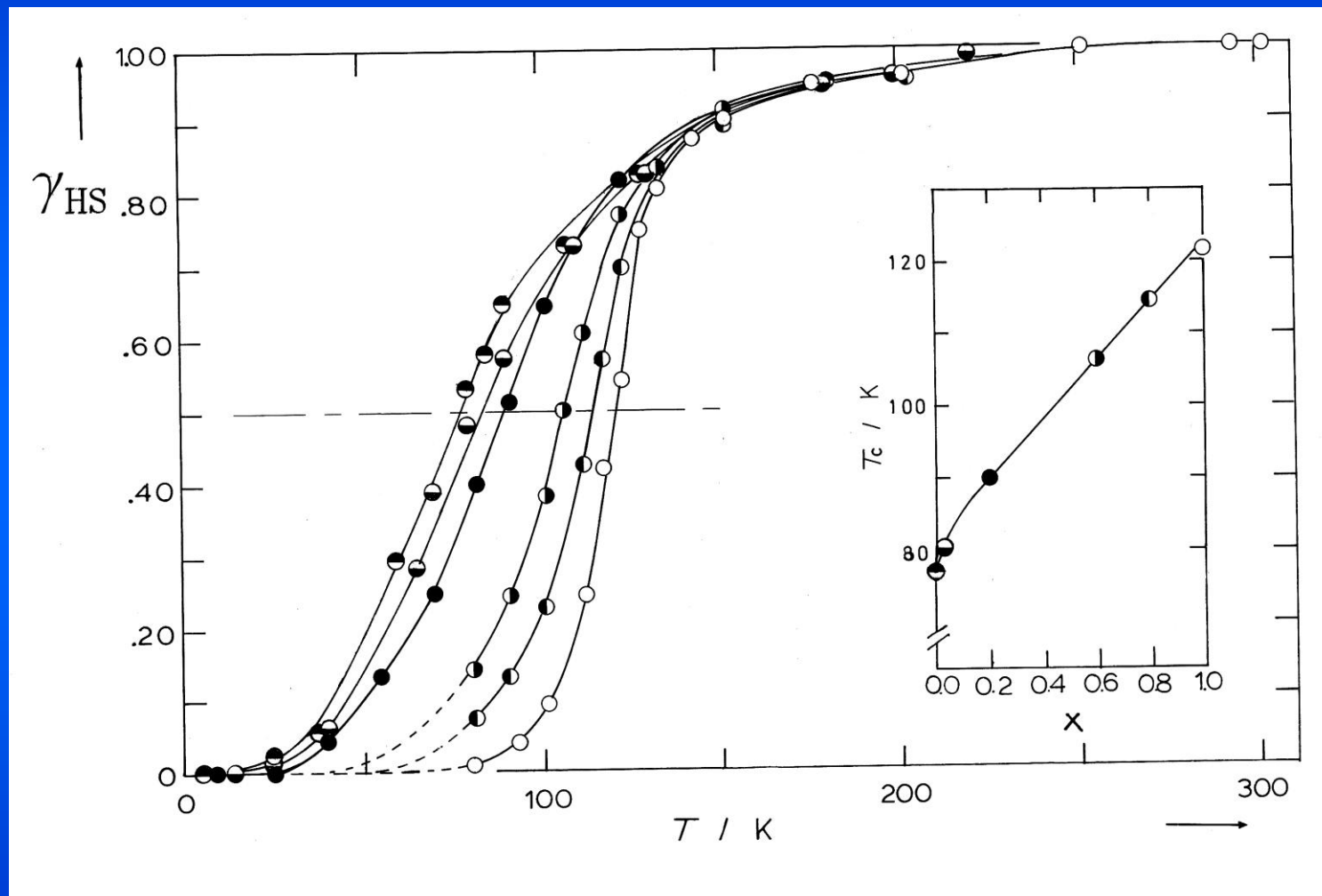
HS state is stabilised with increasing dilution by zinc.

M Sorai, J. Ensling, P. Gütlich, Chem. Phys. 18 (1976) 199

P. Gütlich, R. Link, H.G. Steinhäuser, Inorg. Chem. 17 (1978) 2509

$[\text{Fe}_x\text{Zn}_{1-x}(\text{2-pic})_3]\text{Cl}_2 \cdot \text{EtOH}$

Molar fraction $\gamma_{\text{HS}}(T)$ as function of T and iron content x



M Sorai, J. Enslin, P. Gütlich, Chem. Phys. 18 (1976) 199

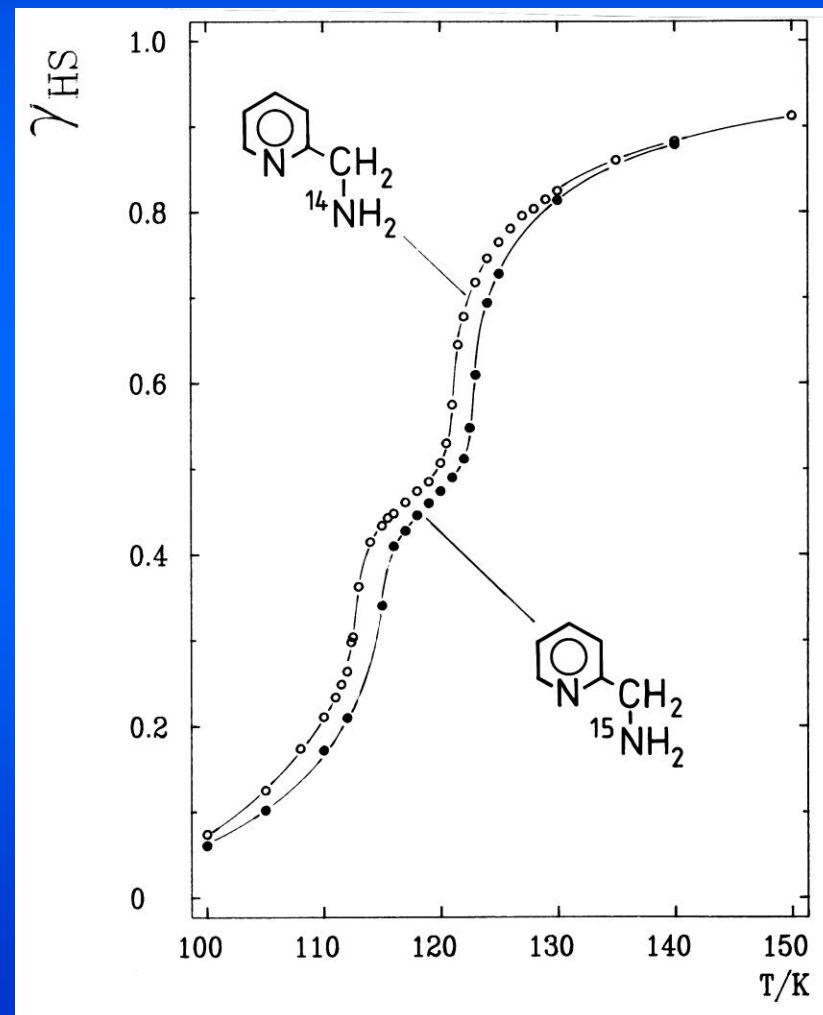
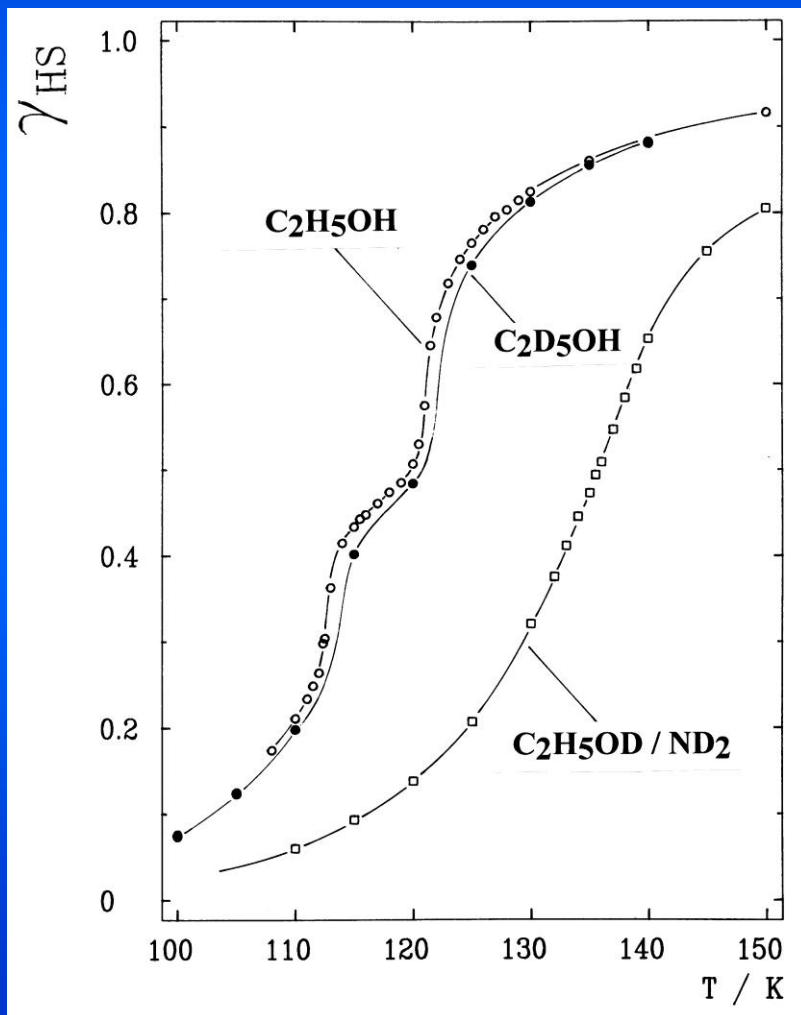
P. Gütlich, R. Link, H.G. Steinhäuser, Inorg. Chem. 17 (1978) 2509

[Fe(2-pic)₃]Cl₂·EtOH

H/D and ¹⁴N/¹⁵N isotopic effects

$\gamma_{\text{HS}}(T)$ from Mössbauer spectra

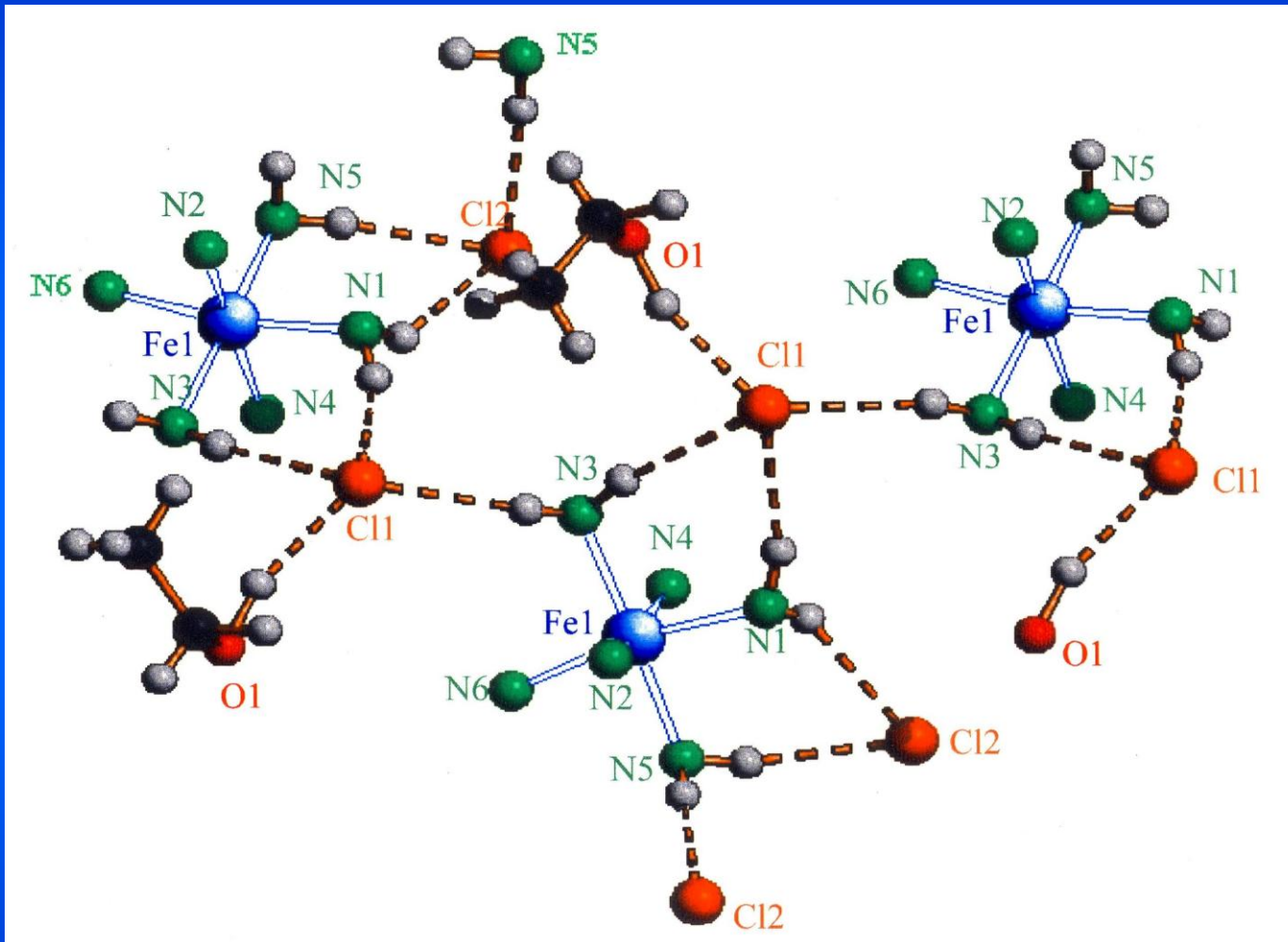
P. Gütlich,
H. Köppen,
H.G. Steinhäuser,
Chem. Phys. Lett.
74 (1980) 475



Note:

- a) When using C_2H_5OD for the H/D substitution, not only the EtOH solvent molecule is replaced, but also the amino groups NH_2 are replaced by ND_2 groups (because of the protic D atoms in EtOD).
- b) When using C_2D_5OH for H/D substitution, this deuterated solvent molecule will be the only deuterated position in the sample.
- c) The H/D isotopic effect is largest in the case of C_2H_5OD/ND_2 , because the positions of substitution are directly built in the hydrogen network, the “communication pathway” from one iron complex to another. In the case of C_2D_5OH , the C_2D_5 group is not directly part of the communication pathway.
- d) The isotopic effect $^{14}N/^{15}N$ is clearly detected. It is, however, considerably less pronounced than the H/D effect because of the much smaller difference in the reduced mass.

[Fe(2-pic)₃]Cl₂·EtOH

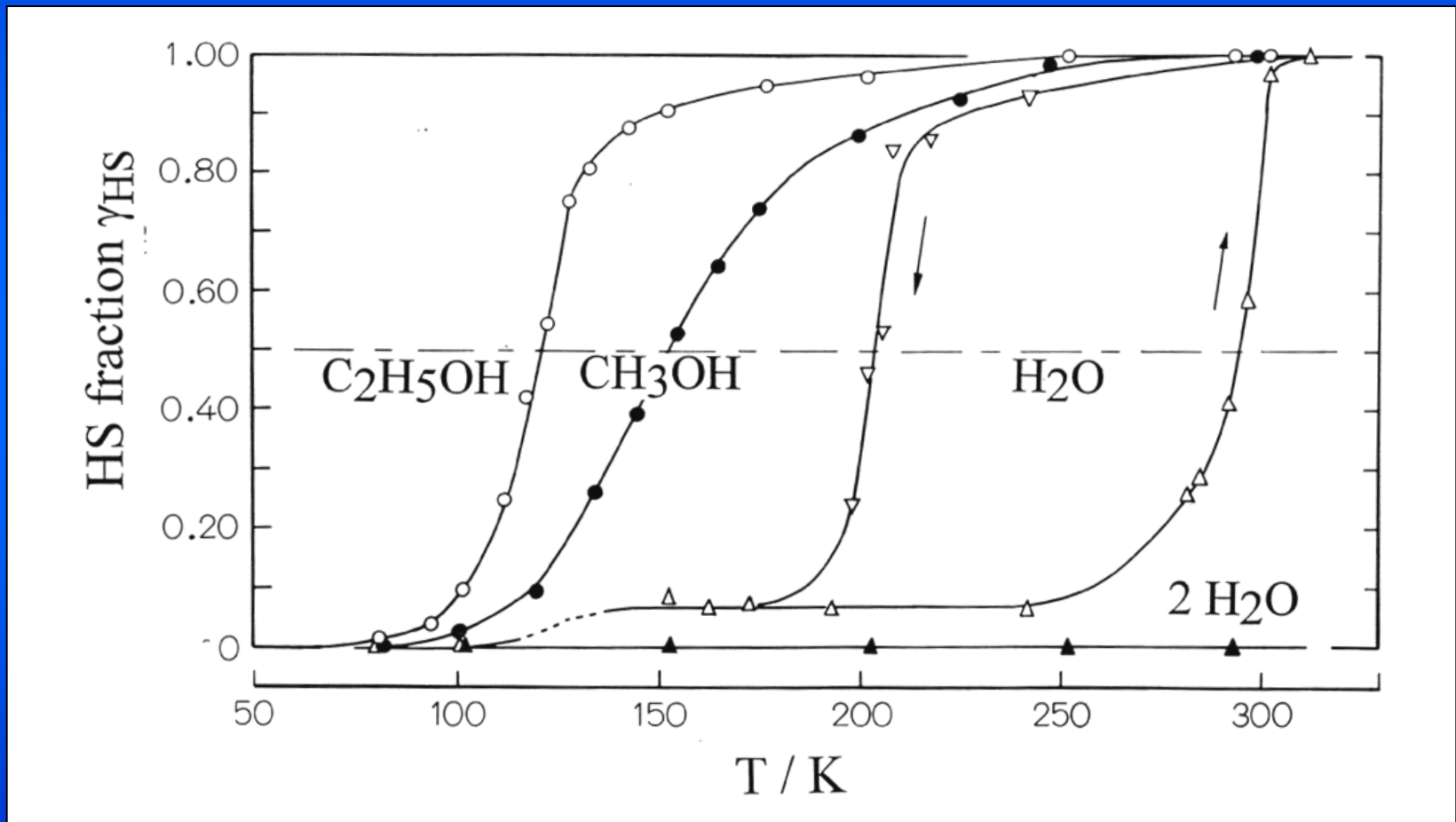


All amino N atoms of the complex are H-bonded to Cl⁻ ions forming a 2-dim. network. The solvate EtOH molecules are H-bonded to Cl⁻ ions.

[Fe(2-pic)₃]Cl₂·Sol

Effect of crystal solvens molecules

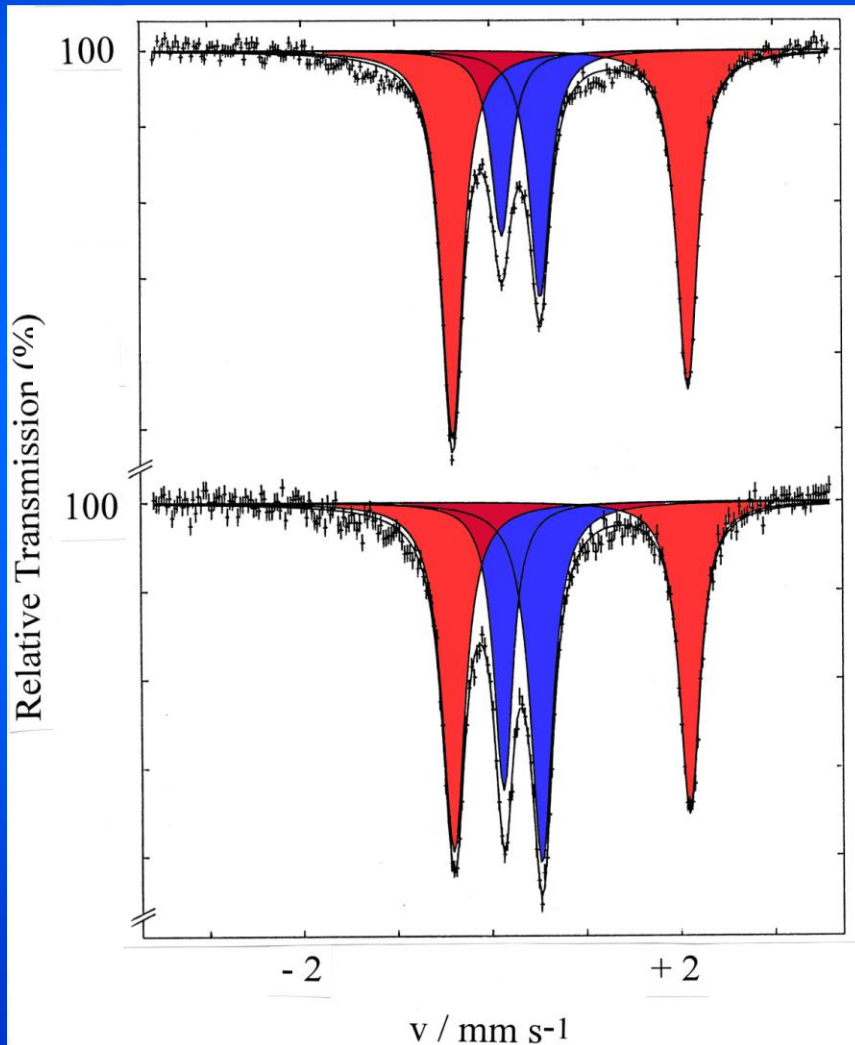
$\gamma_{\text{HS}}(T)$ from Mössbauer spectra



M. Sorai, J. Ensling, K.M. Hasselbach, P. Gülich, Chem. Phys. 20 (1977) 197

$[\text{Fe}(\text{2-pic})_3]\text{Cl}_2 \cdot \text{EtOH}$

Effect of pressure at $T = 125 \text{ K}$

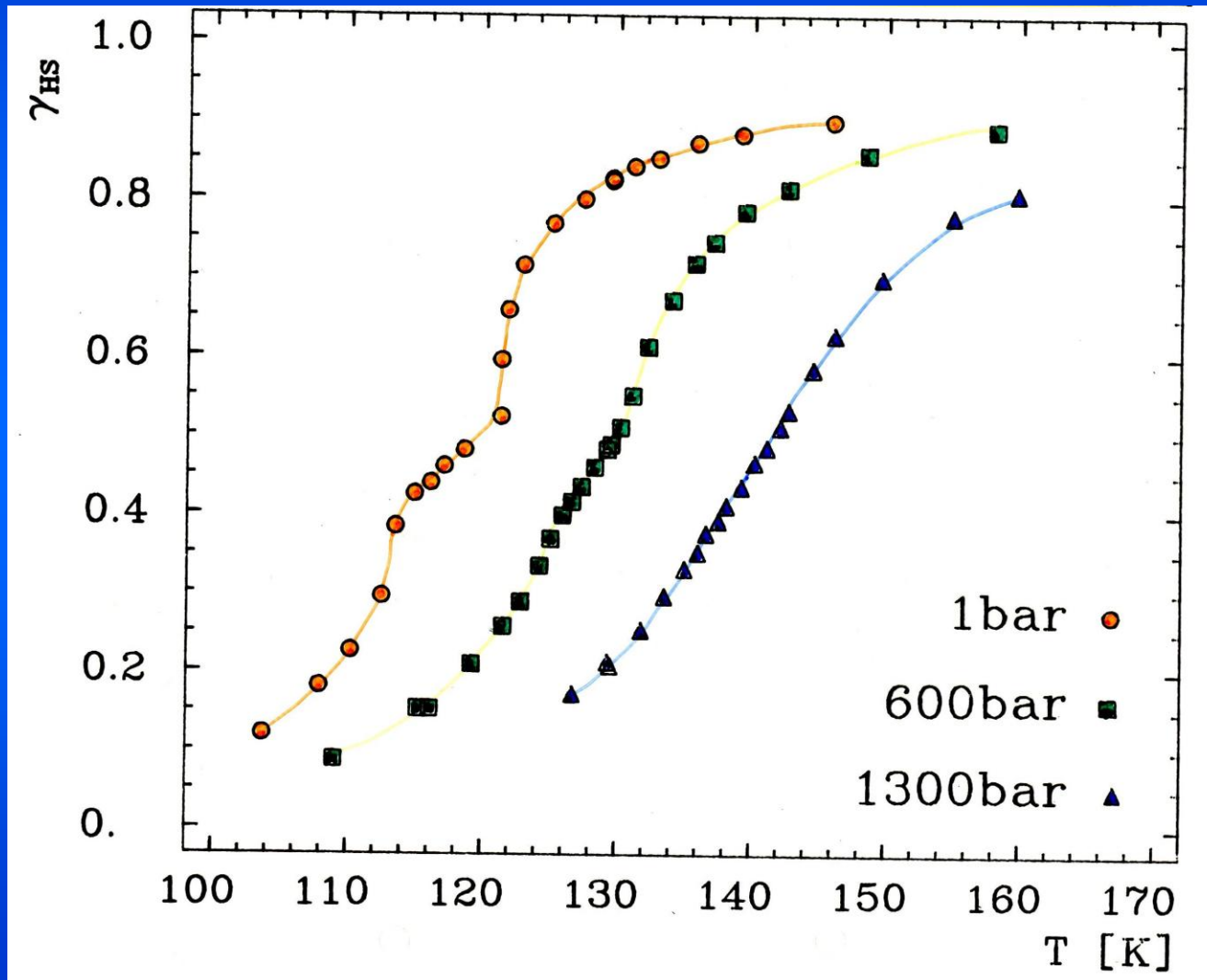


Application of pressure
stabilises the LS state

E. Meissner, H. Köppen, H. Spiering, P. Gülich
Chem. Phys. Lett. 95 (1983) 163

[Fe(2-pic)₃]Cl₂·EtOH

Effect of pressure at variable temperatures



The SCO curve $\gamma_{HS}(T)$ is shifted to higher T , the step disappears under pressure.

E. Meissner, H. Köppen,
H. Spiering, P. Gütlich
Chem. Phys. Lett.
95 (1983) 163

Hydrostatic High Pressure Cells for Magnetic and Mössbauer Studies



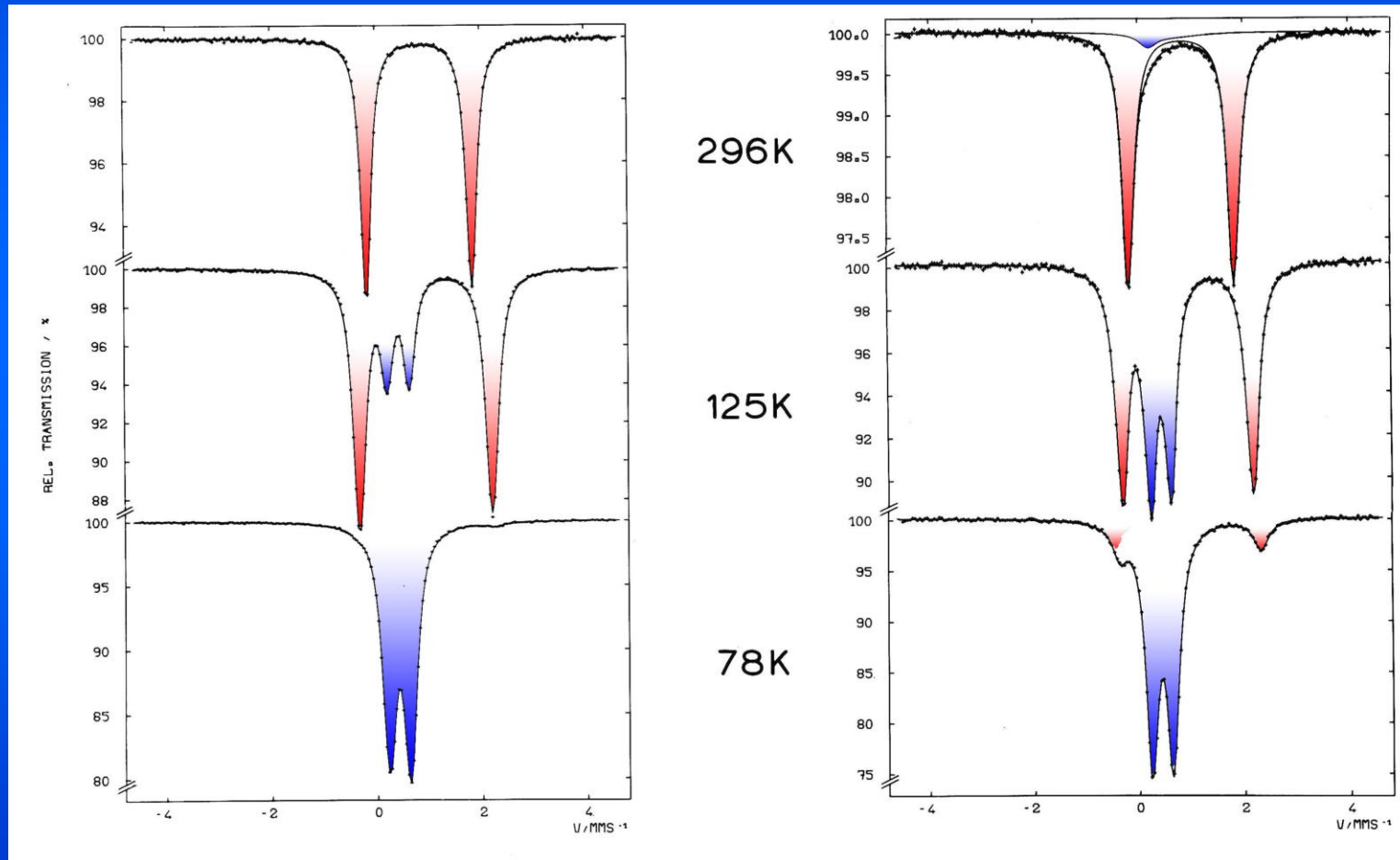
$2 \text{ K} < T < 400 \text{ K}$
 $p < 14 \text{ Kbar}$

[Fe(2-pic)₃]Cl₂·EtOH

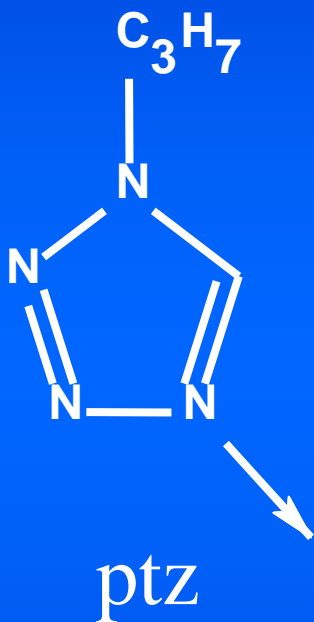
Effect of mechanical treatment (ballmilling)

No treatment

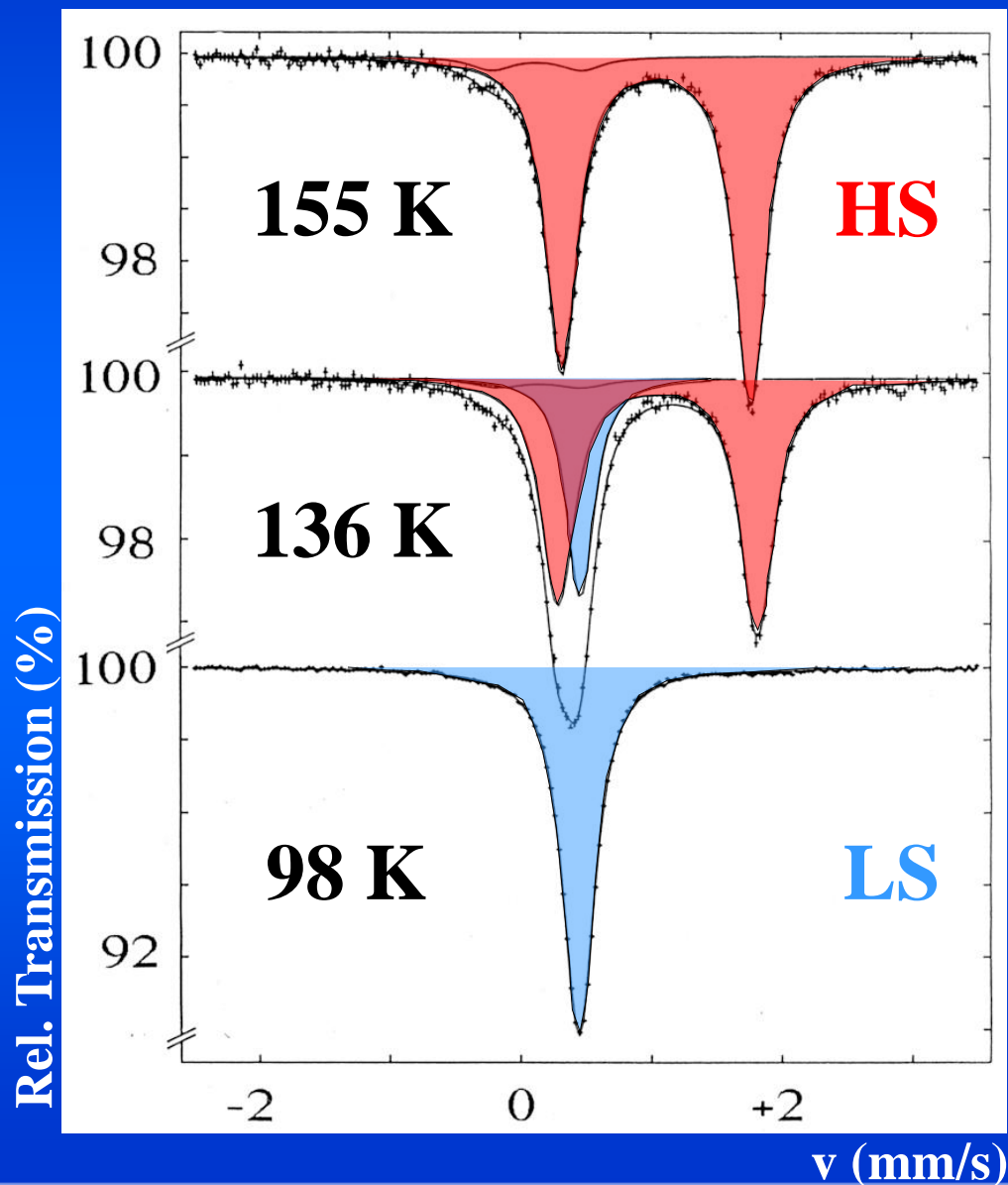
3.5 h Ballmilling



(P. Gülich et al., unpublished)

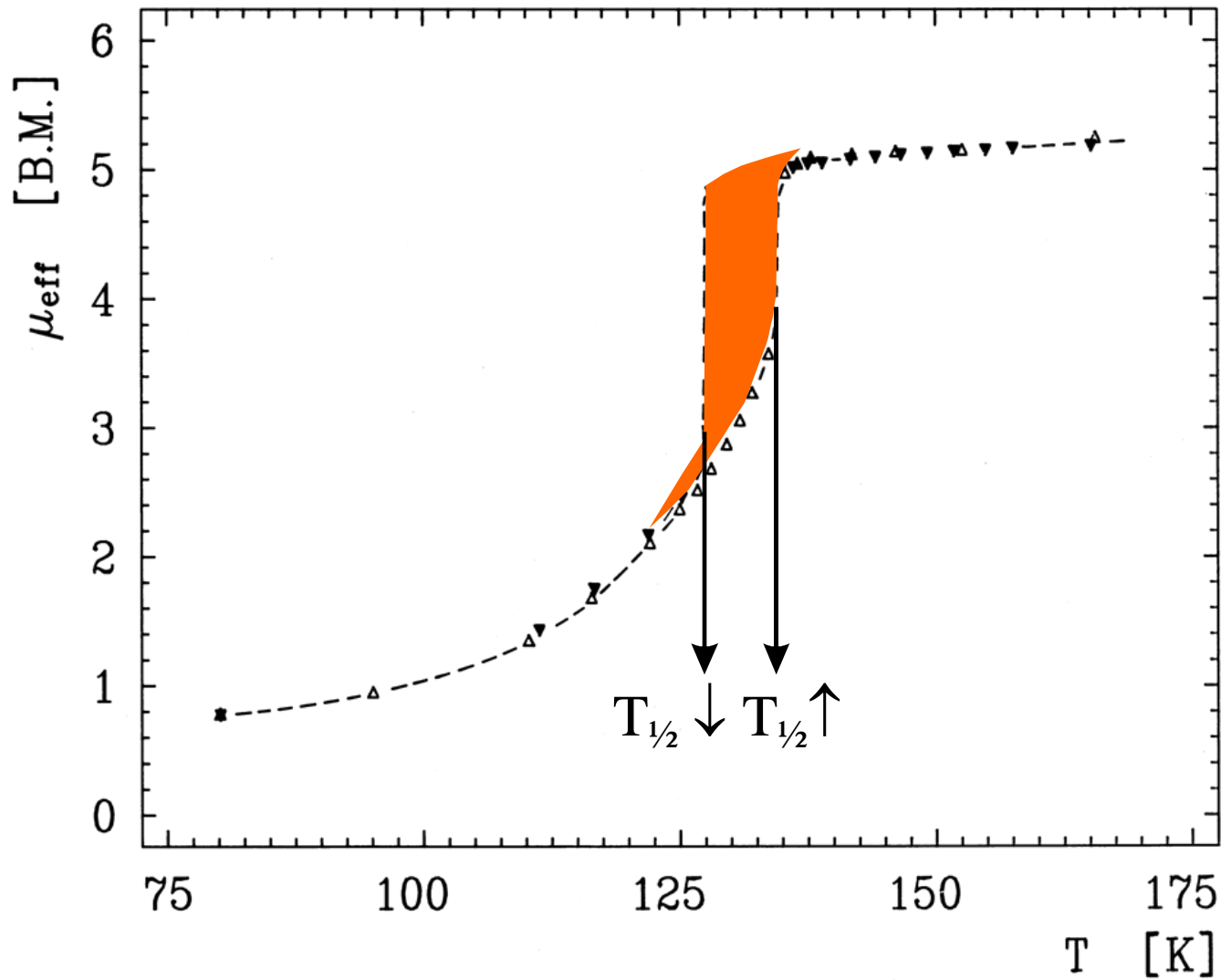


Thermal Spin Crossover



$[\text{Fe}(\text{ptz})_6](\text{BF}_4)_2$, where ptz stands for the ligand molecule 1-propyl-tetrazole as shown in the picture, is another iron(II) coordination compound exhibiting thermal spin crossover with a spin transition temperature $T_{1/2}$ of ca. 135 K. The ^{57}Fe Mössbauer spectra clearly indicate the transition at this temperature between the HS phase (quadrupole doublet shown in red) and the LS phase (singlet shown in blue). Whereas the quadrupole doublet is typical for iron(II) in the HS state, the singlet of the LS state is rarely observed and points at a quasi regular octahedral surroundings at the iron centre. The spin transition in this case occurs with hysteresis as shown by the magnetic measurements in the next picture.

$[\text{Fe}(\text{ptz})_6](\text{BF}_4)_2$

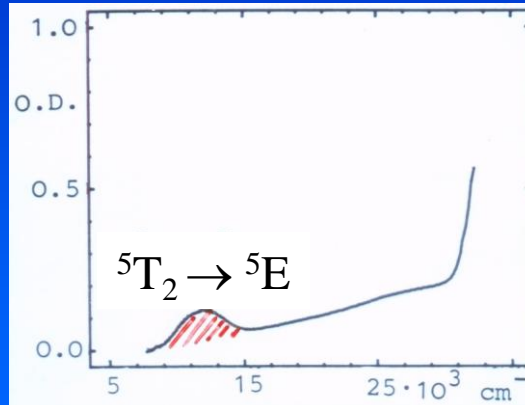
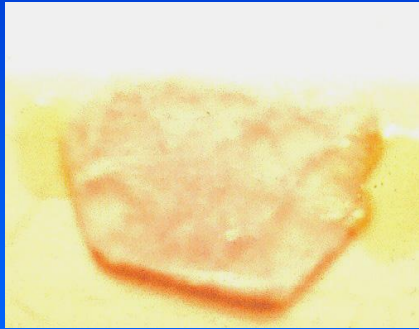


The hysteresis loop is ca. 7 K wide, with transition temperatures of 128 K and 135 K for the cooling and heating branches, respectively. With this compound it was observed for the first time that the spin transition can also be induced by irradiating the crystals with light; green light converts the LS state to the HS state, which can have very long lifetimes, e.g. on the order of days at low temperatures (below ca. 20 K); cf. Decurtins, S.; Gütlich, P.; Köhler, C.P.; Spiering, H.; Hauser, A. *Chem. Phys. Lett.* **1984**, *105* /1, 1.

[Fe(ptz)₆](BF₄)₂

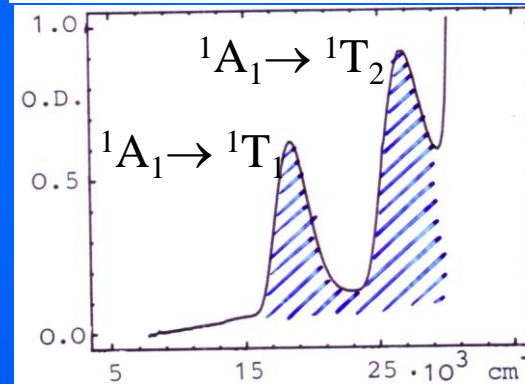
Decurtins
Gütlich
Hauser
Spiering
(1984)

HS



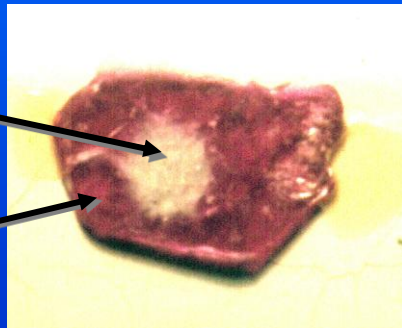
300 K

LS

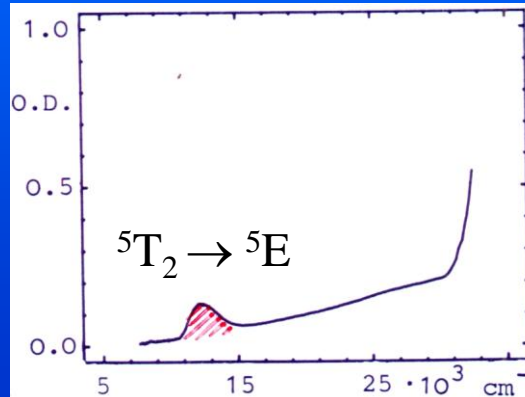


80 K

HS



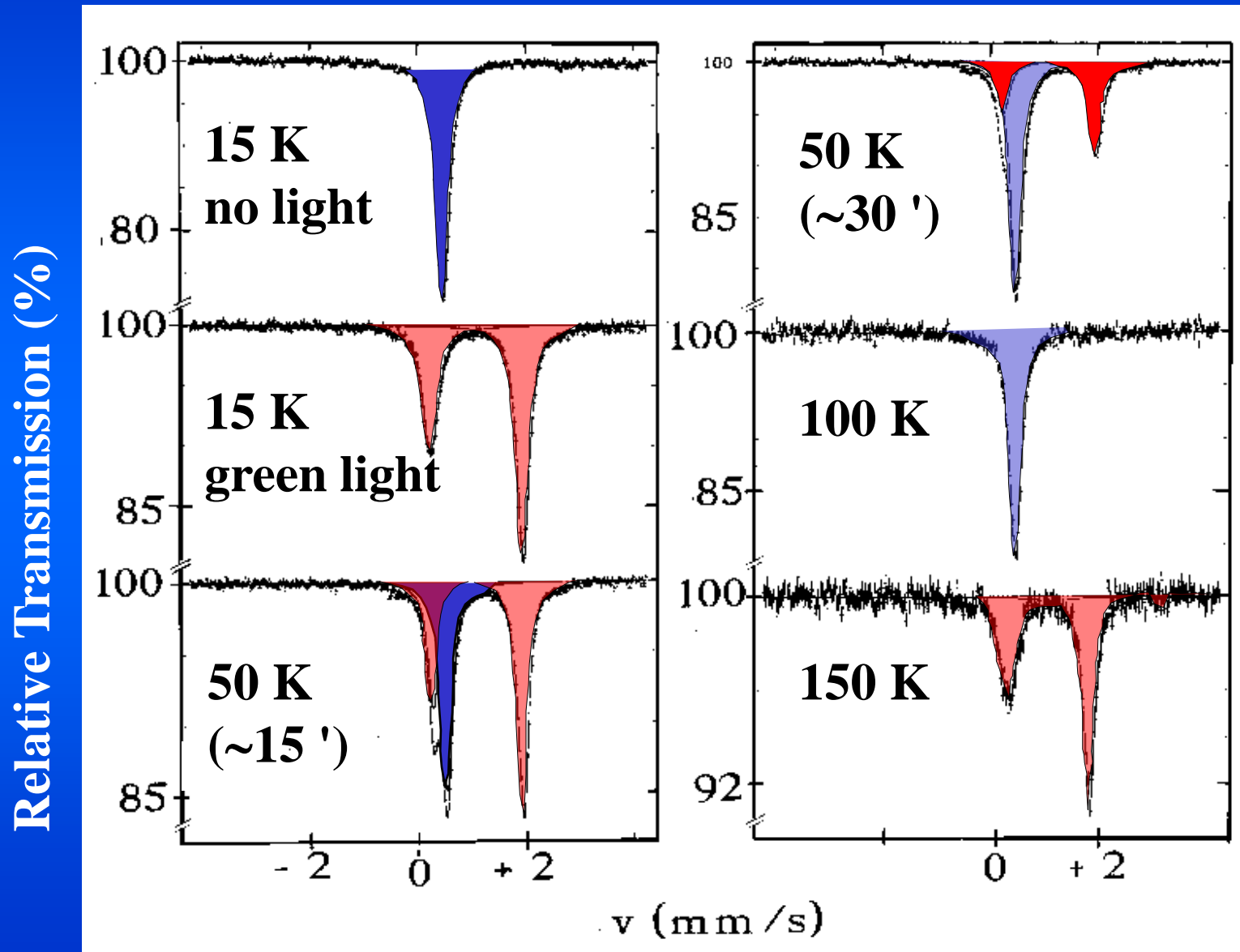
LS



10 K
green light

A single crystal of $[\text{Fe}(\text{ptz})_6](\text{BF}_4)_2$ (size ca. $3 \times 3 \text{ cm}^2$) is colourless at room temperature. The absorption spectrum shows only a weak absorption band at ca. $12\,000 \text{ cm}^{-1}$. At 80 K the crystal has changed totally to the LS state by thermal spin crossover and is now red and absorbs relatively strongly at $18\,000$ and $26\,000 \text{ cm}^{-1}$. Irradiating the crystal at ca. 10 K converts the LS state to the metastable HS state. The optical spectrum of the white spot (ca. 1 mm in diameter) is practically identical to the one recorded at 300 K.

[Fe(ptz)₆](BF₄)₂ : Light-Induced SCO



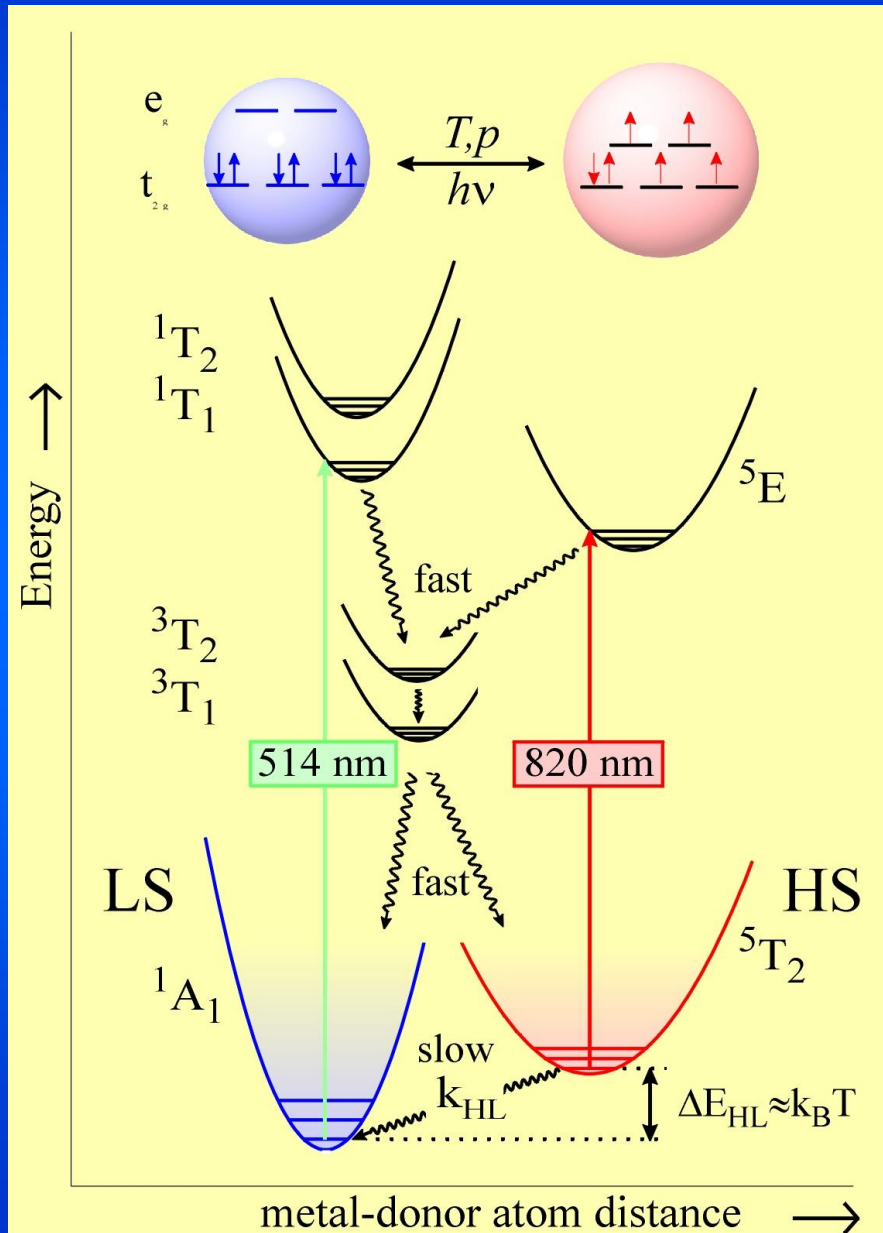
Mössbauer spectroscopy is ideally suited to follow the light-induced spin state conversion in this system as exemplified in the next viewgraph

A polycrystalline sample of $[\text{Fe}(\text{ptz})_6](\text{BF}_4)_2$ was cooled to 15 K. Before irradiation the sample is in the LS state and shows the typical Mössbauer spectrum of the LS state (upper left). After irradiating with green light (xenon lamp with filters or 514 nm band of an Ar ion laser) at 15 K the sample is quantitatively converted to the metastable HS state (middle left). The asymmetry in the intensity of the two components of the quadrupole doublet is due to the plate-like shape of the crystals (texture effect). Thermal relaxation on a 15 minute-timescale sets in at 50 K (lower left and upper right: the sample was heated for 15 minutes at 50 K and then cooled to the measuring temperature of 15 K in two runs). Thermal relaxation to the stable LS state is complete at 10 K. On further heating to 150 K the sample undergoes again thermal spin transition at 135 K to the (now stable) HS state.

This photophysical phenomenon has become known as “**Light-Induced Excited Spin State Trapping**” (LIESST). The processes involved in the LIESST effect are well understood on the basis of ligand field theory (Gütlich, P.; Hauser, A.; Spiering, H. *Angew. Chem. Int. Ed. Engl.* **1994**, *33*, 2024). The next viewgraph explains the mechanisms of LIESST and reverse-LIESST.

Light-Induced Excited Spin State Trapping

“LIESST“



Decurtins, Gütlich, Hasselbach, Hauser, Spiering, *Inorg. Chem.* **24** (1985) 2174

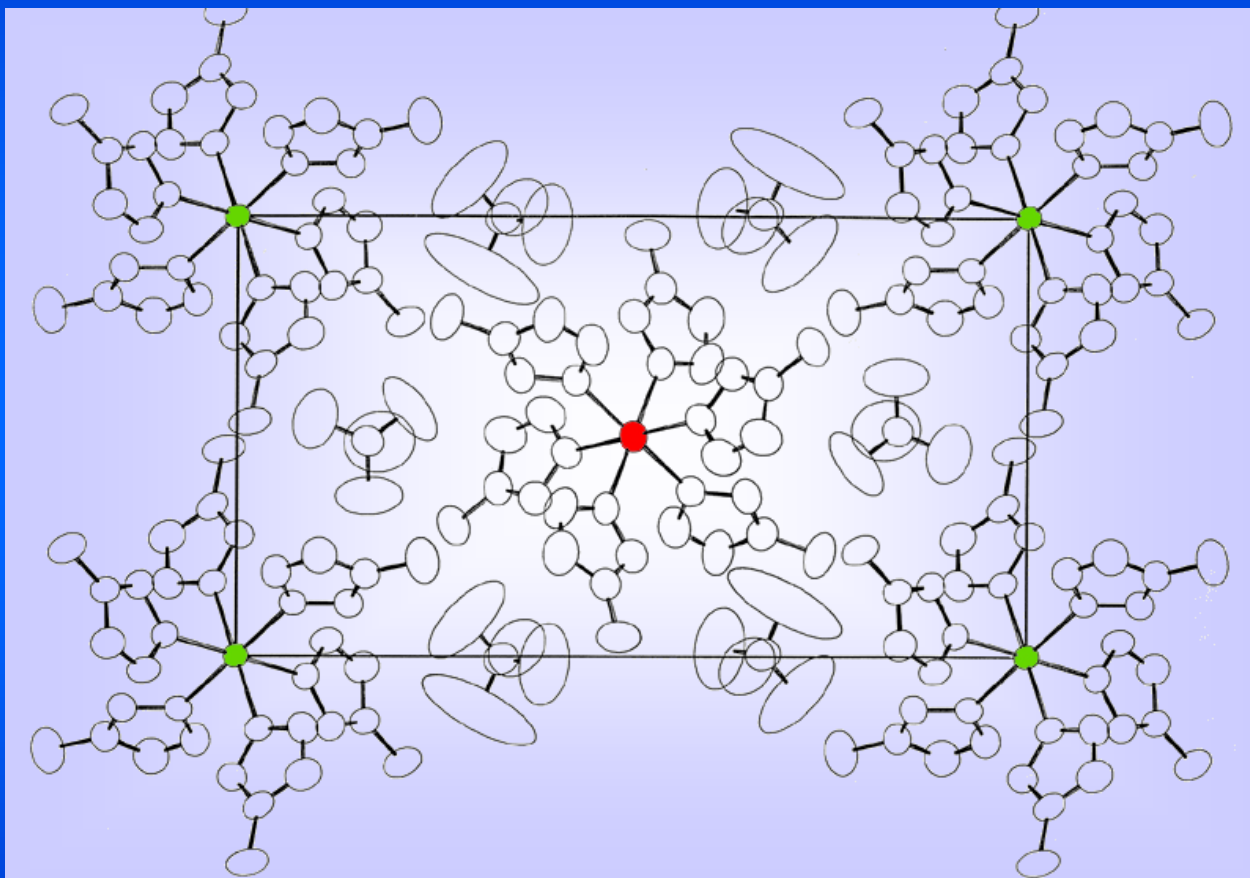
The energy level scheme shows in the uppermost part the distribution of the six valence electrons of iron(II) over the five d-orbitals split in an octahedral ligand field into the subgroups t_{2g} and e_g resulting in the two spin states LS (left) and HS (right), which can be switched forth and back by varying the temperature, applying pressure and by light. The corresponding energy potentials are drawn in the bottom part of the scheme. The complex molecules in the HS state are bigger than those in the LS state due to the fact that the antibonding e_g orbitals are partially occupied in the HS state, whereas in the LS state they are empty. Thus the HS potentials are placed in positions of larger metal-donor atom distances as compared to the LS potentials.

Green light (514 nm) excites the LS state (1A_1) to the 1T_1 and 1T_2 states (spin-allowed, but parity-forbidden), which decay fast via the spin triplet states $^3T_{1,2}$ to the 5T_2 state. This double intersystem crossing decay path is favoured by spin-orbit coupling over the direct decay path back to 1A_1 . Decay of the 5T_2 state to the 1A_1 state is forbidden, the metastable HS state is trapped until radiationless thermal relaxation sets in by nonadiabatic multiphonon processes (Gütlich, P., Hauser, A., Spiering, H., *Angew. Chem. Int. Ed. Engl.*, 1994, 33, 2024). Light-induced back conversion of the metastable LIESST state is possible by irradiating the sample with red light, thereby undergoing again double intersystem crossing processes similar to the LS to HS conversion with green light (reverse-LIESST).

The LIESST phenomenon has been verified in many iron(II) spin crossover complexes. An interesting case is the system with methyl-tetrazole ligands, $[\text{Fe}(\text{mtz})_6](\text{BF}_4)_2$, which will be discussed next.

$[\text{Fe}(\text{mtz})_6](\text{BF}_4)_2$

mtz = 1-methyl-1H-tetrazole



Fe(II) (B)
2.161 (5) Å
2.197 (5) Å
2.207 (4) Å

Fe(II) (A)
2.181 (5) Å
2.181 (5) Å
2.181 (7) Å

The crystal structure of $[\text{Fe}(\text{mtz})_6](\text{BF}_4)_2$ shows that iron(II) ions occupy two slightly different lattice positions, denoted as A and B sites, at a ratio of 1:1. At room temperature the two kinds of Fe(II) ions are in the HS state as confirmed by Mössbauer spectroscopy.



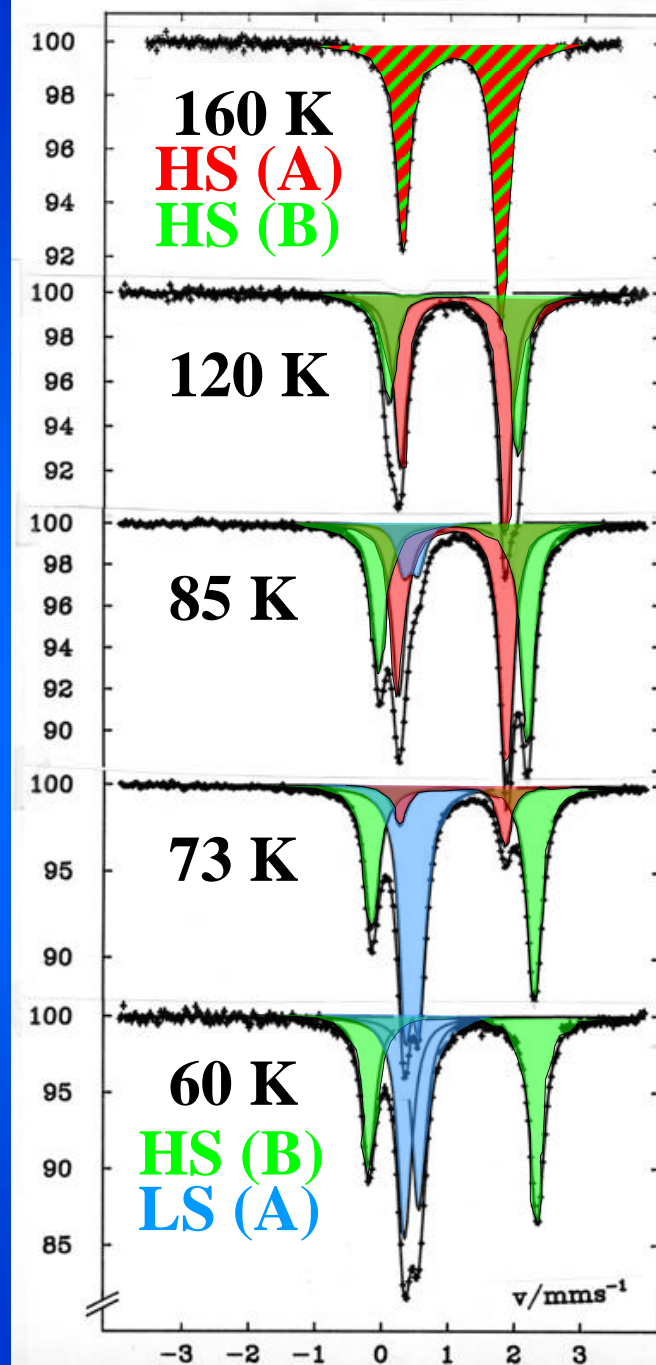
T-dependent
 ^{57}Fe Mössbauer spectra



Thermal Spin
Crossover
at A-sites

Poganiuch, Decurtins, Gülich,
J. Am. Chem. Soc. *112* (1990) 3270

Rel. Transmission (%)

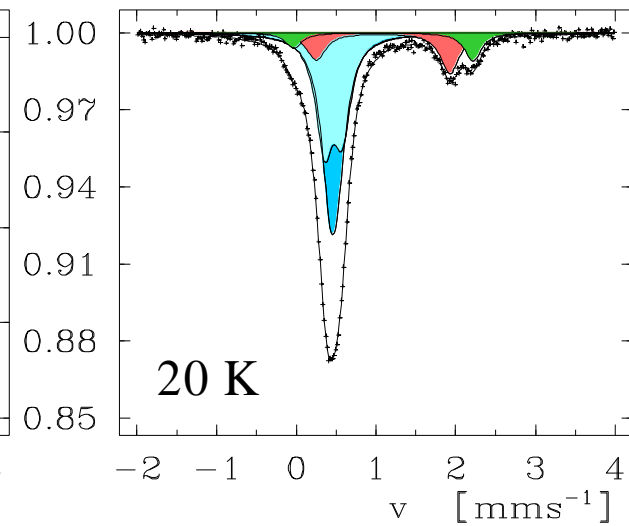
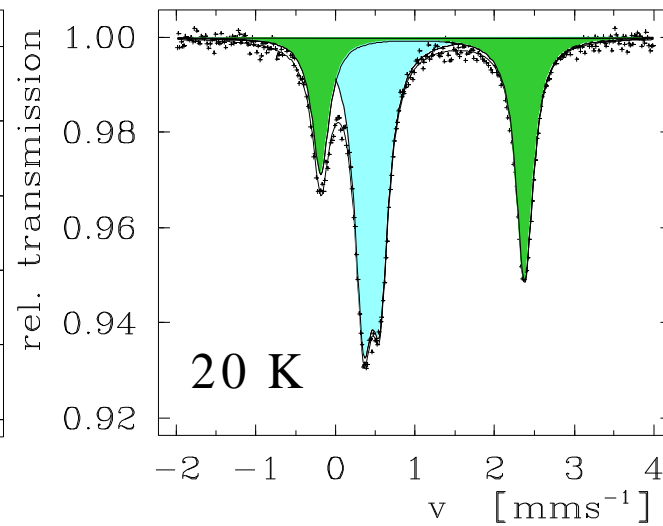
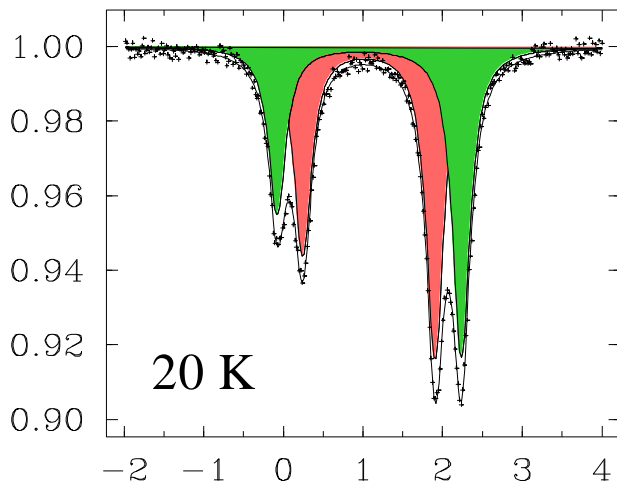
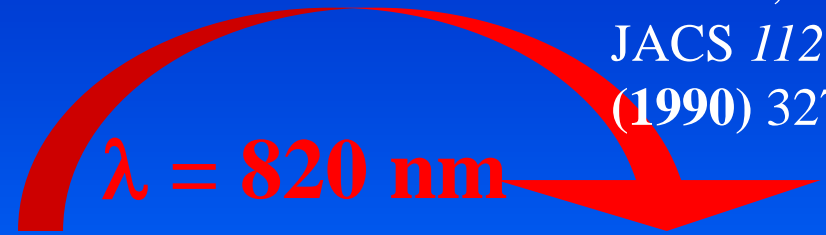
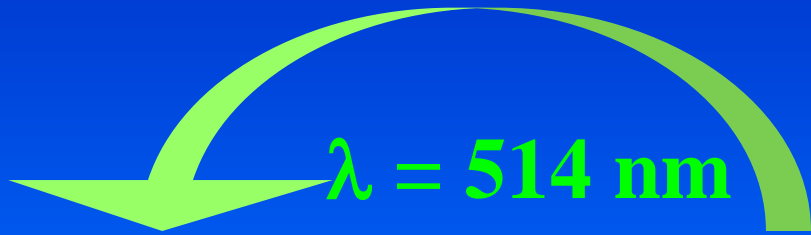


From room temperature down to ca. 160 K, the two kinds of iron ions can not be distinguished by their Mössbauer resonance signals; the quadrupole doublets of HS(A) (red) and HS(B) (green) have the same values within the error limits. At ca. 120 K, however, they become discernible. On further lowering the temperature, HS(A) undergoes spin transition and the intensity of the HS(A) doublet decreases at the favour of a gradually appearing LS(A) signal (blue). The green HS(B) doublet, with an area fraction of ca. 50 % at all temperatures, remains in the HS state throughout. Thus, temperature dependent ^{57}Fe Mössbauer spectroscopy clearly traces the thermal spin crossover process at A-sites only.

This system was also subject to investigations of light-induced spin state conversions (LESST) using Mössbauer spectroscopy. The next picture highlights the results.

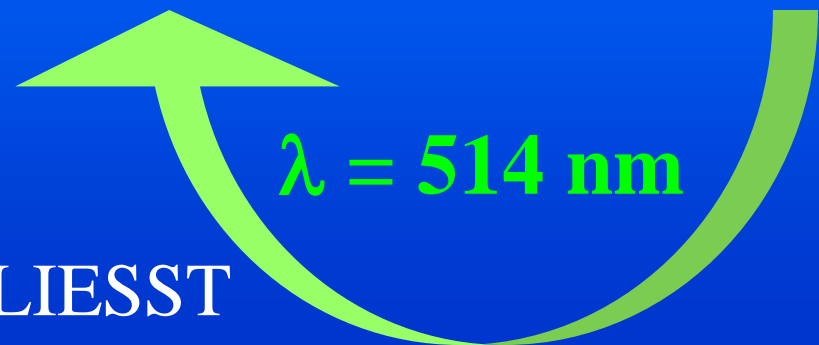
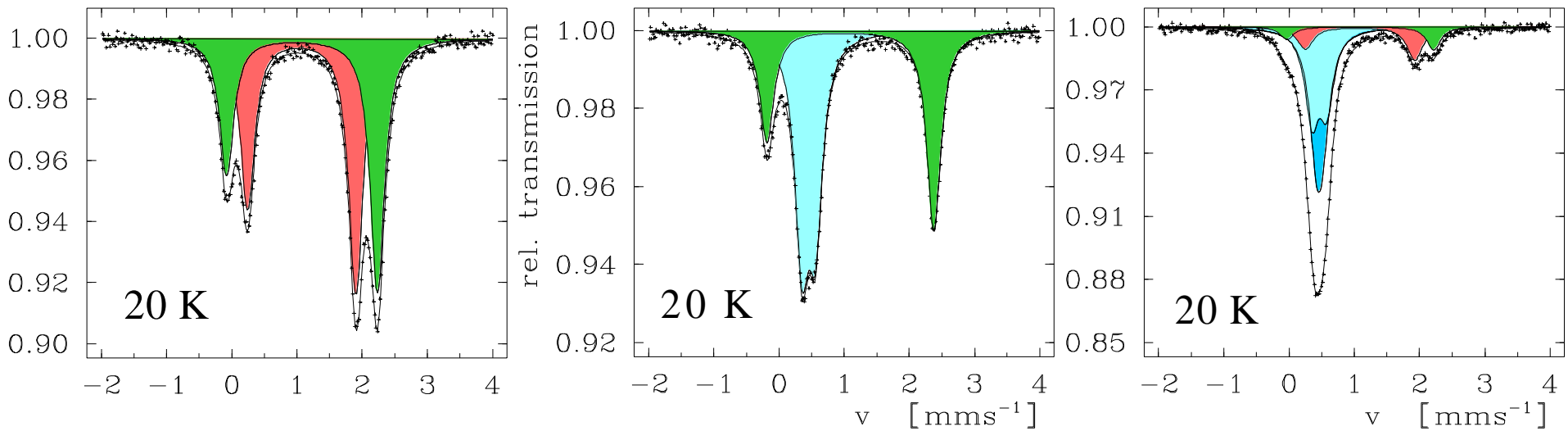
[Fe(mtz)₆](BF₄)₂ LIESST in Sites A and B

Poganiuch,
Decurtins,
Gütlich,
JACS 112
(1990) 3270



A polycrystalline sample of $[\text{Fe}(\text{mtz})_6](\text{BF}_4)_2$ was cooled to 20 K. The recorded Mössbauer spectrum of it is nearly identical to the 60 K spectrum of the previous picture. It shows in blue the LS(A) resonance signal, and in green the HS(B) quadrupole doublet, each species being present to ca. 50 %. After irradiation with green light (514 nm) the LS(A) signal disappears at the favour of a doublet arising from the HS(A) sites. When the sample is warmed to ca. 65 K, thermal relaxation of HS→LS at A sites sets in and the original 20 K spectrum is recorded again. If the sample is irradiated with red light instead of green light, the quadrupole doublet arising from the HS(B) sites mostly disappears and the spectrum mainly contains now LS resonances arising from both LS(A) and LS(B) sites. This way light-induced conversion of a stable HS iron(II) species to a long-lived metastable LS species was observed for the first time. Again, when the sample is heated to ca. 65 K, thermal relaxation of LS→HS at B sites begins and the original 20 K spectrum (middle) is recorded after complete relaxation. ((P.Poganiuch, S. Decurtins, P. Gülich, *J. Am. Chem. Soc.* 112 (1990) 3270).

[Fe(mtz)₆](BF₄)₂ LIESST and Reverse-LIESST



Reverse-LIESST

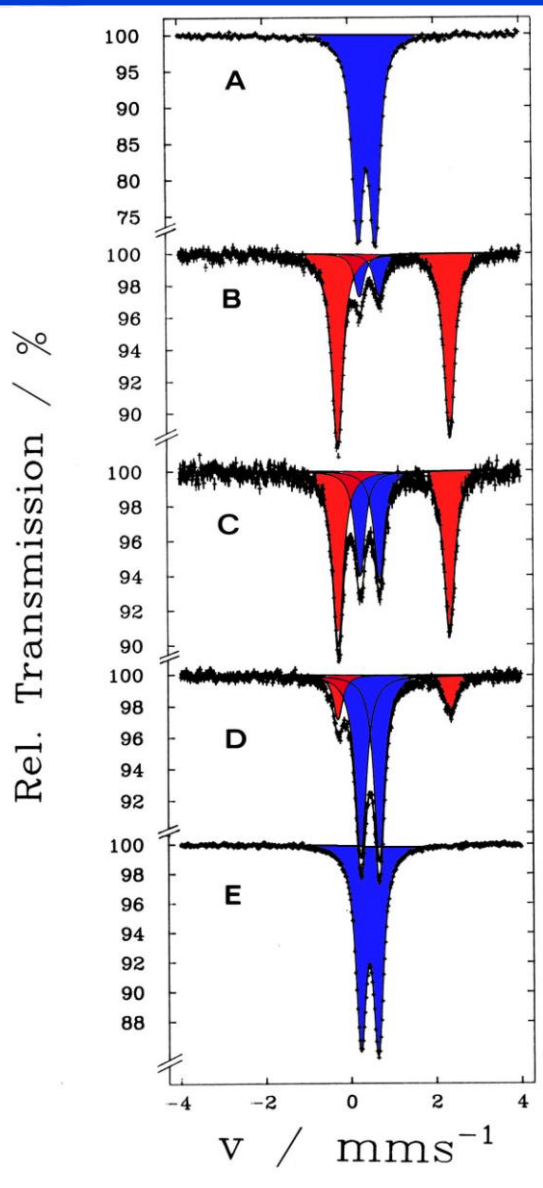
[Fe(2-pic)₃]Cl₂·EtOH - LIESST

No light, 4 K

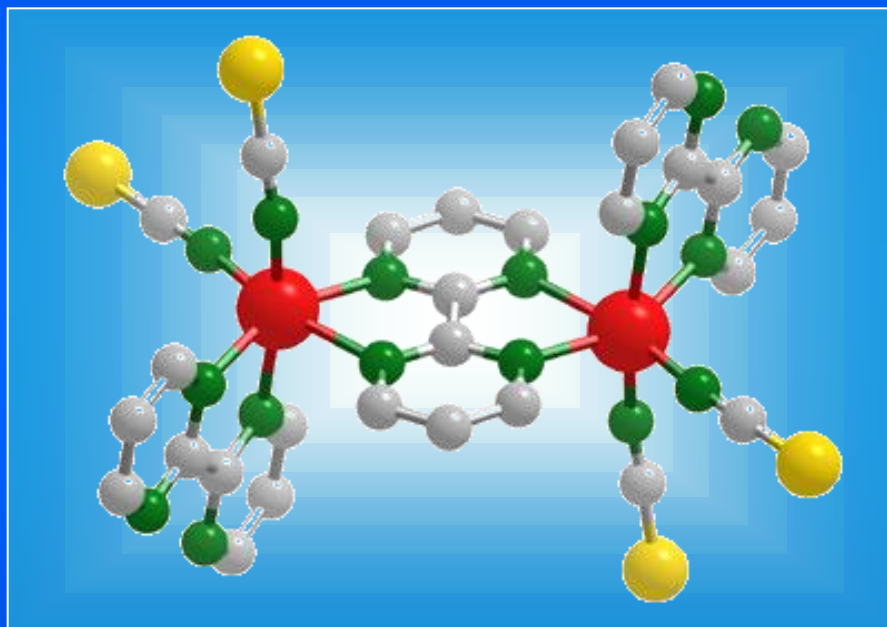
Green light, 4 K

HS→LS relaxation at 30 K

S. Decurtins, P. Gülich, C.P. Köhler, H. Spiering,
J. Chem. Soc. Chem. Commun. 7 (1985) 430



Spin Crossover in dinuclear iron(II) complexes



Gaspar,
Real,
Ksenofontov,
Gütlich et al.
(2001)

A – [Fe bpym (NCS)₂]₂ bpym

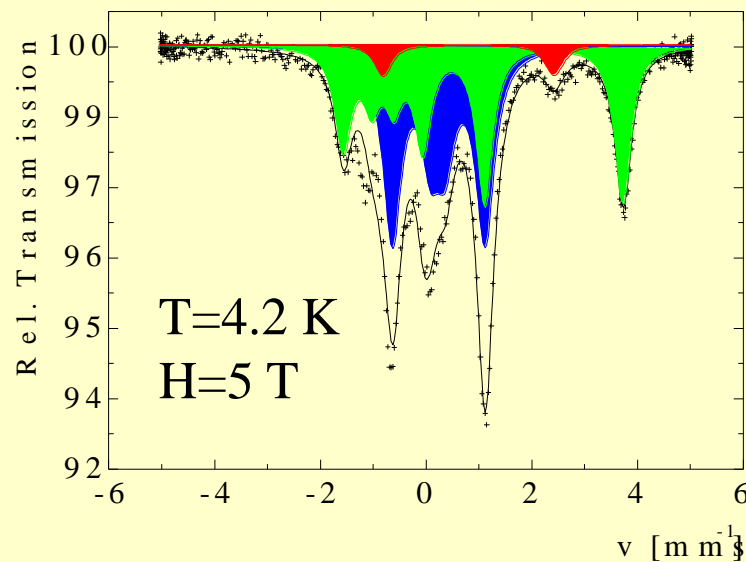
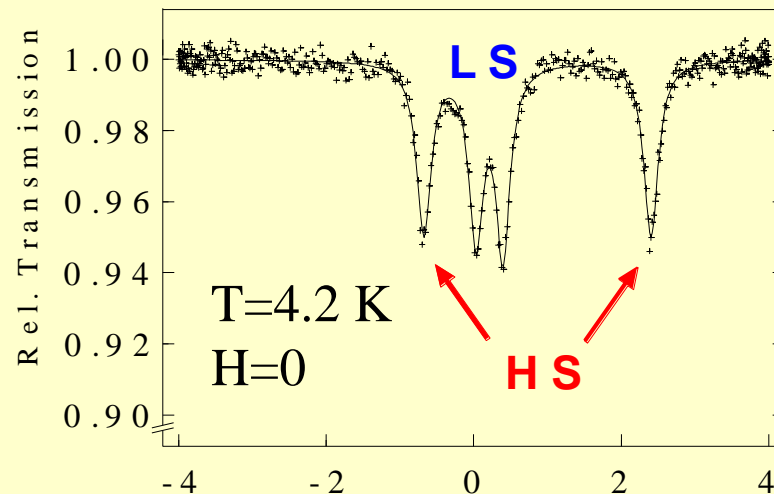
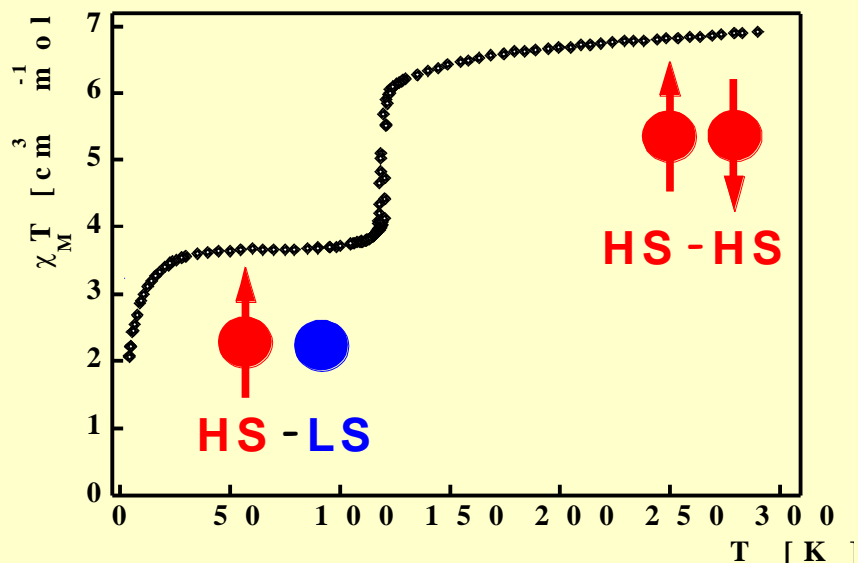
B – [Fe bpym (NCSe)₂]₂ bpym

^{57}Fe Mössbauer spectroscopy is a most elegant tool to follow these photophysical processes.

It has also been employed in investigations of polynuclear systems, i.e. coordination compounds with more than one switchable iron(II) centres in the complex molecules. The simplest ones are dinuclear complexes of iron(II) to be discussed next.

Various members of this class of dinuclear iron(II) compounds were first synthesized and structurally and magnetically characterised in the group of J.A. Real (Valencia). Two selected members A and B are shown here. They differ only slightly in their chemical composition. Compound A, with NCS ligands instead of NCSe (B), the two Fe(II)-HS centres with spin $S = 2$ are antiferromagnetically coupled via the bpym bridge over the whole temperature range under study. Compound B possesses a slightly stronger ligand field strength than A and undergoes thermal spin transition, but encompassing only 50 % of the iron(II) centres as indicated by the plateau in the spin transition curve at $\chi T \approx 3.5 \text{ cm}^3 \text{ mole}^{-1} \text{ K}$.

Mössbauer Spectroscopy of $[\text{Fe bpym}(\text{NCSe})_2]_2\text{bpym}$ in External Magnetic Field



LS in LS-LS and in HS-LS

HS in HS-LS

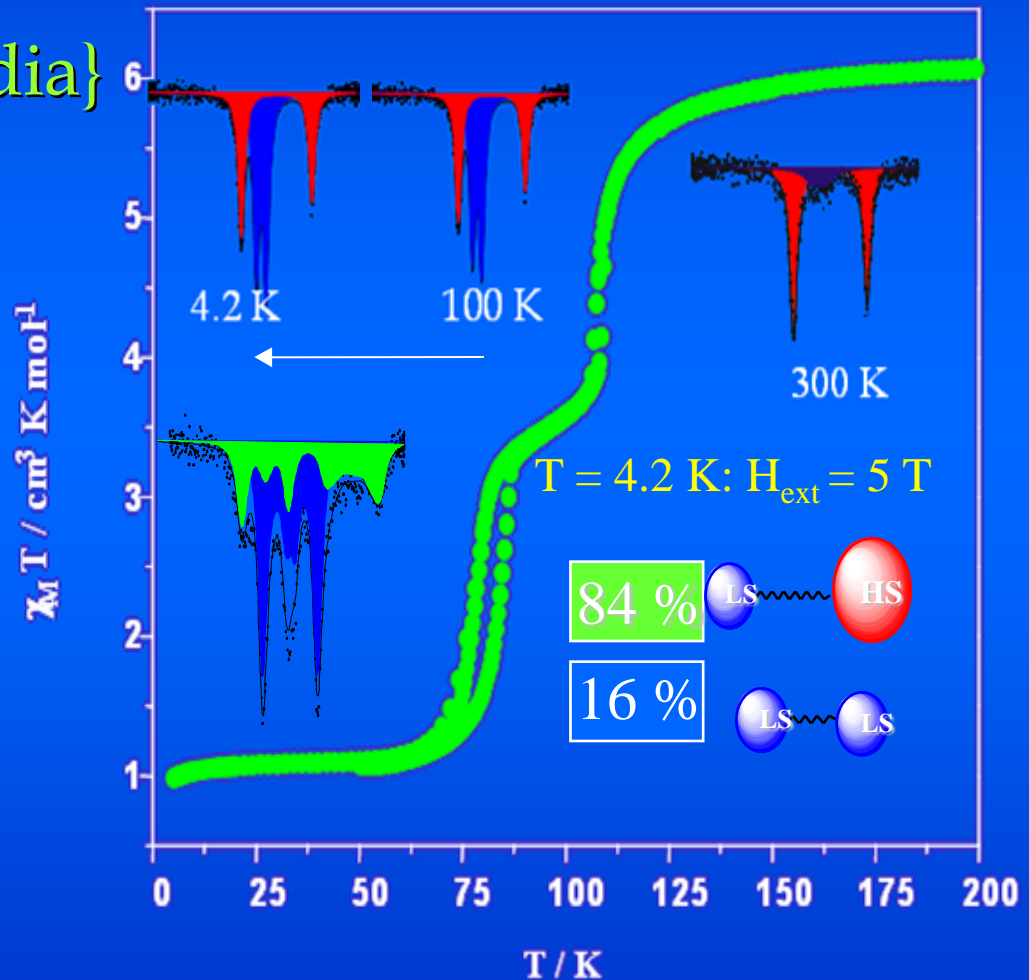
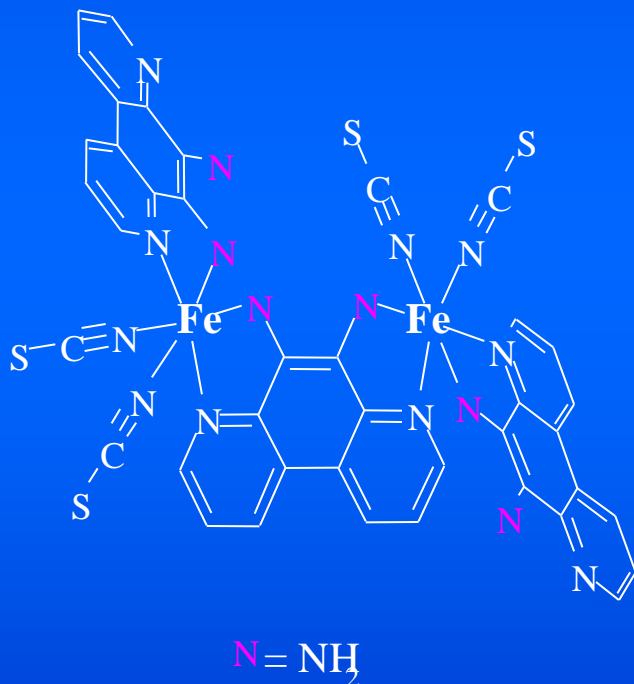
HS-HS

Ksenofontov, Spiering, Reiman, Garcia,
Gaspar, Moliner, Real, Gütlich
Chem. Phys. Lett. 348 (2001) 381

The important question arises whether the spin transition occurs from HS-HS pairs to HS-LS pairs, or whether the plateau arises from a 1:1 mixture of HS-HS and LS-LS pairs. The Mössbauer spectrum recorded without applied magnetic field (see upper right) cannot differentiate between the two possibilities; it reflects the presence of 50 % each of HS and LS Fe(II) ions, but no information about the pair formation. Mössbauer spectroscopy with applied magnetic field, however, solves the problem. The spectrum in the lower right confirms that there is hardly any HS-HS pair formation in the plateau, it consist mainly of HS-LS pairs. (V. Ksenofontov, H. Spiering, S. Reiman, Y. Garcia, A.B. Gaspar, N. Moliner, J.A: Real, P. Gütlich, *Chem. Phys. Letters* 348 (2001)5-6, 381).

Thermal spin transition has also been studied in other dinuclear iron(II) complexes. An example is shown in the following picture, where the spin state in the plateau could be characterised by Mössbauer spectroscopy.

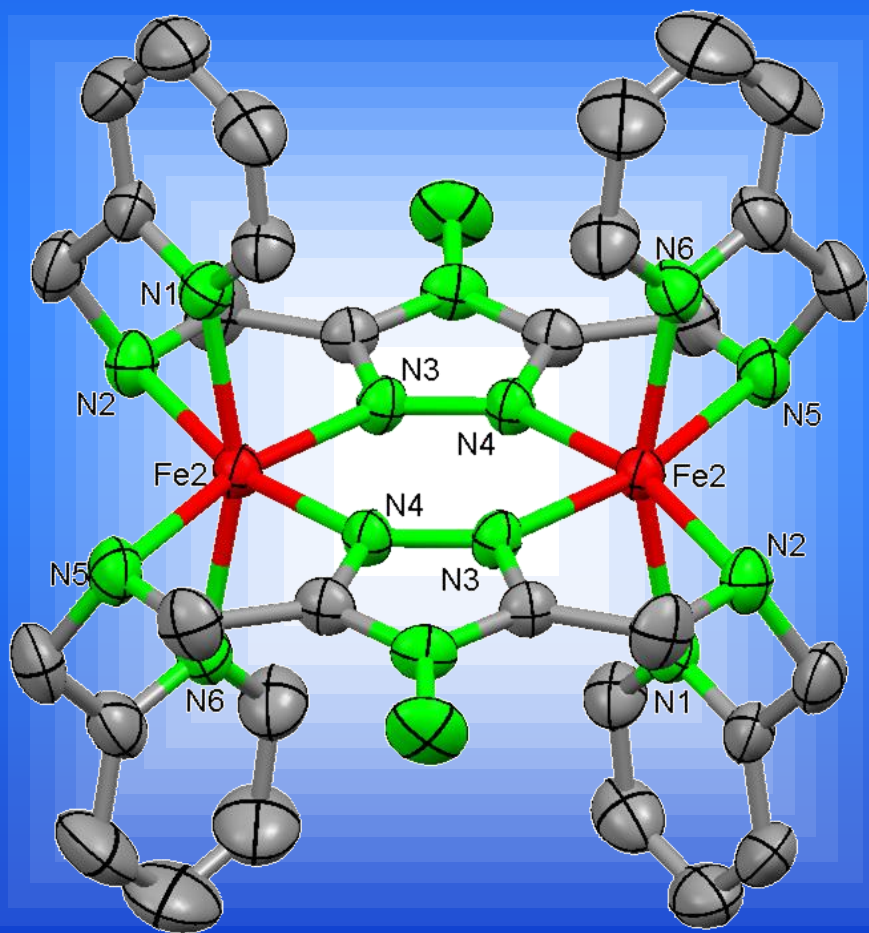
Spin state in the plateau of a dinuclear spin crossover complex



Gaspar, Real, Ksenofontov, Gütlich (2002)

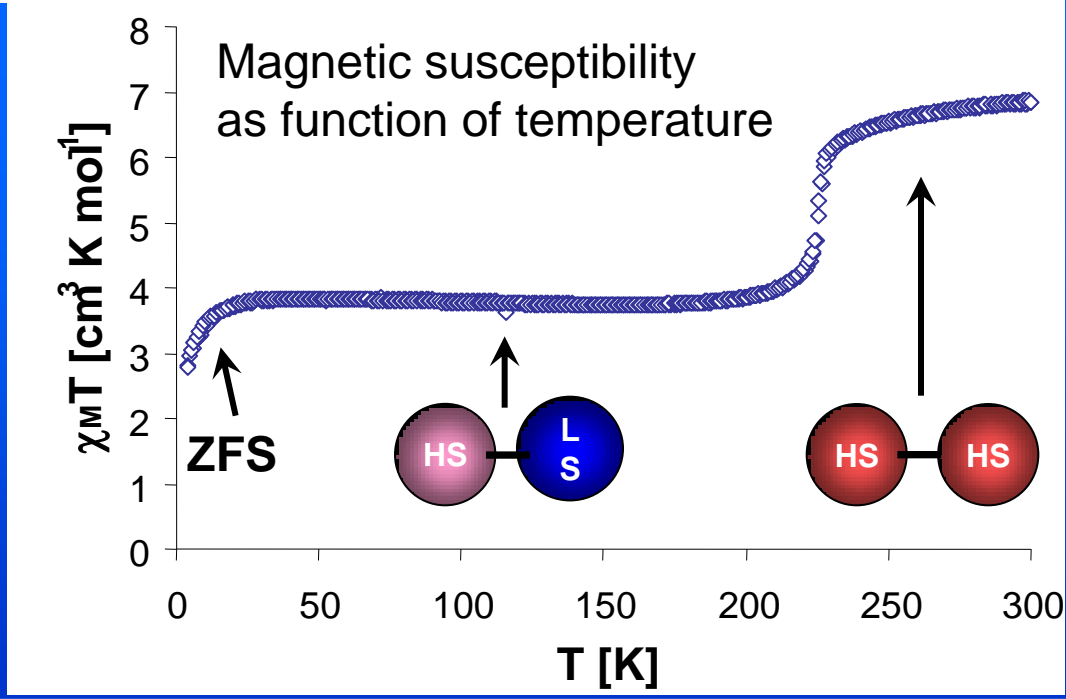
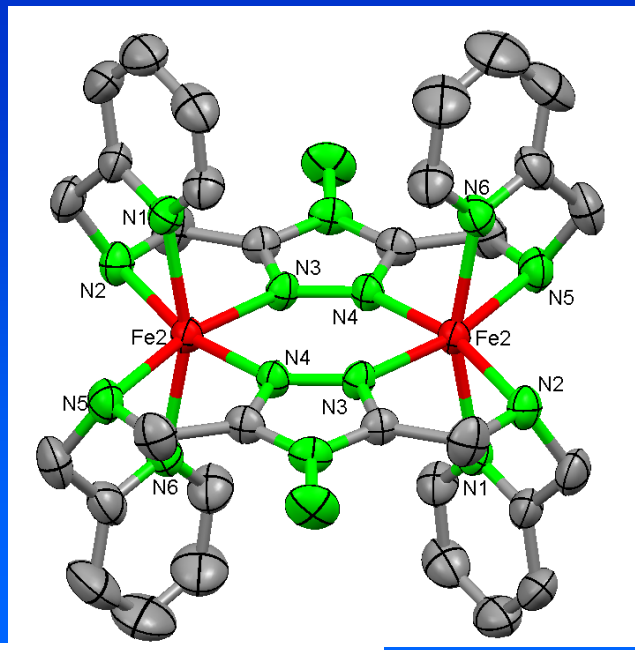
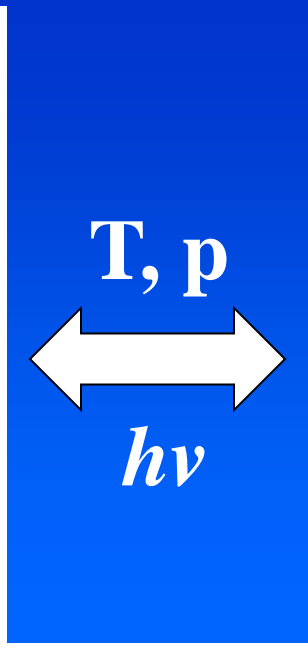
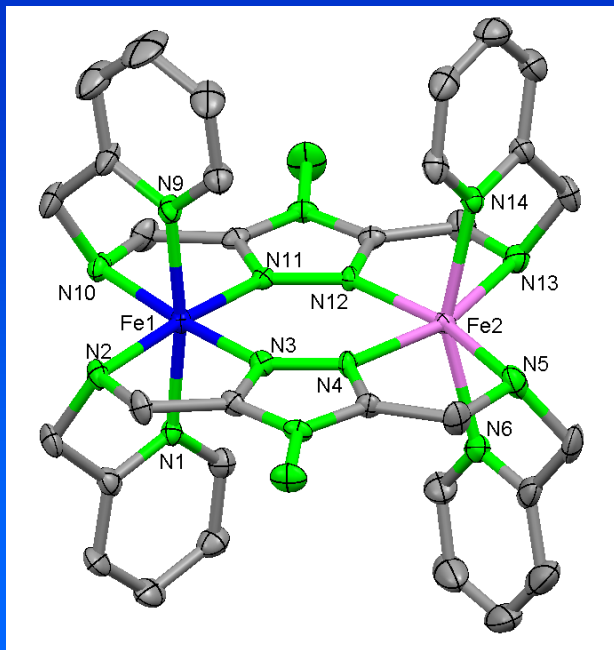
A peculiarity here is that the spin transition curve χT versus temperature from magnetic susceptibility measurements shows a plateau at ca. 50 % spin state conversion. The question arises whether the plateau reflects the presence of 100 % of HS-LS pairs or a mixture of 50 % each of HS-HS and LS-LS pairs. Magnetic susceptibility and conventional Mössbauer measurements do not clarify the situation. At 300 K one observes a typical Fe(II)-HS quadrupole doublet. In the plateau at ca. 100 K one observes the same quadrupole doublet as at 300 K and a typical Fe(II)-LS signal, with intensity ratio of ca. 1:1. These spectra could arise from a mixture of HS-HS and LS-LS pairs as well as from HS-LS pairs only. To solve the problem, the sample was quickly frozen from 100 K to 4.2 K. The Mössbauer spectrum did not change as seen in the picture indicating that the fast trapping procedure was successful. Measuring the Mössbauer effect now in a magnetic field (5 T) yields the spectrum shown in the lower left, with subspectra marked in green and blue arising from LS-HS and LS-LS pairs, respectively. There is no indication for the presence of HS-HS pairs. The answer is clear: The thermal spin transition in this system proceeds from HS-HS via HS-LS (plateau) to LS-LS pairs.

Proof of [HS-LS] Pair Formation in a Dinuclear Spin Transition Complex by Variable Temperature ^{57}Fe Mössbauer Spectroscopy



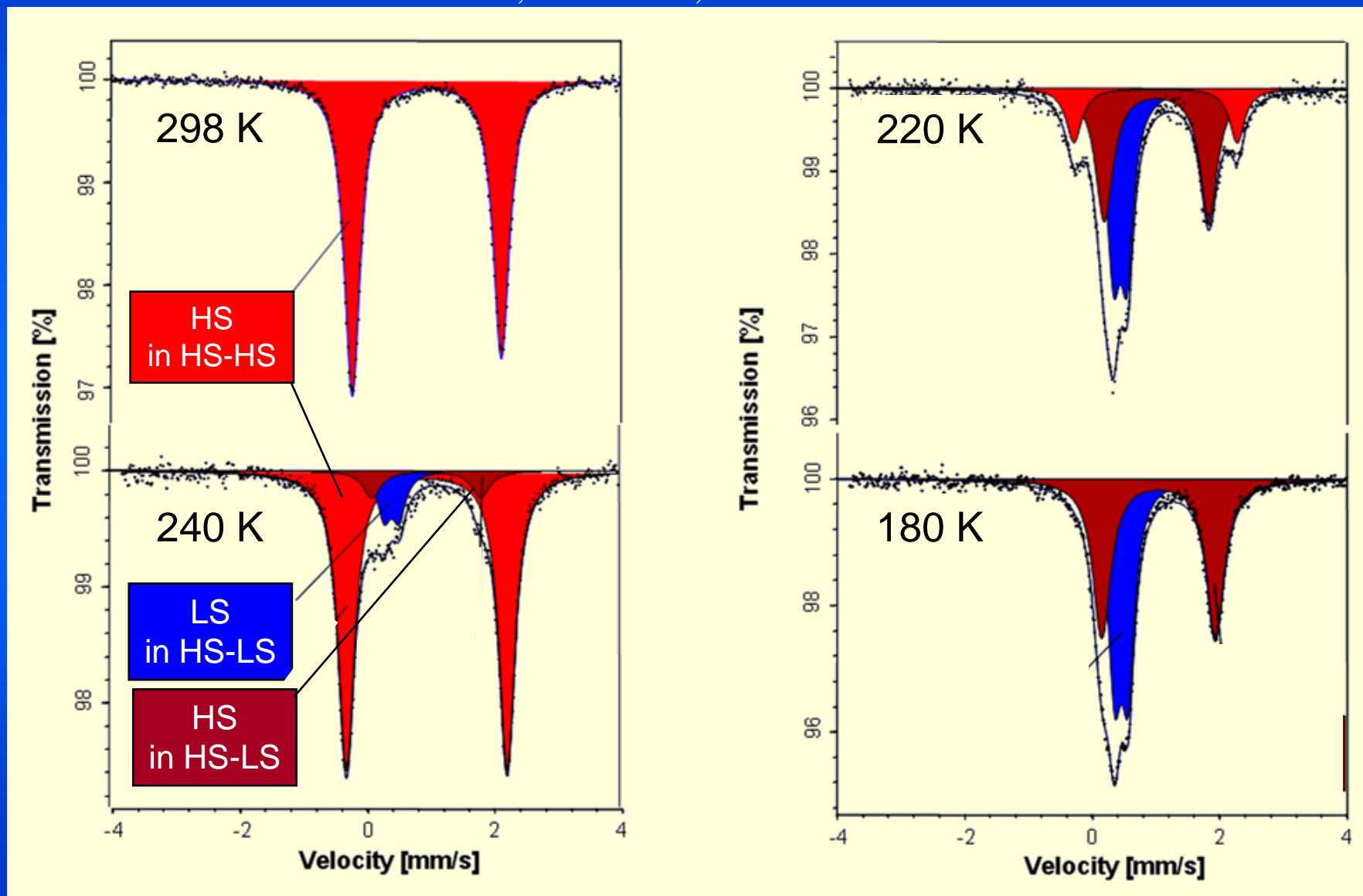
PMAT =
4-amino-3,5-bis
{[(2-pyridyl-methyl)amino]methyl}-
4H-1,2,4-triazole

M. Grunert, S. Brooker, P. Gülich et al.,
Angew. Chem. 2008



Proof of [HS-LS] Pair Formation in a Dinuclear Spin Transition Complex by Variable Temperature ^{57}Fe Mössbauer Spectroscopy

M. Grunert, S. Brooker, P. Gülich et al. 2007

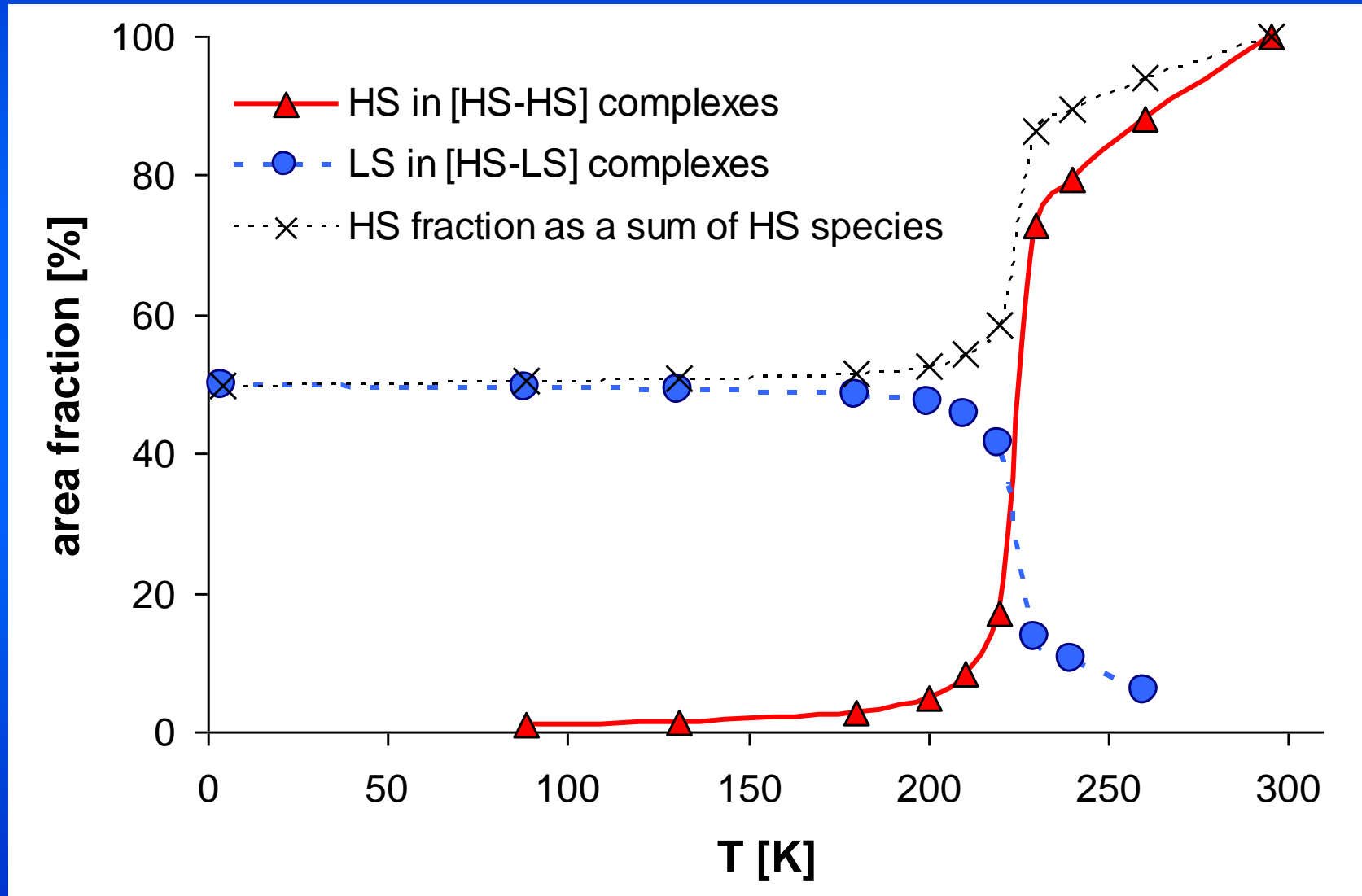


At 298 K there is only one quadrupole doublet with isomer shift $\delta = 0.96 \text{ mm s}^{-1}$ (relative to α -iron) and quadrupole splitting $\Delta E_Q = 2.34 \text{ mm s}^{-1}$. These values are characteristic of Fe(II) in the HS state and prove the presence of only [HS-HS] pairs. The slight intensity asymmetry is due to texture. As the temperature is decreased, to 240 K, two new doublets (blue & brown) appear at the expense of the original HS doublet (red). The blue signal, with $\delta = 0.36 \text{ mm s}^{-1}$, $\Delta E_Q = 0.26 \text{ mm s}^{-1}$ and area fraction $A = 10.3 \%$, arises from LS-Fe(II) in a [HS-LS] pair, formed as a result of a thermal HS to LS transition at this site. The brown signal, a quadrupole doublet with $\delta = 0.96 \text{ mm s}^{-1}$, $\Delta E_Q = 1.66 \text{ mm s}^{-1}$, and area fraction $A = 10.3 \%$, is unambiguously due to HS-Fe(II) in HS-LS pairs. The original red HS-Fe(II) doublet arising from the [HS-HS] pairs now has a reduced area fraction of 79.6 %. With further lowering of the temperature the original HS doublet (red) arising from [HS-HS] pairs continues to lose intensity in favor of the new doublets (brown and blue) with equal area fractions arising from LS-Fe(II) and HS-Fe(II) in the [HS-LS] pairs. In the plateau region, at 180 K and below, the half ST is complete and the original HS doublet (red) has vanished, the remaining signals are those due to HS (brown) and LS (blue) Fe(II) in the [HS-LS] pairs, with intensity ratio 1:1.

The present Mössbauer study confirms the conclusion from single crystal X-ray crystallography that the thermal ST in this dinuclear complex occurs from [HS-HS] pairs to [HS-LS] pairs rather than to a mixture of [HS-HS] and [LS-LS] pairs. In addition, it elegantly demonstrates the role of the rigid bridging ligands in communicating the message of the spin state change at one Fe(II) center to the neighboring Fe(II), because the newly created neighboring LS state causes distortions in the coordination sphere of the second Fe(II) centre.

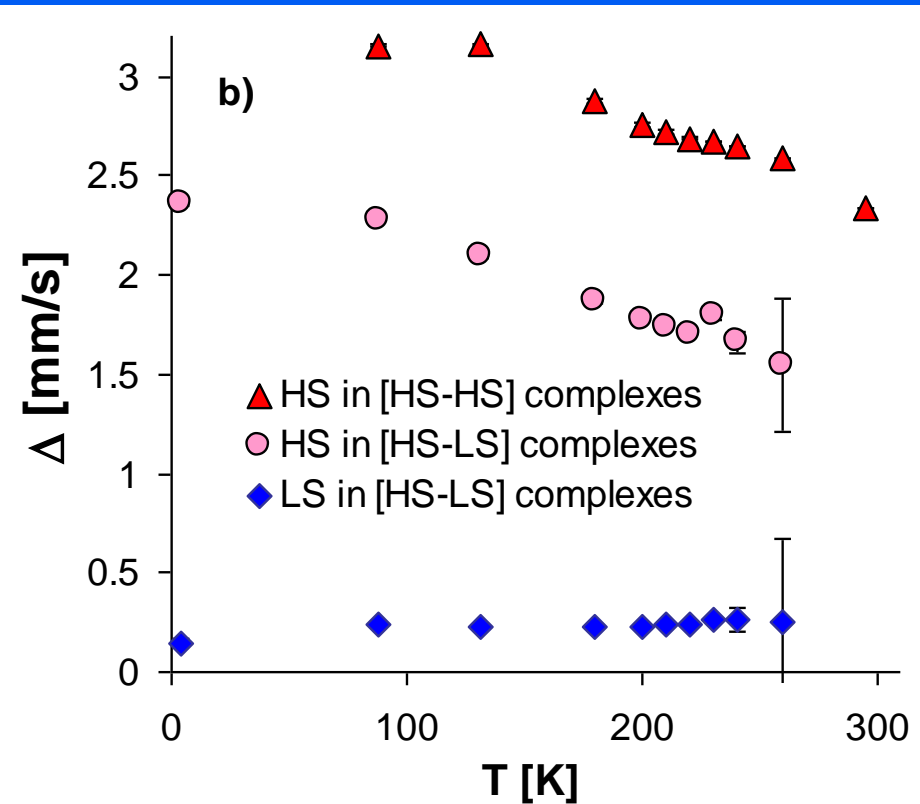
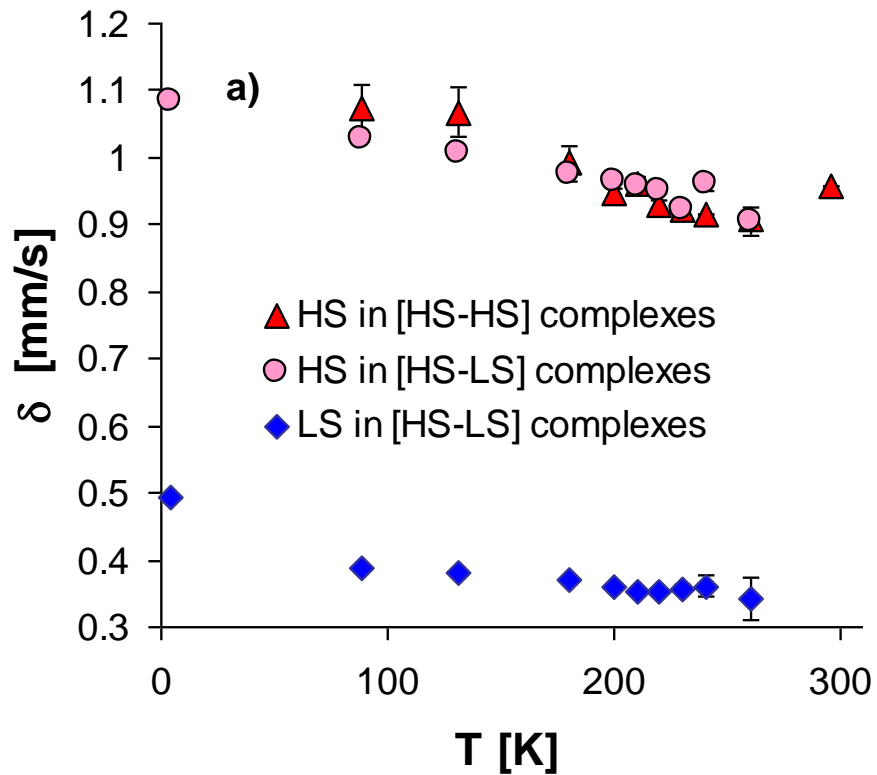
This is the first study where the mechanism of spin crossover in a dinuclear complex – whether it is via a [LS-HS] species or a 1:1 mixture of [LS-LS]:[HS-HS] species – has been identified by standard, easily accessible, temperature-dependent Mössbauer spectroscopy, i.e. without the need to access and employ tedious magnetic field measurements.

Area fractions of the Mössbauer resonance signals as a function of temperature



The area fractions for the three signals are plotted as a function of temperature. The curve for the HS-Fe(II) in [HS-HS] pairs shows a very sharp decrease near 225 K, consistent with the spin transition temperature determined from magnetic susceptibility measurements. In the same temperature range the area fractions of both HS-Fe(II) and LS-Fe(II) (blue data points) in [HS-LS] pairs are identical within the error limits and increase sharply, reaching a plateau at the 50 % level.

Isomer shift and quadrupole splitting of Mössbauer resonance signals as a function of temperature



The δ values for both HS species, HS in [HS-HS] pairs and HS in [HS-LS] pairs, are practically identical, implying no noticeable change of electron density at the ^{57}Fe -HS nucleus due to the spin transition in the neighboring iron site. The slight increase of the δ values with decreasing temperature is due to the second-order Doppler effect (here with a value of $(d\delta/dT) \approx 5 \times 10^{-4} \text{ mm s}^{-1} \text{ K}^{-1}$). The ΔE_Q of the LS doublet is temperature independent, which is typical for LS-Fe(II) species with no valence electron contribution and only little (temperature independent) lattice contribution to the field gradient. Typically, the ΔE_Q values of the two HS species increase with decreasing temperature.

A Journal of the Gesellschaft Deutscher Chemiker

Angewandte Chemie

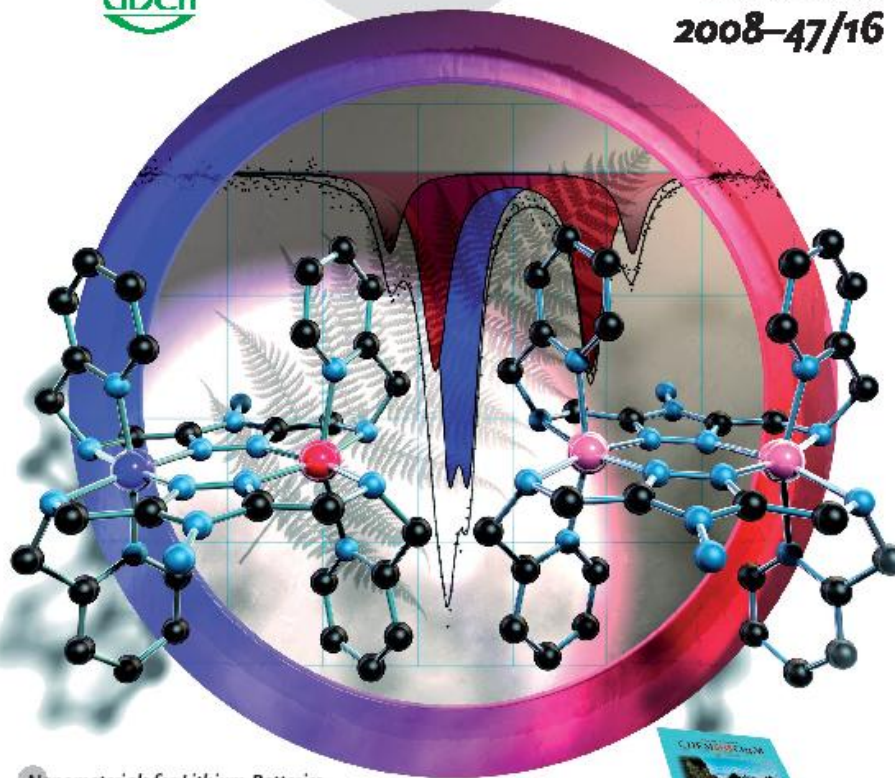
International Edition

GDCh

www.angewandte.org

2008-47/16

D 3461



Nanomaterials for Lithium Batteries

P. G. Bruce et al.

Prebiotic Chemistry

P. Cintas

Total Synthesis of Spirastrellolide A

M. V. Perkins

[3+2] Cycloadditions of Trimethylenemethane

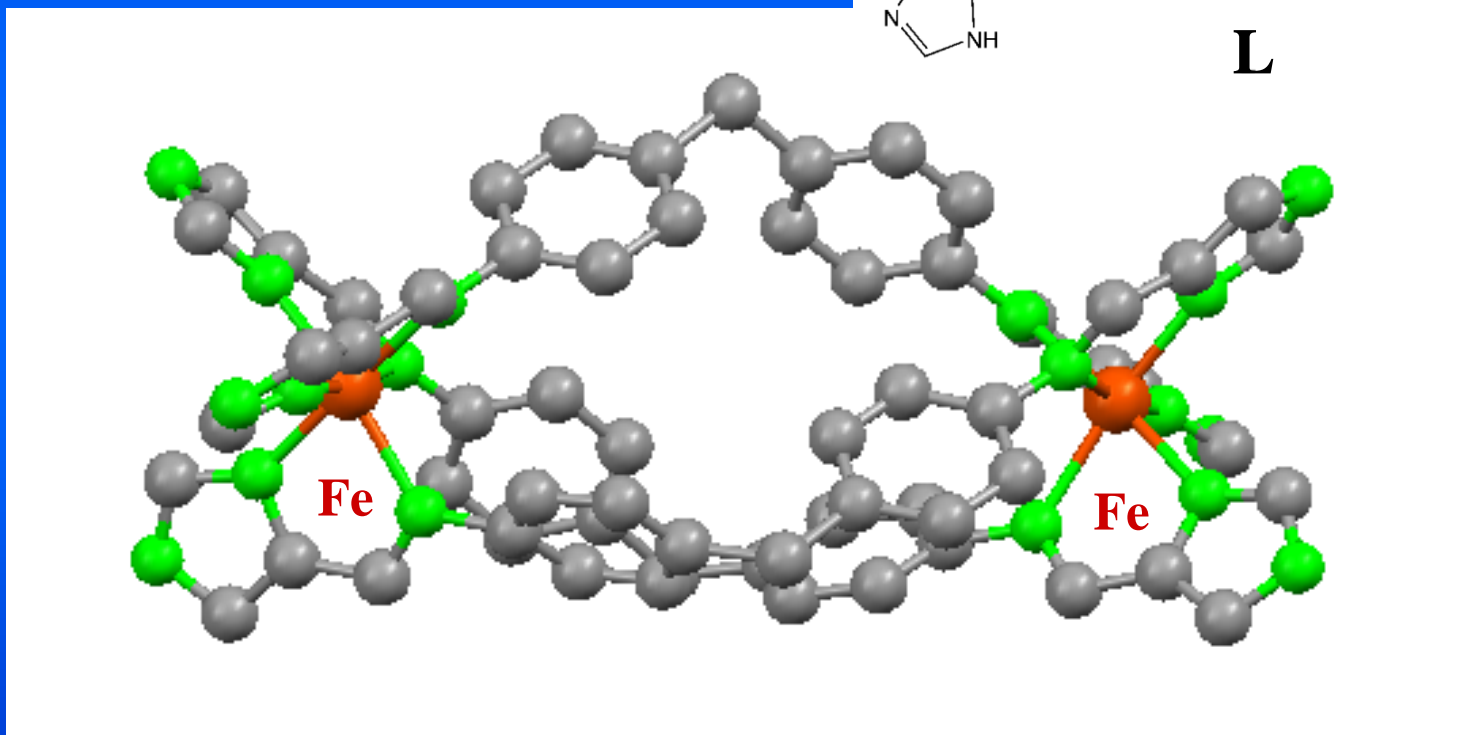
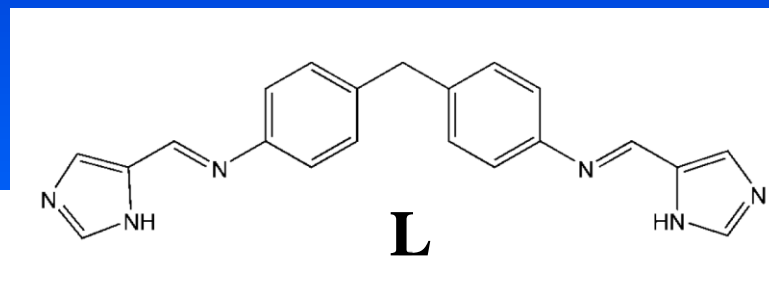
W. Tam and P. Le Marquand

ACEFS 47 (16) 2893-3066 (2008) · ISSN 1433-7851 · Vol. 47 · No. 16



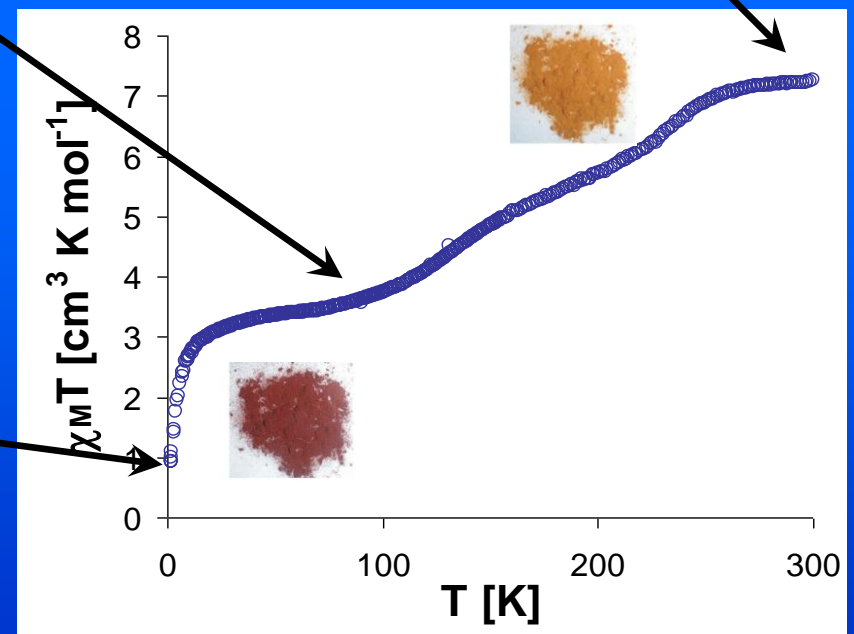
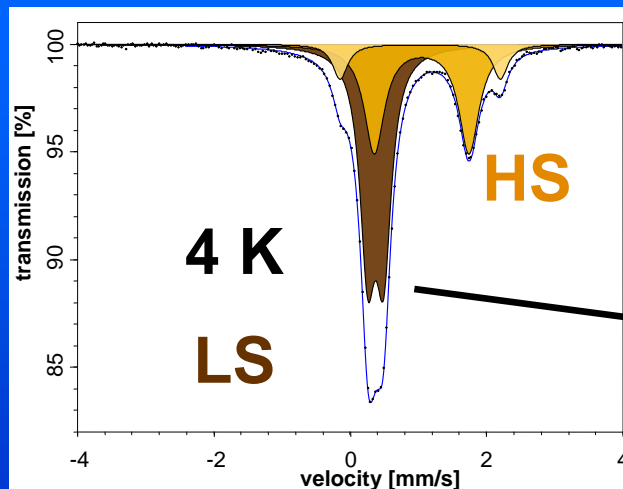
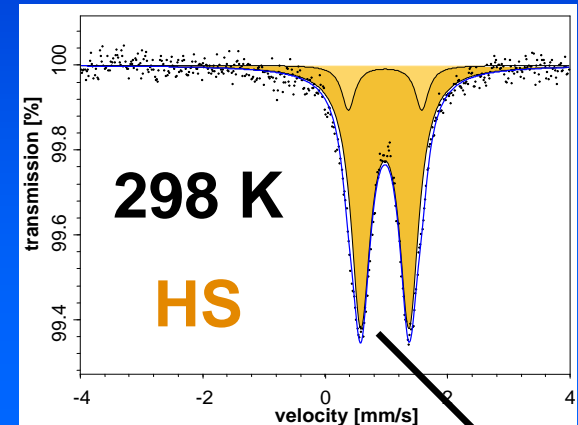
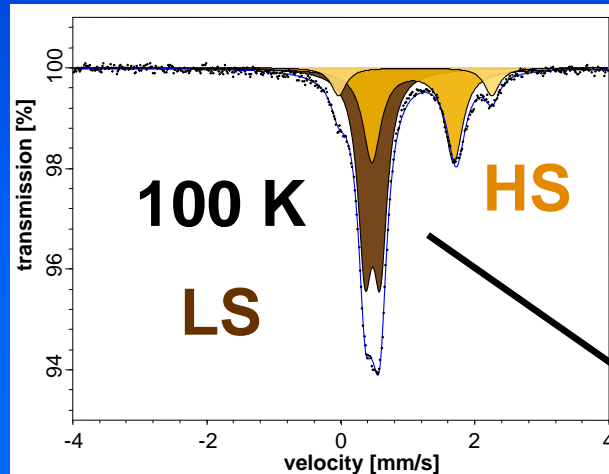
 WILEY-VCH

$[\text{Fe}_2(\text{L})_3](\text{ClO}_4)_2 \cdot 2\text{H}_2\text{O}$

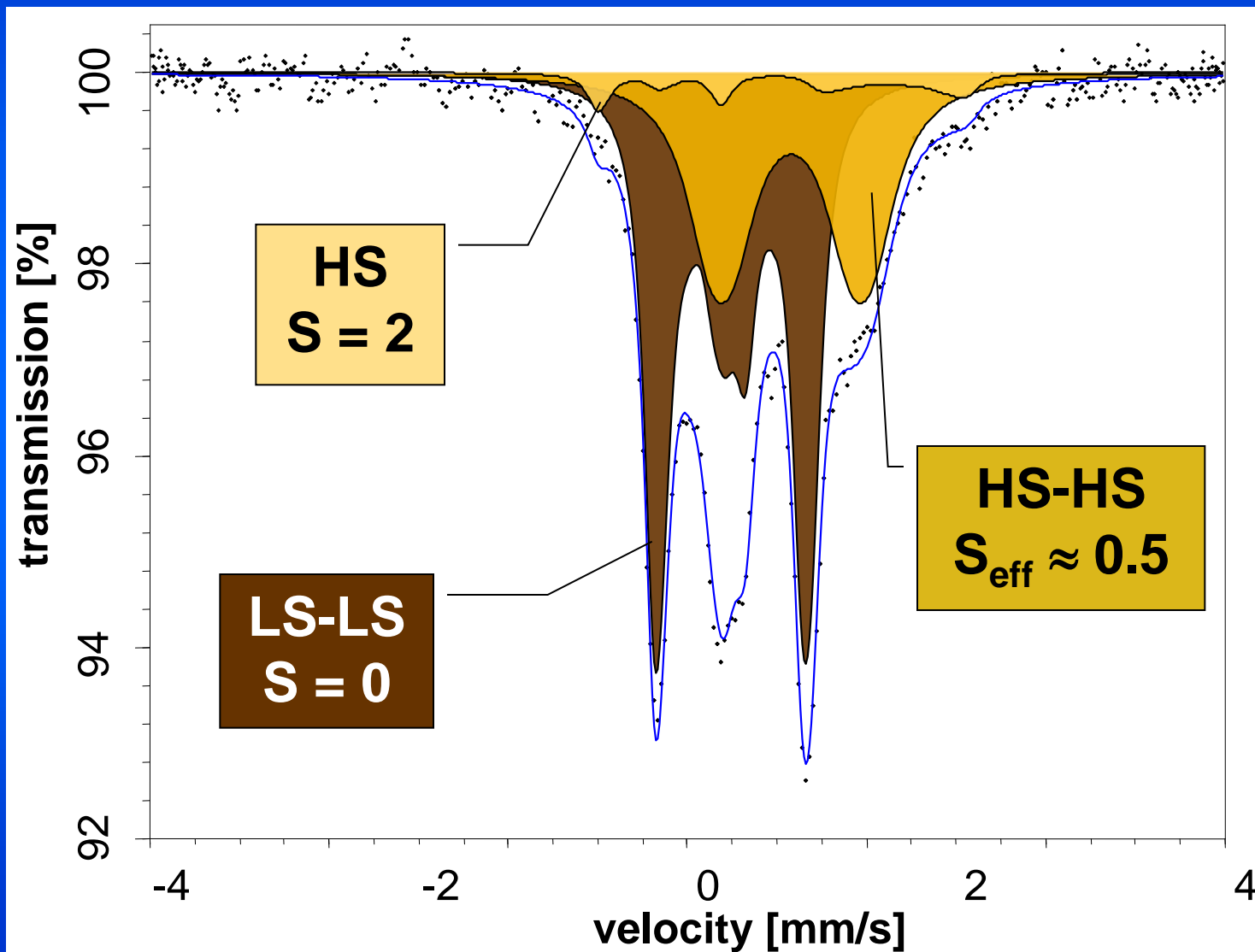


F. Tuna, M. R. Lees, G. J. Clarkson and M. J. Hannon, *Chemistry - A European Journal* **10** **22**, 5737-3750, **2004**

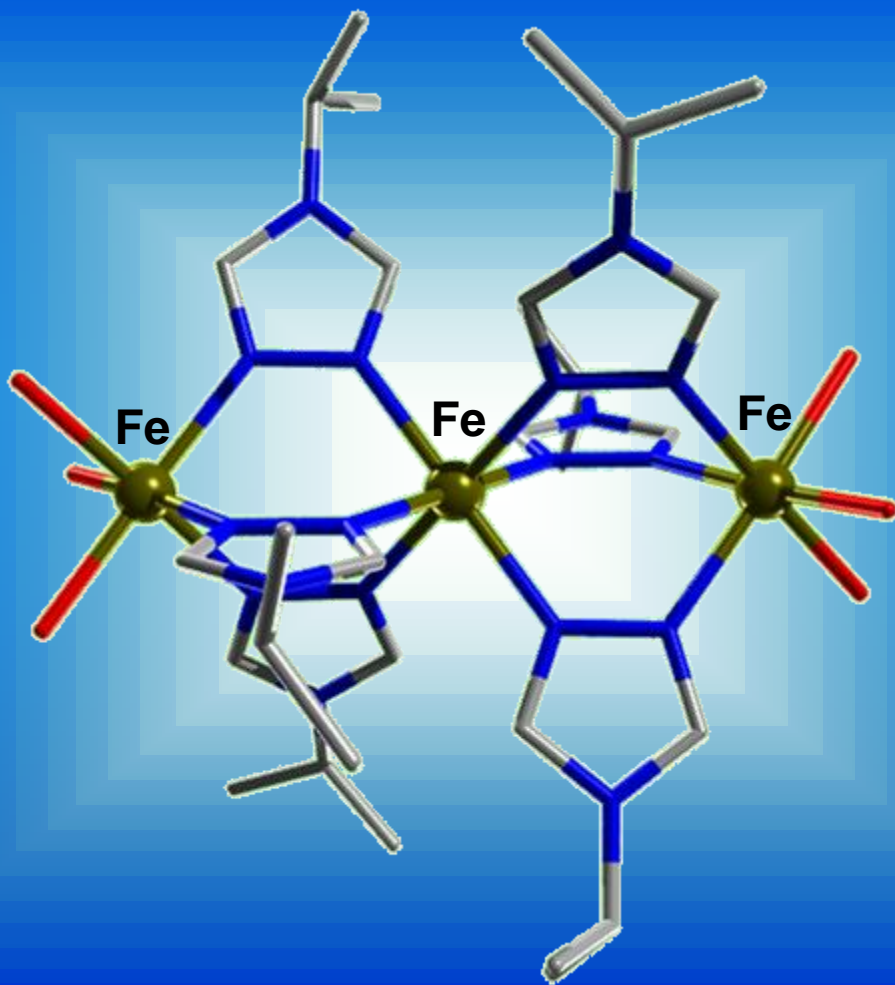
Magnetic and Mössbauer Measurements



^{57}Fe -Mössbauer spectrum at 4 K, $H = 5$ T

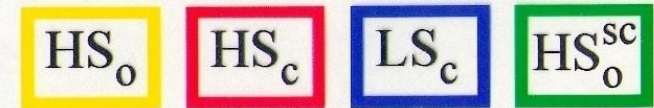
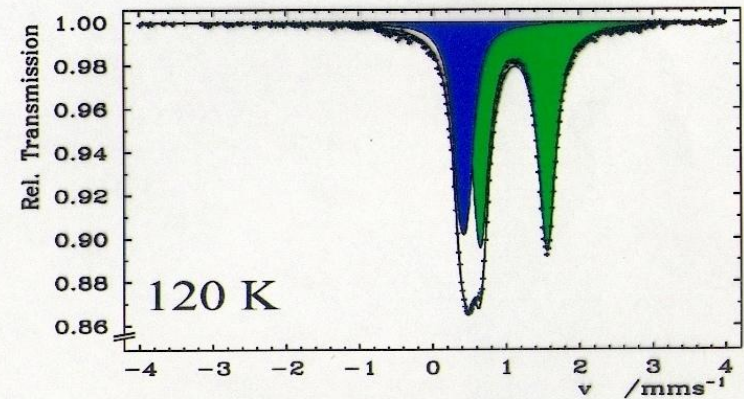
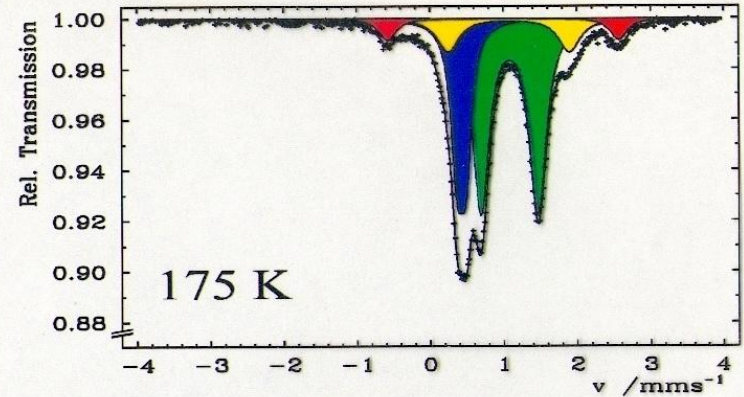
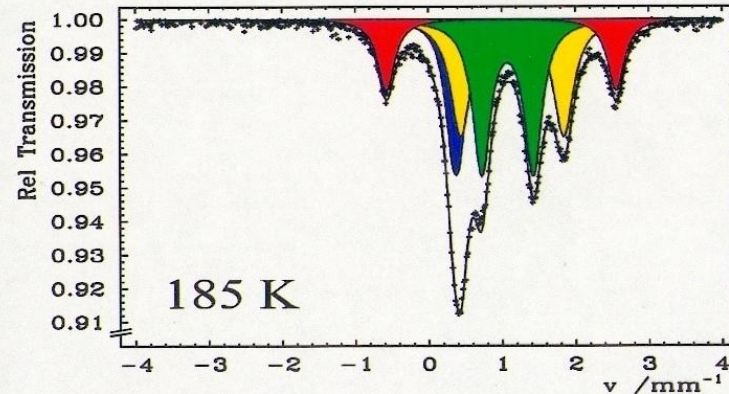
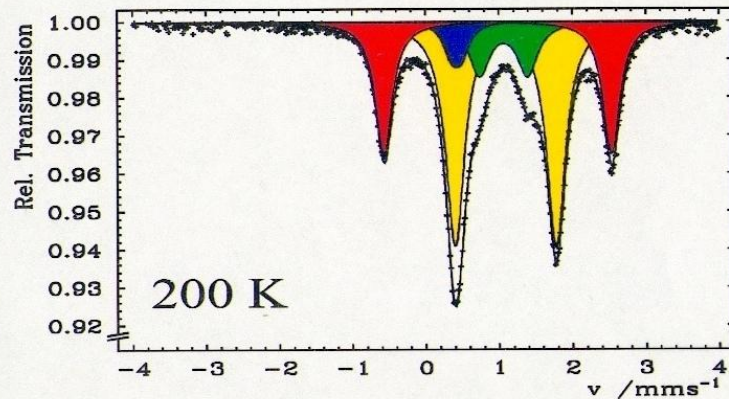
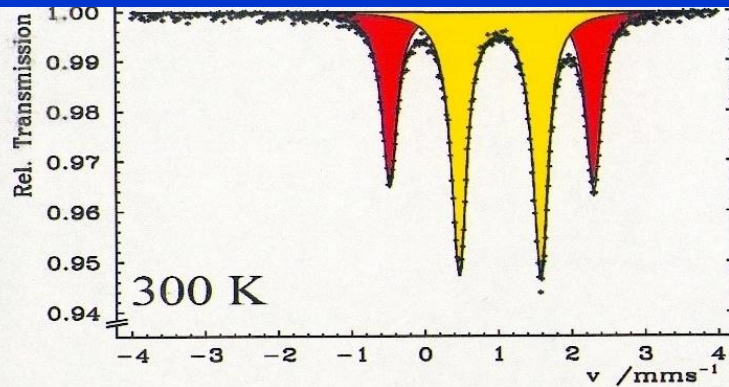
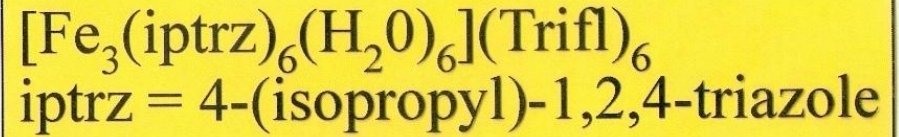


Thermal spin transition in the trinuclear iron(II) complex $[\text{Fe}_3(\text{iptrz})_6(\text{H}_2\text{O})_6](\text{Trifl})_6$



iptrz =
4-(isopropyl)-1,2,4-triazole

Kolnaar, Kooijman, Spek,
Ksenofontov, Gülich,
Haasnoot, Reedijk,
Inorg. Chem. 36(1997)2433

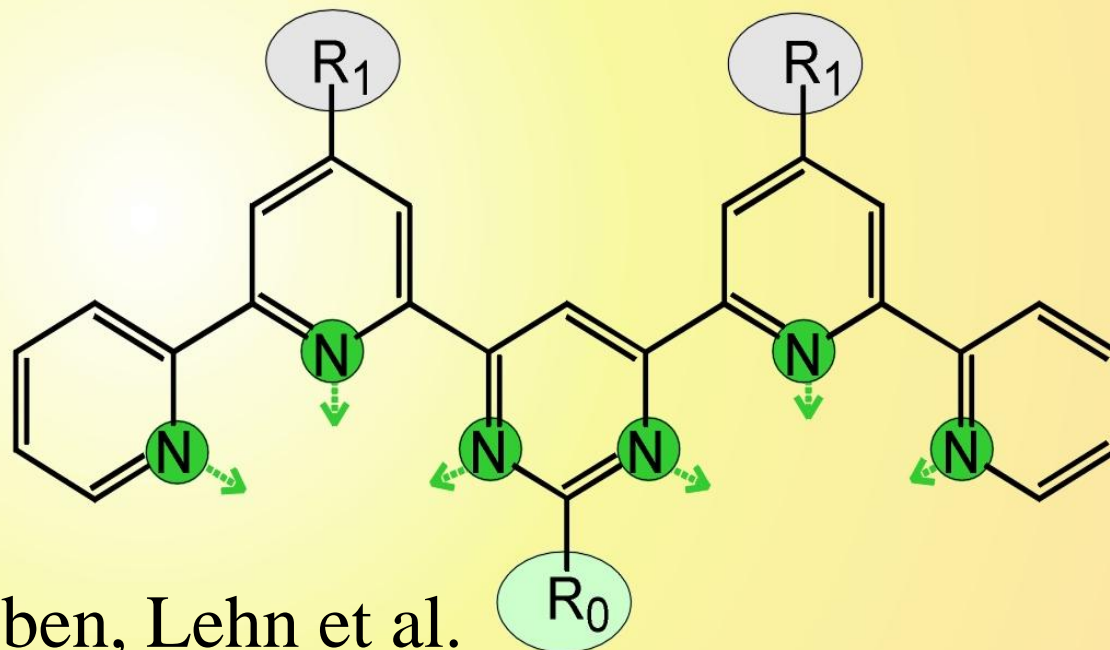


The central iron(II) is coordinated to three 1,2,4-triazole units and thus has FeN_6 core suitable to undergo thermal spin transition. The outer two iron(II) sites are each coordinated to three 1,2,4-triazole units and are capped by three water molecules, thus each having an FeN_3O_3 core, the ligand field strength of which is too weak for iron(II) to undergo spin transition. All three iron(II) centers are high spin at **300 K** as confirmed by Mössbauer spectroscopy. The quadrupole doublet shown in red, marked HS_c , with the large splitting refers to the central Fe(II). The large splitting arises mainly from the valence electron contribution to the EFG; the lattice contribution is small due to the relatively high symmetry (close to O_h) of the FeN_6 core. The quadrupole doublet shown in yellow, marked HS_o , refers to the two outer two Fe(II) sites. The considerably smaller quadrupole splitting in this case arises from a relatively large lattice contribution to the EFG due to the low symmetry of the FeN_3O_3 core, this is opposite in sign to the valence electron contribution and thus reduces the total EFG giving a smaller quadrupole splitting. The intensity ratio of the doublets of HS_o to HS_c is 1:2 as expected.

As the temperature is lowered, thermal spin transition from HS to LS takes place only at the central Fe(II). While the intensity of the yellow doublet of HS_o remains unchanged, that of the red doublet of the central Fe(II) diminishes at the favour of a new signal, shown in blue, referring to the low-spin state of the central Fe(II), marked by LS_c . At the same time, a new quadrupole doublet (green) arising from the outer Fe(II)-HS sites in HS-LS-HS trinuclear species, denoted as HS_o^{SC} , with twice the intensity of the blue LS_c resonance signal. This 2:1 intensity ratio for $\text{HS}_o^{\text{SC}} : \text{LS}_c$ (green to blue) remains on further lowering the temperature. The same 2:1 intensity ratio remains for $\text{HS}_o : \text{HS}_c$ (yellow to red) at any temperature until they entirely disappear after the spin transition is complete. The Mössbauer spectrum recorded at 120 K shows only the resonance signals for HS-LS-HS species. Clearly, the outer Fe(II)-HS sites “feel” the process of thermal spin transition in the center, which is being communicated through the three triazole bridges.

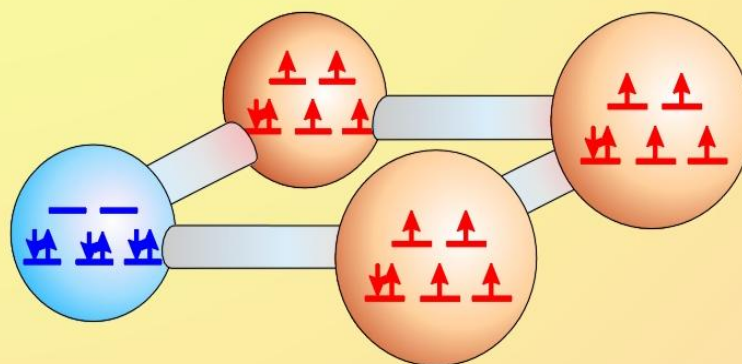
This is another “textbook example” for the high sensitivity of Mössbauer spectroscopy similar to the Mössbauer study of the $[\text{FeII}_2(\text{PMAT})_2](\text{BF}_4)_4 \cdot \text{DMF}$ discussed earlier. The slight distortion felt by the outer Fe(II)-HS sites, which is caused by the spin transition from HS to LS in the center, is hardly detectable by diffraction techniques.

Tetranuclear Iron(II) Complexes



Ruben, Lehn et al.

Renz, Gütlich. et al.

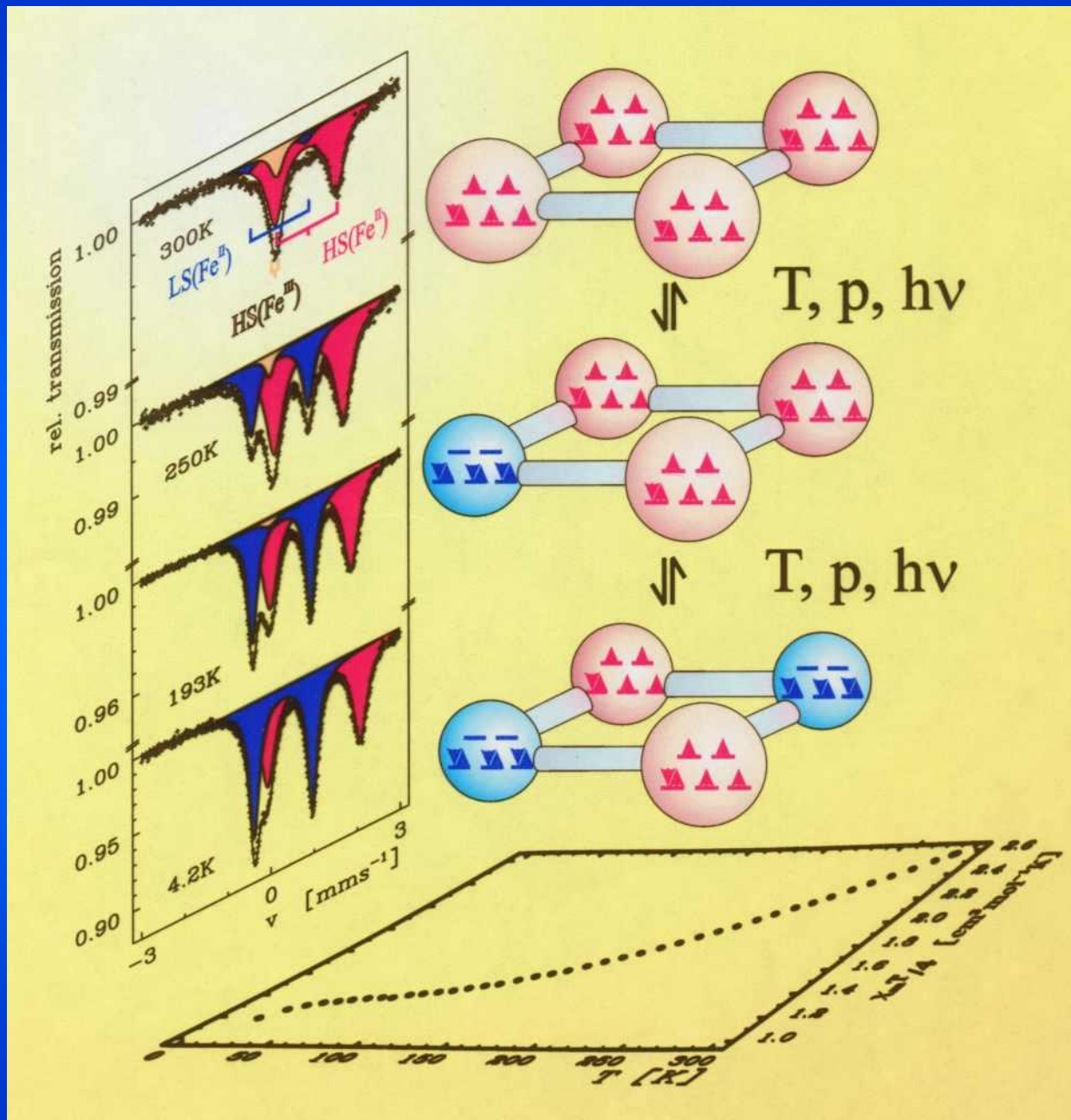


le1in.cdr cfr991118

Four iron(II) ions are held together in these tetranuclear complex molecules by four ligand molecules of the type shown in the upper part of the picture. The nitrogen donating atoms (green) of the ligand molecules coordinate to the iron centres as indicated by the arrows such that each centre is surrounded by six nitrogen atoms. The tetranuclear complex molecule is schematized in the lower part of the picture, where the spheres in red and blue represent the HS and LS centres, respectively, with their respective electron arrangements, and the rods represent the ligand molecules.

The four iron centres undergo thermal spin transition upon lowering the temperature. Results of Mössbauer and magnetic susceptibility measurements are depicted in the next viewgraph.

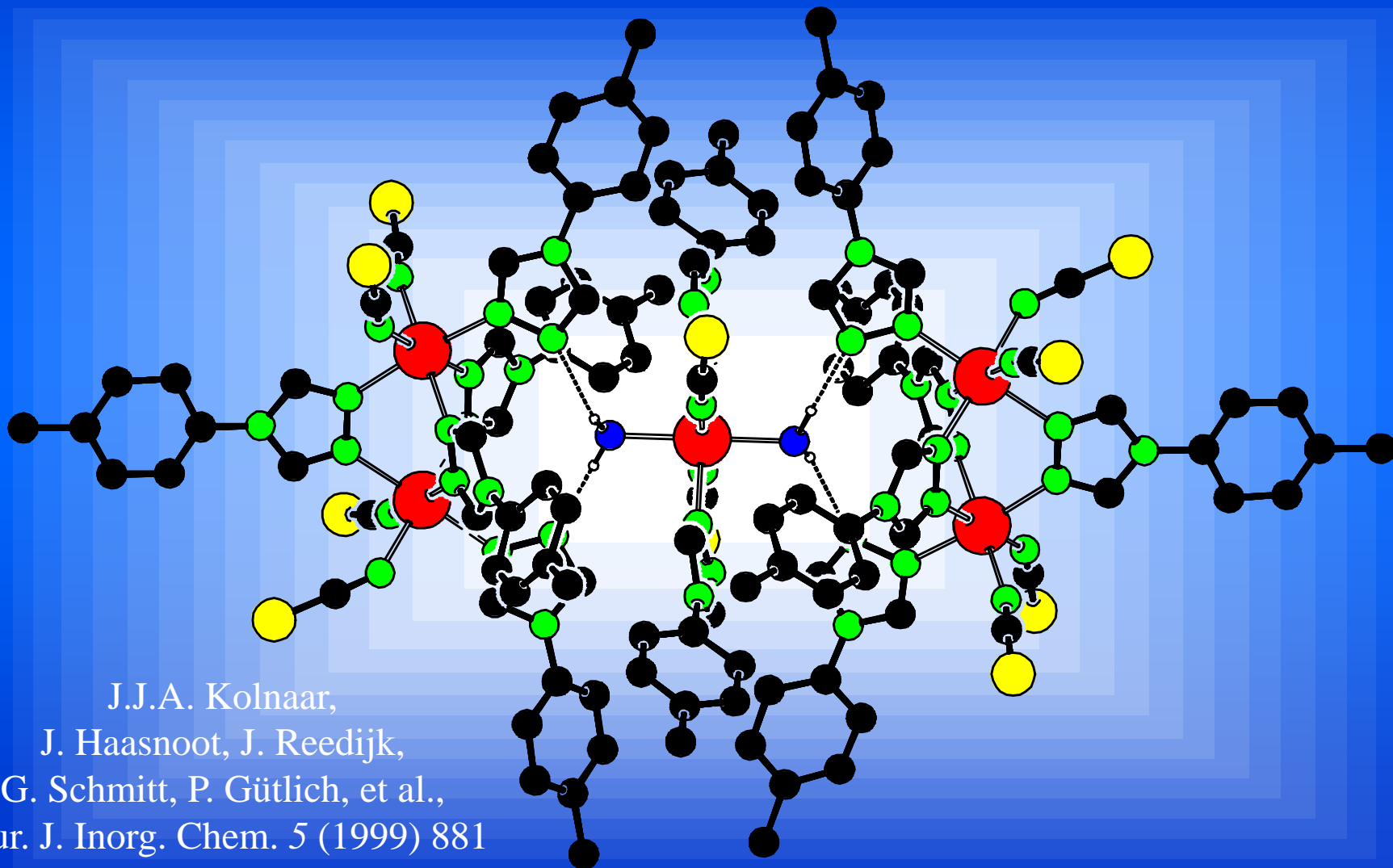
M. Ruben, E. Breuning, J. M. Lehn, V. Ksenofontov, F. Renz, P. Gütlich and G. B. M. Vaughan, *Chemistry-a European Journal*; 9 (2003) 18, 4422-4429



The 300 K spectrum indicates that essentially all four iron centres per complex molecule are in the HS state at room temperature. On cooling, the iron centres successively turn to the LS state. At 4.2 K two of the iron centres are still in the HS state. The spin transition is very gradual due to the fact that the iron centres do not switch simultaneously and that the cooperative interactions apparently are rather weak. The spin transition can also be effected by applying pressure, because the complex molecules are bigger in the HS than in the LS state. The LIESST phenomenon has also been verified in these systems.

(E. Breuning, M. Ruben, J.M. Lehn, F. Renz, Y. Garcia, V. Ksenofontov, P. Gütlich E. Wegelius, K. Rissanen, *Angew. Chem. Int. Ed.* 39 (2000) 14, 2504).
M. Ruben, E. Breuning, J. M. Lehn, V. Ksenofontov, F. Renz, P. Gütlich and G. B. M. Vaughan, *Chemistry-a European Journal*; 9 (2003) 18, 4422-4429

Pentanuclear Iron(II) Triazole Complex



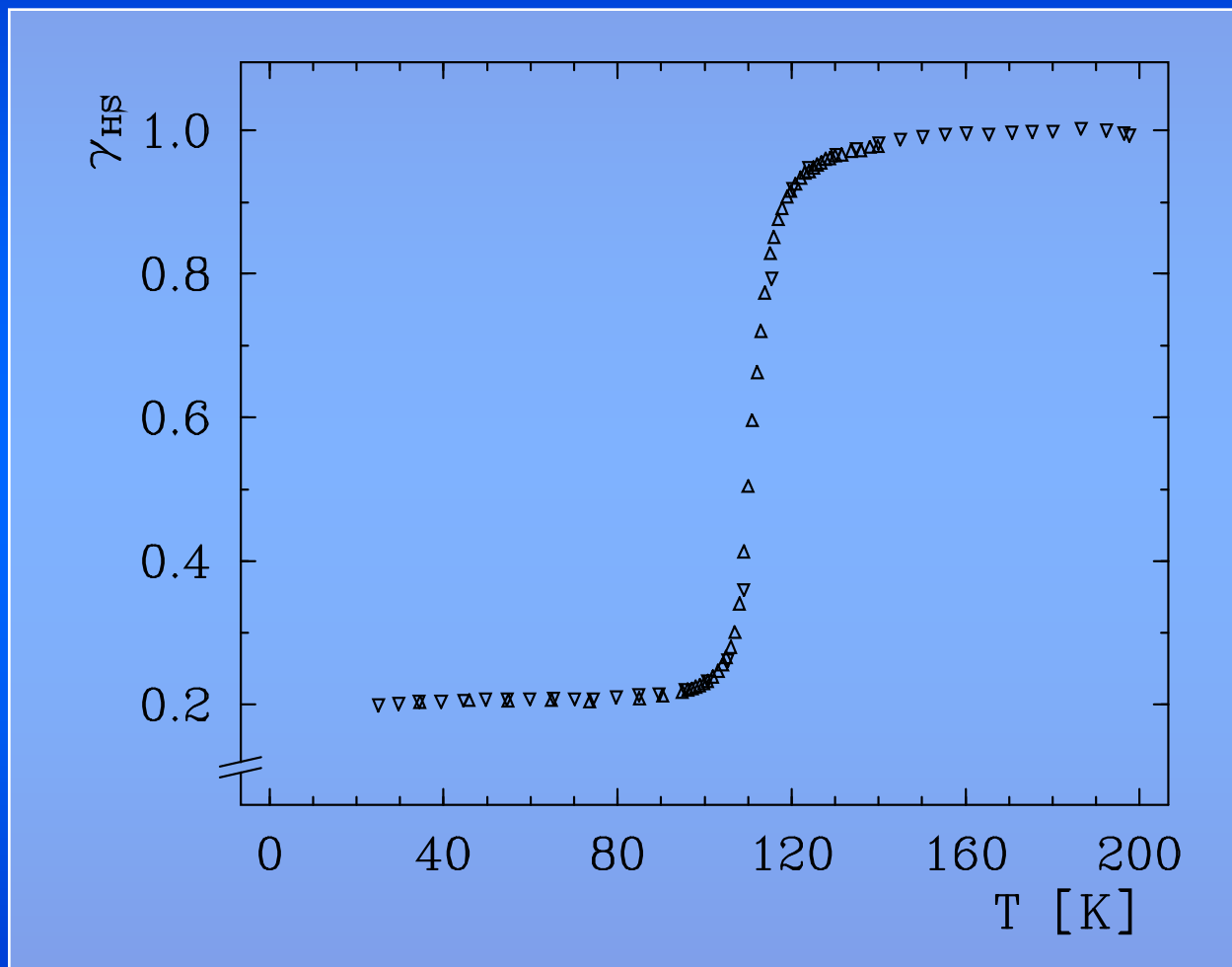
J.J.A. Kolnaar,

J. Haasnoot, J. Reedijk,

G. Schmitt, P. Gülich, et al.,

Eur. J. Inorg. Chem. 5 (1999) 881

$[\text{Fe}_2(\text{TolTrz})_5(\text{NCS})_4]_2[\text{Fe}(\text{TolTrz})_2(\text{NCS})_2\text{H}_2\text{O}]_2 \cdot \text{H}_2\text{O}$ Molar fraction $\gamma_{\text{HS}}(\text{T})$ from magn. susceptibility measurements

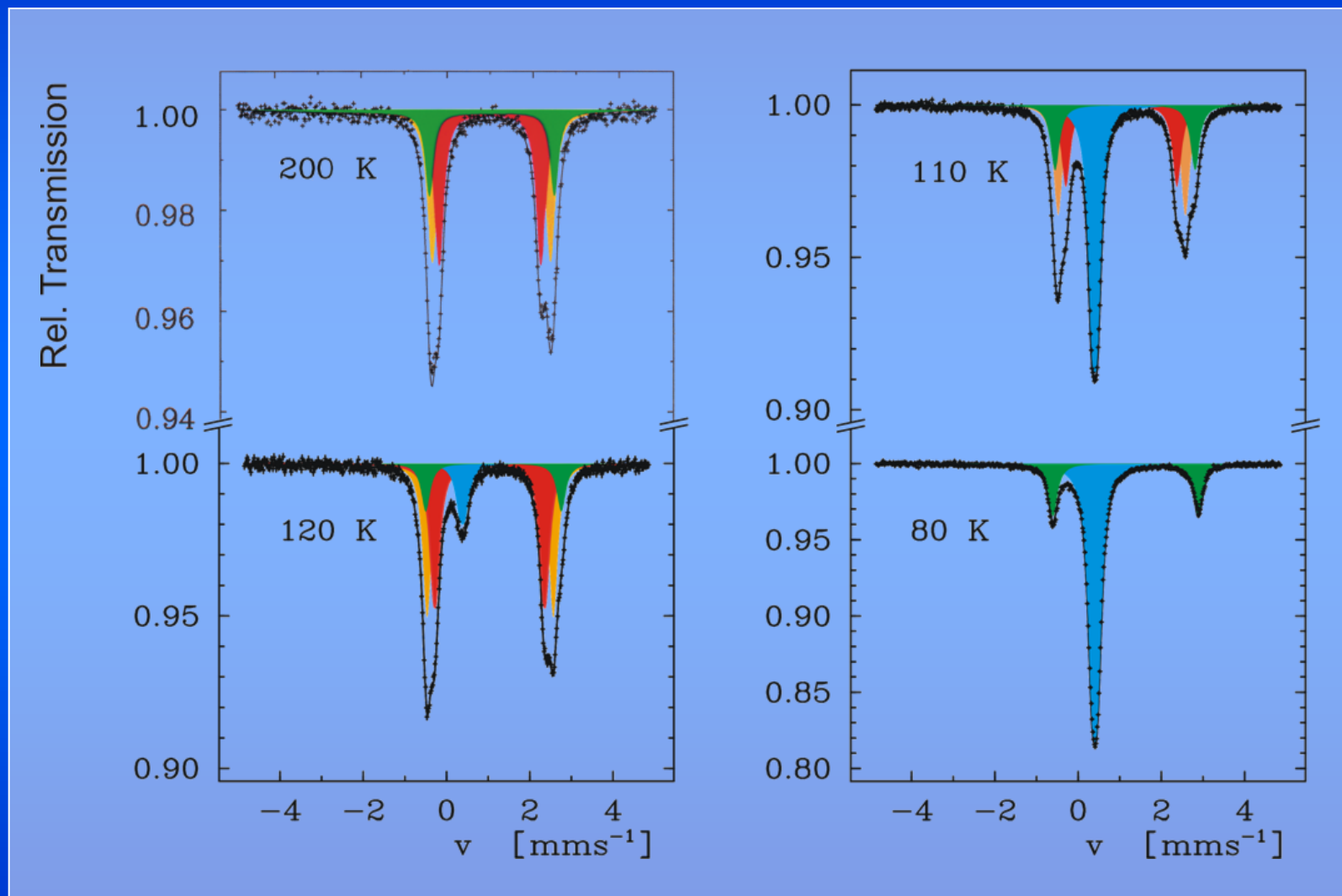


Four Fe(II) sites,
with FeN_6 core,
undergo thermal
spin transition.
One Fe(II) site, with
 FeN_4O_2 core,
remains in HS state.

J.J.A. Kolnaar, J. Haasnoot, J. Reedijk, G. Schmitt, P. Gülich, et al.,
Eur. J. Inorg. Chem. 5 (1999) 881



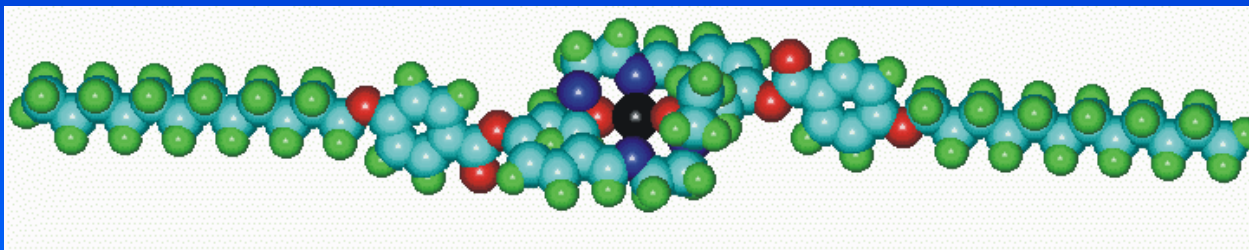
Mössbauer spectra as function of temperature



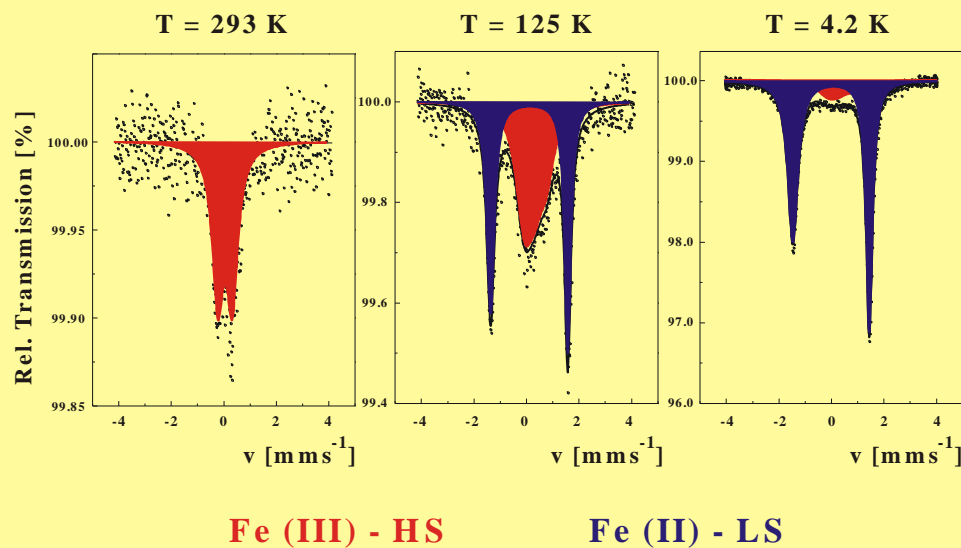
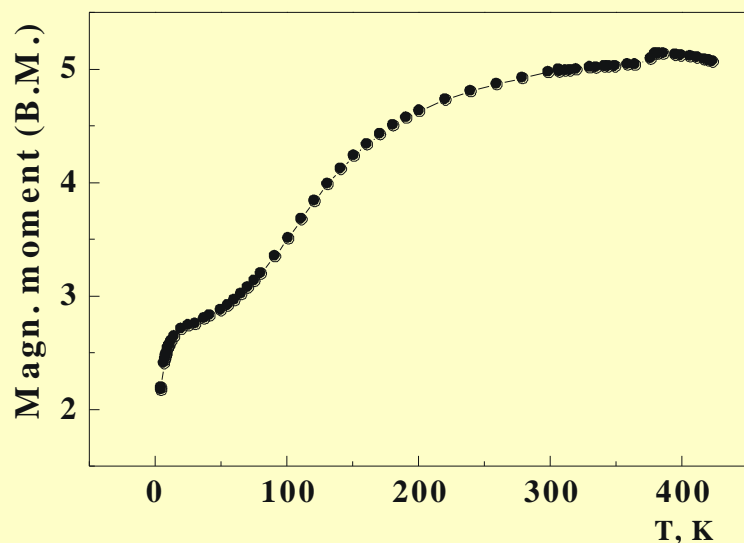
J.J.A. Kolnaar, J. Haasnoot, J. Reedijk, G. Schmitt, P. Gülich, et al., *Eur. J. Inorg. Chem.* 5 (1999) 881

P. Gülich, University of Mainz, Lecture Notes "Mössbauer Spectroscopy"

Coexistence of Spin Transition and Liquid Crystal Properties



Iron(III) complex with dodecyloxysalicyliden-N-ethyl-N-ethylendiamine ligands



Galyametdinov, Ksenofontov, Prosvirin, Ovchinnikov, Ivanova, Gülich, Haase, *Angew. Chem. Int. Ed.* **40** (2001) 4269

A topic of great actuality in molecular magnetism research is designing coordination compounds exhibiting synergistic effects, i.e. systems showing more than one dynamic electronic structure phenomena such as spin crossover, molecular magnetic interaction, electron transfer resulting in mixed valency and valence tautomerism, liquid crystal properties. An example is displayed in this picture.

The iron(III) complex with long-chain ligands shows liquid crystal properties above and spin crossover behaviour below room temperature. The latter is documented by the strong temperature dependence of the magnetic moment (lower left) and the Mössbauer spectra recorded at three different temperatures.

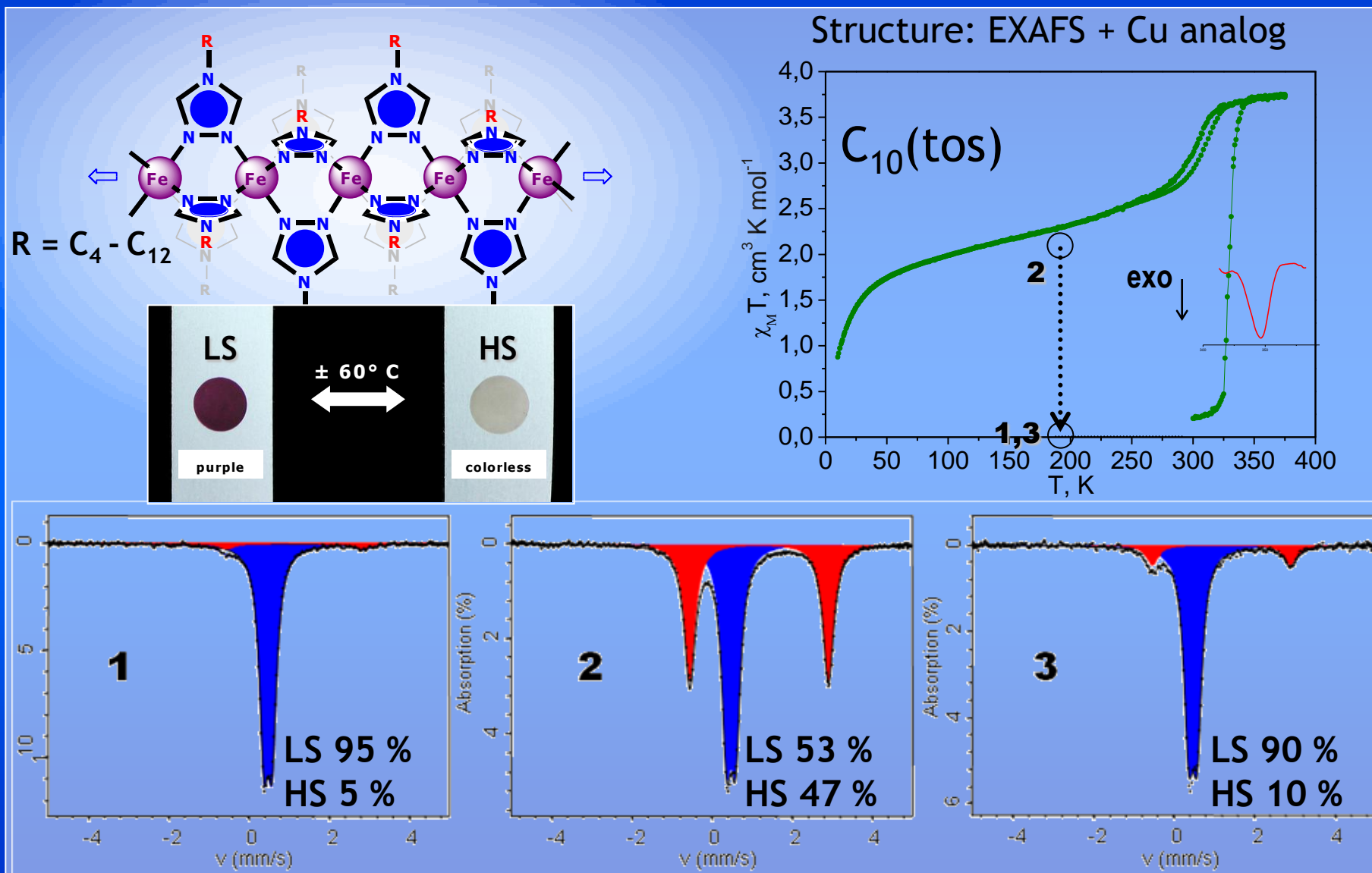
First example of coexistence of thermal spin transition and liquid-crystal properties

Y. Galyametdinov, V. Ksenofontov, A. Prosvirin, I. Ovchinnikov, G. Ivanova, P. Gütlich and W. Haase

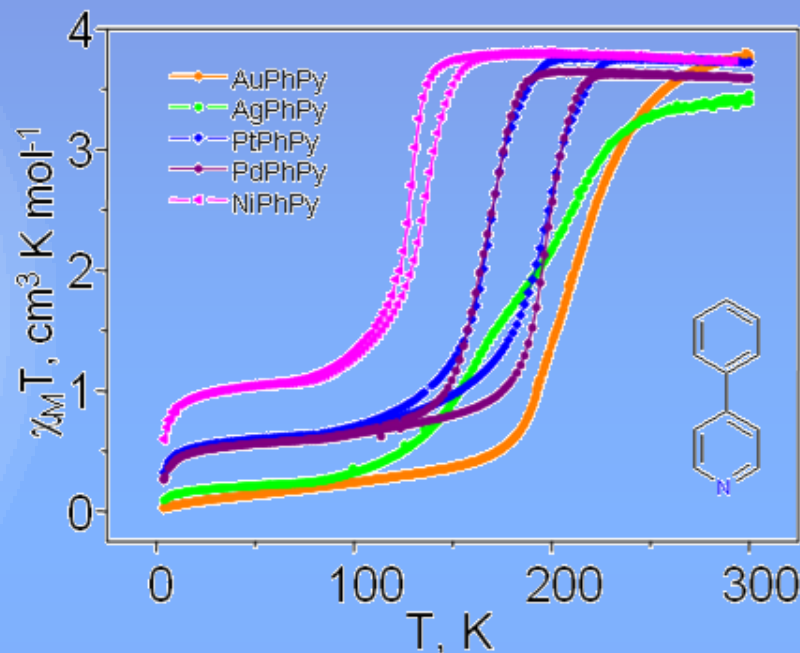
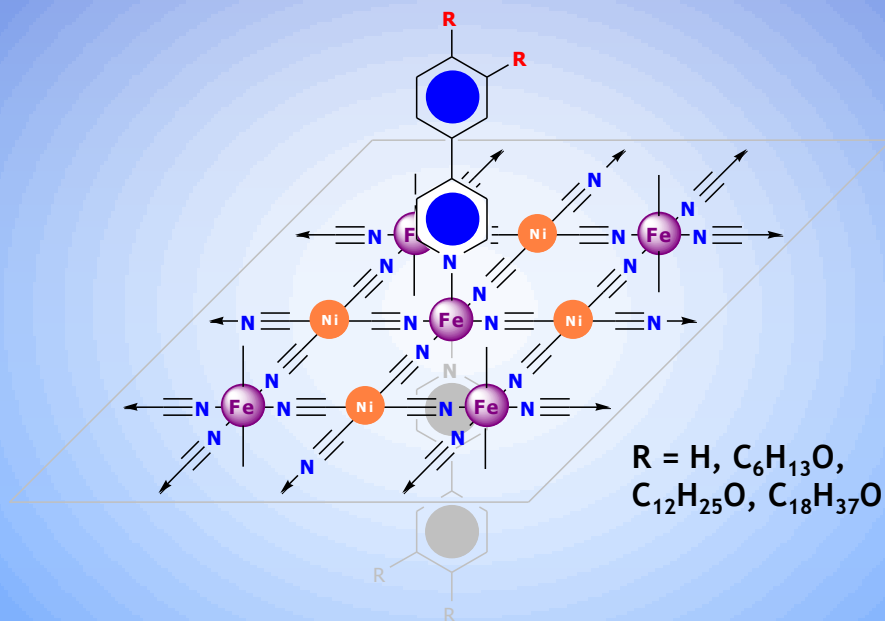
Angewandte Chemie-International Edition; 40 (2001) 22, 4269-4271

One-dimensional triazole-based SCO-LC complexes

M. Seredyuk, A.B. Gaspar, P. Gülich, 2007

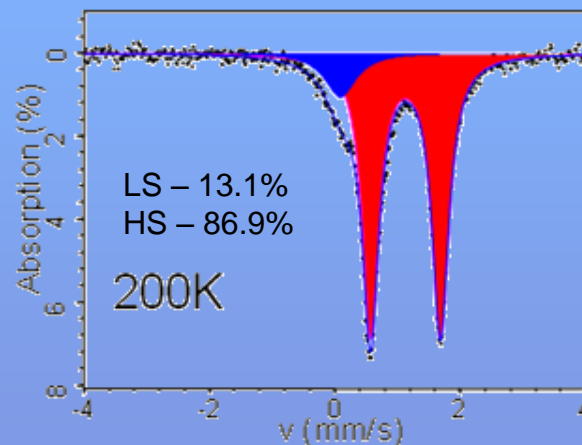
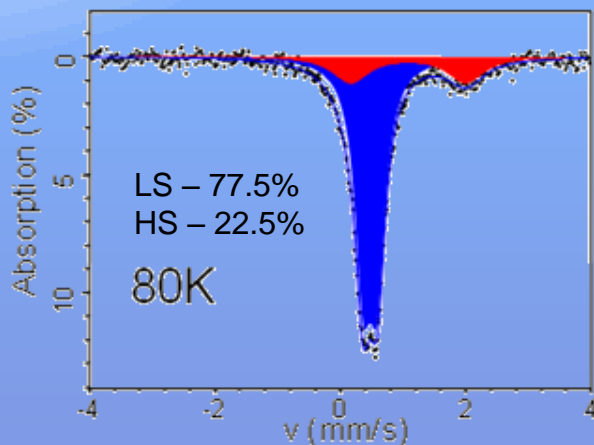


Two-dimensional Hofmann clathrate complexes



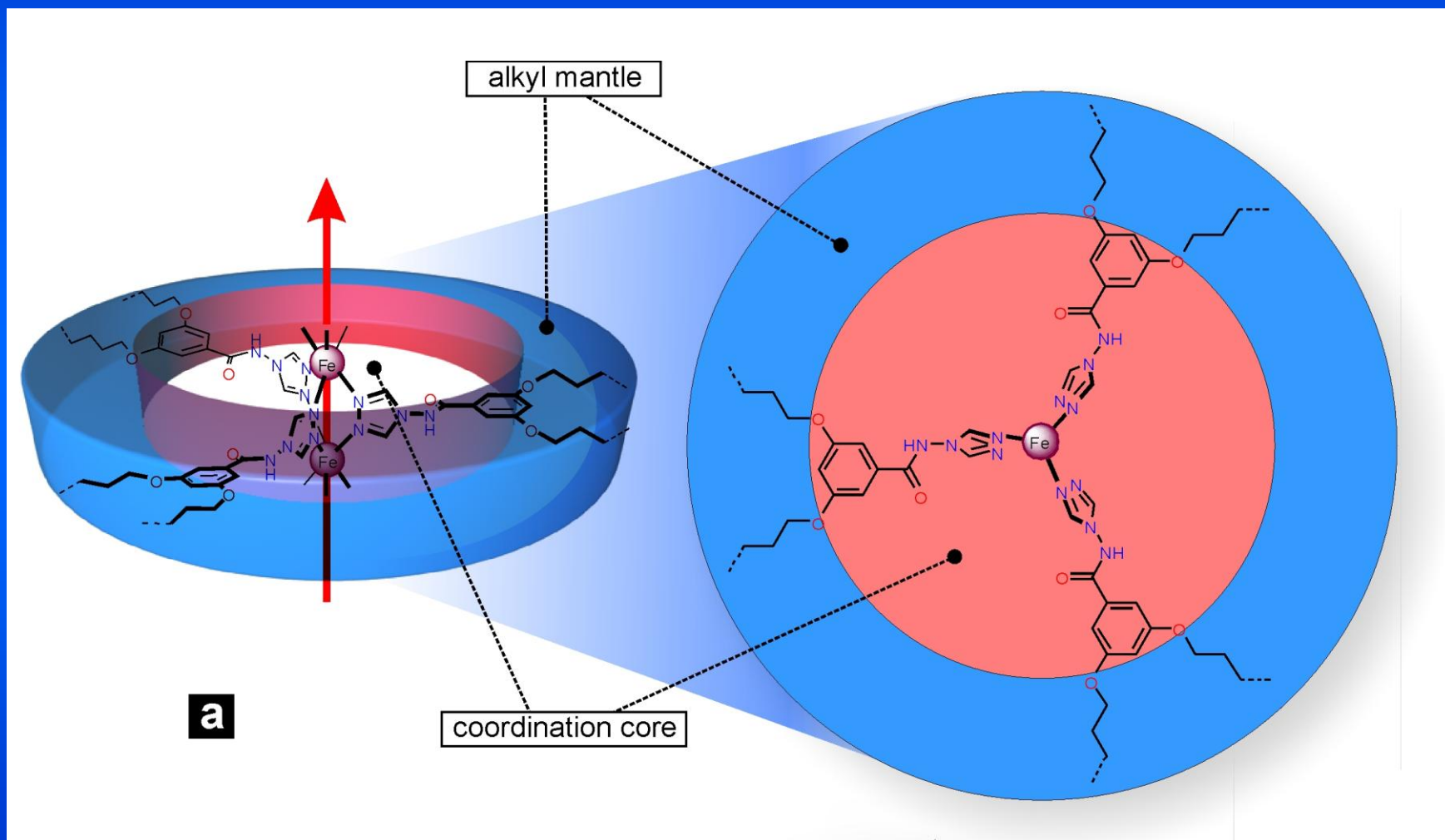
Mössbauer studies of the $\text{Fe}\{\text{[Ni(CN)}_4\text{] (PhPy)}_2\}$

Methods:
 DSC
 TGA
 XRD
 EXAFS
 Mössbauer
 SQUID



$[\text{Fe}(\text{C}_4\text{-tba})_3](\text{CF}_3\text{SO}_3)_2 \cdot 0.5\text{H}_2\text{O}$

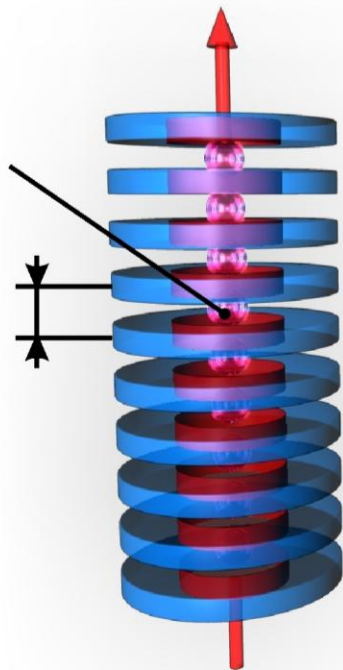
$\text{C}_4\text{-tba} = (5\text{-bis(butyloxy)-}N\text{-(4}H\text{-1,2,4-triazol-4-yl)benzamide})$



M. Seredyuk, A. B. Gaspar, P. Gülich 2008

Fe(II), low spin
 $d^{\text{Fe-N}} \sim 1.98 \text{ \AA}$

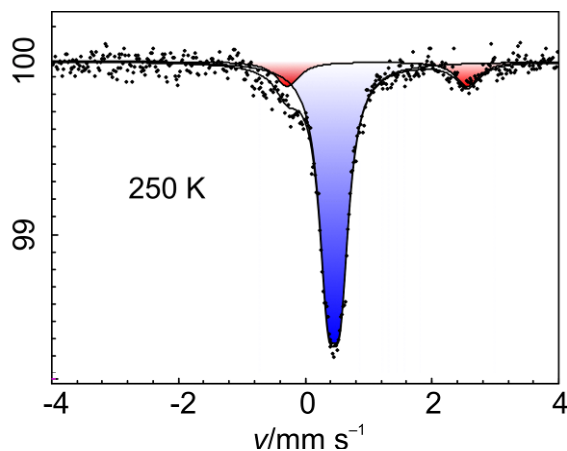
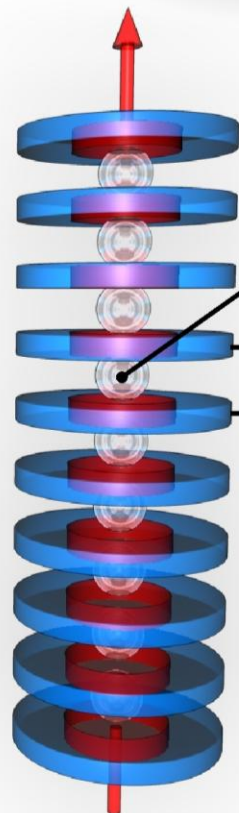
3.7 \text{ \AA}



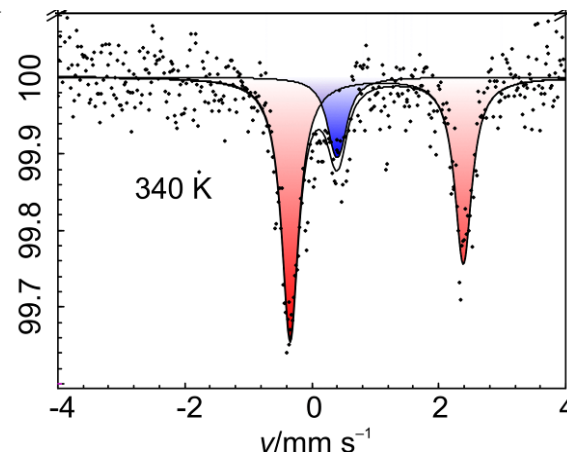
b

Fe(II), high spin
 $d^{\text{Fe-N}} \sim 2.15 \text{ \AA}$

3.9 \text{ \AA}



Temperature induced increase of distance changes spin state: LS \rightarrow HS

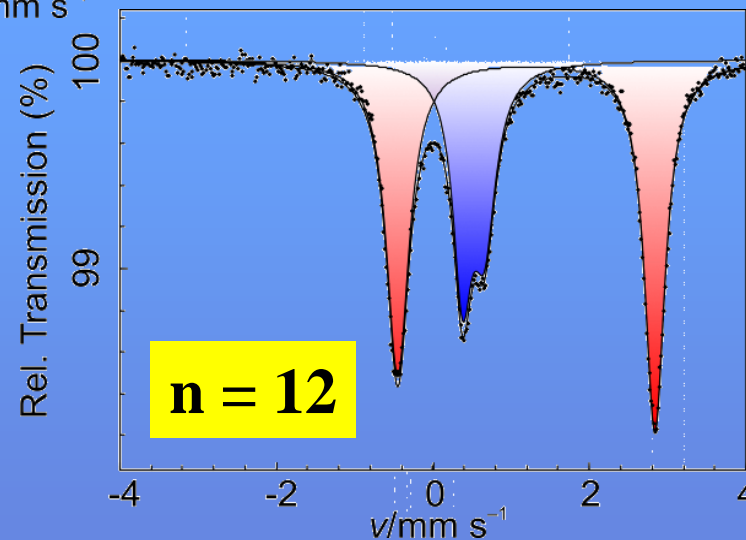
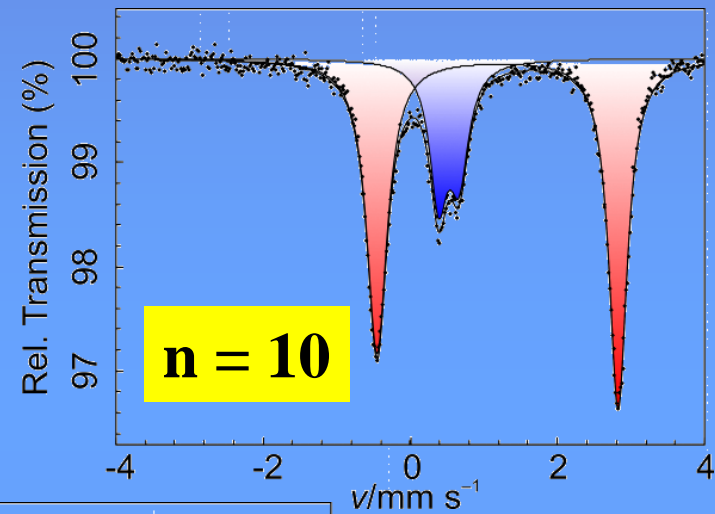
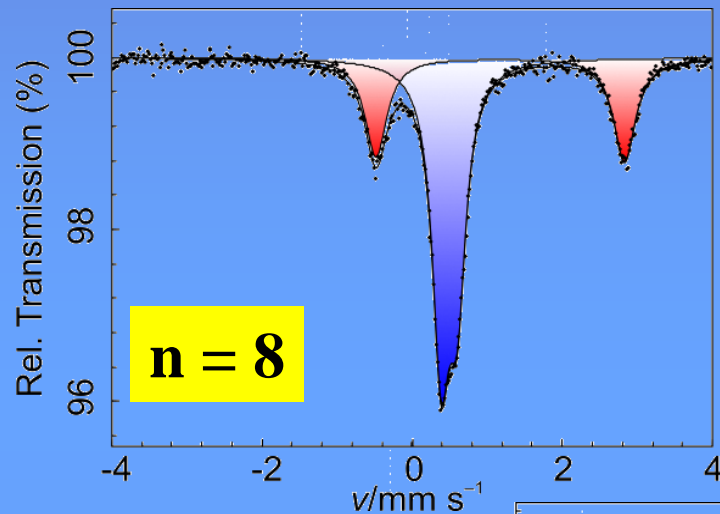


M. Seredyuk, A. B. Gaspar, P. Gütlich 2008

Effect of chain-length in $[\text{Fe}(\text{C}_n\text{-tba})_3](\text{BF}_4)_2 \cdot \text{H}_2\text{O}$

$n = 8, 10, 12$; $T = 80 \text{ K}$

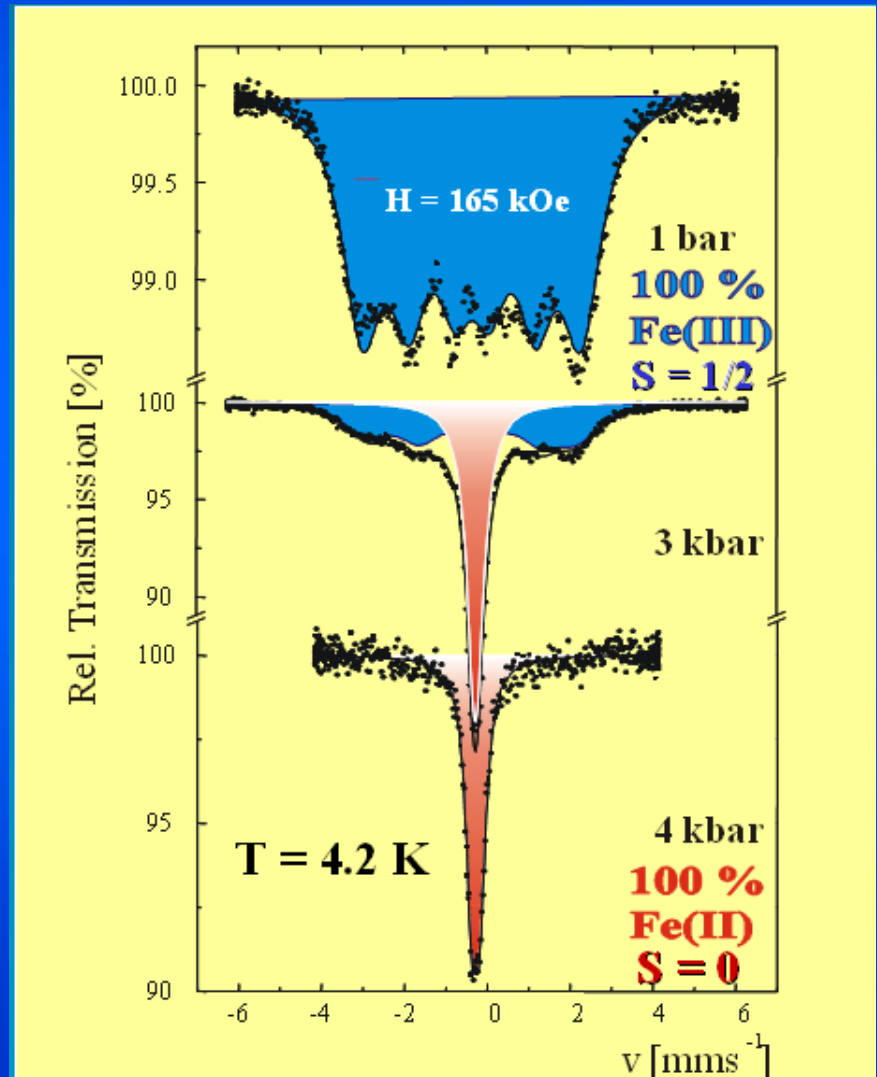
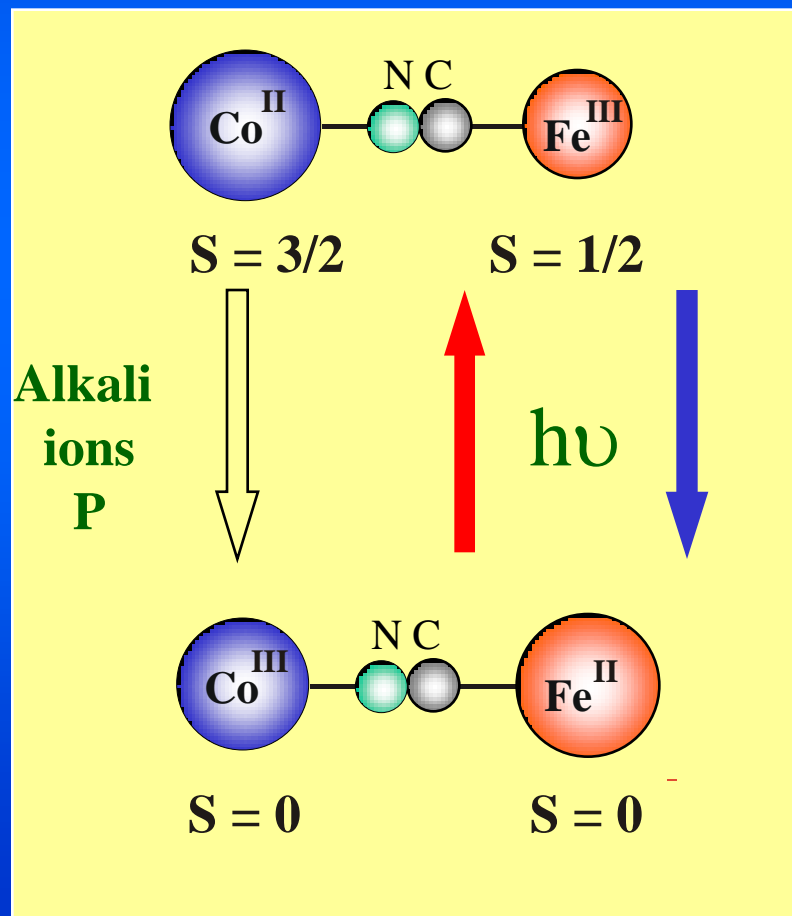
$\text{C}_n\text{-tba} = (5\text{-bis(alkoxy)-}N\text{-(4}H\text{-1,2,4-triazol-4-yl)benzamide})$



M. Seredyuk,
A. B. Gaspar,
P. Gütlich 2008

Pressure-induced electron transfer in ferrimagnetic Prussian blue analogs

Ksenofontov, Bleuzen, Verdaguer, Gütlich et al. (Phys. Rev. B, 2003)



The cobalt(II)-iron(III) cyano complex, when doped with potassium ions, may undergo a thermally induced electron transfer around 20 K from the Co(II)-HS ion with spin $S=3/2$ over the NC bridge to the Fe(III)-LS ion with spin $S=1/2$, whereby the Co(II)-HS centre turns to Co(III)-LS with spin $S=0$ and the Fe(III)-LS to Fe(II)-LS with spin $S=0$. The diamagnetic pair Co(III)-Fe(II) (total spin $S = 0$) can be converted to the paramagnetic pair Co(II)-Fe(III) (total spin $S = 2$) by irradiation with red light, while the latter pair can be converted back to the diamagnetic pair with blue light. It has been observed that the formation of the diamagnetic pairs can be enhanced by increasing the potassium concentration or doping with more voluminous alkali ions like rubidium or caesium. Apparently, chemical pressure favours the electron transfer and the formation of the diamagnetic pairs, which are smaller in molecular volume than the paramagnetic pairs. This was proven by measuring the Mössbauer spectra under applied pressure of a sample as shown here, which has very little potassium and does not show a thermally induced electron transfer at ambient pressure. At 4.2 K, the spectrum is magnetically split into a sextet with a local magnetic field of 165 kOe arising from the $S=1/2$ Fermi contact field. At a pressure of 3 kbar, most of the sextet intensity has disappeared at the favour of a singlet arising from the Fe(II)-LS sites. At 4 kbar the pressure-induced electron transfer from Co(II)-HS to Fe(III)-LS is complete and the spectrum shows only the typical Fe(II)-LS singlet.

V. Ksenofontov, G. Levchenko, S. Reiman, P. Gütlich, A. Bleuzen, V. Escax, M. Verdaguer, *Phys. Rev. B* 68(2003)024415

Pressure cells for Mössbauer and magnetic susceptibility measurements at variable hydrostatic pressures up to ca. 14 kbar in the temperature range 400 K to 4.2 K have been developed by the Mainz group of P. Gütlich and are shown in the next picture.

Mössbauer Emission Spectroscopy

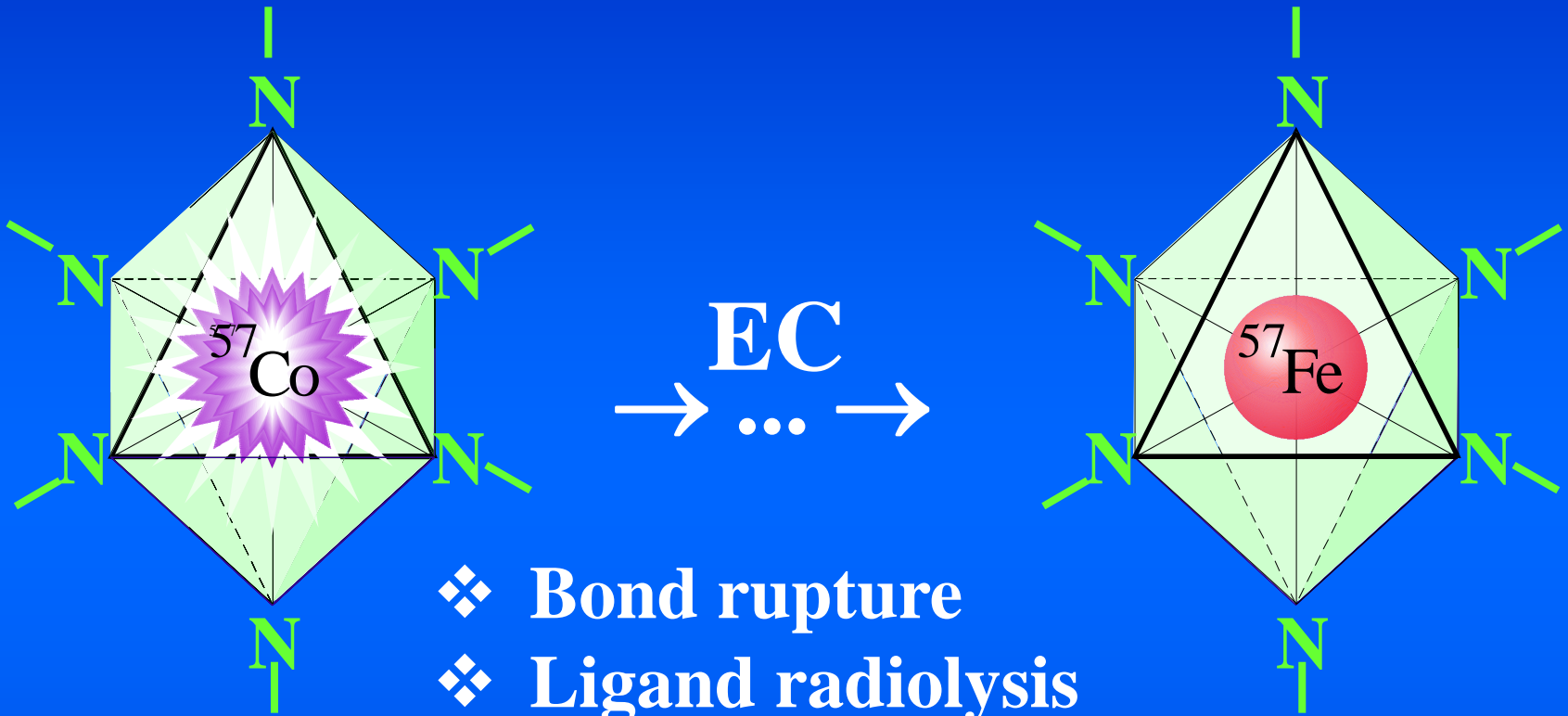
MAS and MES Experiments

	MAS	MES
Source	Single line ($^{57}\text{Co/Rh}$)	Sample under Study
Absorber	Sample under study	Single line $\text{K}_4[\text{Fe}(\text{CN})_6]$

In conventional Mössbauer spectroscopy one uses a “single-line” source, e.g. ^{57}Co embedded in a rhodium matrix in the case of ^{57}Fe spectroscopy, and the iron containing material under study as absorber. This technique is termed “Mössbauer absorption spectroscopy” (MAS) in order to distinguish it from the so-called source experiment, also known as “Mössbauer emission spectroscopy” (MES). In a MES experiment one uses a “single-line” absorber, e.g. $\text{K}_4[\text{Fe}(\text{CN})_6]$, and a ^{57}Co doped sample under study as source. In this case, the recorded Mössbauer spectrum refers to the hyperfine interactions in the source material, i.e. it yields information on the chemical and physical properties of the excited ^{57}Fe atoms before they decay. The MES technique has been widely used to investigate chemical and physical *after-effects* of nuclear decay in various materials, particularly in poorly conducting coordination compounds.

If the radioactive ^{57}Co ions are embedded in a metallic matrix, electron relaxation processes are very fast, and at ca. 100 ns after the nuclear decay, when the “Mössbauer time window” (corresponding to the lifetime of the excited nuclear state) is reached, electronic relaxation processes have become thermally equilibrated and one usually observes no noticeable after-effects in metallic matrices. This, however, is different in the case of poorly conducting coordination compounds, e.g. with nitrogen donating ligand molecules. As schematized in the viewgraph, the electron capture decay of radioactive ^{57}Co , whereby an electron from the K shell is captured by the ^{57}Co nucleus and turned into ^{57}Fe , may lead to a variety of after-effects like bond rupture, ligand radiolysis, change of charge states and excited ligand field states to name the most important consequences of nuclear decay in solid coordination compounds. These after-effects may have lifetimes on the order of 10 to 500 ns. It is possible to cover this time regime with “time-integral” and “time-differential” Mössbauer emission spectroscopy.

After-Effects of $^{57}\text{Co}(\text{EC})^{57}\text{Fe}$ Decay



- ❖ Bond rupture
- ❖ Ligand radiolysis
- ❖ Change of charge state
- ❖ Excited ligand field states

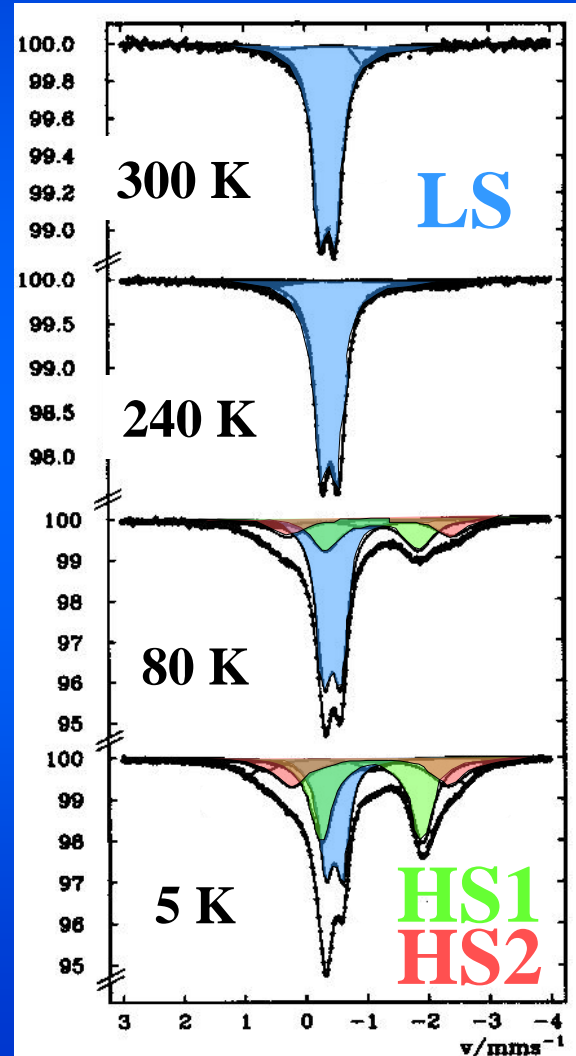
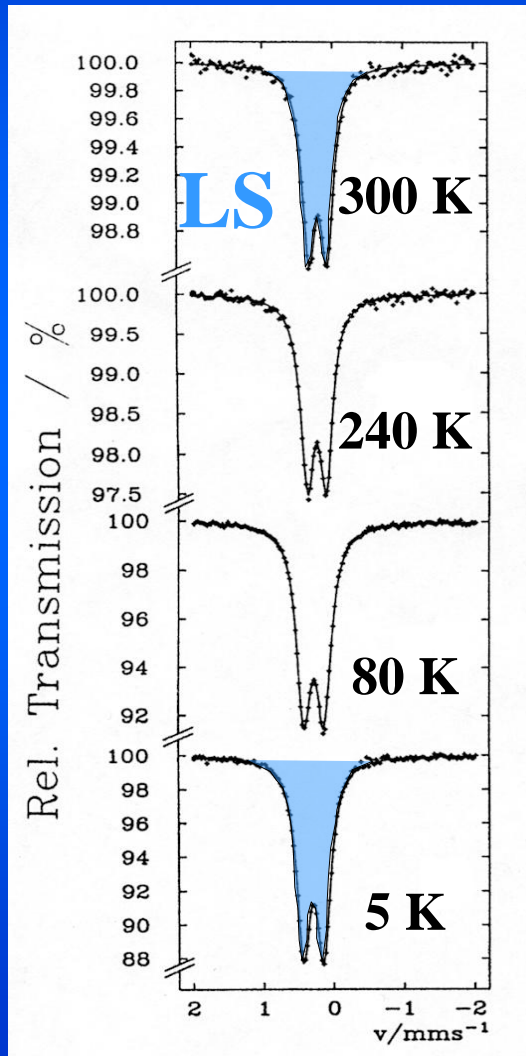
Time window: 10 – 500 ns

$[M(\text{phen})_3](\text{ClO}_4)_2$

$$M = {}^{57}\text{Fe}_x/\text{Co}_{1-x} \quad M = {}^{57}\text{Co}_x/\text{Co}_{1-x}$$

($x = 0.001$)

Source:
 ${}^{57}\text{Co}/\text{Rh}$
295 K



Absorber:
 $\text{K}_4[\text{Fe}(\text{CN})_6]$
295 K

The coordination compound $[\text{Co}^{\text{II}}(\text{phen})_3](\text{ClO}_4)_2$ (phen = 1,10-phenanthroline) doped with 0.1 % of ^{57}Fe was studied by Mössbauer absorption spectroscopy using a $^{57}\text{Co}/\text{Rh}$ source (spectra on the left). The three phen ligands create a relatively strong ligand field at the iron(II) center, the compound shows LS behaviour at all temperatures under study (see MAS spectra on the left). The same system, however doped with ^{57}Co as Mössbauer source, was studied by Mössbauer emission spectroscopy using $\text{K}_4[\text{Fe}(\text{CN})_6]$ as absorber. The MES spectra (right) also show the typical Fe(II)-LS signal at 300 K down to ca. 200 K. On further cooling, the intensity of this signal decreases and at the same time two Fe(II)-HS doublets, HS1 and HS2, appear with increasing intensity. These unusual spin states are excited ligand field states with temperature-dependent lifetimes on the order of ca. 100 ns. Similar experiments were carried out with systems whose corresponding iron(II) compounds possess intermediate ligand field strengths and show thermal spin crossover. An example is discussed in the next picture.

Recent review article: **Nuclear-decay-induced excited spin trapping**

P. Gülich in “Spin Crossover in Transition Metal Compounds”

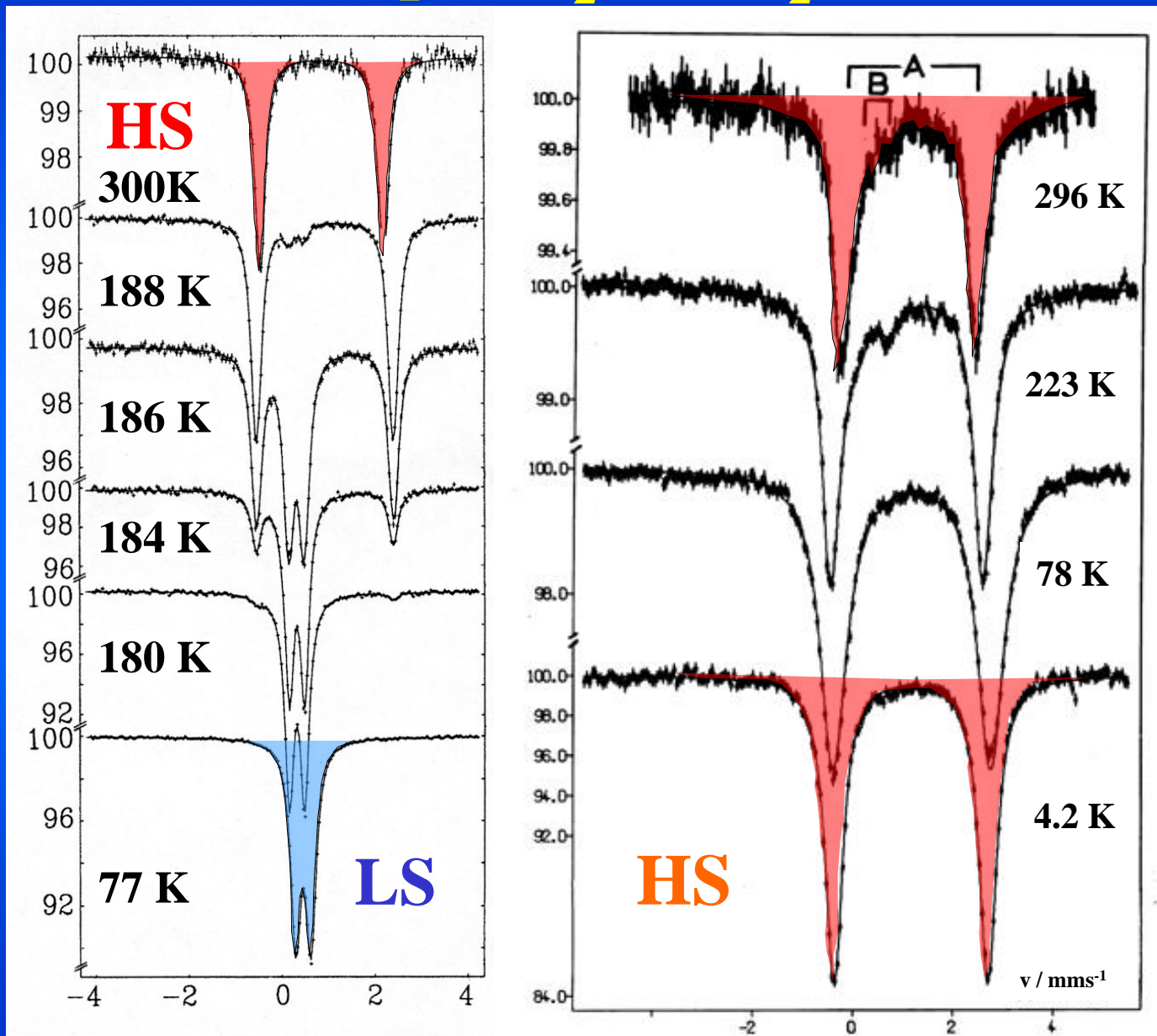
P. Gülich and H.A. Goodwin (Editors), *Topics in Current Chemistry*, Vol. 234 (2004), Springer, Heidelberg, Berlin, p. 231-260

M : ^{57}Fe



M : ^{57}Co

Rel. Transmission (%)



[Fe(phen)₂(NCS)₂] undergoes thermal spin transition as already discussed above. The temperature dependent MAS spectra are shown on the left. The analogous cobalt(II) compound doped with ⁵⁷Co and used as Mössbauer source (or the corresponding iron compound doped with ⁵⁷Co as source which gives the same results) yield the temperature dependent MES spectra shown on the right. The main result is that in the temperature region, where the MAS spectra reflect the transition to the LS state, the MES spectra still show the typical HS signals arising from excited ligand field states.

The mechanism of the formation of the excited ligand field states as a consequence of the EC nuclear decay of radioactive ⁵⁷Co is well understood. It is much related to that of the LIESST phenomenon and has therefore been termed “Nuclear-Induced Excited Spin State Trapping” (NIESST). The main difference between the two phenomena lies in the primary step of excitation, which is the application of a light source in the case of LIESST, whereas in NIESST the nuclear decay serves quasi as an intrinsic molecular excitation source.

The ligand field strength at the nucleogenic ^{57}Fe centre is of utmost importance for the lifetime of the excited $^5\text{T}_2$ state. The stronger the ligand field, the larger is the energy difference ΔE_{HL} , and the shorter is the lifetime of the $^5\text{T}_2$ state of the nucleogenic ^{57}Fe ion (Gütlich, P., Hauser, A., Spiering, H., *Angew. Chem. Int. Ed. Engl.*, 1994, 33, 2024). This is clearly confirmed by MES experiments with strong-field and intermediate-field complexes as discussed above.

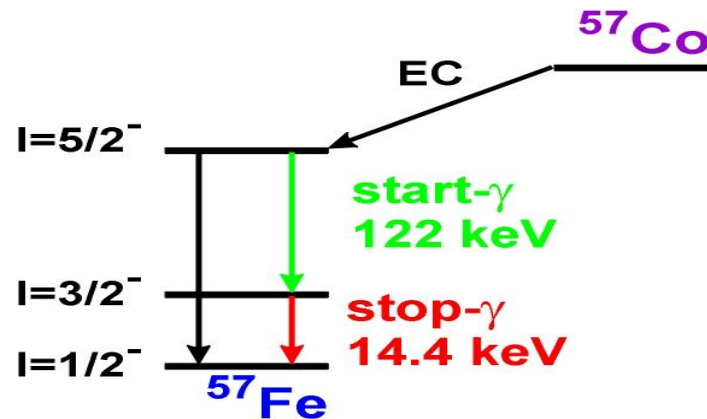
Lifetime measurements on ^{57}Co doped strong-field complexes have been carried out by time-differential MES experiments using a specially constructed Mössbauer coincidence spectrometer developed by the Mainz group. The following scheme gives an idea how the method works.

Kajcsos, Zs.; Alflen, M.; Spiering, H.; Gütlich, P.; Albrecht, R.; Schulze, R.; Kurz, R. *Hyperfine Interactions* **1986**, 29, 1551;

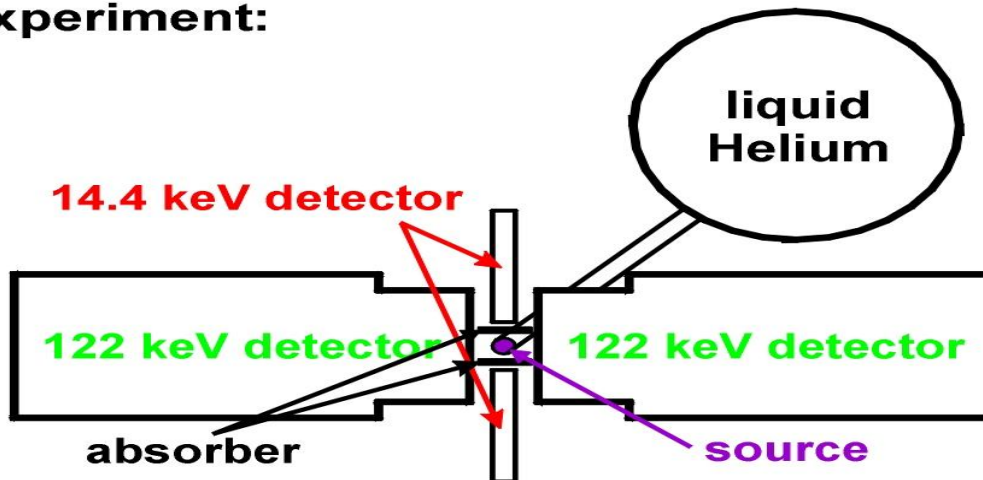
Albrecht, R.; Alflen, M.; Gütlich, P.; Kajcsos, Zs.; Schulze, R.; Spiering, H.; Tuczek, F. *Nucl. Instr. Meth. Phys. Res. A* **1987**, 257, 209;

Tuczek, F.; Spiering, H.; Gütlich, P., *Hyperfine Interactions* **1990**, 62, 109

Time-Differential Mössbauer Emission Spectroscopy



Experiment:



Lifetimes of excited electr. states: 10 - 500 ns
Resolution : ca. 5 ns

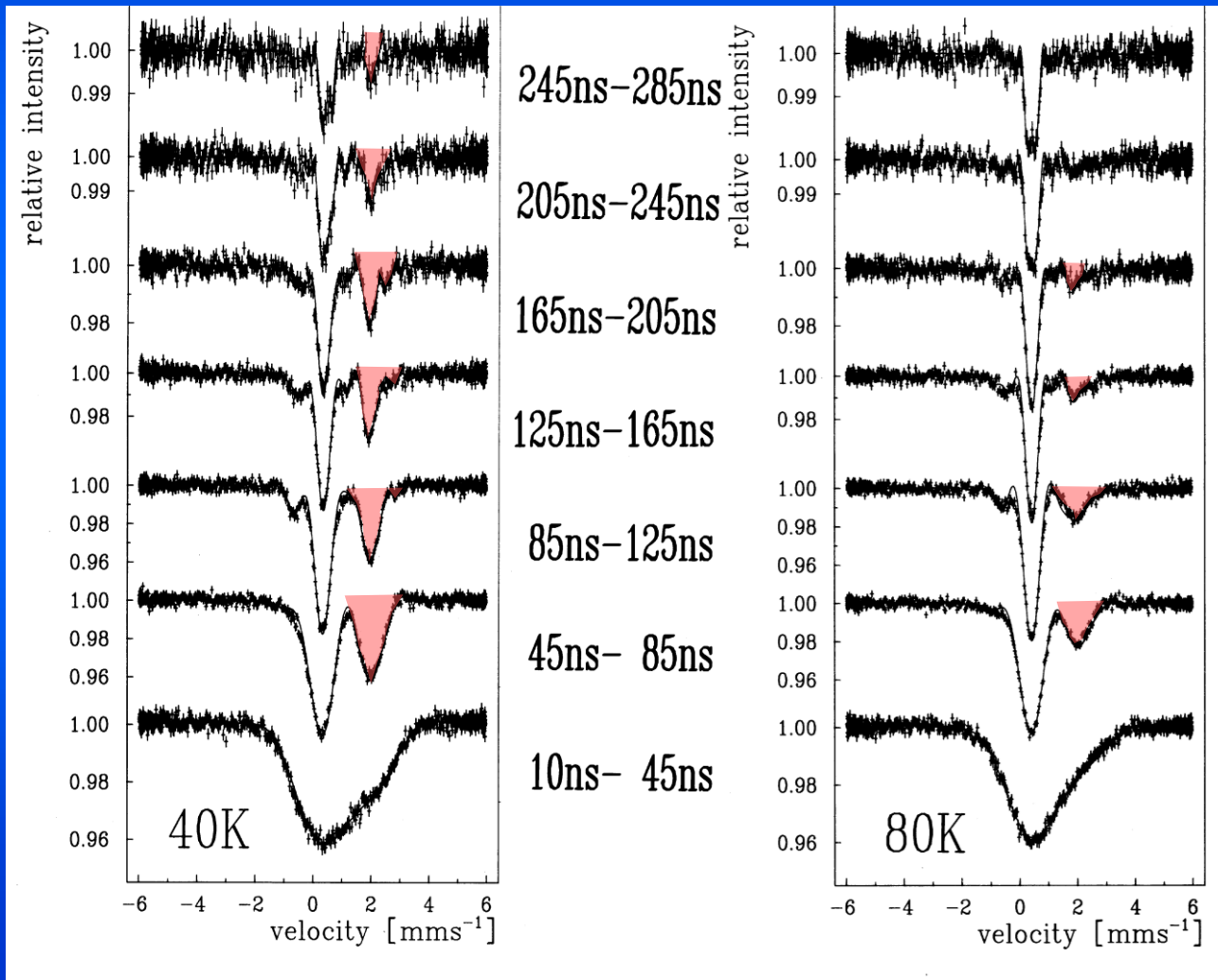
Time-differential Mössbauer emission spectroscopy of ^{57}Co -doped cobalt or iron compounds makes use of the 122 keV γ -Quanta arising from the decaying 136 keV nuclear state of ^{57}Fe as the start signal, and the 14.4 keV γ -Quanta of the “Mössbauer transition” as the stop signal. The source is mounted in a cryostat for temperature dependent measurements down to the liquid helium range, and the single-line absorber ($\text{K}_4[\text{Fe}(\text{CN})_6]$) is moved relative to the absorber outside at ambient temperature. Specially designed sodium iodide detectors are used as detectors for the 122 and 14 keV γ -Quanta. Information on the electronic parts and the data acquisition and data reduction methods can be found in the literature: R. Albrecht, M. Alflen, P. Gütlich, Z. Kajcsos, R. Schulze, H. Spiering, F. Tucek, *Nucl. Instr. Meth. Phys. Res. A* 257 (1987) 209; M. Alflen, C. Hennen, F. Tucek, H. Spiering, P. Gütlich, Z. Kajcsos, *Hyperfine Interactions* 47 (1989) 115).

Lifetime measurements of excited electronic states formed after the EC decay of ^{57}Co in transition metal compounds have been carried out in the time window of ca. 10 to 500 ns with a resolution of ca. 5 ns. An example showing two series of time-differential Mössbauer emission spectra of $[\text{Co}^{\text{II}}(\text{phen})_3](\text{ClO}_4)_2$ (phen = 1,10-phenanthroline) recorded at 80 and 40 K, respectively, is displayed in the next figure.

$[^{57}\text{Co}/\text{Co}(\text{phen})_3](\text{ClO}_4)_2$

Time Differential Mössbauer Emission Spectra

40 K



80 K

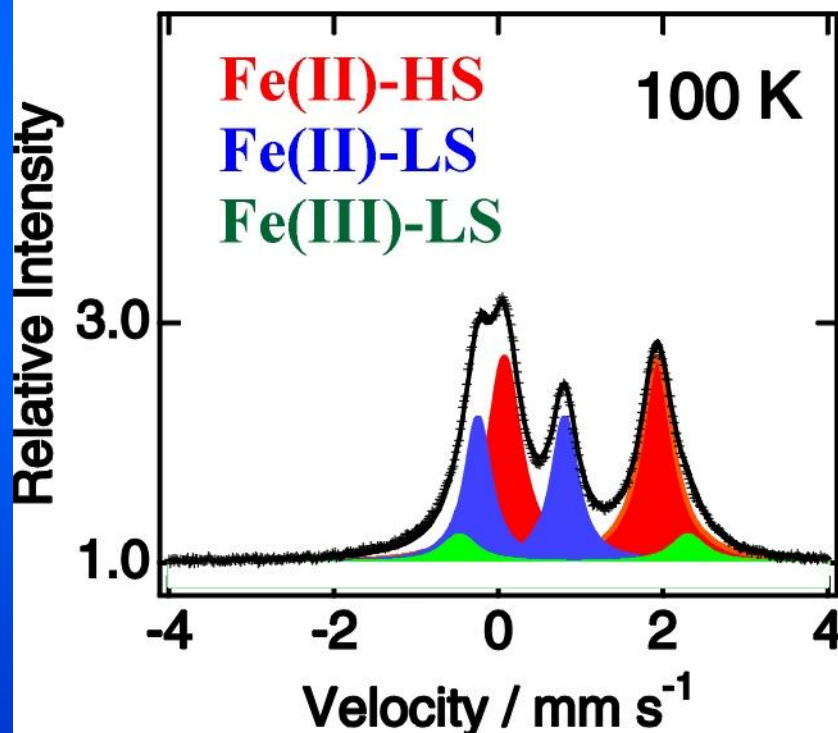
The resonance signal marked in red is one component of the quadrupole doublet of the metastable $^{57}\text{Fe(II)-HS}$ state, the intensity of which decreases with increasing temperature and the time elapsed after nuclear decay. The derived lifetimes of the $^{57}\text{Fe(II)-HS}$ state have been found to be 390 ns (10 K), 300 ns (25 K), 205 ns (47 K) and 100 ns (80 K). Very similar lifetimes have been measured by optical methods after laser excitation of the corresponding iron(II) compound. This confirms that the relaxation mechanism is the same for both the nuclear decay-induced and the light-induced “excited spin state trapping” (NIESST and LIESST).

It has been found in NIESST experiments with other cobalt coordination compounds that the lifetime of the nucleogenic metastable $^{57}\text{Fe(II)-HS}$ states depends decisively on the ligand field strength of the corresponding iron(II) coordination compound. The weaker the ligand field strength, the longer is the lifetime, i.e. the higher is the intensity of the metastable state at a given temperature. A convincing example confirming this finding is seen in the next picture with the emission spectra of the terpyridyl complex of Co(II) doped with ^{57}Co and two different kinds of anions. The spectra were recorded at 100 K using a resonance detector

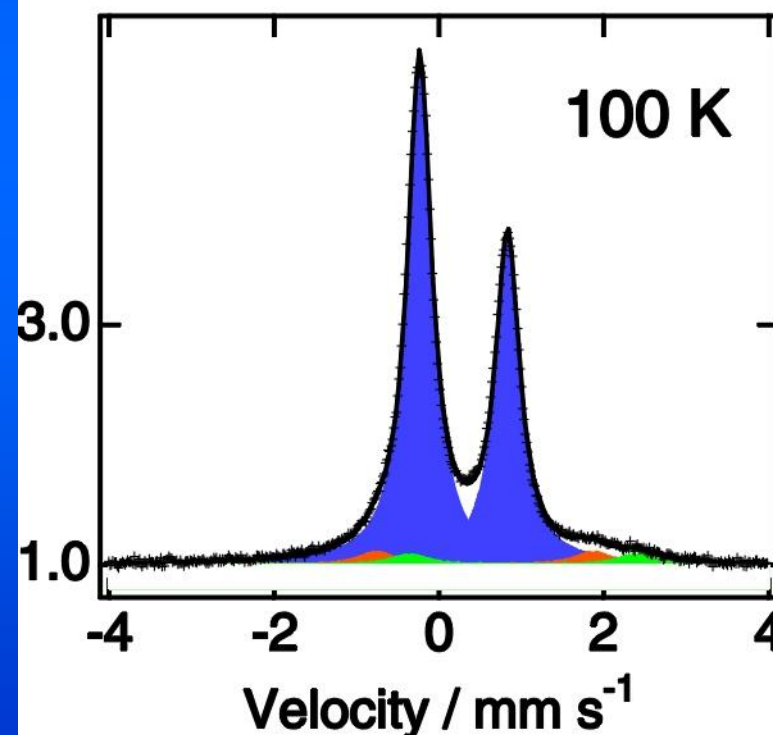
Emission Spectra
of
[⁵⁷Co/Co(terpy)₂]₂X₂
vs. enriched ⁵⁷Fe - SS
as absorber (293 K)

NIESST in $[^{57}\text{Co}/\text{Co}(\text{terpy})_2]\text{X}_2$

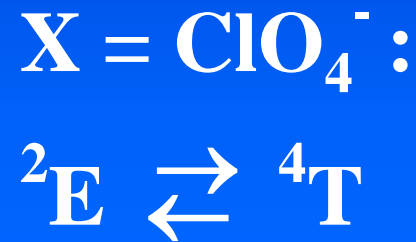
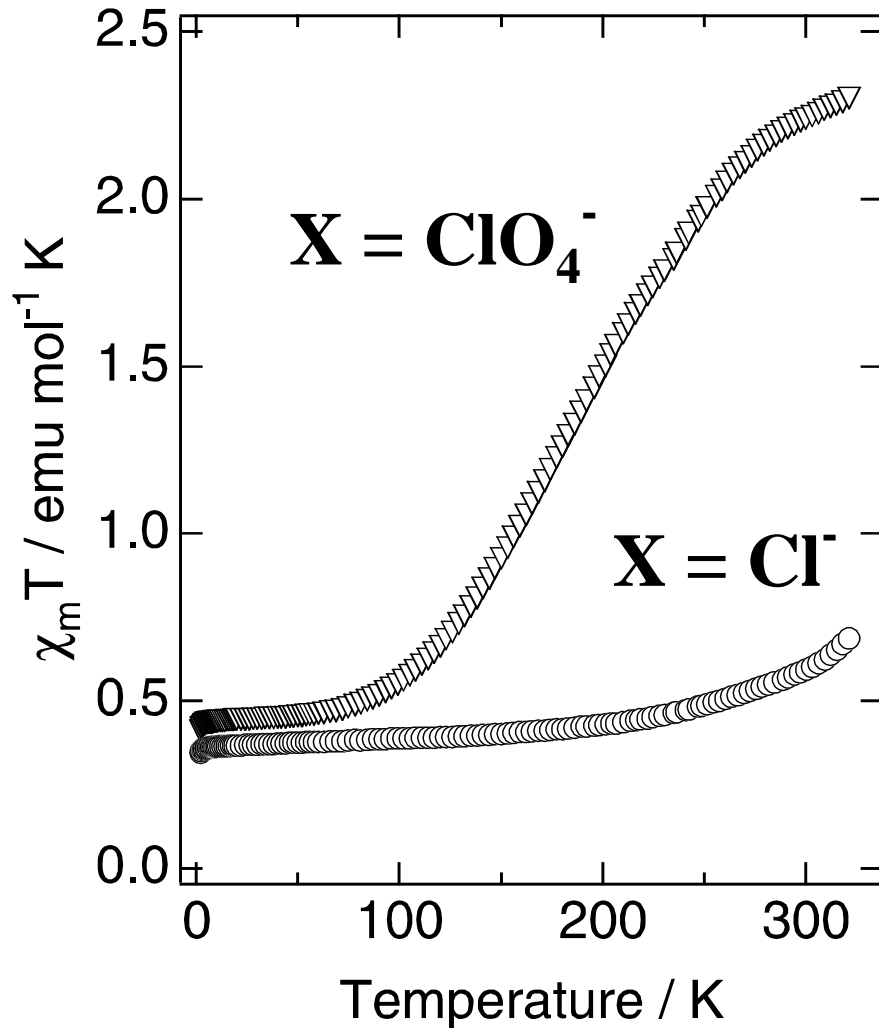
$\text{X} = \text{ClO}_4$
Weaker Ligand Field



$\text{X} = \text{Cl}$
Stronger Ligand Field



[Co(terpy)₂]X₂



Oshio, Spiering,
Ksenofontov, Renz, Gütlich
(2001)

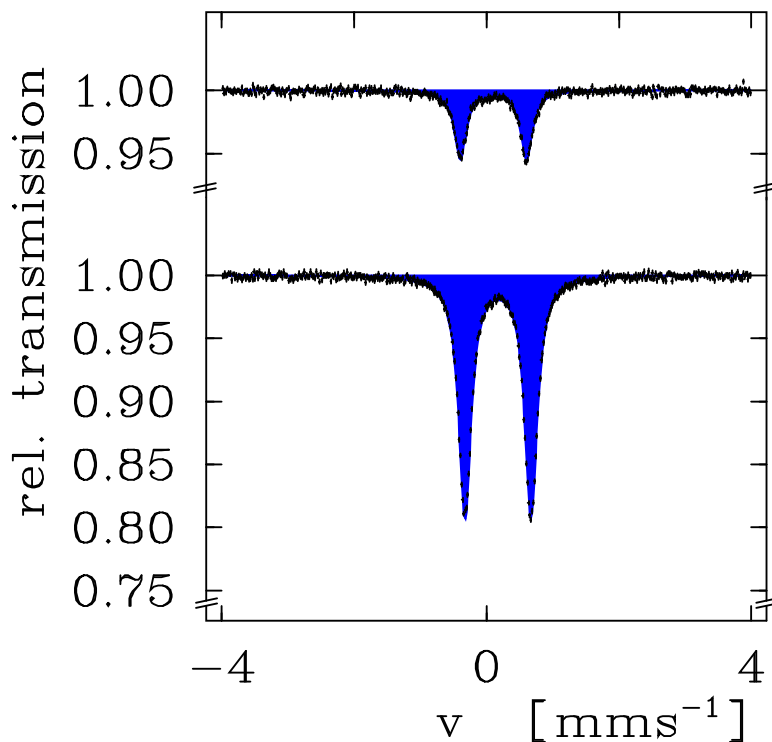
As observed with temperature dependent magnetic susceptibility measurements the perchlorate compound shows a thermally induced spin transition, whereas the chloride compound is low-spin still at room temperature, i.e. the former has a weaker ligand field strength than the latter compound. The emission spectra displayed here clearly show that the intensity of the metastable $^{57}\text{Fe}(\text{II})\text{-HS}$ (red) state is considerably higher in the system with the weaker ligand field strength (left) as compared to that in the stronger ligand field.

As the lifetime of the metastable $^{57}\text{Fe}(\text{II})\text{-HS}$ states responds to the chemical pressure created by the nearby surroundings in a crystal lattice, this method can be employed to probe the pore and cavity dimensions of a crystal lattice.

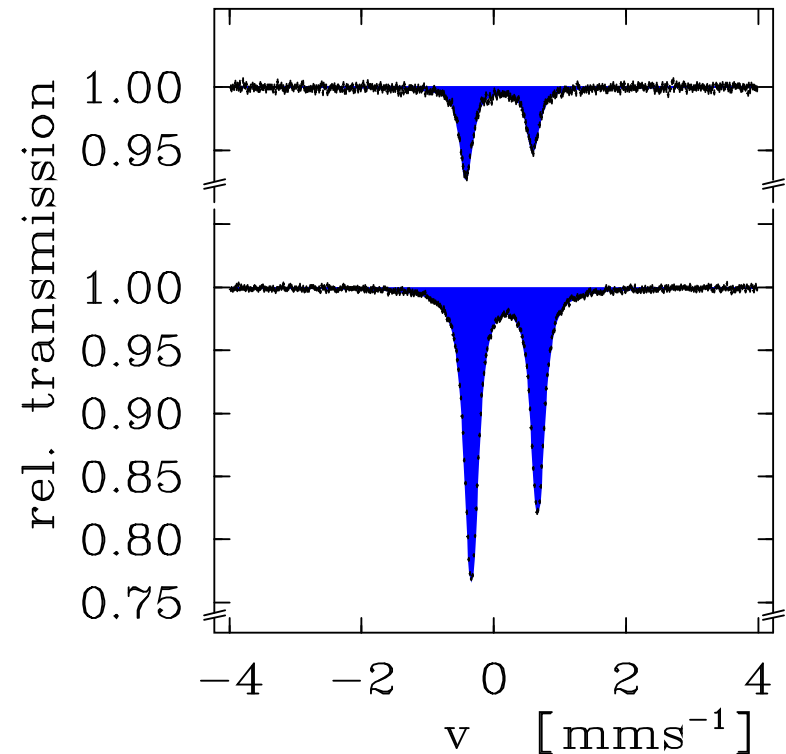
A comprehensive coverage of Mössbauer emission spectroscopy experiments may be found in a recently published review article: P. Gütlich, in *Spin Crossover in Transition Metal Compounds II*, P. Gütlich and H.A. Goodwin (eds.), *Topics in Current Chemistry*, Vol. 234, Springer, Berlin Heidelberg New York, **2004**, pp. 231-260.

Mössbauer Absorption Spectra of $[^{57}\text{Fe}_{0.05}\text{Co}_{0.95}(\text{terpy})_2]\text{X}_2$

X = ClO_4^-



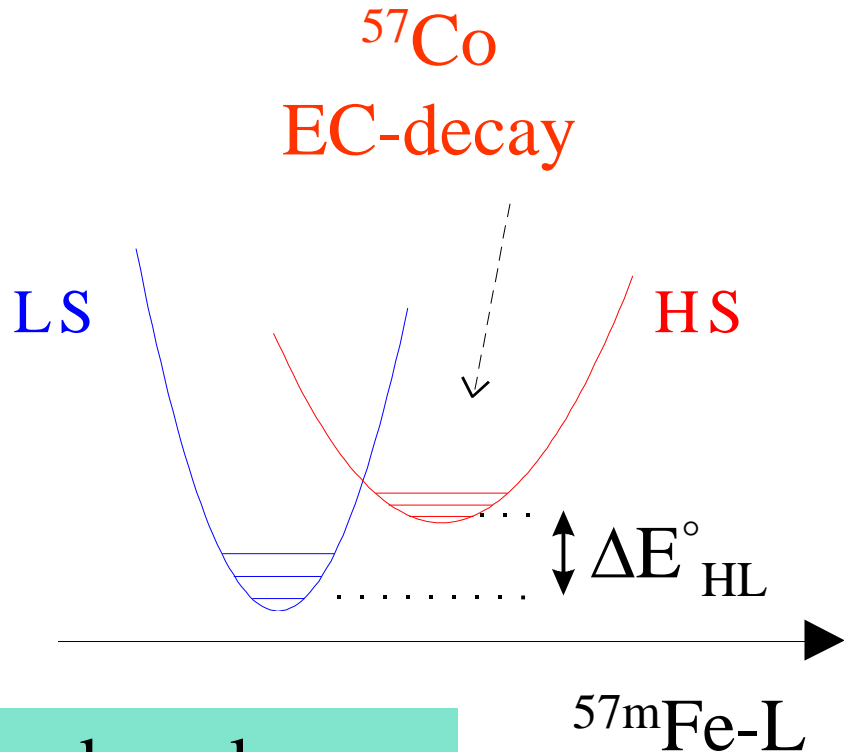
X = Cl^-



HS \rightarrow LS Relaxation after NIESST in $[^{57}\text{Co}/\text{Co}(\text{terpy})_2]\text{X}_2$



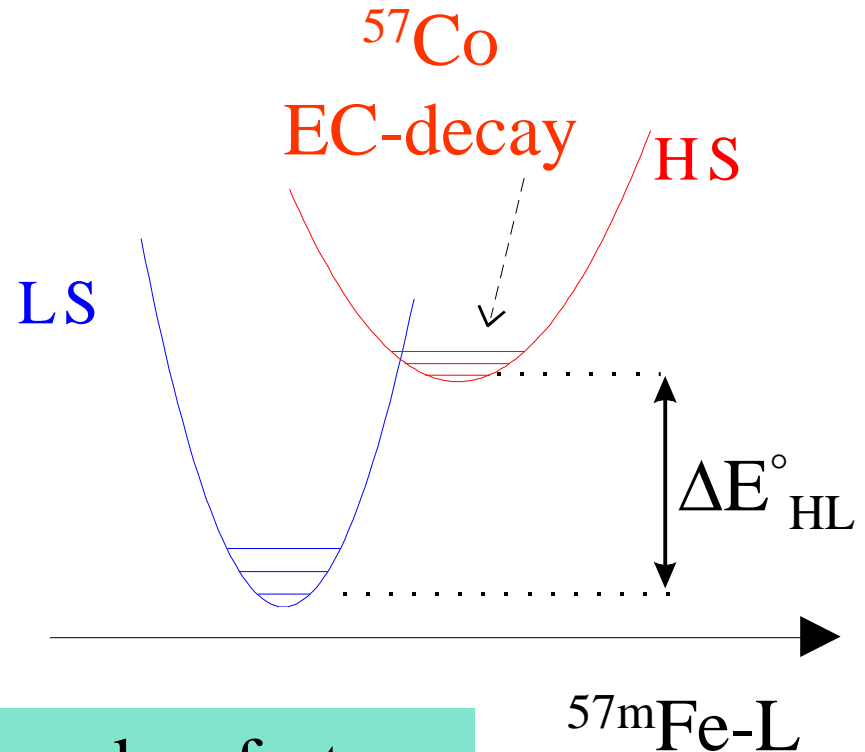
Weak Ligand Field



k_{HL} slow

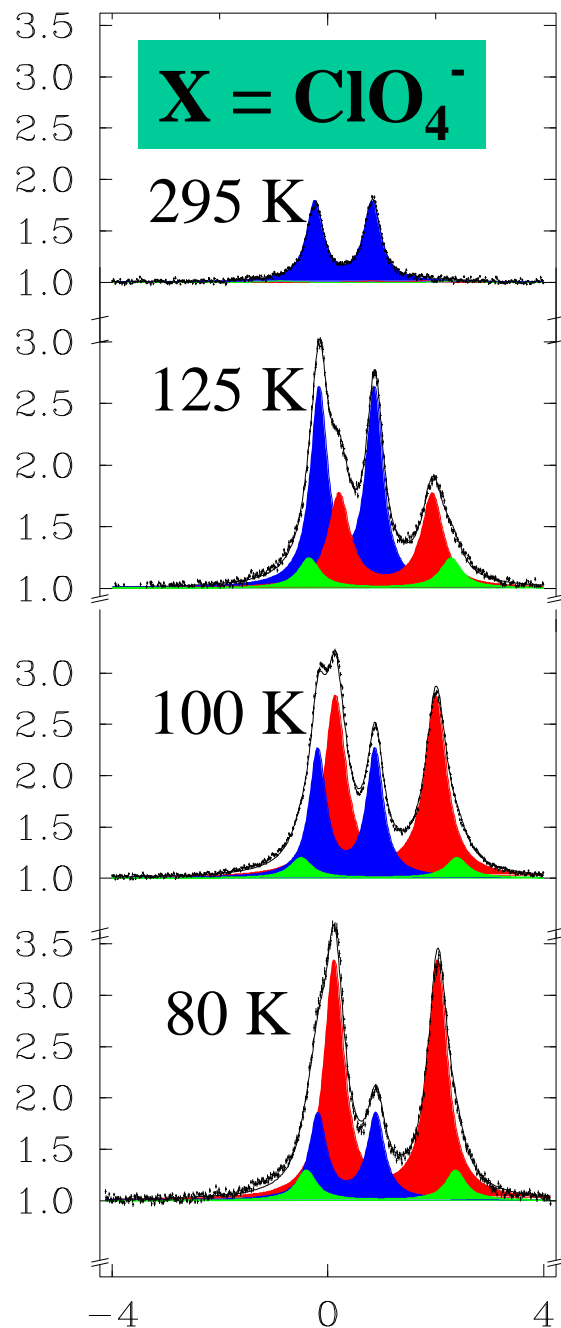


Strong Ligand Field



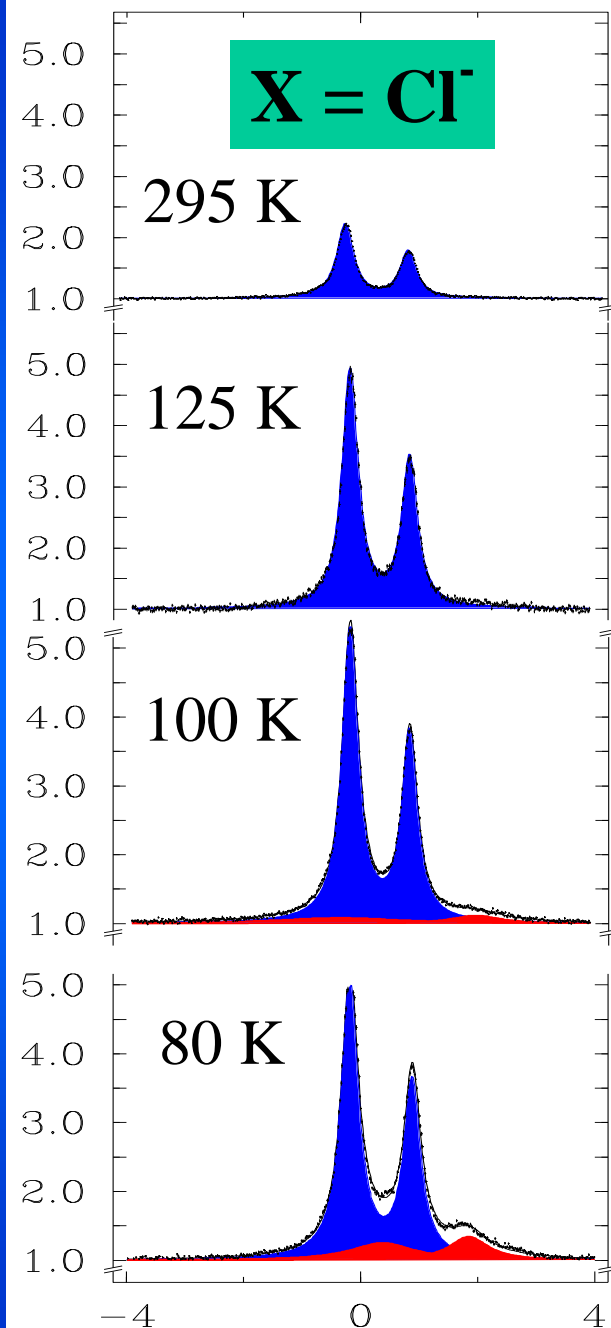
k_{HL} fast

Relative Intensity



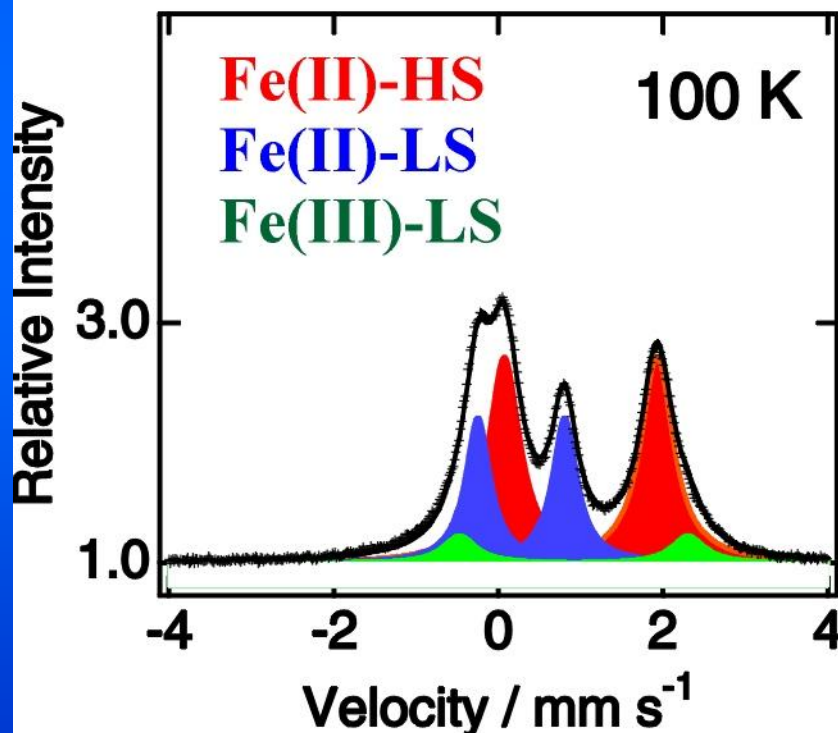
Fe(II)-HS
Fe(II)-LS
Fe(III)-LS

v [mms⁻¹]

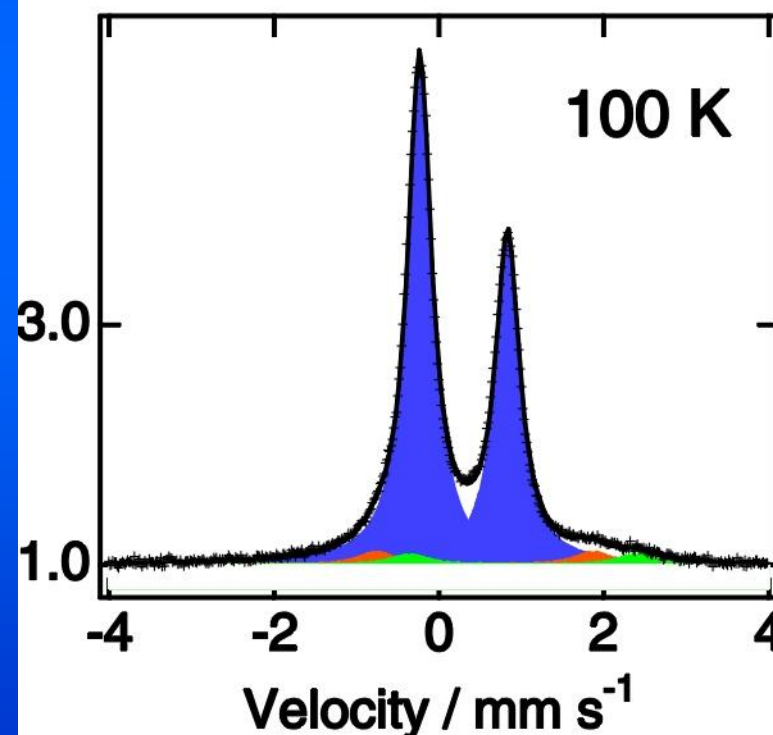


NIESST in $[^{57}\text{Co}/\text{Co}(\text{terpy})_2]\text{X}_2$

$\text{X} = \text{ClO}_4$
Weaker Ligand Field



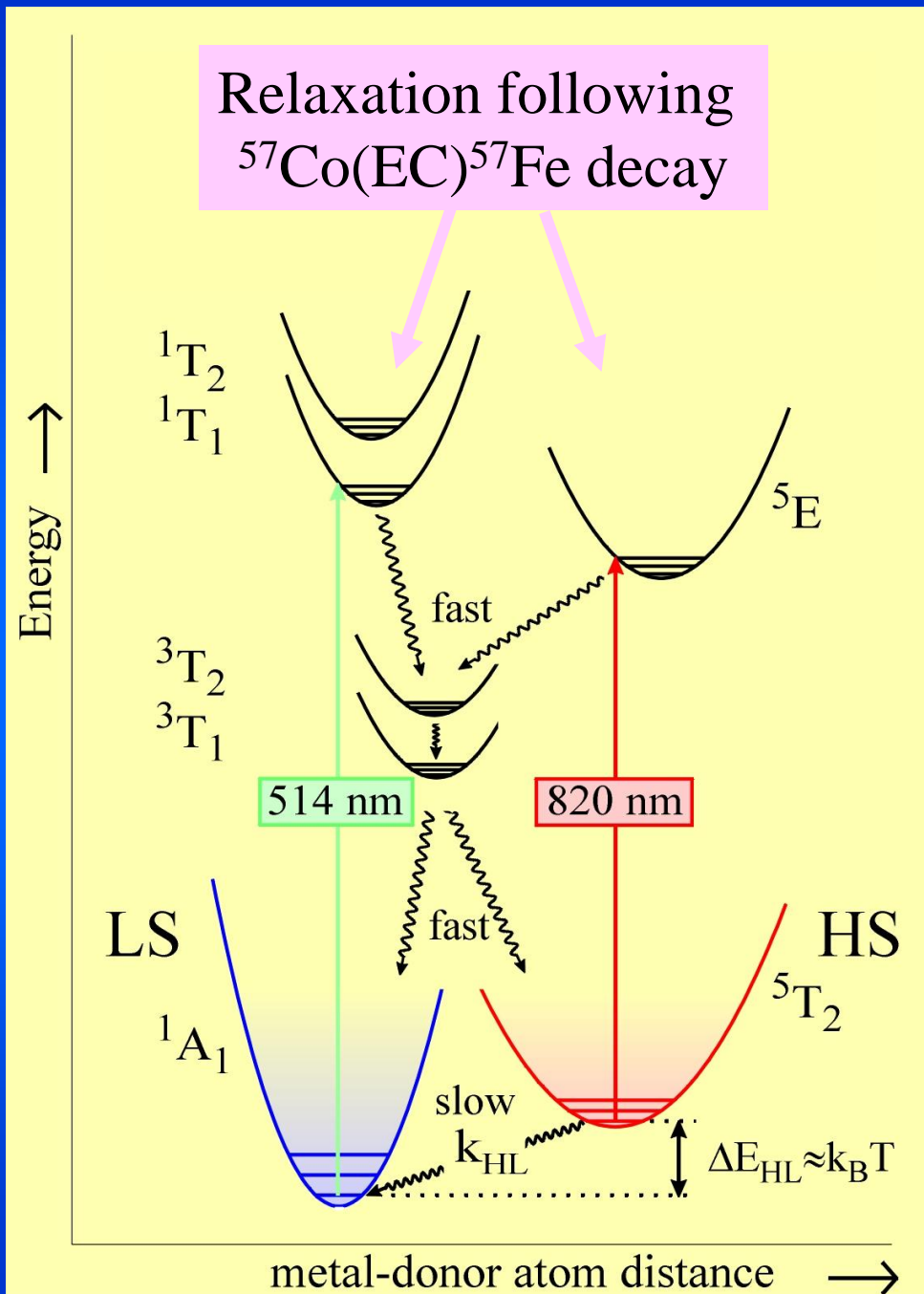
$\text{X} = \text{Cl}$
Stronger Ligand Field



Nuclear Decay- Induced Excited Spin State Trapping NIESST

$^{57}\text{Co}(\text{EC})^{57}\text{Fe}$ decay
is intrinsic light source

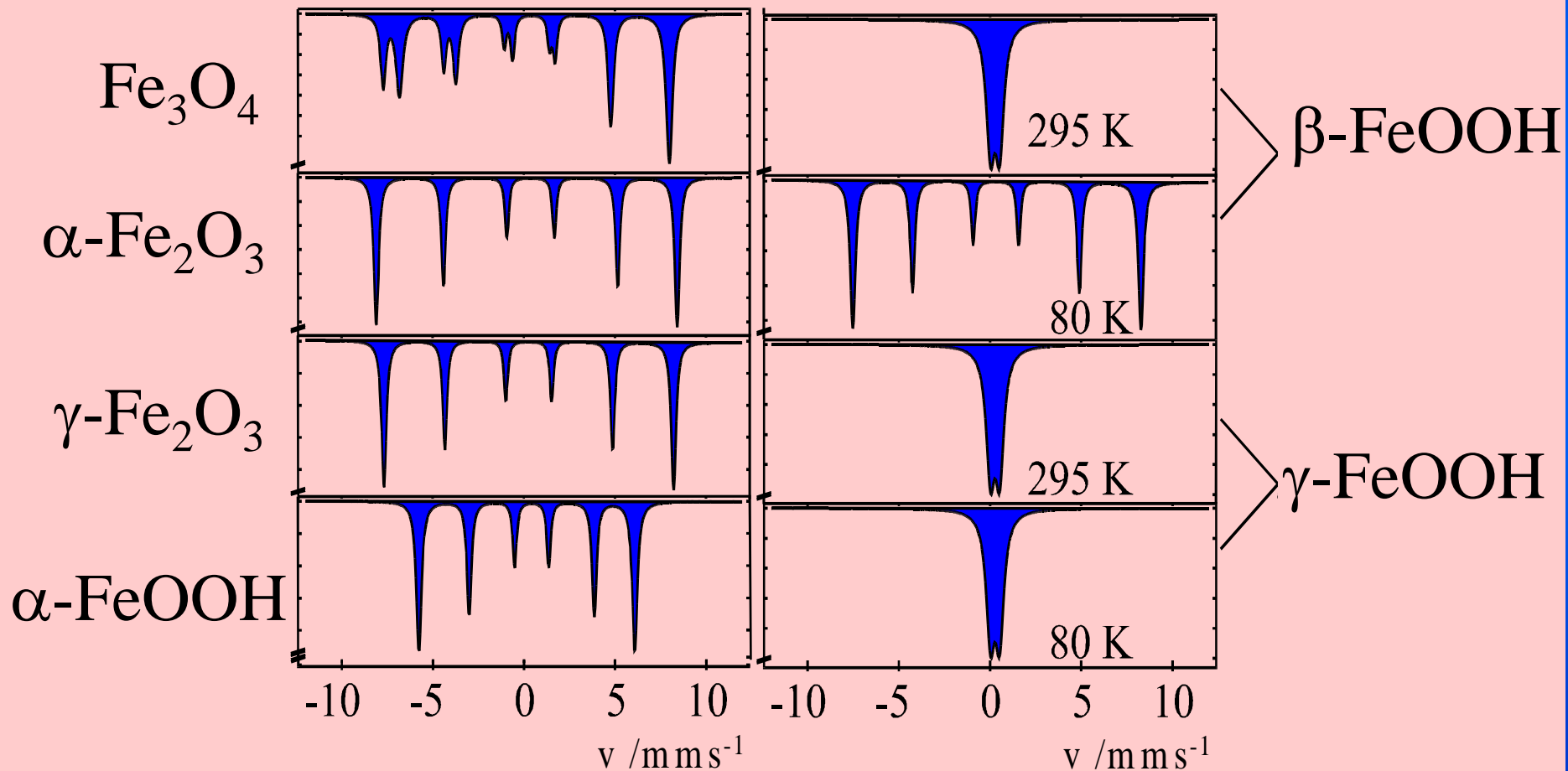
**Mechanisms for
LIESST and NIESST
The same!**



INDUSTRIAL APPLICATIONS

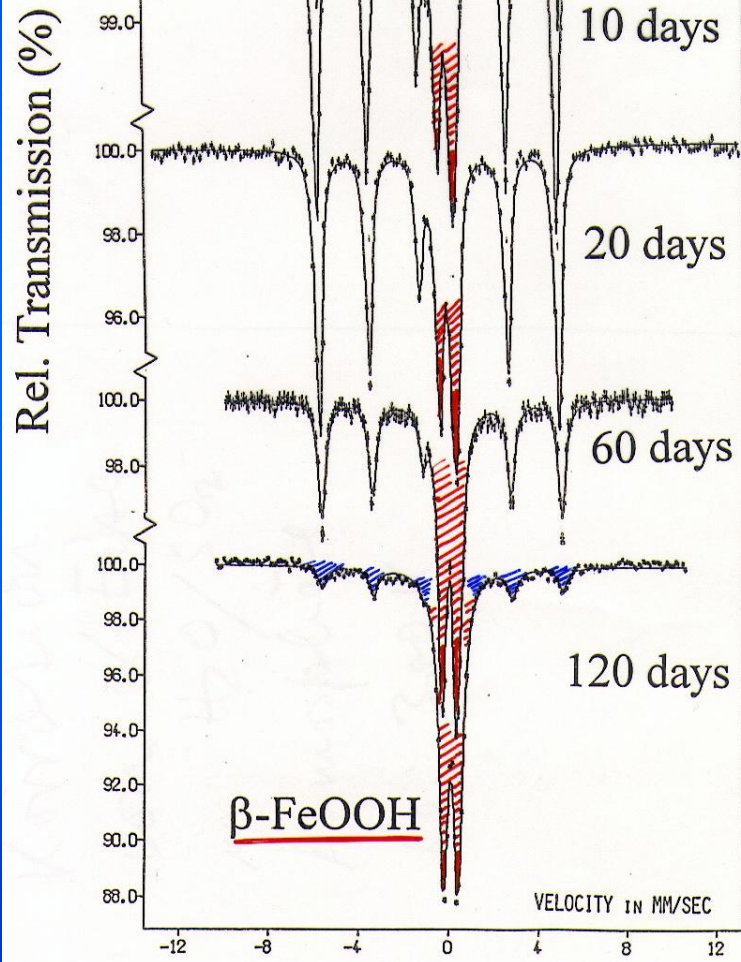
- **Corrosion Studies**
- **Magnetic Tape**
- **Glass Manufacturing**
- **Nitrification of Steel**
- **Martensitic phase transformation in
gold alloys**

^{57}Fe Mössbauer Spectra of Corrosion Products



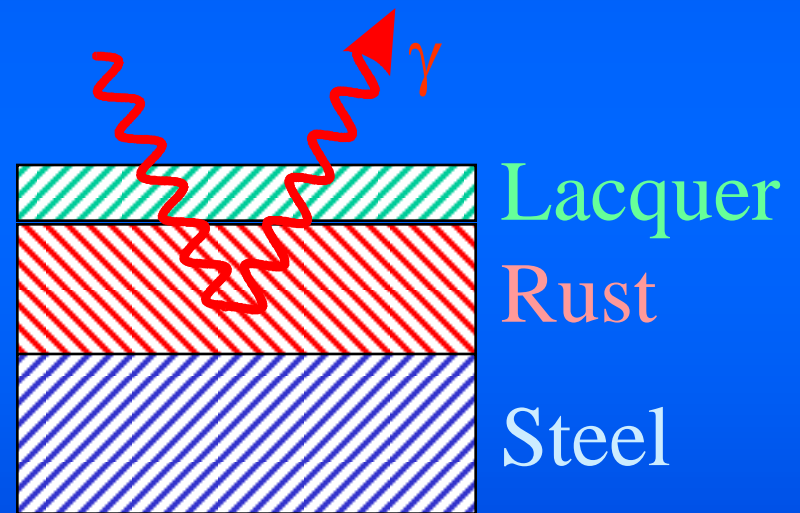
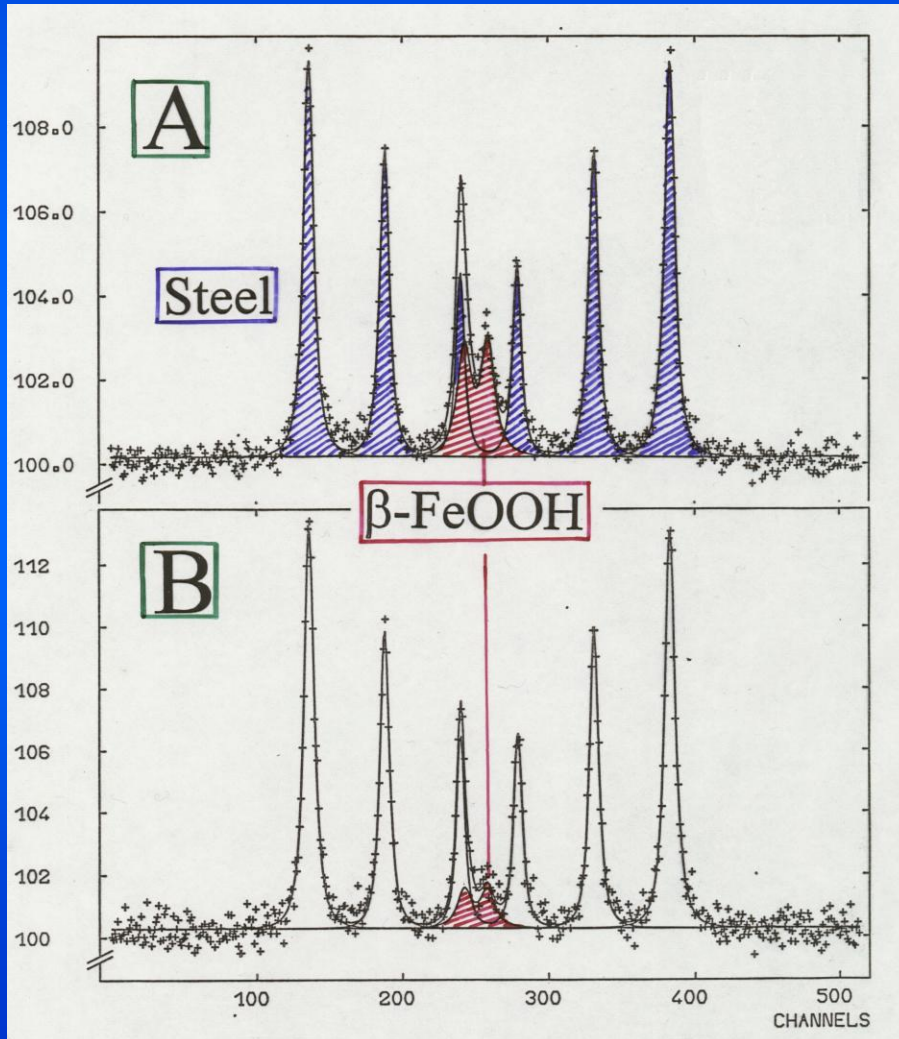
Roughly 6 different iron oxides and oxyhydroxides of iron are known as corrosion products, which may be formed by corrosion reactions in steel and iron containing alloys under different conditions. These corrosion products can be distinguished by ^{57}Fe Mössbauer spectroscopy. Magnetite, Fe_3O_4 , is characterised by two overlapping sextets, one arising from Fe(III) ions in tetrahedral sites, the other one is a time-averaged sextet arising from Fe(II) and Fe(III) ions in octahedral sites with fast electron fluctuations between them (faster than the inverse of the lifetime of the 14.4 keV nuclear level). The oxides α - and γ - Fe_2O_3 show a magnetically split sextet with a slightly different size of the internal magnetic field. The oxyhydroxides α -, β - and γ - FeOOH can be distinguished by temperature dependent Mössbauer spectroscopy. While α - FeOOH (Goethite) shows a magnetically split sextet at room temperature, β - and γ - FeOOH have the same poorly resolved quadrupole doublet and therefore cannot be distinguished at room temperature. At liquid nitrogen temperature (ca. 80 K), however, β - FeOOH is magnetically ordered and shows the typical magnetically split sextet, whereas γ - FeOOH still shows the same poorly resolved quadrupole doublet as at 295 K. This phase orders magnetically only below ca. 30 K yielding then a similar sextet as the other modifications.

Corrosion of α -Iron in $\text{H}_2\text{O}/\text{SO}_2$ atmosphere at 300 K



Corrosion product is
 β -FeOOH

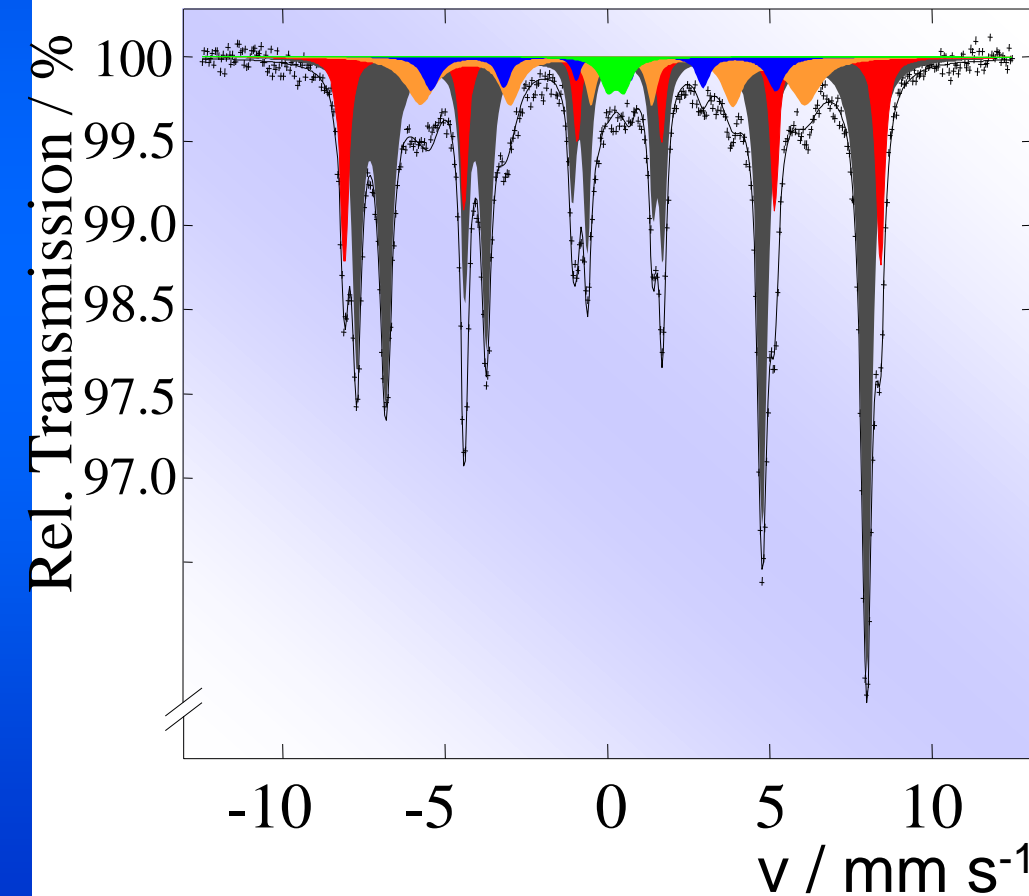
Lacquer Coating Against Corrosion of Steel



**A, B : Different lacquers,
Same corrosion conditions**

The quality of various lacquer coatings on steel, as used e.g. in the fabrication of cars, was investigated with respect to resistance against corrosion. The steel samples were coated with the lacquers and then exposed to aggressive media under the same conditions. After certain exposure times Mössbauer spectra were recorded in the gamma ray reflection technique without destroying the lacquer layer (see scheme). Two selected spectra are reproduced in the picture. In both cases β -FeOOH was identified as the corrosion product (typical quadrupole doublet in the middle of the sextet of the steel substrate). It is clearly seen that the intensity of the β -FeOOH signal is much bigger in the A experiment than in B. This means that the protecting quality of lacquer B is better than that of A.

Corrosion Products in Cooling Systems of Power Plants



Constituents	A/%
Hematite, $\alpha\text{-Fe}_2\text{O}_3$	16
Magnetite, Fe_3O_4	64
Goethite, $\alpha\text{-FeOOH}$	13
Martensite	5
$\beta/\gamma\text{-FeOOH}$	2

This example is taken from routine Mössbauer analysis of finely dispersed particles in a cooling system of a power plant. The particles were collected from the coolant with a special filter and analysed with standard transmission Mössbauer spectroscopy. The spectrum is a superposition of the spectra of five different iron-containing species with percentages given in the table. Such measurements have been carried out routinely in the context of regular maintenance works in nuclear and conventional power plants.

Effect of Corrosion Inhibitors

DEDA : Diethanol-dodecanylamine

BBA : m-Benzoylbenzoic acid

Conversion Electron Mössbauer Spectroscopy at 300 K

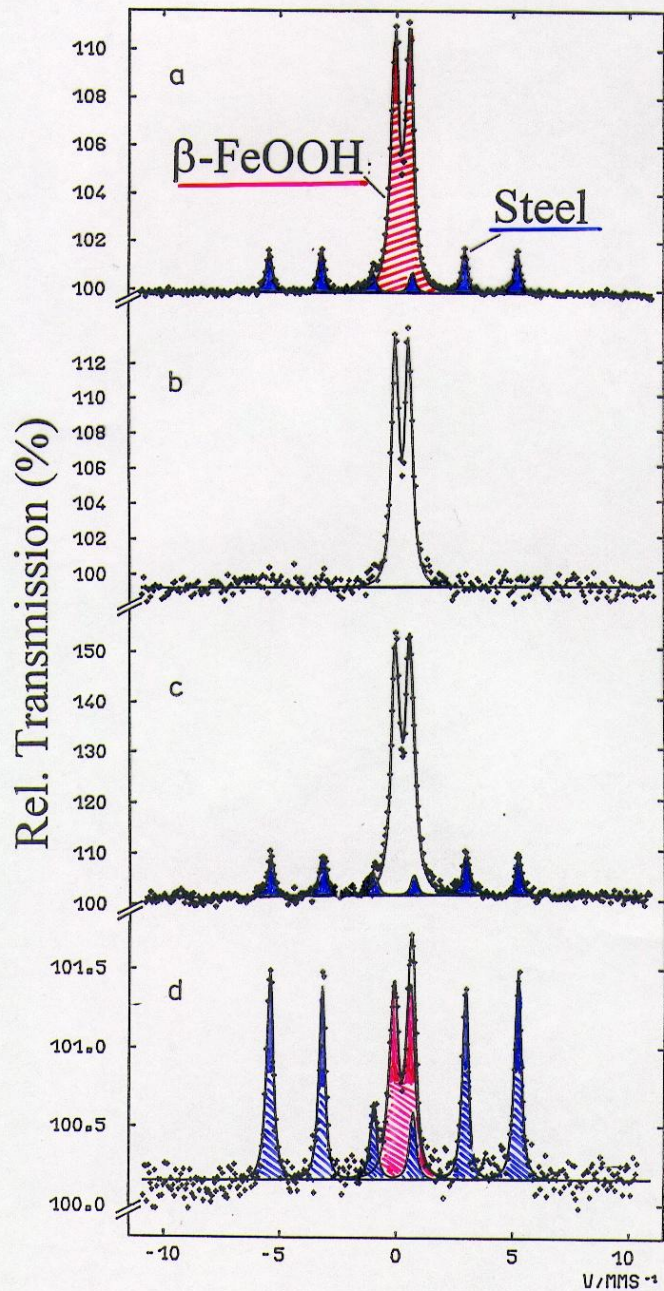
Effect of Corrosion Inhibitors

16 hours
no inhibitor

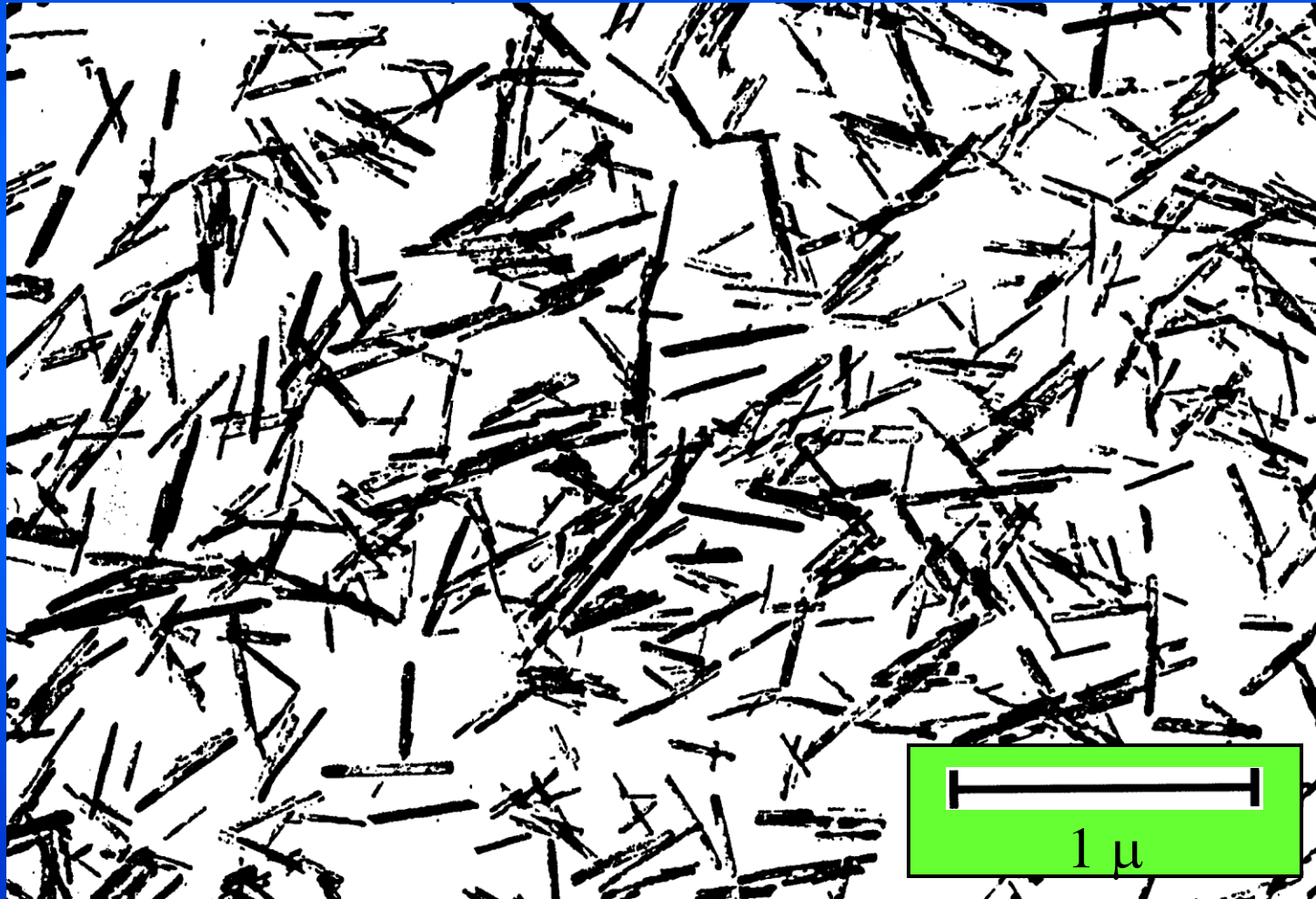
3 days
no inhibitor

8 days
400 ppm DEDA

8 days
400 ppm each DEDA + BBA



Fe-doped CrO_2 -Particles for Magnetic Tapes(BASF)



A collaboration with the BASF company was conducted with the specific objective to improve the magnetic properties of CrO_2 particles for audio- and video-magnetic tapes. As sketched in the next picture, iron can enter the CrO_2 lattice in two ways, one improving and the other worsening the magnetic properties. Samples from many different batches, differing in the preparation parameters, were analysed by ^{57}Fe Mössbauer spectroscopy.

Fe-doped Chromium Dioxide Particles for Magnetic Tapes

Problem: Fe enters CrO_2 lattice as



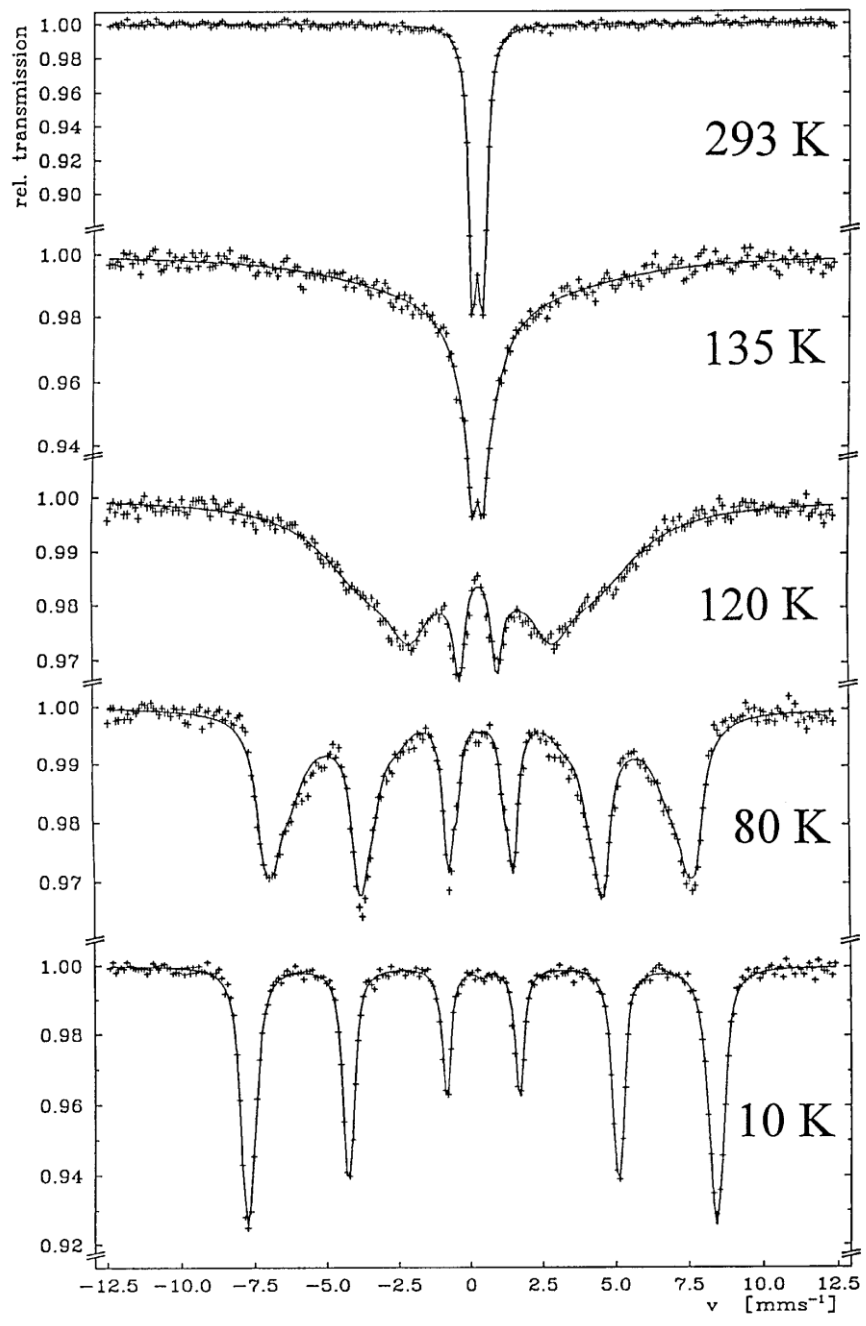
NOT wanted!

Deteriorates magnetic properties



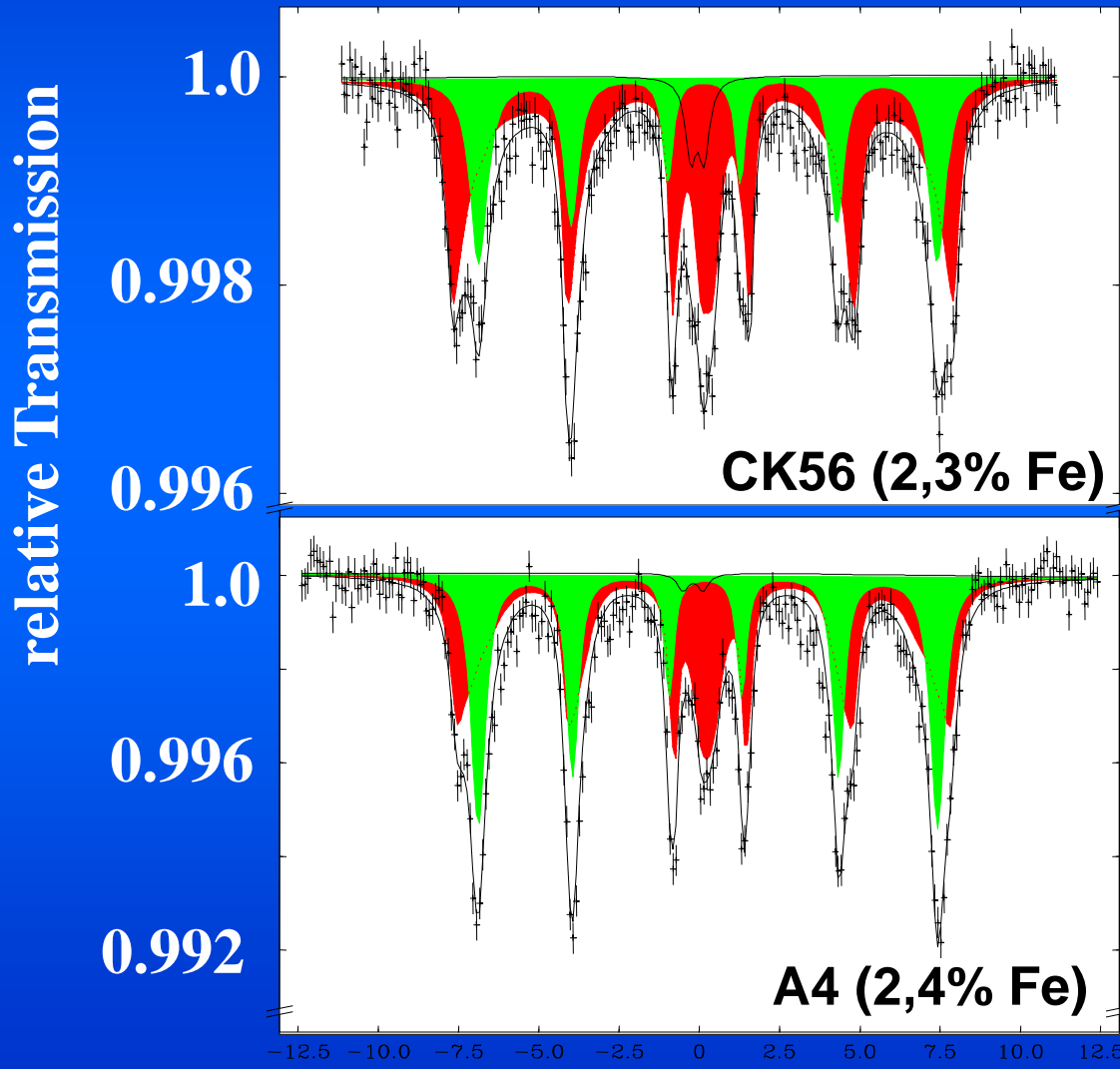
Wanted!

Improves magnetic properties



**^{57}Fe -Mössbauer Spectra
of $\alpha\text{-(Cr}_{1-x}\text{Fe}_x)_2\text{O}_3$ ($x=0.2$)
at variable temperatures**

^{57}Fe Mössbauer Spectra (293 K) of Fe-doped CrO_2 particles



$\alpha\text{-(Cr}_{1-x}\text{Fe}_x)_2\text{O}_3$
magnetic

$\alpha\text{-(Cr}_{1-x}\text{Fe}_x)_2\text{O}_3$
paramagnetic

$(\text{Cr}_{1-x}\text{Fe}_x)\text{O}_2$

- Shown here are the Mössbauer spectra of Fe-doped CrO_2 particles of two samples from different preparation procedures. The green magnetic sextet refers to iron accommodated in Cr positions, the desired version that improves the magnetic properties for recording tapes by ca. 10 % as compared to the “old” preparation method (see table). So Mössbauer spectroscopy has helped to find the better preparation procedure for magnetic tapes of higher quality.

Klinger, R.; Enslin, J.; Meisel, W.; Gütlich, P.; Jachow, H.; Schwab, E., *J. Magn.Magn. Mat.* **1995**, *150*, 277

Improvement of Magnetic Properties

	CK56	A4
Coercivity (Oe)	700	770
Remanence (emu/g)	33.7	37.0
Saturation Magnetization (emu/g)	68.8	74.4

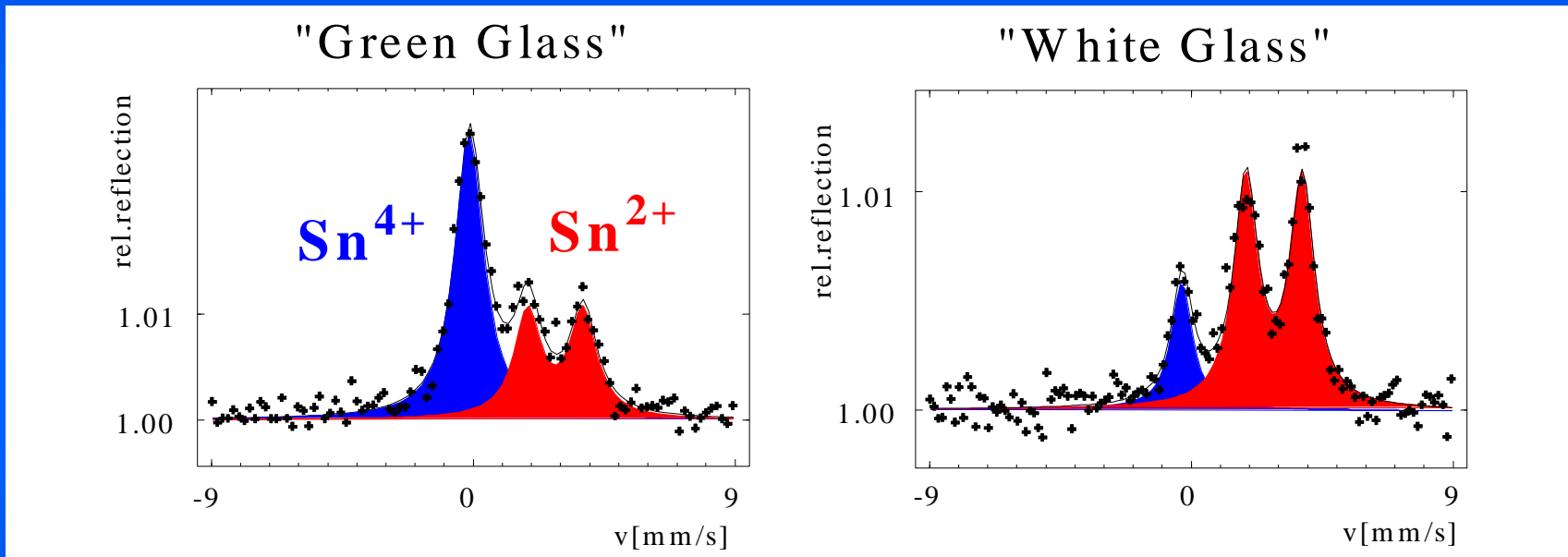
Problems in Glass Manufacturing

**Collaboration with Schott Glas
Mainz**

Tin in Surface of Floatglass

Problem:

Surface properties depends on oxidation state of tin.



Quantative determination of $\text{Sn}^{2+} / \text{Sn}^{4+}$
by CEMS in dependence of

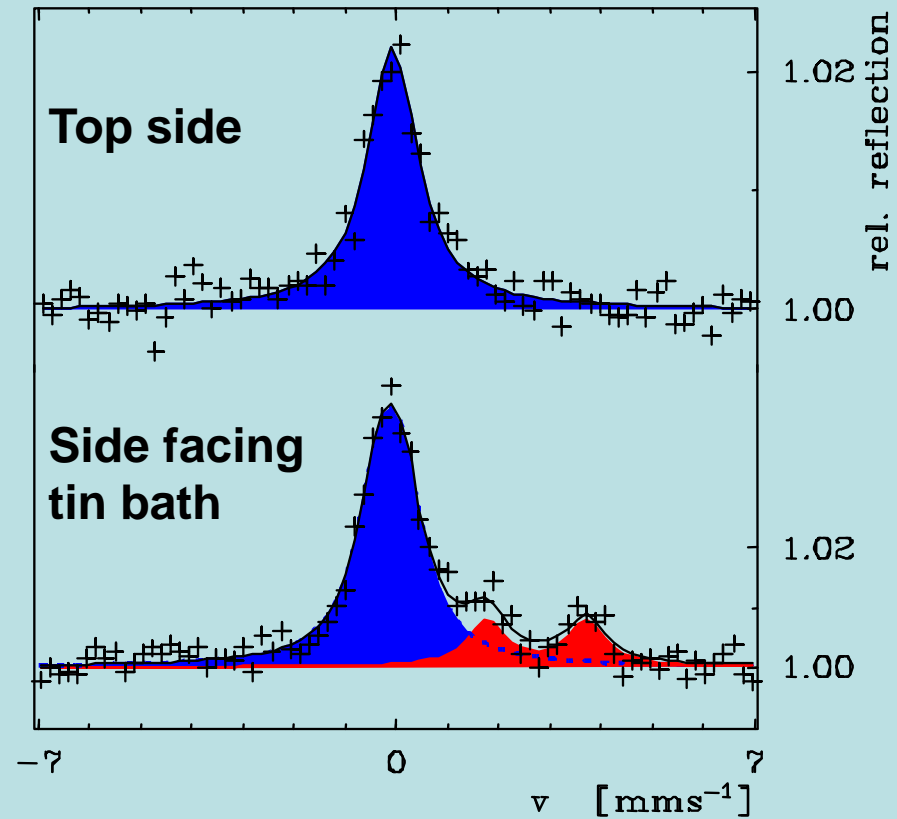
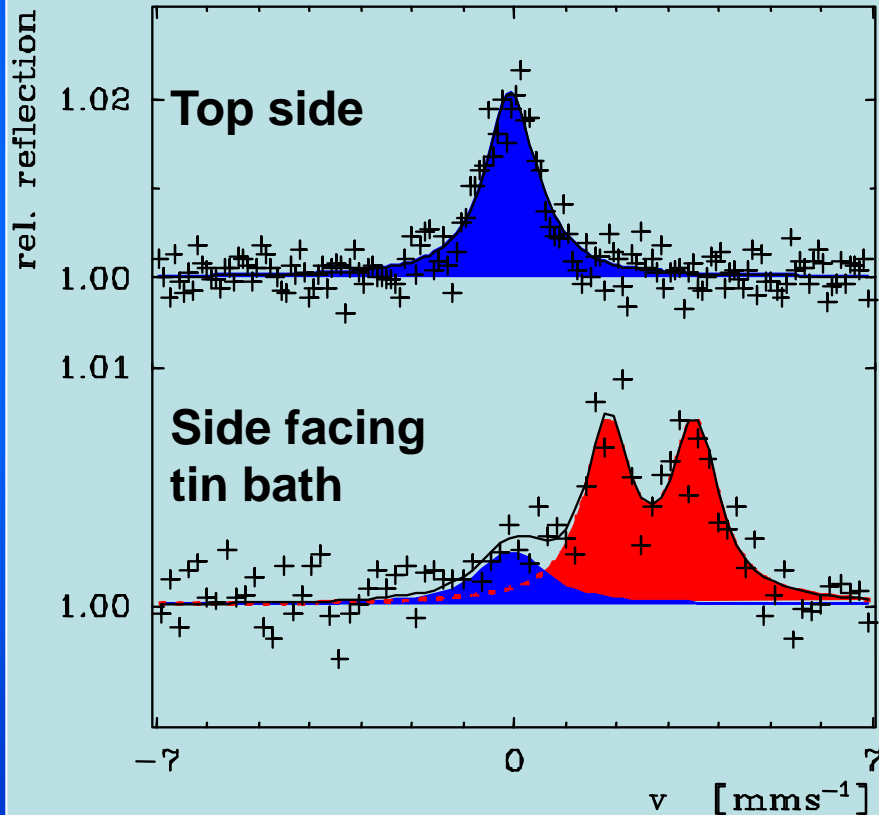
- Glass composition
- Production conditions

Tin is usually an additive in the production of floatglass. It has been found that the surface properties of floatglass depends on the oxidation state of tin. In order to have control over the surface properties it is necessary to control the oxidation state of tin, which is difficult to do with conventional methods. In a collaboration with SCHOTT company (Mainz) we have applied ^{119}Sn Mössbauer spectroscopy using the conversion electron detection. The two spectra shown here confirm convincingly that the oxidation state of tin in floatglass can be determined qualitatively and quantitatively. The production of floatglass can now be conducted considering various parameters like glass composition and production conditions.

^{119}Sn Mössbauer spectra (CEMS) of KN-floatglass before and after thermal treatment

untreated

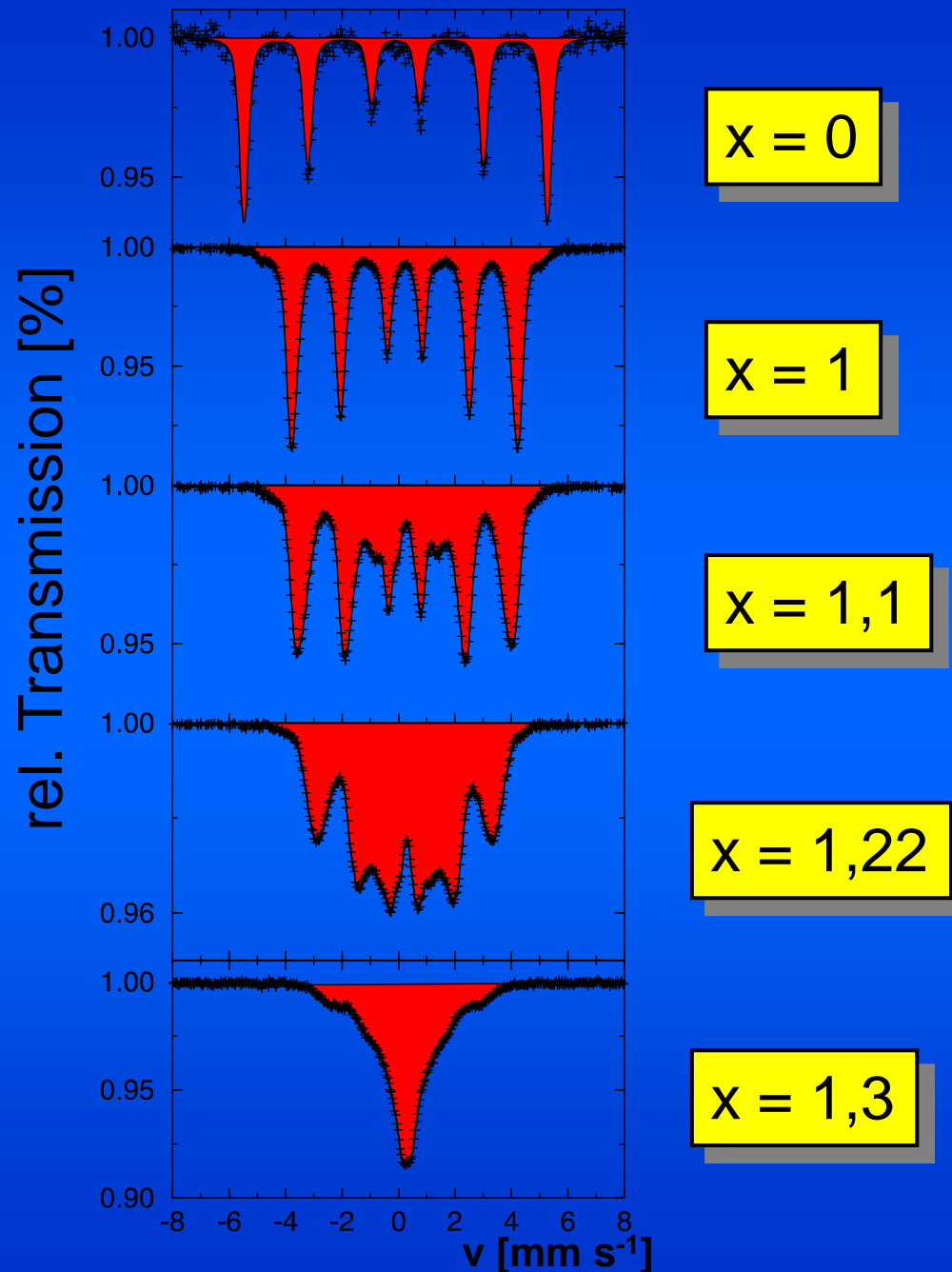
treated 7 min, 730°C



Metallurgy

High-Temperature Nitrification of Steel

Fe_3N_x at 293 K



Hydrogen Storage

LaNi₅/H₂

(H. Rummel, P. Gütlich, unpublished)

The alloy LaNi₅ has proven to be suitable as battery material for hydrogen storage. In a long-term stability test the material was analyzed by Ni-61 Mössbauer spectroscopy after many loading/unloading cycles.

It was found that the material shows noticeable segregation into lanthanum hydride and metallic nickel after ca. 2000 cycles of loading/unloading.

^{61}Ni Mössbauer Spectroscopy of LaNi_5/H_2

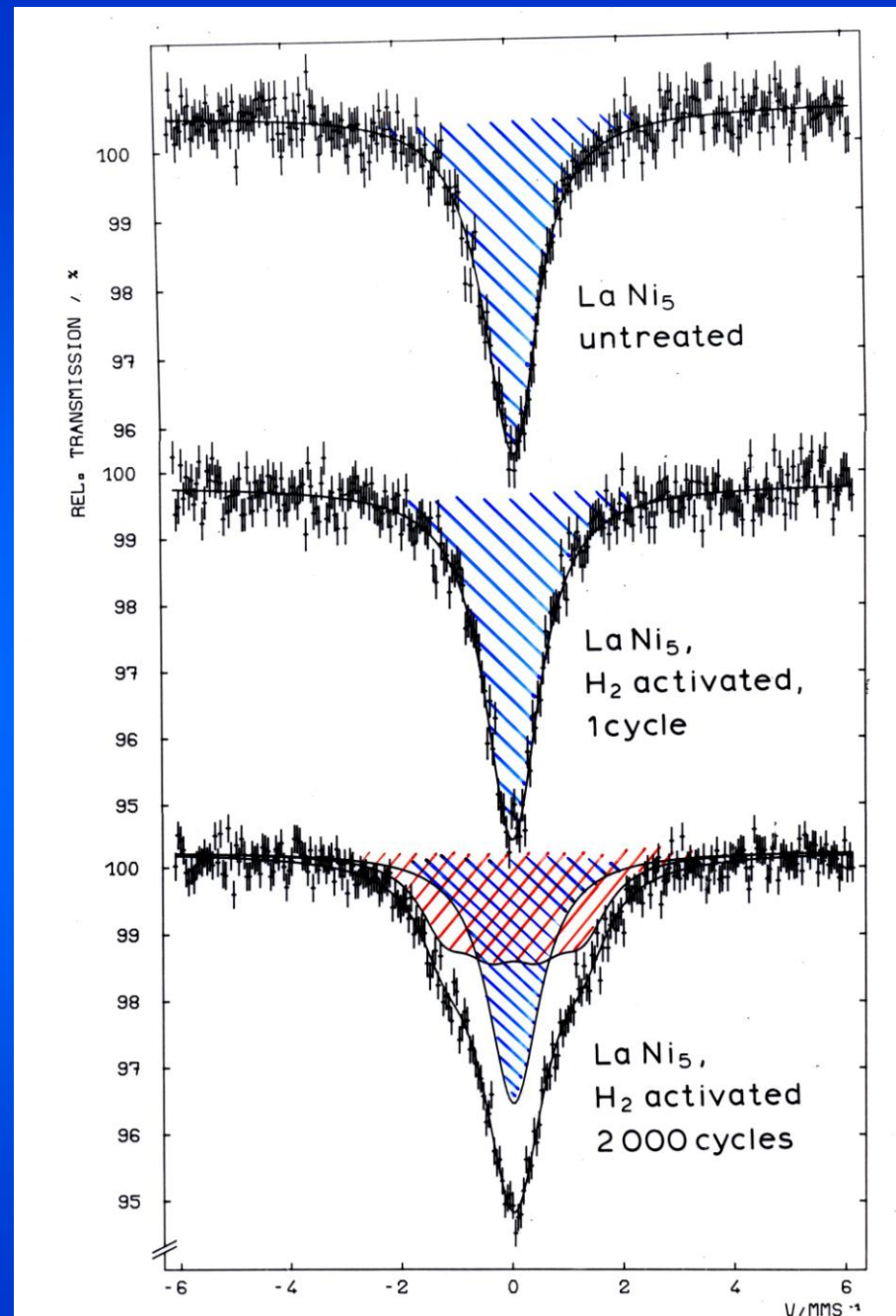
(H. Rummel, P. Gütlich, unpublished)

Source: $^{61}\text{Co}(^{62}\text{Ni}_{0.85}\text{Cr}_{0.15})$ at 4.2 K
activated with Bremsstrahlung from
electron beam of Mainz Mikrotron:
 $^{62}\text{Ni}(\gamma, p)^{61}\text{Co}$

Absorber: LaNi_5/H_2 at 4.2 K

Result:

LaNi_5 untreated and loaded with H_2 show nearly the same Mössbauer single line. After ca. 2000 cycles of loading/unloading of hydrogen the single resonance line (blue) of the original material LaNi_5 begins to reduce in intensity at the favour of a hyperfine-broadened signal arising from metallic nickel. Thus, the battery material is stable up to ca. 2000 cycles.

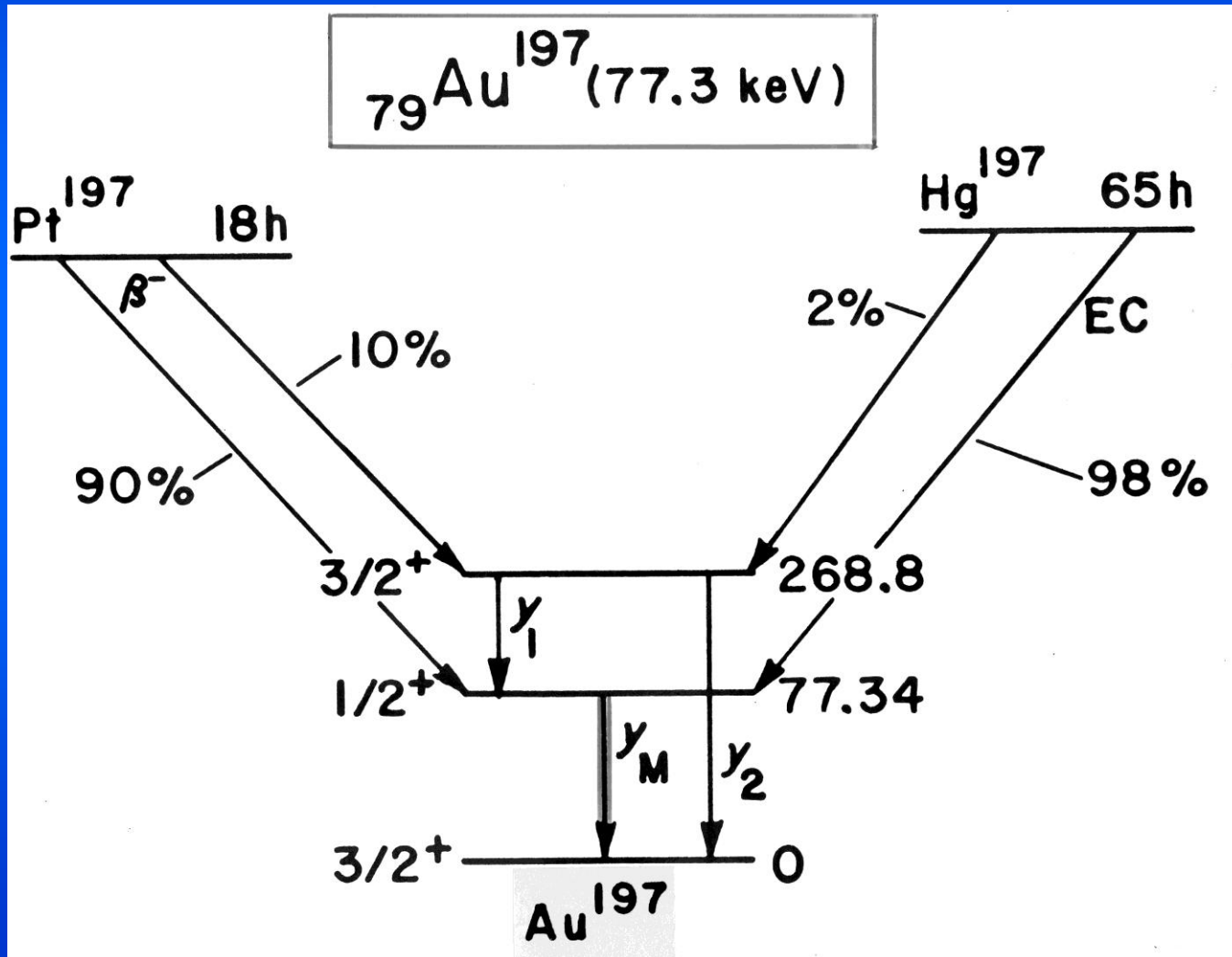


**Martensitic
Phase Transformation
in
Au-Zn Alloys**

by

^{197}Au Mössbauer Spectroscopy

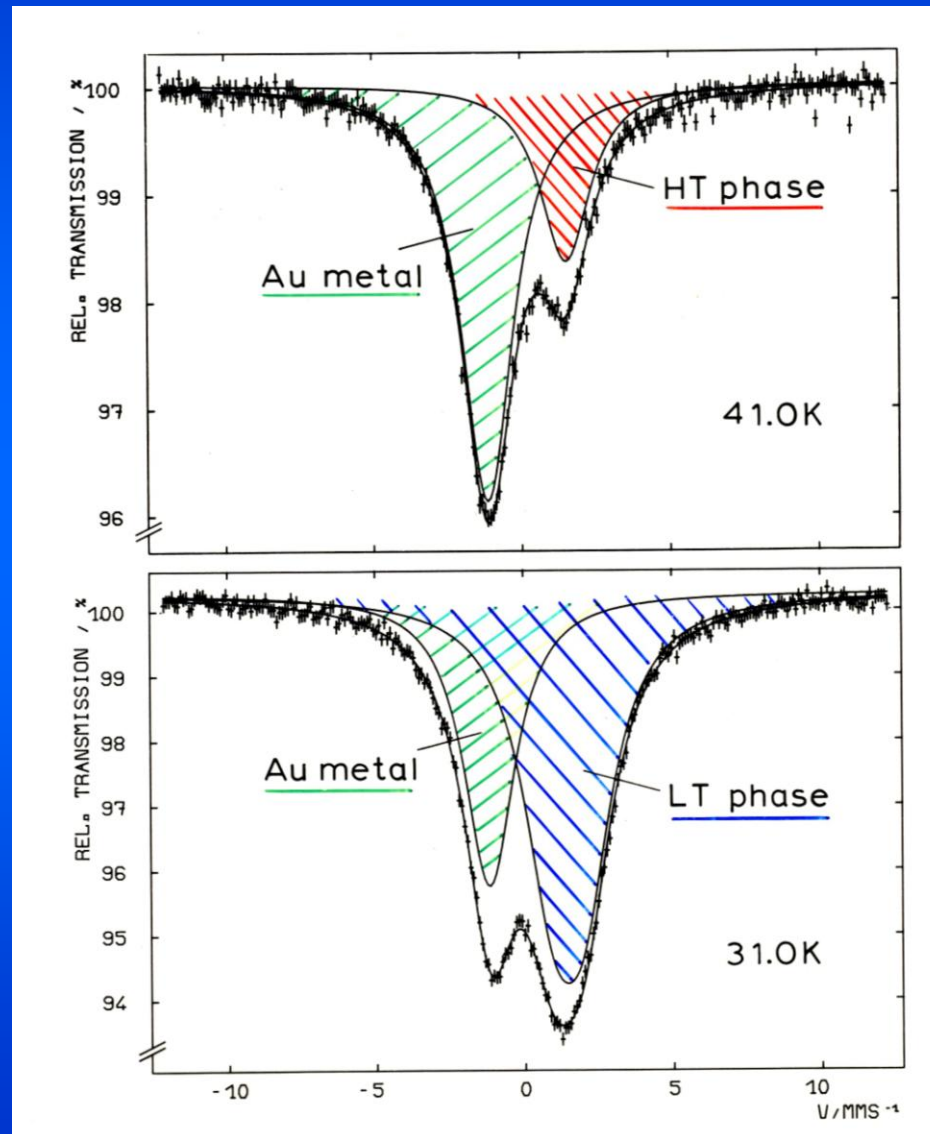
^{197}Au Mössbauer source



Nuclear reactor:
 $^{196}\text{Pt}(n,\gamma)^{197}\text{Au}$

Electron
 accelerator:
 $^{198}\text{Pt}(\gamma,n)^{197}\text{Pt}$

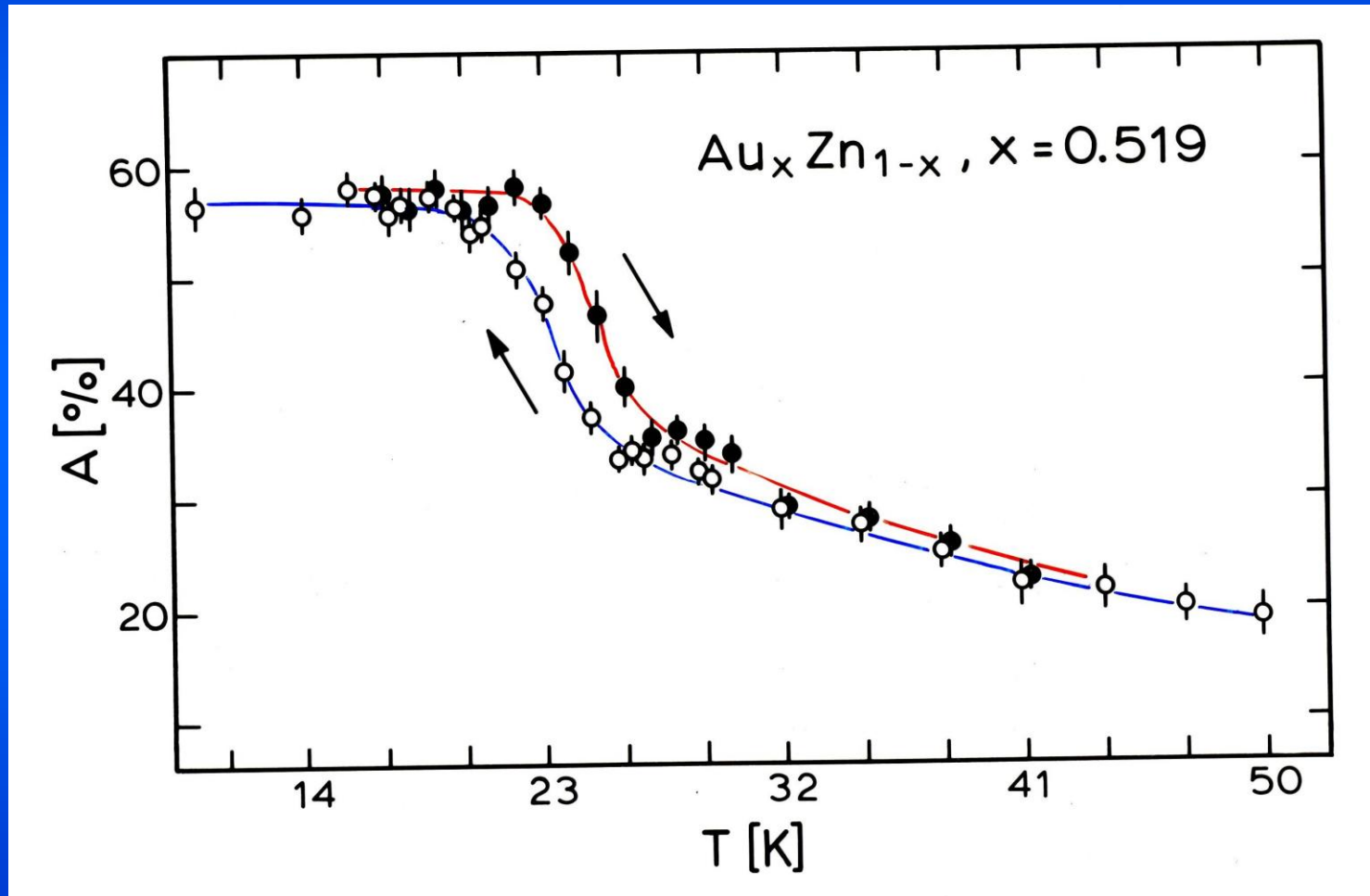
$\text{Au}_x\text{Zn}_{1-x}$ ($x = 0.52$), $T = 4.2 \text{ K}$



K. Römhild,
P. Gütlich
(unpublished)

$\text{Au}_x\text{Zn}_{1-x}$ ($x = 0.52$)

Resonance area fraction as function of T[K]



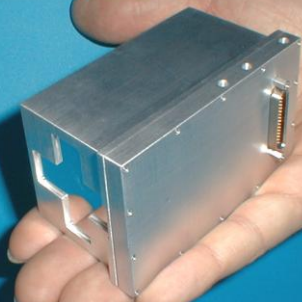
K. Römhild, P. Gütlich (unpublished)

Mobile Mössbauer Spectroscopy

**G. Klingelhöfer, E. Kankeleit,
J. Foh, B. Bernhardt,
P. Gütlich**

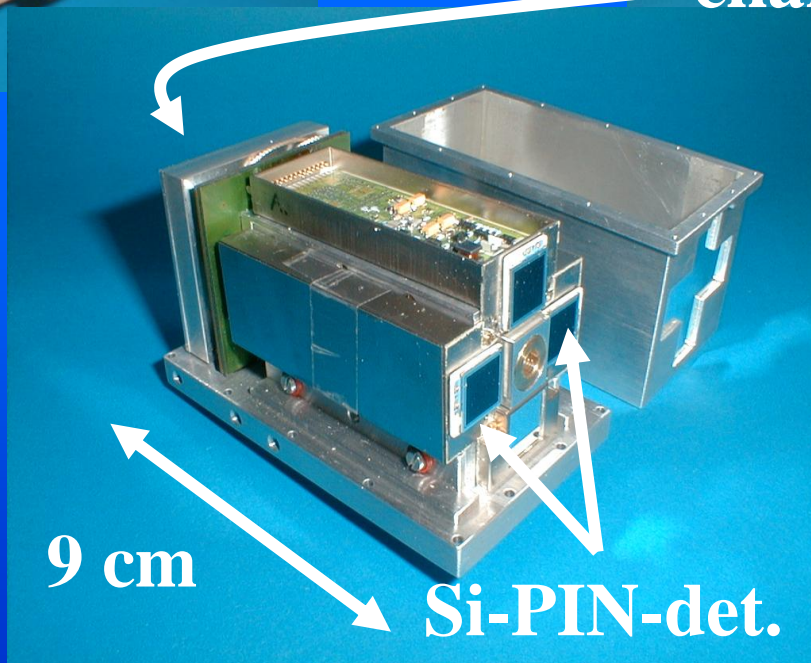
Initiated by Professor Egbert Kankeleit (Darmstadt) around 1990 and extensively pursued by his student Göstar Klingelhöfer and the two excellent electronics experts Josef Foh and Bodo Bernhardt a Mössbauer spectrometer was miniaturised by scaling down a laboratory apparatus by a factor of ca. 100. After E. Kankeleit's retirement in 1998 the project continued with G. Klingelhöfer in the research group of P. Gütlich at the University of Mainz. The goal has been reached most successfully. The miniaturised spectrometer (abbreviated as MIMOS), operating in the gamma backscattering mode, was chosen by NASA to be sent to the planet Mars in two missions in 2003. After a flight time of ca. 7 months the two rovers, *Spirit and Opportunity*, landed safely on the surface of Mars in January 2004. Since then the two MIMOS instruments, one each mounted together with other instruments on a robotic arm of the rovers, are recording Mössbauer spectra (in backscatter mode) of outstanding quality. As of April 2008, both rovers are still operational. The spectra are being sent down to earth and received at the Jet Propulsion Laboratory in Pasadena. They are analyzed and interpreted by an international group of specialists.

Miniaturized Mössbauer Spectrometer (MIMOS)



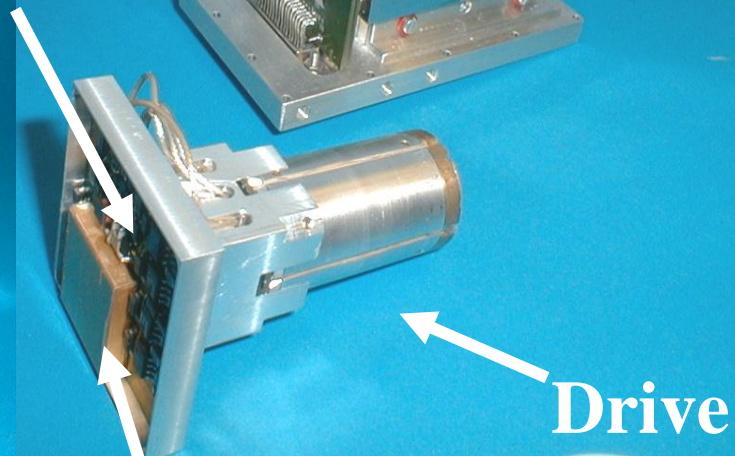
Sensor Head

Reference
channel



9 cm

Si-PIN-det.



Drive

Drive Control unit

The sensor head of the miniaturised Mössbauer spectrometer MIMOS II has the dimensions $9 \times 9 \times 5 \text{ cm}^3$ and weighs only ca. 450 g. Both 14.4 keV gamma rays and 6.4 keV X-rays are detected simultaneously by 4 Si-PIN diodes. The drive unit carries the main Mössbauer source in front and a reference source for velocity calibration in the back. The electronics board is placed in a thermostated housing.

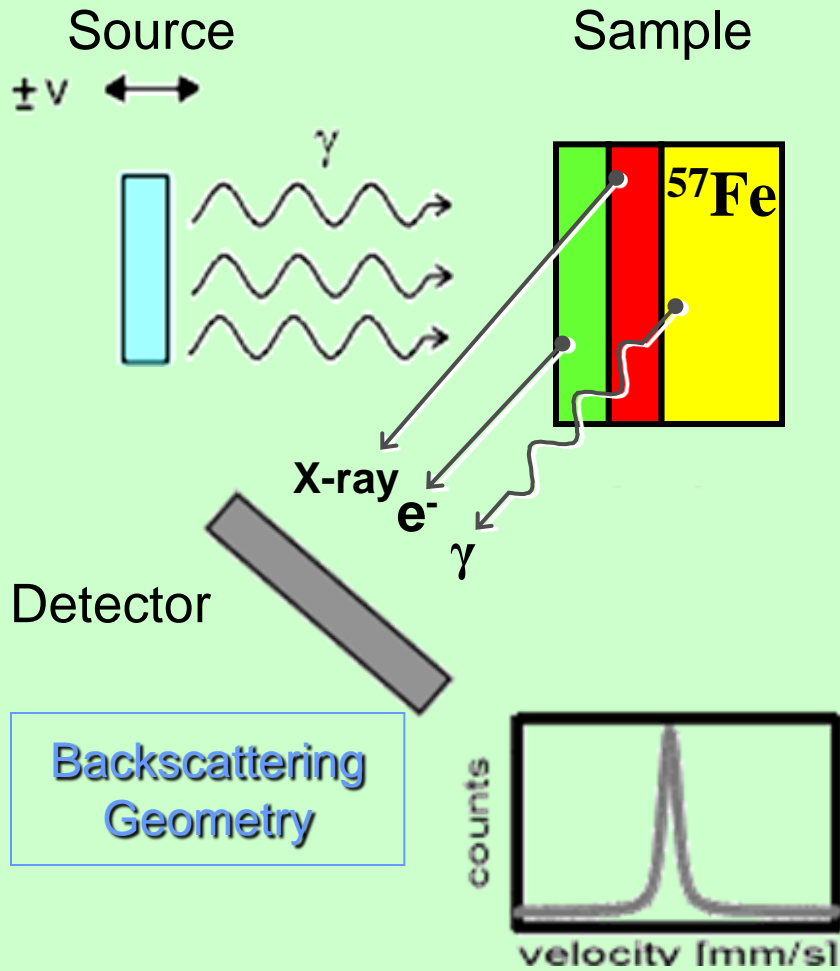
For measurements on planetary surfaces, the instrument has to meet special requirements. In the case of Mars, MIMOS II is able to work at temperatures as low as -133°C and an average atmospheric pressure of 7 mbar.

Due to the instrumental setup in backscattering geometry, sample preparation is not needed, which is a great advantage for a space mission.

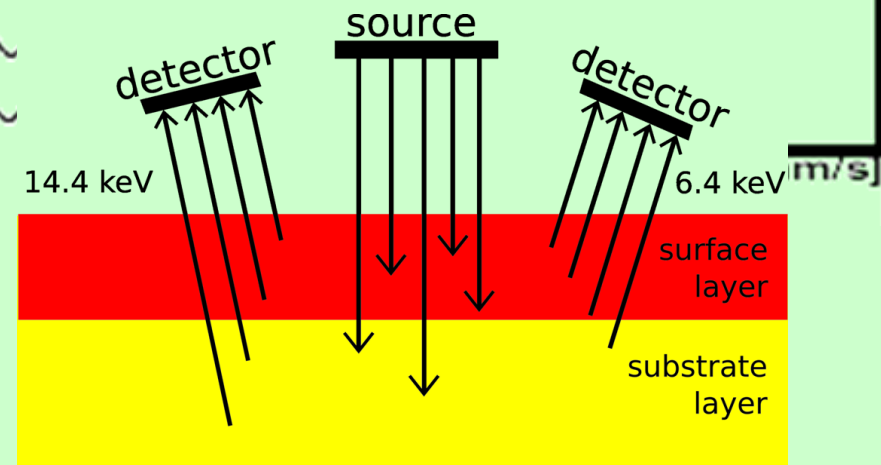
MIMOS II can obtain 14.4 keV gamma ray spectra and 6.4 keV X-ray spectra simultaneously in backscattering geometry. Comparing 6.4 keV and 14.4 keV spectra yields depth selective information about a sample and allows for the detection and characterization of thin coatings or weathering rinds.

From: Klingelhöfer, G., et al. (2003), Athena MIMOS II Mössbauer Spectrometer Investigation, *J. Geophys. Res.*, 108

Mössbauer Spectroscopy: Transmission and Backscattering

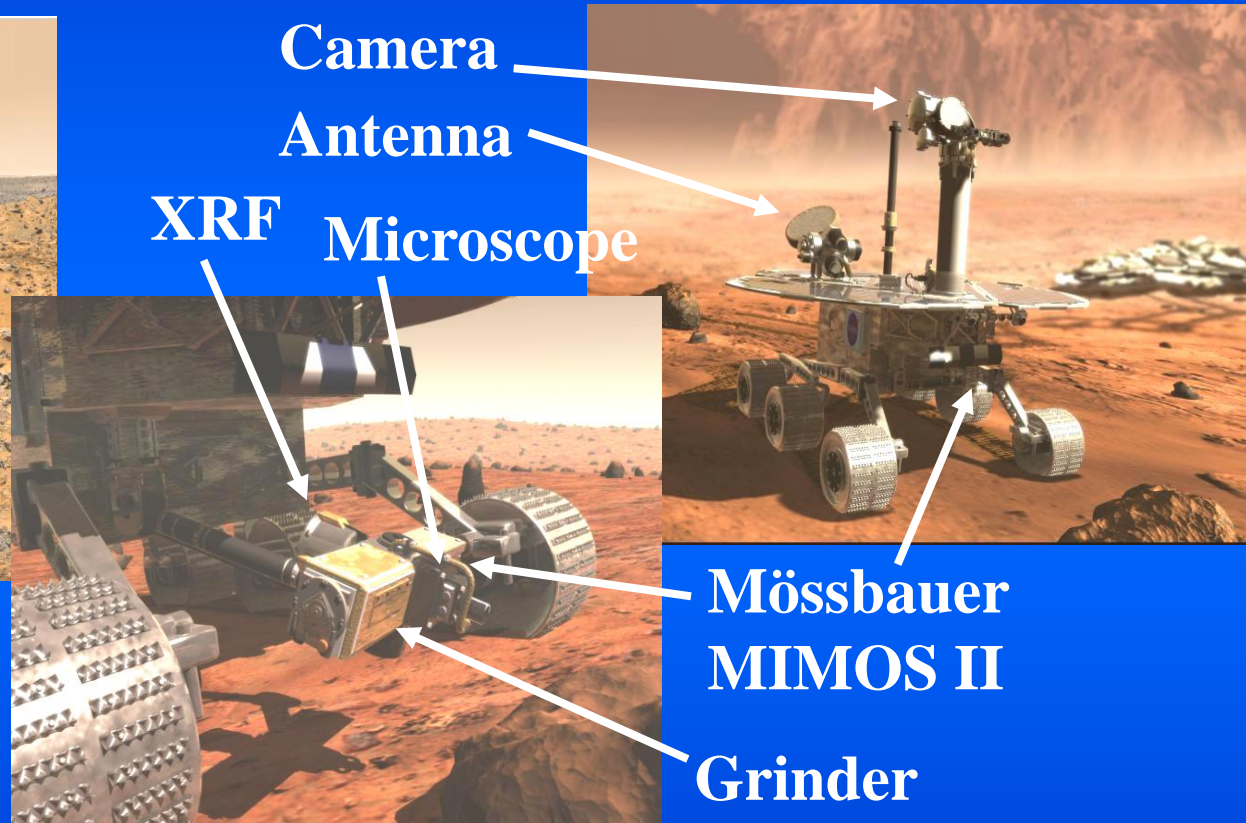


Depth selective Mössbauer spectroscopy:
simultaneous detection of
14.4 keV γ -rays and 6.4 keV X-rays



Mars Exploration Rover 2003

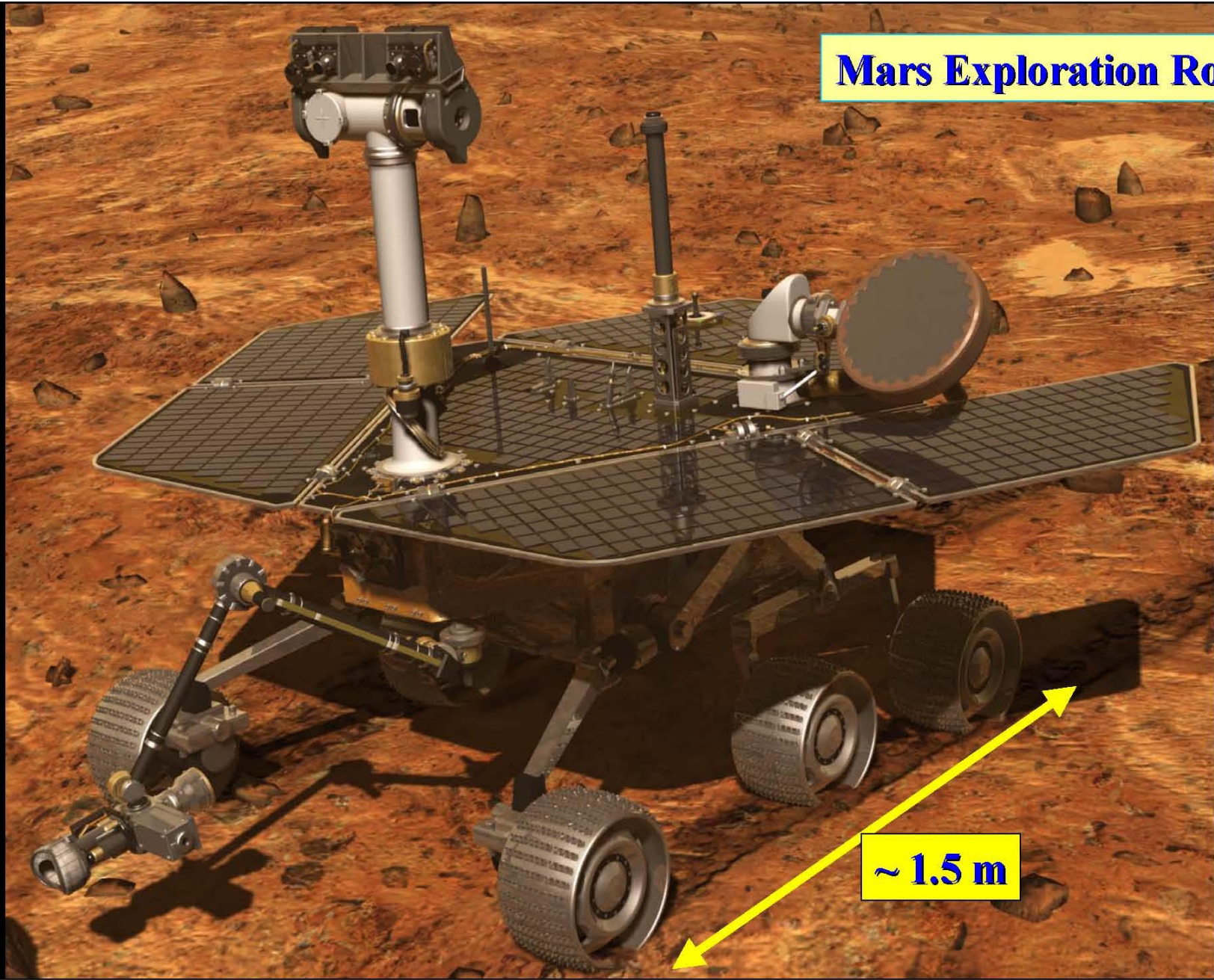
Spirit and Opportunity



Launch: June 2003

Landing: January 2004

Mars Exploration Rover



~ 1.5 m

Pancam Image of the IDD instruments (Sol 287)

MIMOS II

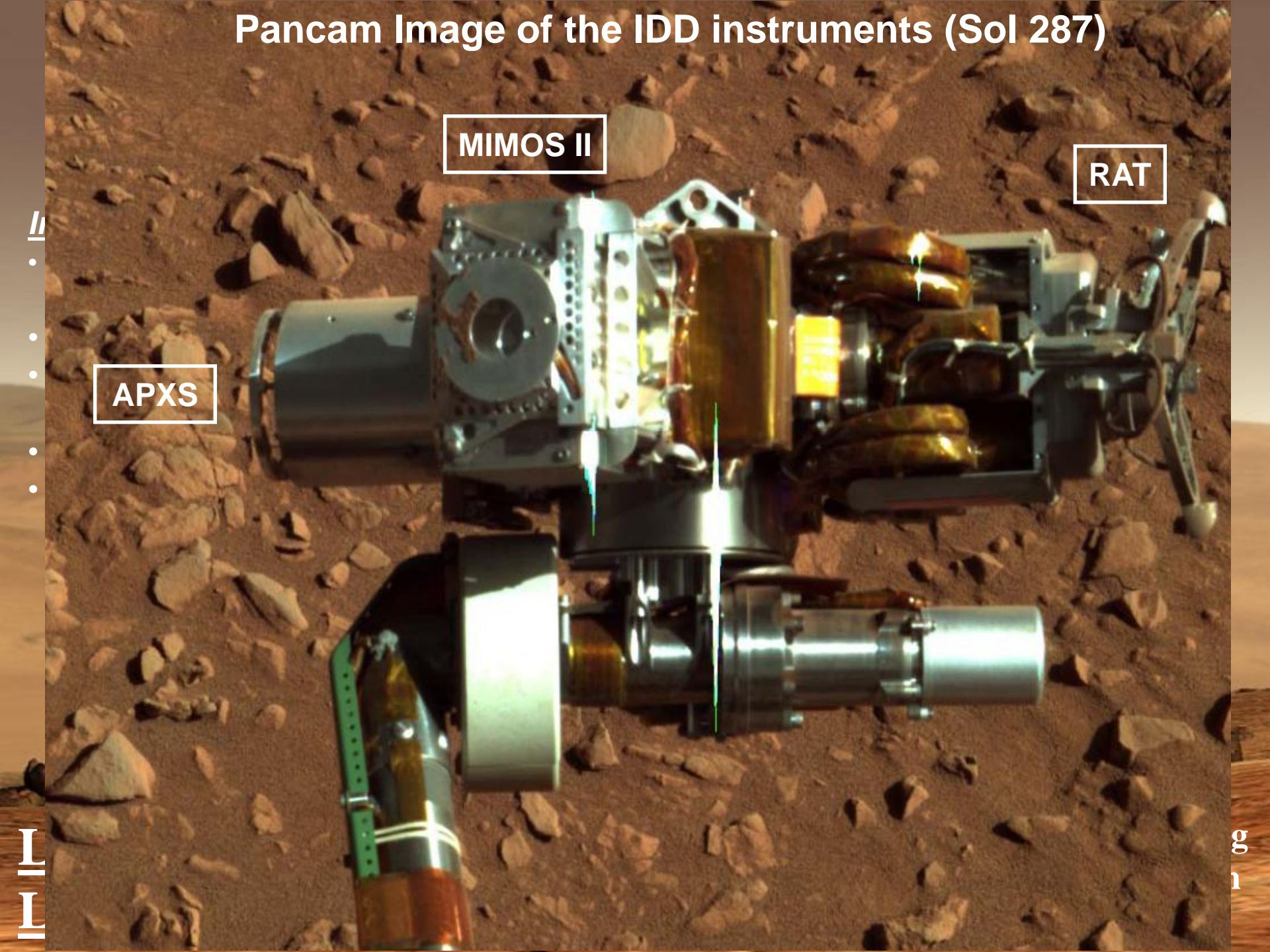
RAT

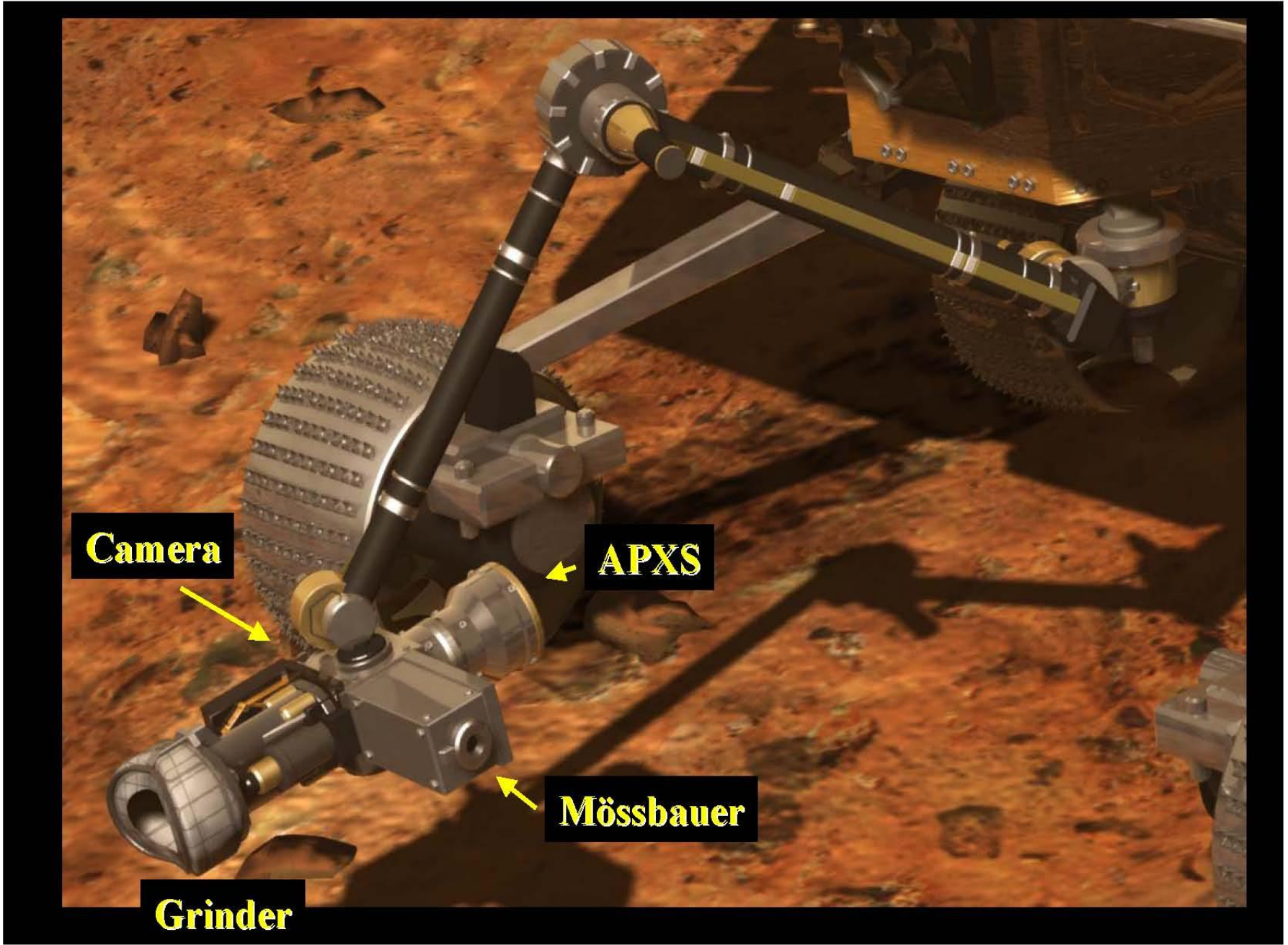
APXS

//
•
•
•
•
•

L
L
L

50
P





Camera

APXS

Mössbauer

Grinder

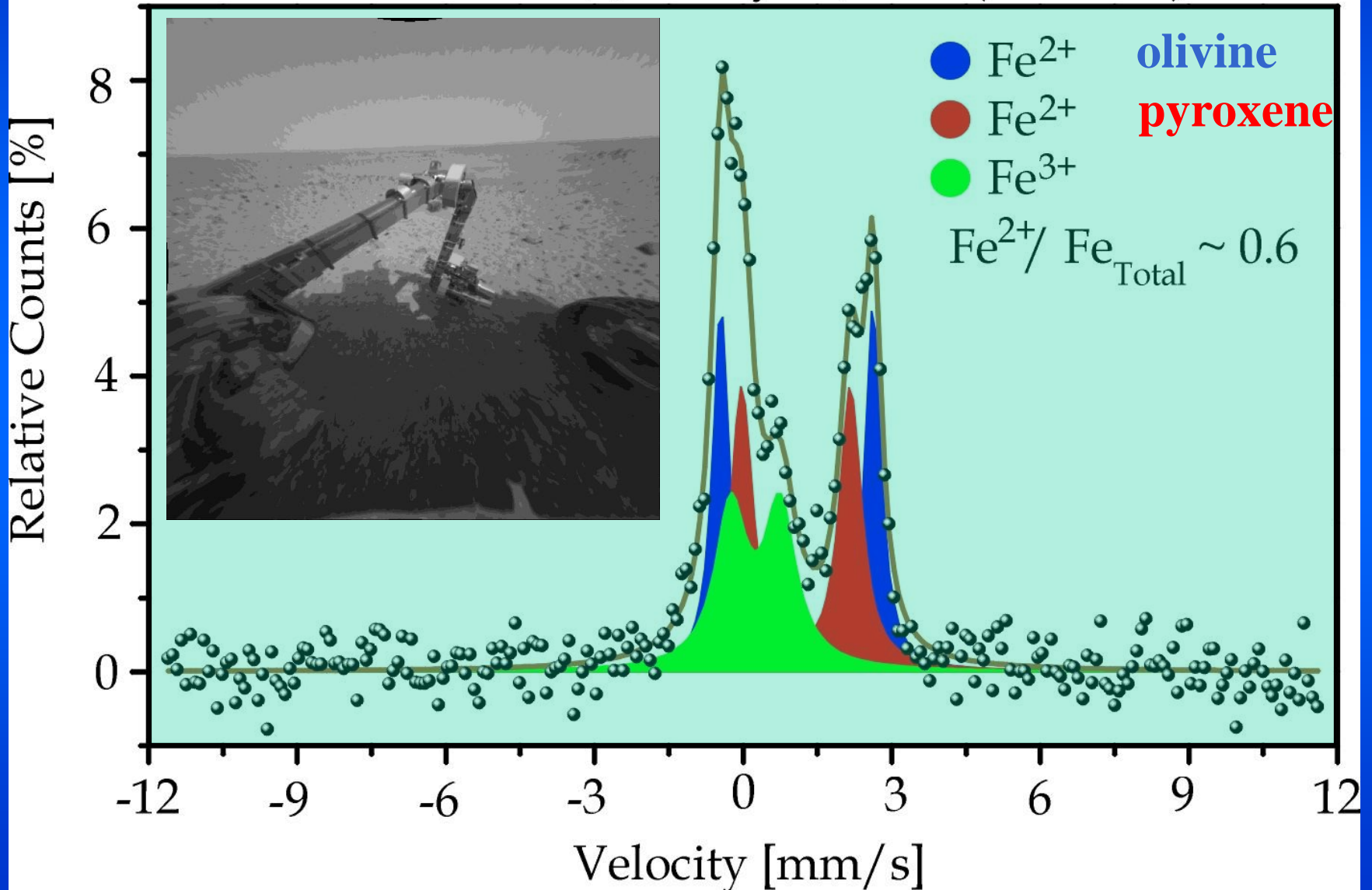
A MIMOS II instrument was mounted on the robotic arm of each of two identical rovers, called *Spirit* and *Opportunity*, which were launched separately in June 2003 (from Kennedy Space Center, Florida) and landed successfully on Mars in January 2004, *Spirit* in Gusev Crater and *Opportunity* in Meridiani Planum (opposite side of Mars).

The rovers are ca. 1.5 m long and ca. 1.5 m high and weigh ca. 175 kilograms each. The solar panels and a lithium-ion battery system provide a power of 140 watts on Mars surface. The rovers are programmed to cover distances of up to a few kilometres taking photographs, recording Mössbauer and X-ray fluorescence spectra of rock and soil on their way. Typical measuring times for Mössbauer spectra are a few hours. Temperatures vary between ca. -70 and $+10$ °C.

The robotic arm carries the Mössbauer spectrometer MIMOS II, an Alpha-Particle-X-ray-Spectrometer (APXS) for elemental analysis (developed at the Max Planck-Institute in Mainz, a Microscopic Imager, and a Rock Abrasion Tool for polishing rocks and drilling holes up to ca. 5 mm into rocks. The first Mössbauer spectrum recorded on the Martian surface was obtained on soil at Spirit's landing site in Gusev crater and shows a basaltic signature (olivine and pyroxene). Soil and dust were found to be globally distributed on Mars: spectra obtained on soil at Opportunity's landing site in Meridiani Planum are almost identical to those recorded in Gusev crater.

First Mössbauer Spectrum Recorded on Martian Surface

Gusev Crater, January 17, 2004 (3h25min)

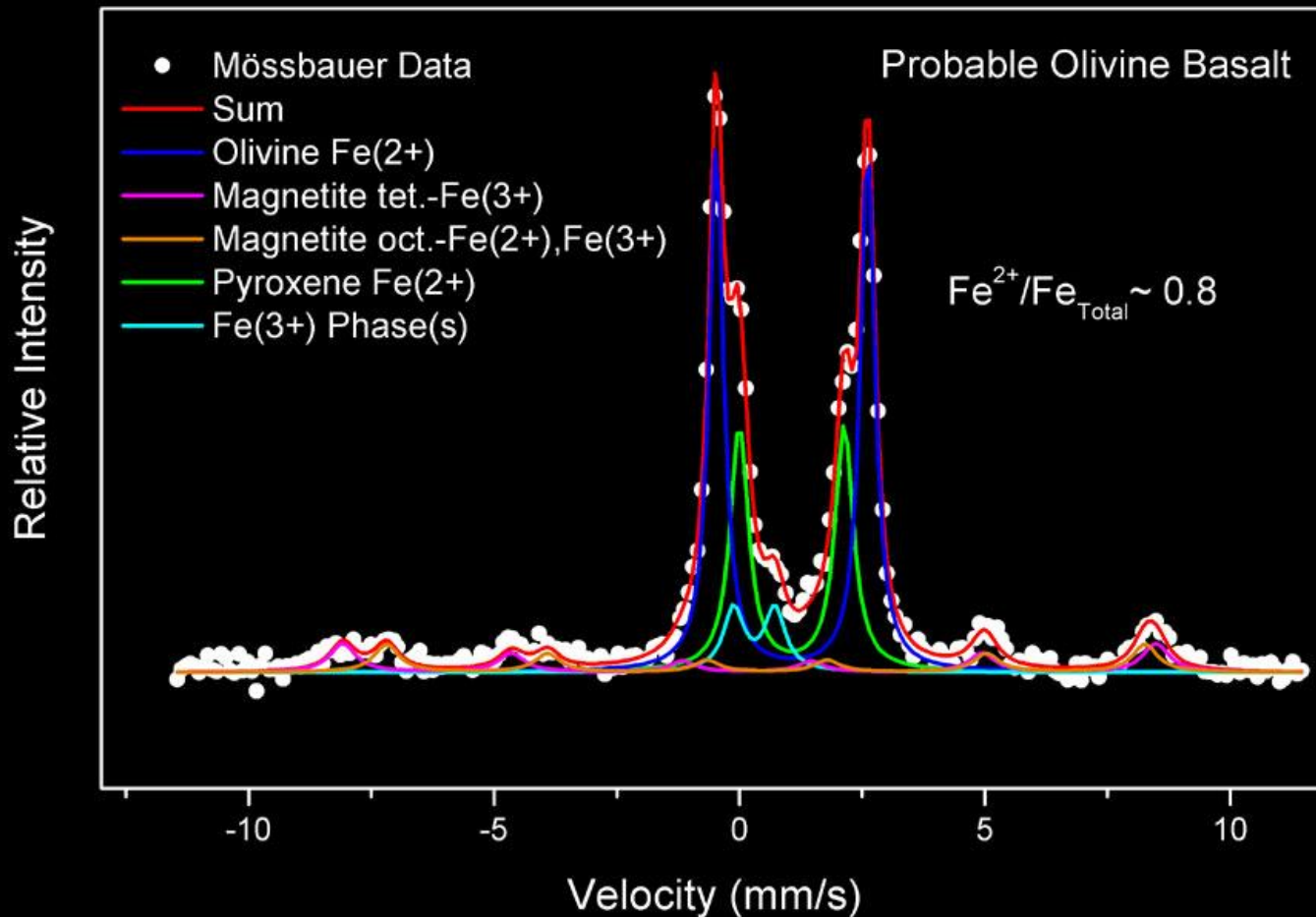


Rock *Adirondack*



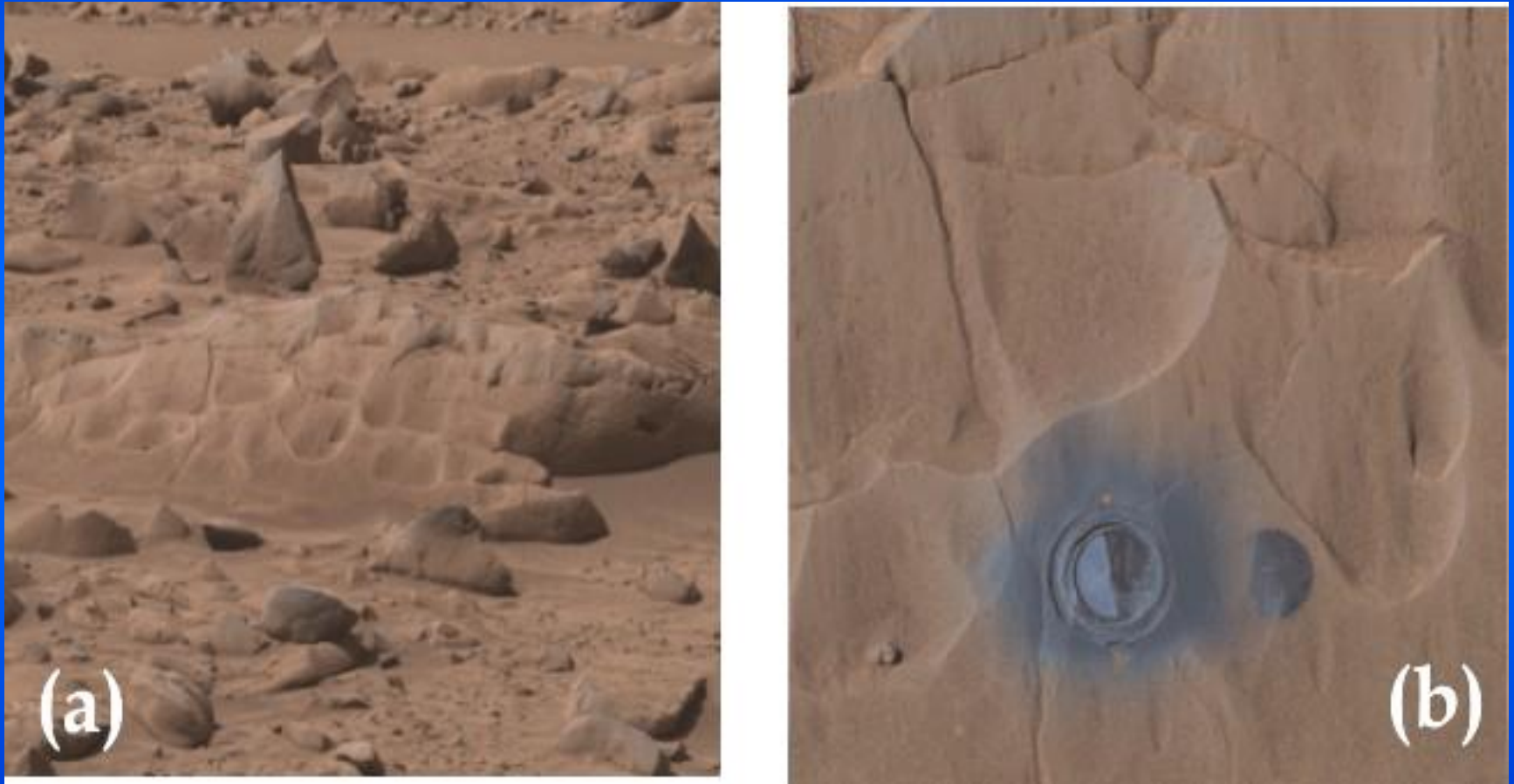
Adirondack has the size of a football.

Mössbauer Spectrum of Adirondack Rock
(Sol 18, Gusev Crater, Mars)



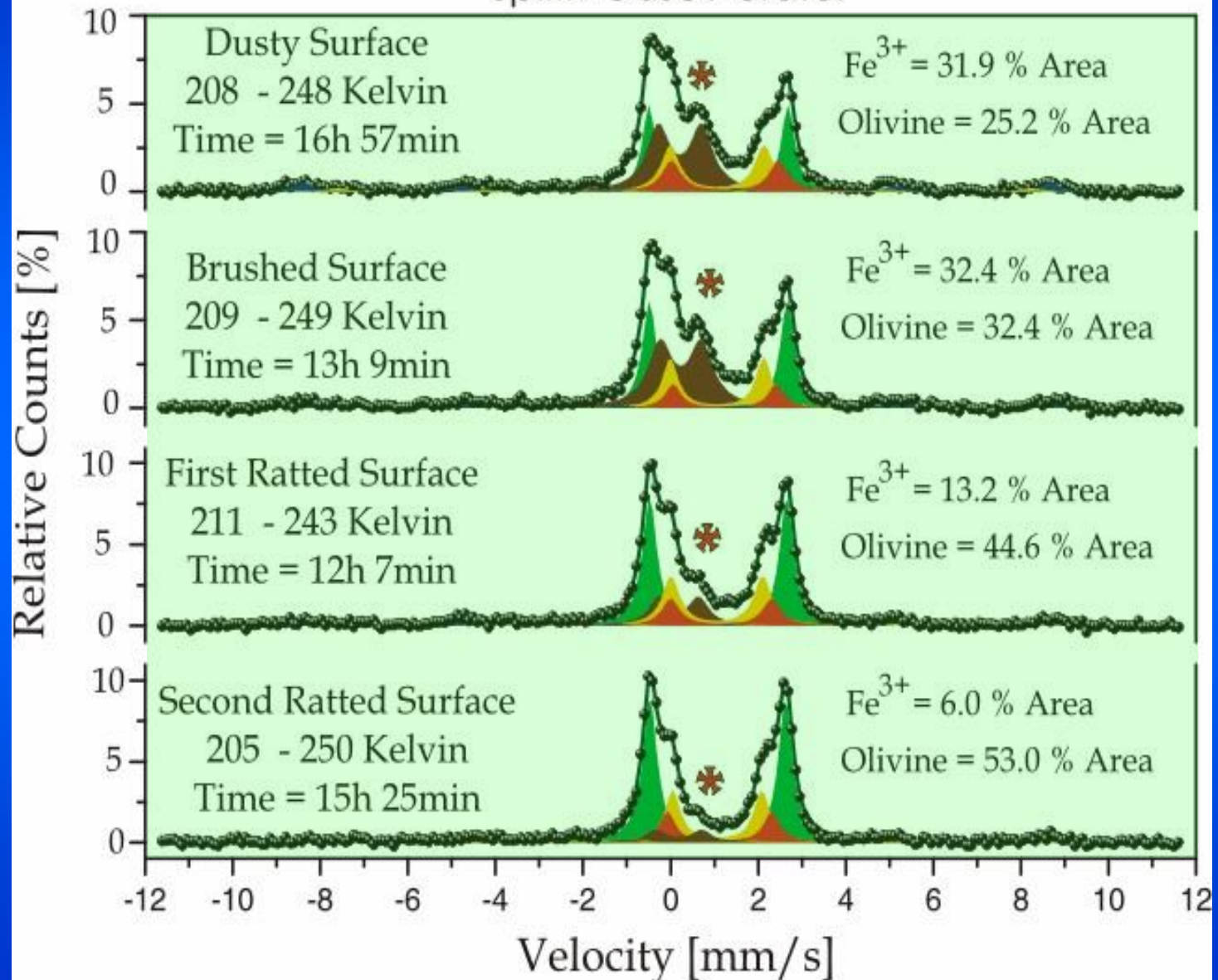
The Mössbauer spectrum of Adirondack taken 18 Mars days (sol) after landing reveals mainly olivine and pyroxene, and a small concentration of magnetite.

The Rock *Mazatzal* at Gusev Bonnevillite crater



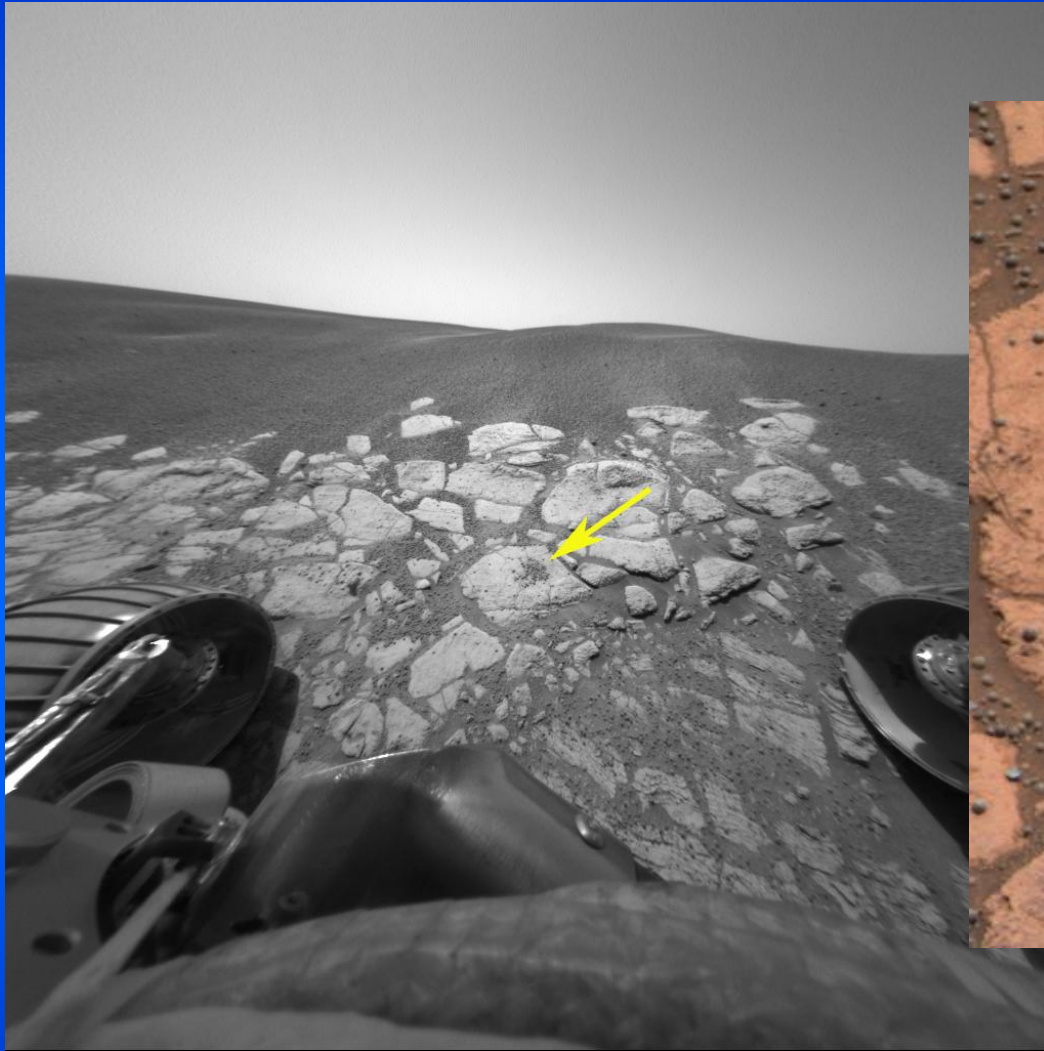
The grinder drills a hole of ca. 5 cm diameter and variable depth into the rock and MIMOS takes the following depth-selective Mössbauer spectra.

Mössbauer Measurements on Mazatzal Rock Spirit: Gusev crater



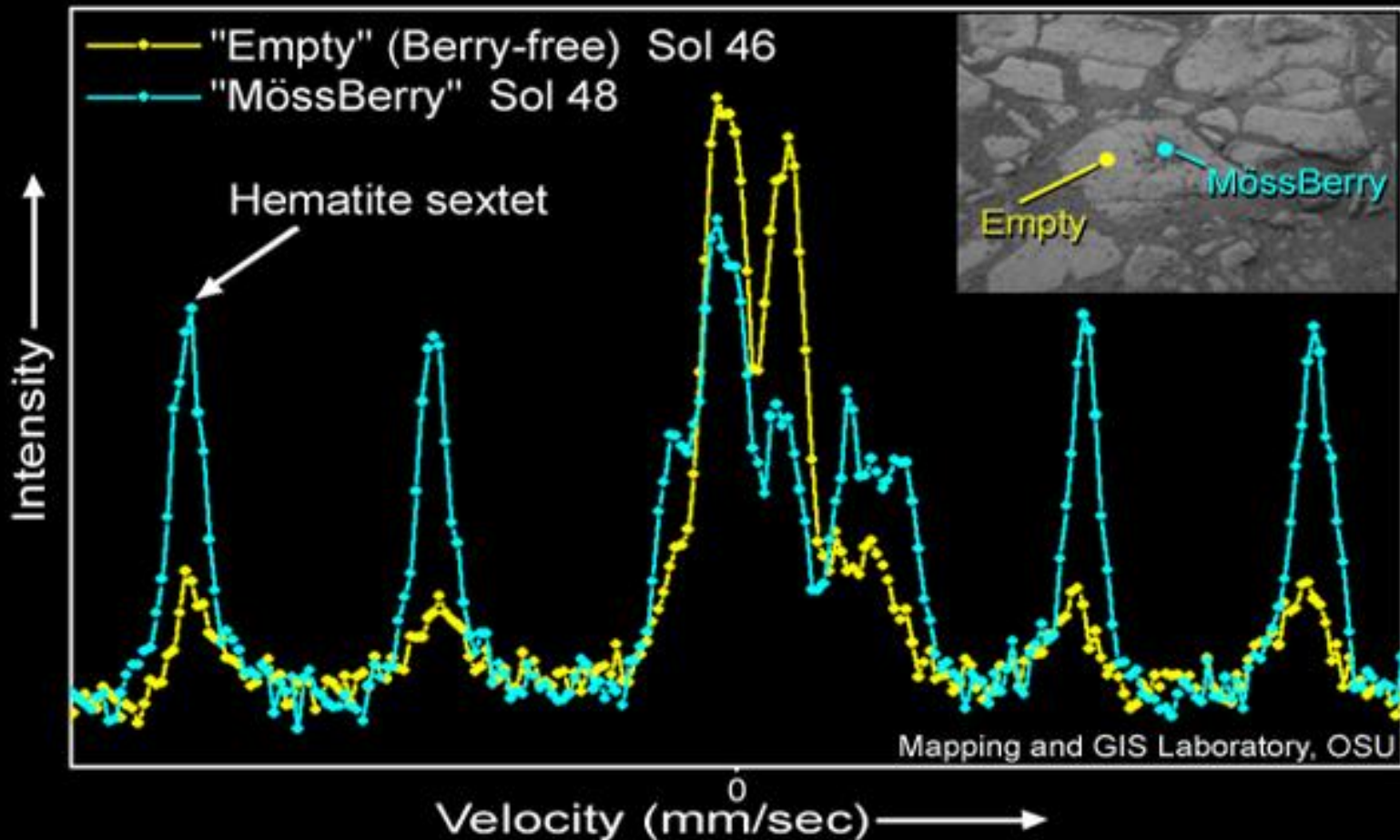
The spectra show that the olivine content varies on going from the untreated dusty surface to a brushed surface and then into the interior of the rock. Indicated are the measuring times and the changes of the ambient temperature during the measurements.

The “Berry Bowl”



Black spherules (ca. 5 mm diameter), looking like blueberries, spread out in a rocky outcrop are analysed with MIMOS, 46 and 48 Mars days after landing.

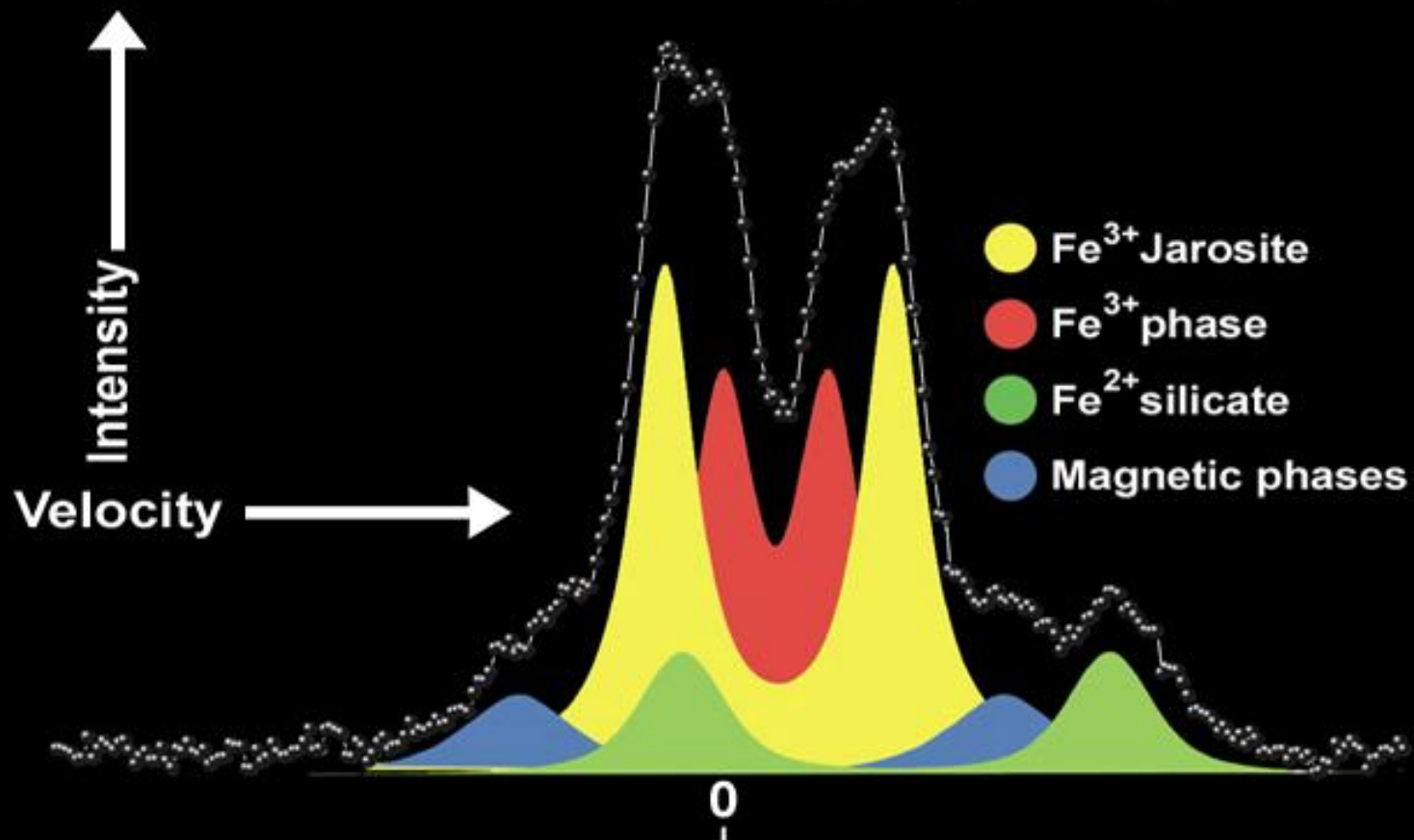
Mössbauer spectra of the BlueBerry bowl and bare outcrop at Meridiani Planum



The blueberry-spherules show a high concentration of hematite, much higher than the berry-free rock.

Mössbauer spectra of El Capitan

Mössbauer Spectrum of El Capitan: Meridiani Planum
Jarosite: $(K, Na, X^{+1})Fe_3(SO_4)_2(OH)_6$



The most exciting Mössbauer spectrum recorded on Mars (Meridiani Planum) so far points at the presence of the mineral Jarosite. The chemical formula of Jarosite as given in the picture contains 6 OH groups per formula unit. This means that the mineral must have been formed in the presence of water. Thus the detection of the mineral Jarosite is clear evidence for the presence of water on Mars in the past or even until now in the form of deep frozen ice.

Reprint Series

Science

6 August 2004

Vol. 305 No. 5685
Pages 737-900 \$10

“Mineralogy at Gusev Crater
from the
Mössbauer Spectrometer
on the Spirit Rover”

Spirit
at Gusev Crater



Reprint Series

Science

3 December 2004

Vol. 306 No. 5702
Pages 1633-1844 \$10

“Jarosite and Hematite
at Meridiani Planum
from Opportunity’s
Mössbauer Spectrometer”

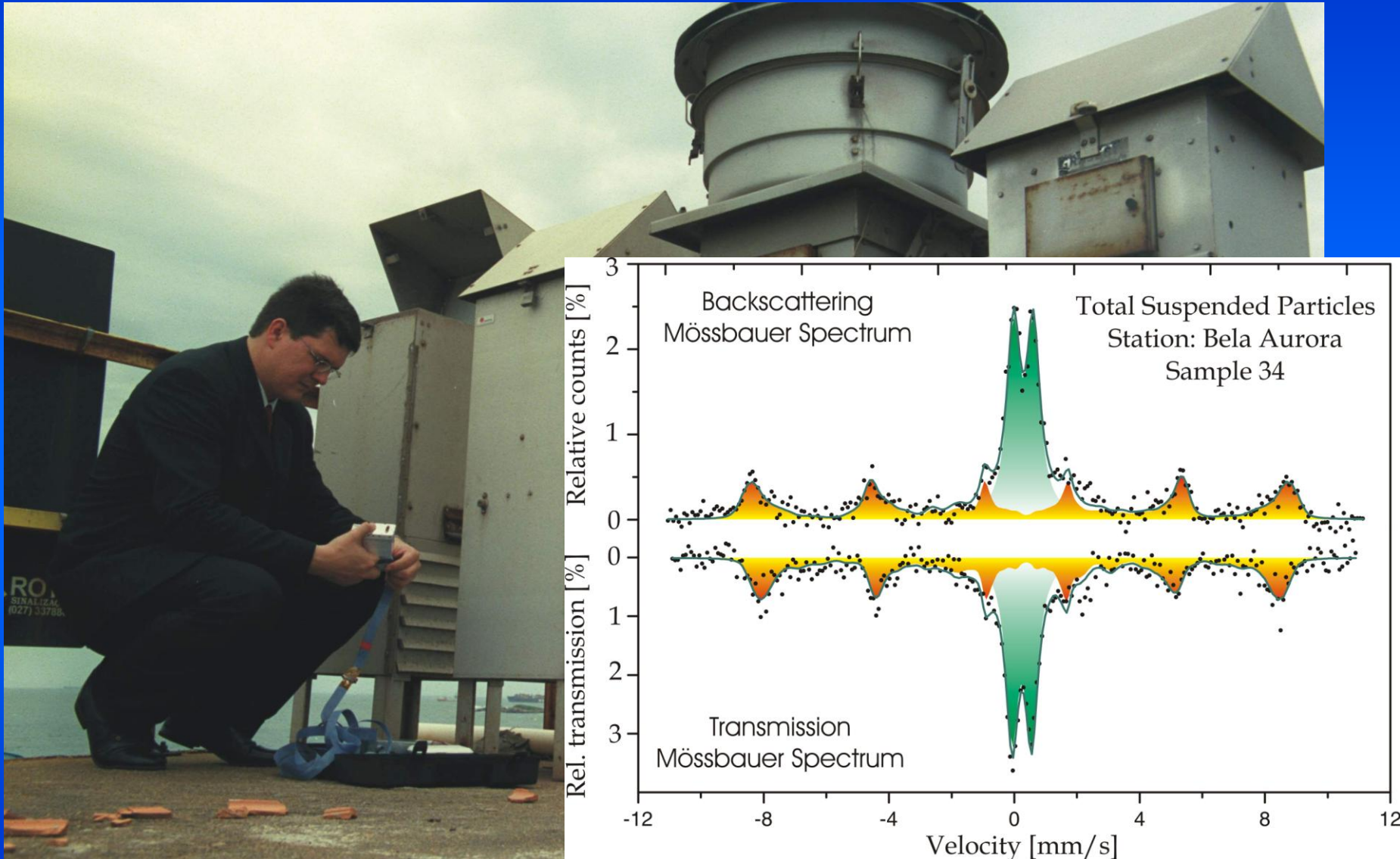
Opportunity
at Meridiani Planum



Mobile Mössbauer Spectroscopy on Earth with MIMOS



In situ Air Pollution Investigation



P. A. de Souza Jr., et al. *94th AWMA Meeting, 2001, Sect. AB-2D, 569.*

Monitoring of Iron Mineralogy and Oxidation States in the Field: the Green Rust Mineral

Electronics-box
with digital board
and positioning-
mechanism.

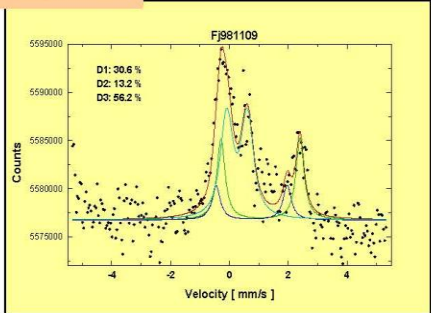


- long tube with windows located in different depths.
- MIMOS II is moved within the tube to different depth.

Depth
(with respect to
surface)

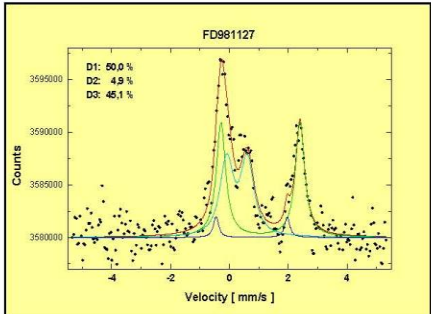
$\text{Fe}^{\text{II}}/\text{Fe}^{\text{III}}$

69 cm



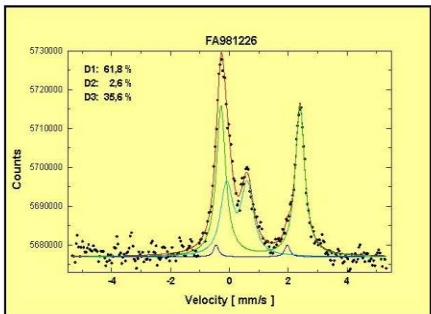
0,78

34 cm



1,22

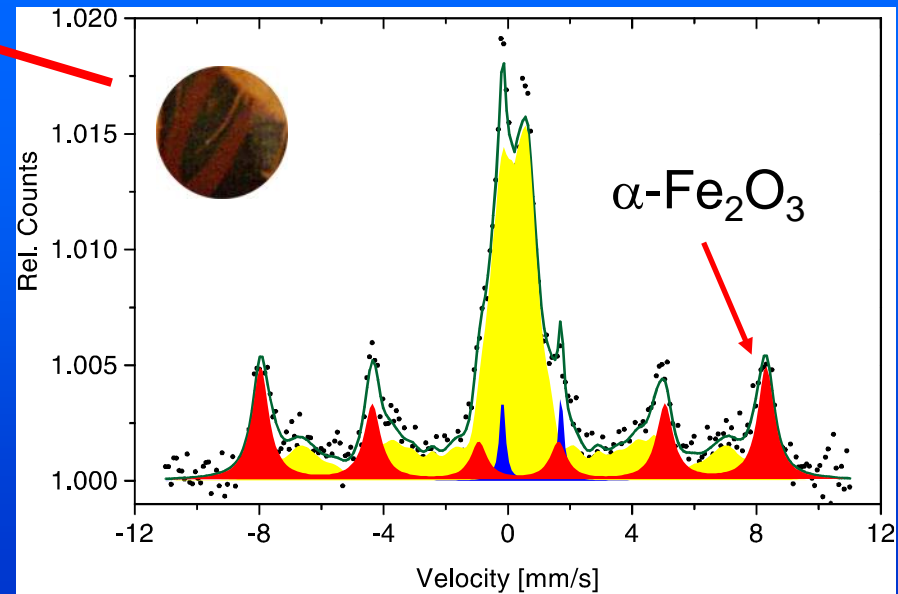
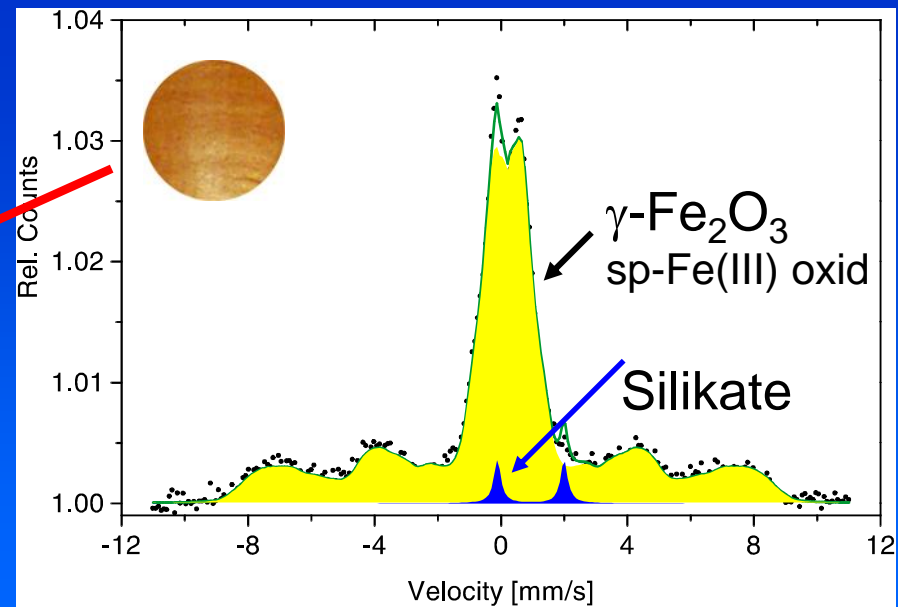
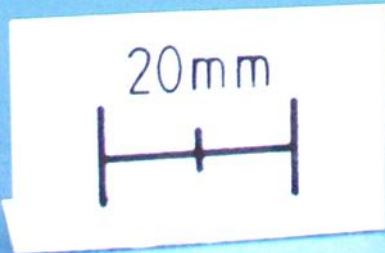
9 cm



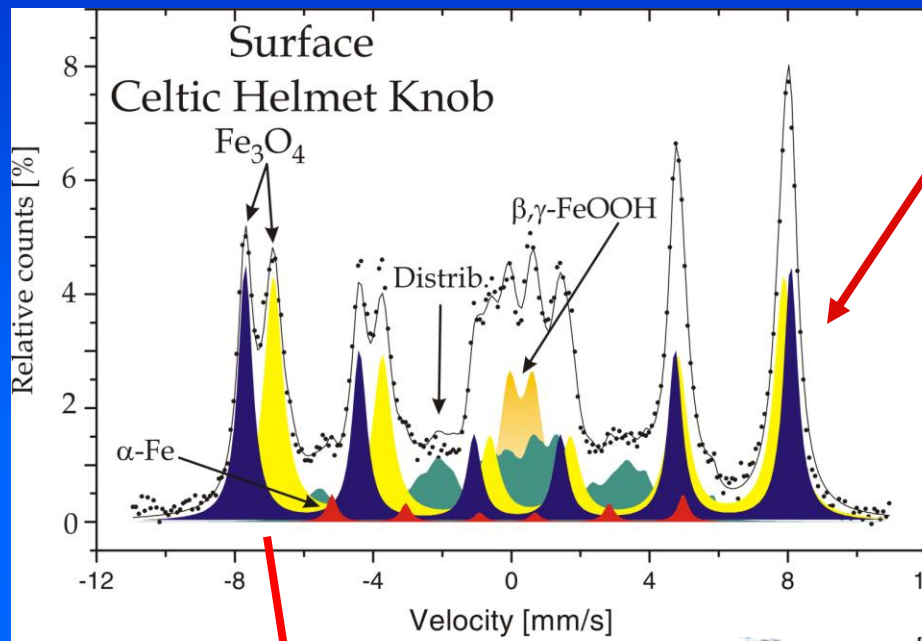
1,81

Lekythos 500 b. C.

Röm.-germ.
Zentralmuseum
Mainz

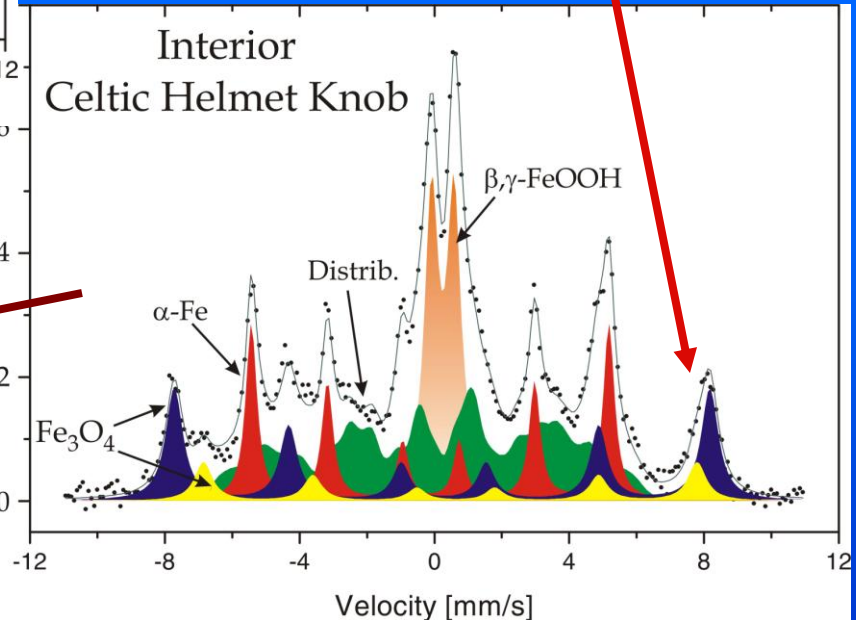
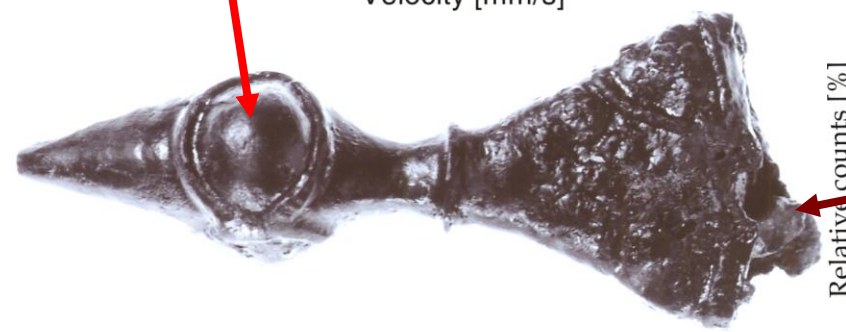


Celtic Helmet Knob

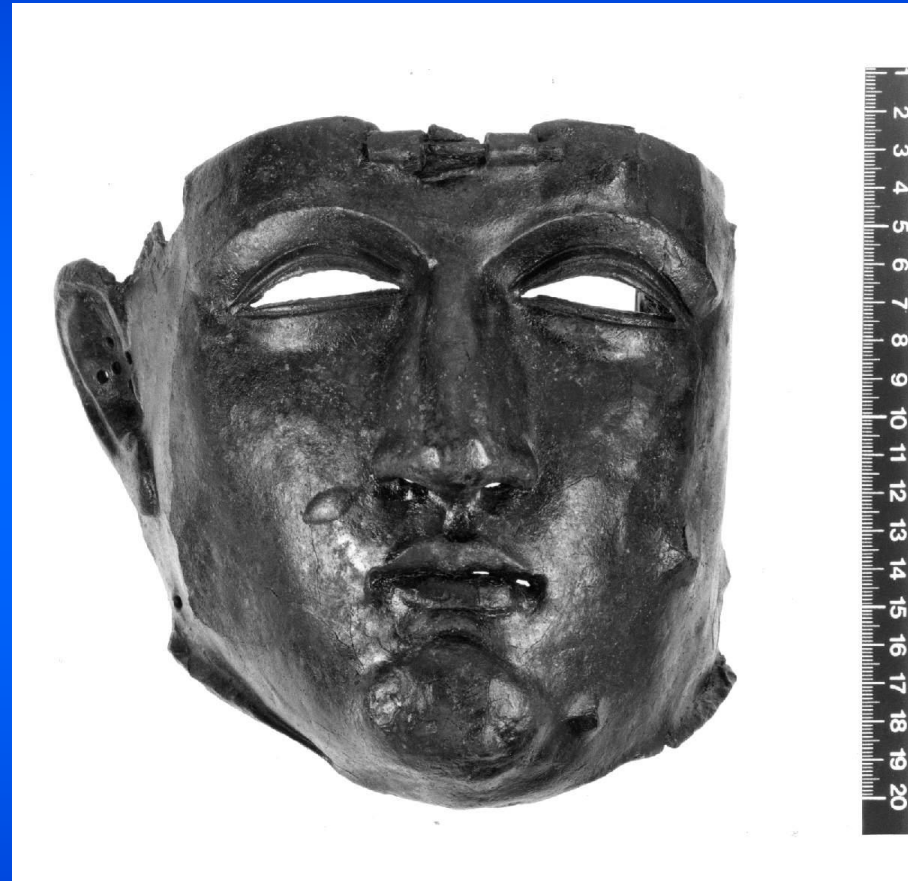
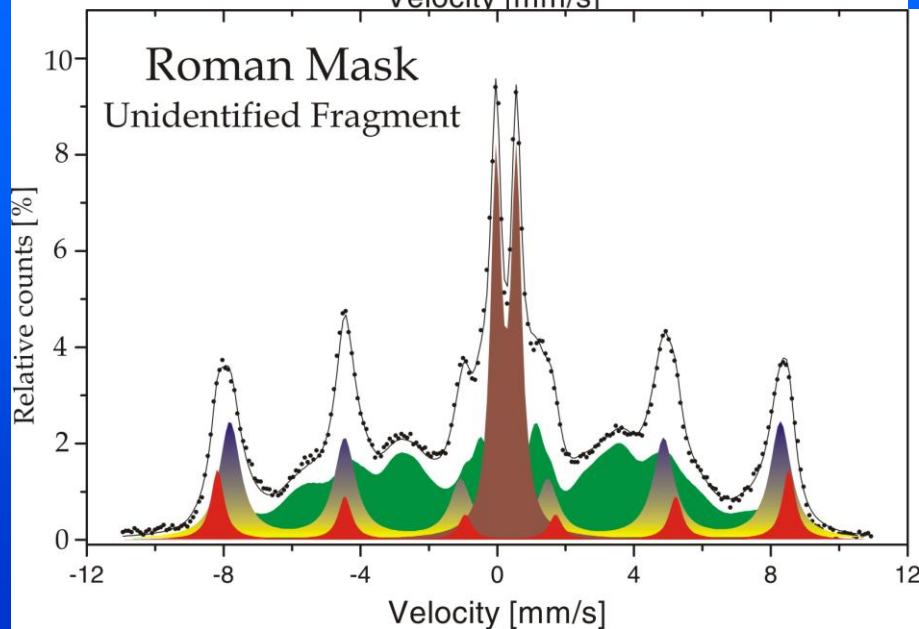
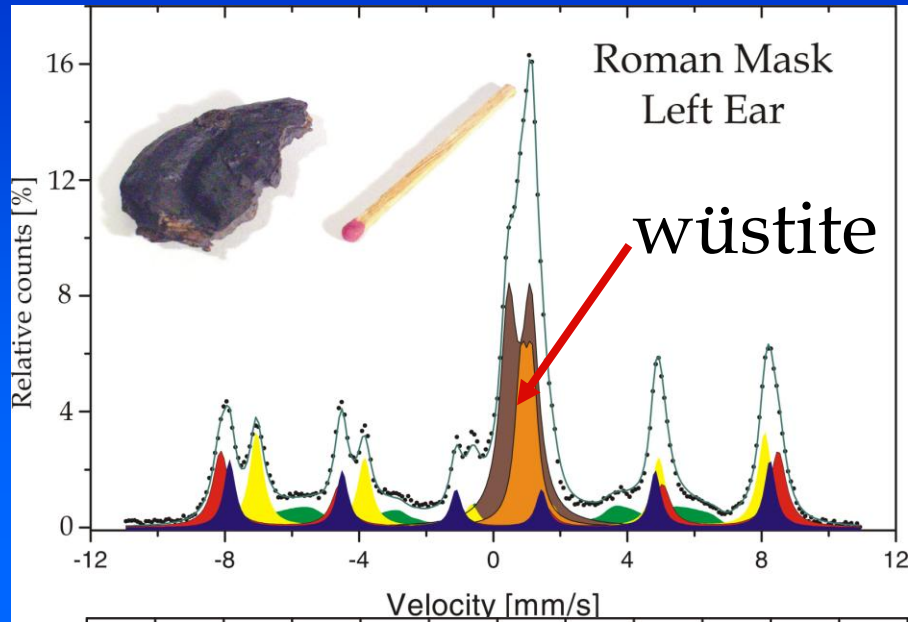


Magnetite

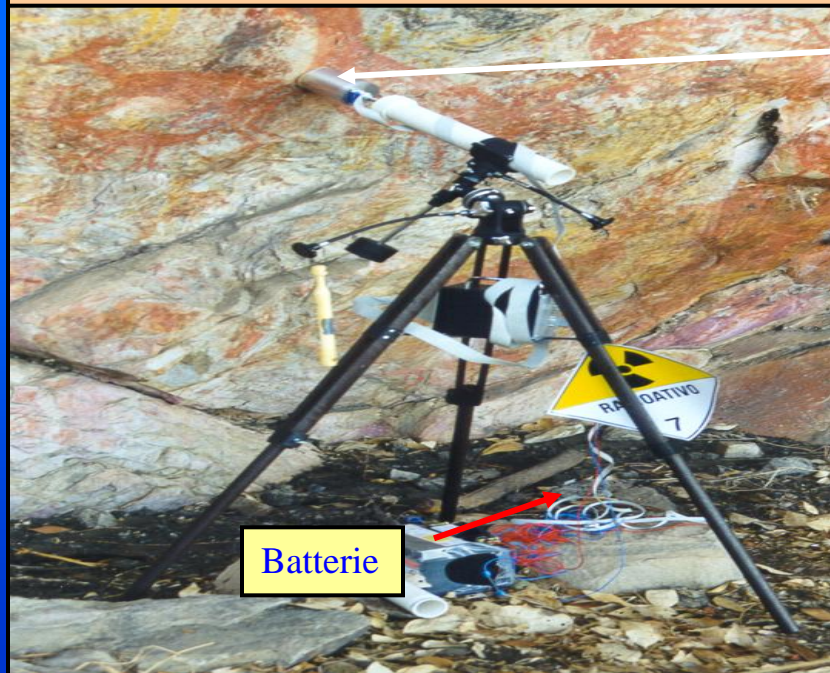
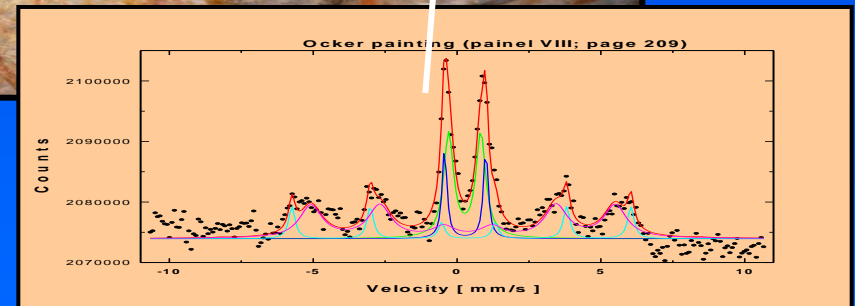
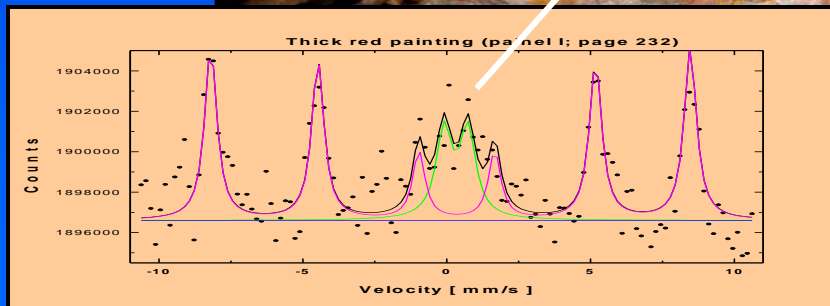
Magnetite
and
Maghemite



Restoration of a Roman Mask



Ancient rockpainting in Brazil (Santana do Riacho)



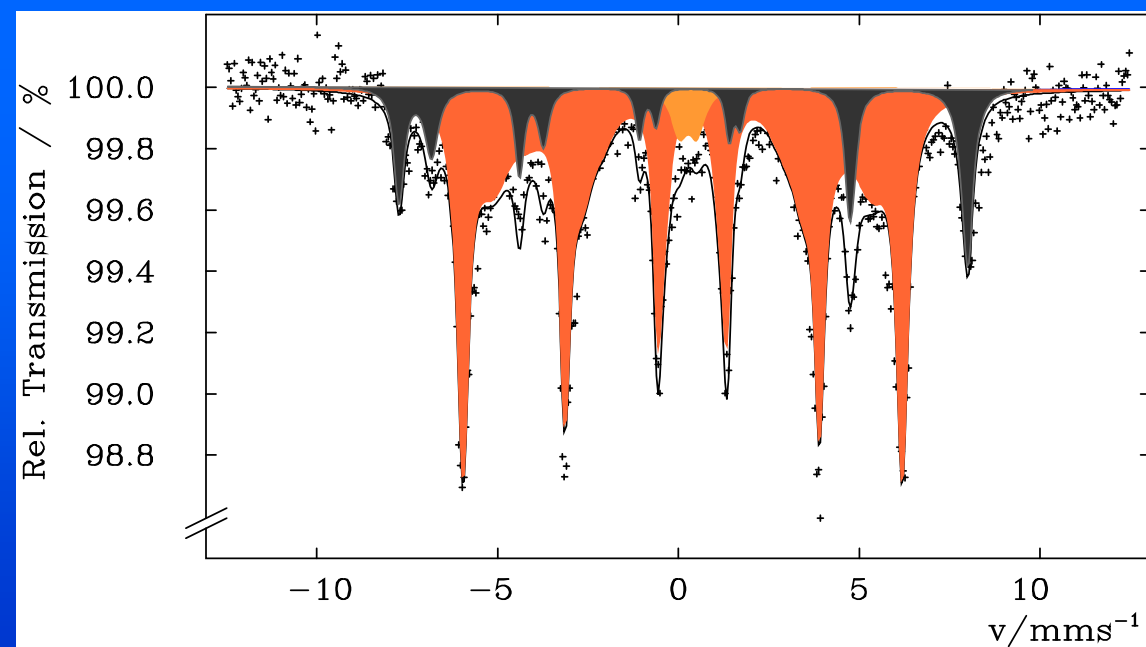
Batterie

MIMOS II Mössbauer-Spectrometer

Non-destructive analysis with MIMOS of ancient rockpainting in Brazil (near Belo Horizonte, Minas Gerais).

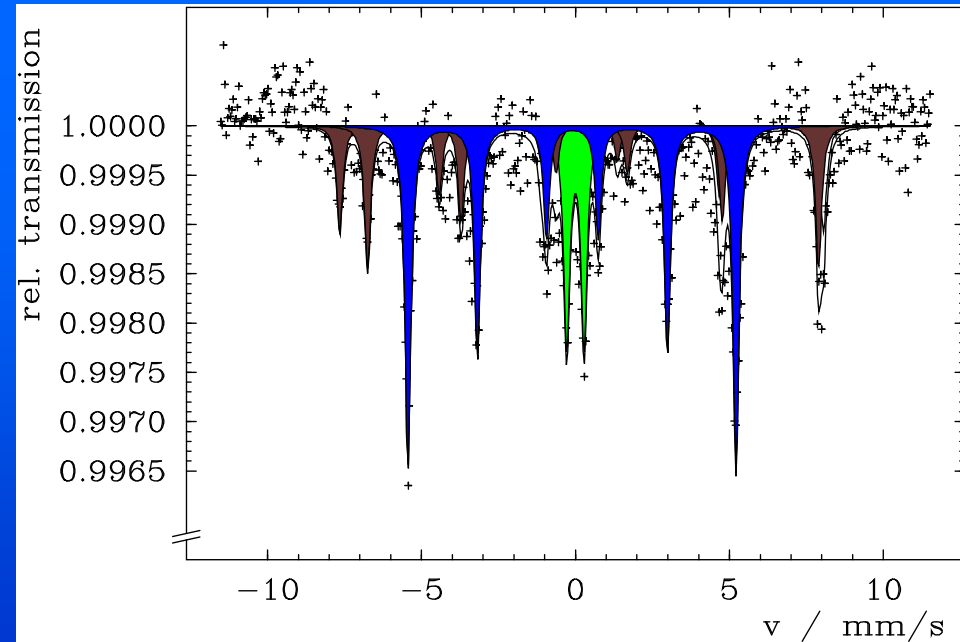
MIMOS is mounted on a support and touches the painting on the wall for measurement. Two spectra were recorded, one of a darker paint, the other for a light-coloured paint. With Mössbauer spectroscopy it is possible to distinguish between different iron oxide pigments.

^{57}Fe Mössbauer Spectrum of a 1 US-Dollar Bill



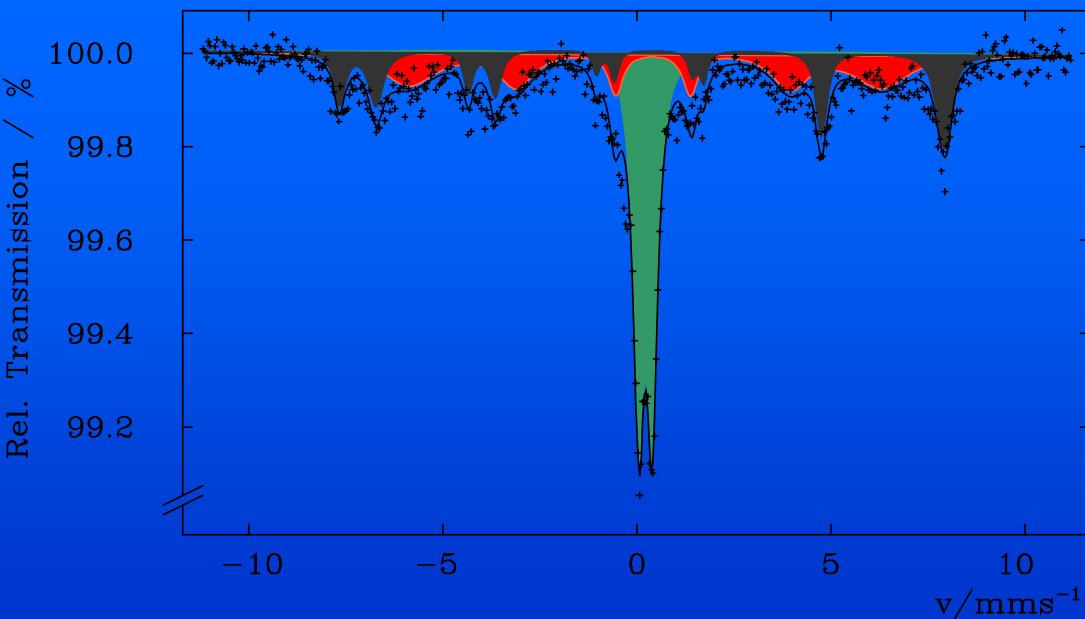
<u>Constituents</u>	<u>area-%</u>
Magnetite, Fe_3O_4	20
Goethite, $\alpha\text{-FeOOH}$	80

^{57}Fe Mössbauer Spectrum of a 50 Euro Bill



<u>Constituents</u>	<u>area-/%</u>
α Iron	48
Magnetite	36
doublet	16

^{57}Fe Mössbauer-Spectrum 10000 Yen



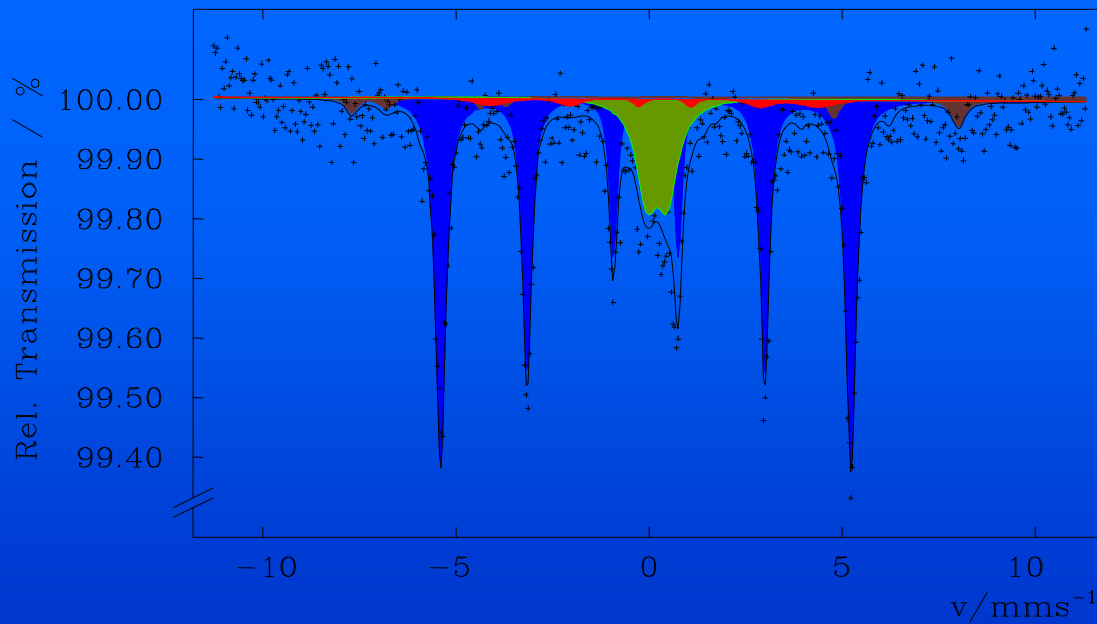
Komponenten: Fläche %

Magnetit, Fe_3O_4 27

Superpara-
magnetisches
Eisenoxid 36

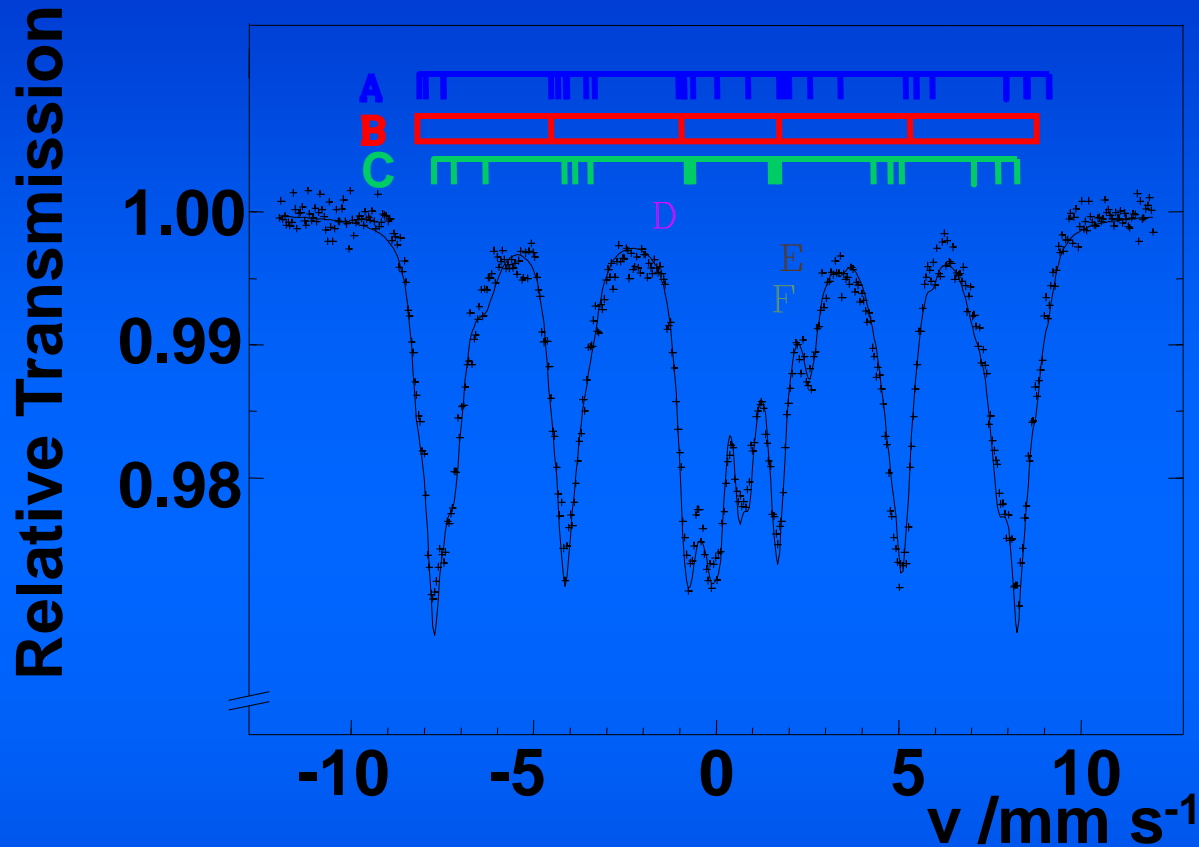
Goethit, $\alpha\text{-FeOOH}$ 37

^{57}Fe -Mössbauer-Spectrum 100 DM



<u>Komponenten</u>	<u>Fläche %</u>
Metallisches Eisen	70
Superpara- magnetisches Eisen-(III)oxid	18
Magnetit	6
Hämatit	6

Iron containing particles in aerosols



A: Fe₃O₄, Magnetite 9,8

B: α-Fe₂O₃, Haematite 7,5

C: α-FeOOH, Goethite 60,8

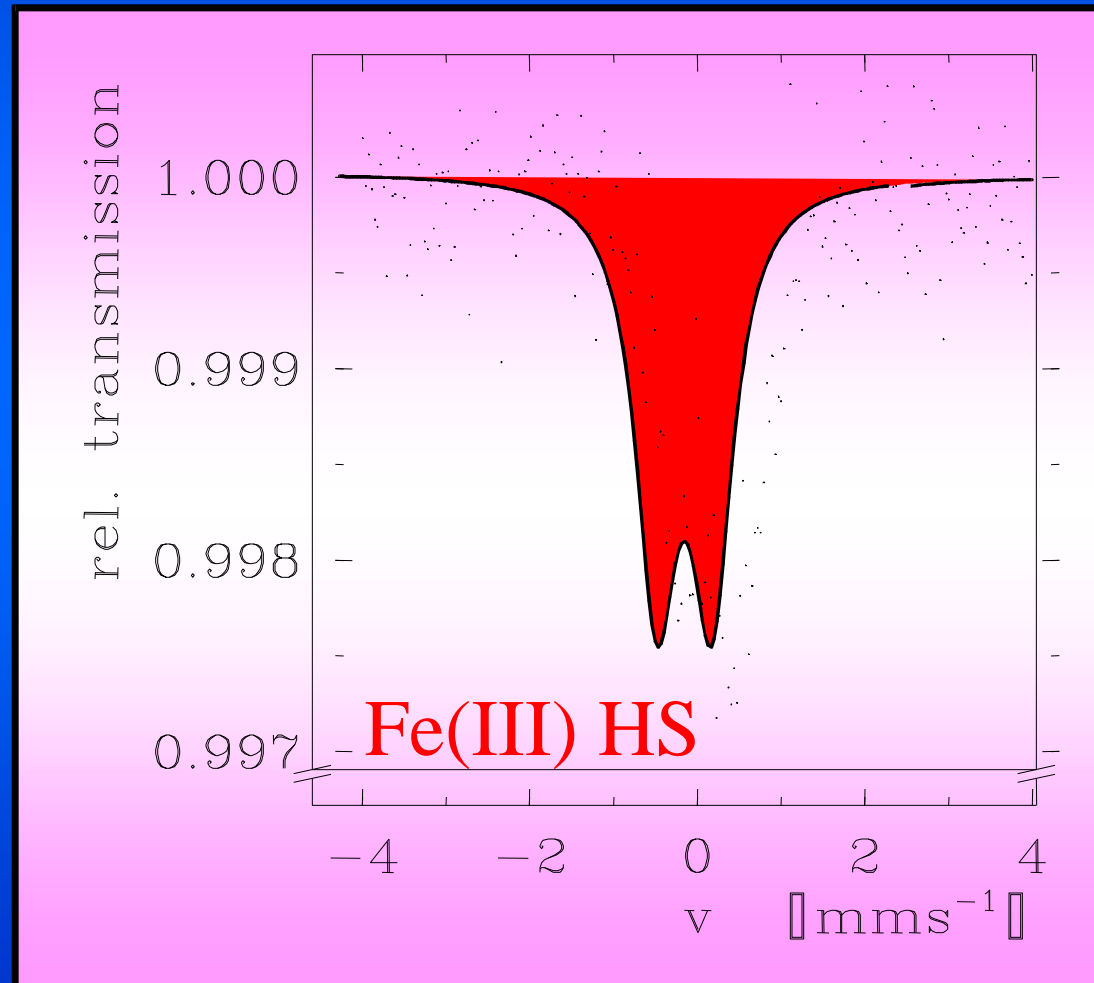
D: Silikat Fe²⁺ 9,4

E: Silikat Fe³⁺ (I) 6,8

F: Silikat Fe³⁺ (II) + 5,7

Superparamag. Goethite

Iron in french red wine





Iron in spinach

